INFORMATION TO USERS

This manuscript has been reproduced from the microfilm master. UMI films the text directly from the original or copy submitted. Thus, some thesis and dissertation copies are in typewriter face, while others may be from any type of computer printer.

The quality of this reproduction is dependent upon the quality of the copy submitted. Broken or indistinct print, colored or poor quality illustrations and photographs, print bleedthrough, substandard margins, and improper alignment can adversely affect reproduction.

In the unlikely event that the author did not send UMI a complete manuscript and there are missing pages, these will be noted. Also, if unauthorized copyright material had to be removed, a note will indicate the deletion.

Oversize materials (e.g., maps, drawings, charts) are reproduced by sectioning the original, beginning at the upper left-hand corner and continuing from left to right in equal sections with small overlaps.

Photographs included in the original manuscript have been reproduced xerographically in this copy. Higher quality 6" x 9" black and white photographic prints are available for any photographs or illustrations appearing in this copy for an additional charge. Contact UMI directly to order.

ProQuest Information and Learning
300 North Zeeb Road, Ann Arbor, MI 48106-1346 USA
800-521-0600

UMI®

Spatially Controlled Engineering of Myocardial Tissue

Todd C. McDevitt

A dissertation submitted in partial fulfillment of the
requirements for the degree of

Doctor of Philosophy

University of Washington

2001

Program Authorized to Offer Degree: Bioengineering

UMI Number: 3036506

ProQuest Information and Learning Company
300 North Zeeb Road
P.O. Box 1346
Ann Arbor, MI 48106-1346

In presenting this dissertation in partial fulfillment of the requirements for the Doctoral degree at the University of Washington, I agree that the Library shall make its copies freely available for inspection. I further agree that extensive copying of the dissertation is allowable only for scholarly purposes, consistent with "fair use" as prescribed in the U.S. Copyright Law. Requests for copying or reproduction of this dissertation may be referred to Bell and Howell Information and Learning, 300 North Zeeb Road, Ann Arbor, MI 48106-1346, to whom the author has granted "the right to reproduce and sell (a) copies of the manuscript in microform and/or (b) printed copies of the manuscript made from microform."

Signature Todd R. McDavitt

Date 11/20/01

University of Washington
Graduate School

This is to certify that I have examined this copy of a doctoral dissertation by

Todd C. McDevitt

and have found that it is complete and satisfactory in all respects,
and that any and all revisions required by the final
examining committee have been made.

Chair of Supervisory Committee:

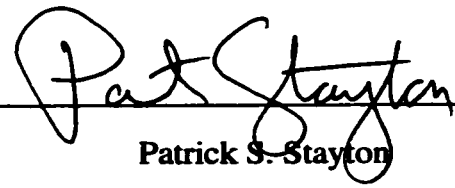

Patrick S. Stayton

Reading Committee:

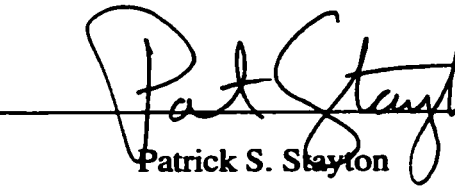

Patrick S. Stayton

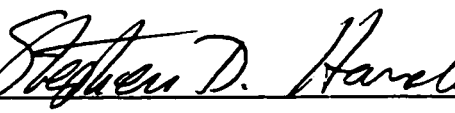

Stephen D. Hauschka

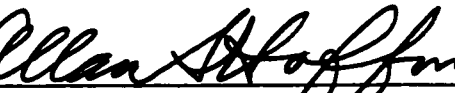

Allan S. Hoffman

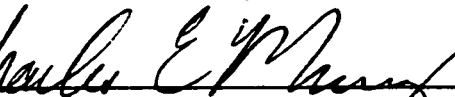

Charles E. Murry

Date: 11/30/01

University of Washington

Abstract

Spatially Controlled Engineering of Myocardial Tissue

Todd C. McDevitt

Chair of the Supervisory Committee:
Professor Patrick S. Stayton
Bioengineering

Developmental biology and tissue regeneration processes utilize specific spatial adhesive cues to direct the assembly of cells into complex, organized tissues. Microfabrication methods provide analogous technologies to accurately control the displacement of proteins and cells *in vitro* to mimic their natural spatial organization. Thus, we have investigated how spatially controlled engineering of protein interfaces can be used to direct cellular response and the organized assembly of tissues. Adhesive extracellular matrix proteins were micropatterned directly by microcontact printing onto a number of different substrates and shown to spatially control the attachment of various anchorage dependent mammalian cell types. Specifically, micropatterned lanes of laminin were used to guide the adhesion and organization of cardiomyocytes on polymeric surfaces such that they exhibited a more mature and fully differentiated phenotype. Morphological features of native myocardium, such as the dimensions of individual cardiomyocytes, myofibril assembly and organization, intercalated disk localization and synchronous contractile behavior, were reproduced by micropatterned cultures of cardiomyocytes on polystyrene substrates. The true myocardium, however, is

an organized, heterogeneous tissue composed of various cell types, thus a spatially defined co-culture system was developed, utilizing an engineered streptavidin mutant, to facilitate secondary cell adhesion between patterned rows of cardiomyocytes. Comparable cardiomyocyte patterns were also achieved on thin films of resorbable polymers (i.e. PLGA and biodegradable polyurethane), in order to engineer organized sheets of cardiomyocytes. Dense, highly aligned layers of cardiomyocytes could contract thin elastomeric polyurethane films and were successfully grafted onto the surface of the heart in nude mice. This method represents a novel therapeutic approach to potentially repair infarcted myocardium by transplanting spatially organized layers of cardiac tissue. In addition to tissue engineering applications, patterned cardiomyocyte cultures are also applicable to *in vitro* cell biology and physiological studies or diagnostic applications, such as pharmacological screening, that require more accurate reproduction of native myocardial architecture.

TABLE OF CONTENTS

Page

List of Figures vi

List of Tables xi

Chapter 1: Introduction 1

1.1 Overview 1

1.2 Myocardial infarction and left ventricular remodeling 1

1.3 "Replacement" therapies for myocardial repair 2

1.4 "Regenerative" therapies for myocardial repair 5
- 1.4.1 Cellular cardiomyoplasty 5
- 1.4.2 Cardiac tissue engineering 8
- 1.4.3 Regenerative potential of cardiac muscle 10

1.5 Stem cells for myocardial repair 12
- 1.5.1 Embryonic stem cells 12
- 1.5.2 Adult stem cells 13

1.6 Conclusions 14

Chapter 2: Materials and Methods 15

2.1 Materials 15
- 2.1.1 Proteins 15
- 2.1.2 Antibodies 15
- 2.1.3 Substrates 16

2.2 Methods 16
- 2.2.1 Streptavidin expression and purification 16
- 2.2.2 Microfabrication 18
- 2.2.3 Microcontact printing of proteins 19
- 2.2.4 Fluorescent labeling of proteins 21
- 2.2.5 Biotinylation of proteins 21
- 2.2.6 Cell culture 22
- 2.2.7 Immunostaining 24
- 2.2.5 Microscopy 24
- 2.2.6 Image processing 25

2.3 Tables 27

2.4 Figures 28

Chapter 3: Constrained Cell Recognition Peptides Engineered into Streptavidin 29

3.1 Abstract 29

3.2 Introduction 30

3.3 Methods 31
3.3.1 Construction and production of mutants 31
3.3.2 Protein analysis 32
3.3.3 Cell adhesion 32
3.3.4 Apoptosis assay 34

3.4 Results 35
3.4.1 Characterization of streptavidin mutants 35
3.4.2 Cell adhesion 35
3.4.3 Modulation of cell adhesion 37
3.4.4 Apoptosis assays 38

3.5 Discussion 39

3.6 Figures 43

Chapter 4: Spatially Organized Assembly of Extracellular Matrix Proteins on Surfaces to Direct Cellular Response 55
4.1 Abstract 55

4.2 Introduction 56

4.3 Methods 58
4.3.1 Protein printing methods 58
4.3.2 Cell patterning 59
4.3.3 Surface analysis techniques 59

4.4 Results 59
4.4.1 Properties of matrix protein printing 59
4.4.2 Mechanism of protein printing 61
4.4.3 Protein and cell pattern stability 64
4.4.4 Bioactivity of printed protein patterns 65
4.4.5 Printing onto protein layers 67

4.5 Discussion 70

4.6 Tables 74

4.7 Figures 76

Chapter 5: In vitro Generation of Differentiated Cardiac Myofibers on Micropatterned Laminin Surfaces 88

5.1 Abstract 88

5.2 Introduction 89

5.3 Methods 91
5.3.1 Preparation of micropatterned substrates 91
5.3.2 Cell culture 91
5.3.3 Immunostaining 92
5.3.4 Morphometric analysis 92
5.3.5 Microscopy 93
5.3.6 Quantifying contraction rates 93

5.4 Results 94
5.4.1 Cardiomyocyte patterning 94
5.4.2 Geometric dependence of cardiomyocyte organization 95
5.4.3 Myofibril alignment 97
5.4.4 Formation of intercalated disks 98
5.4.5 Contractile activity 99
5.4.6 Organization on PLGA surfaces 100

5.5 Discussion 101

5.6 Figures 103

Chapter 6: Spatially and Temporally Controlled Generation of Heterotypic Cell Co-cultures 120

6.1 Abstract 120

6.2 Introduction 121

6.3 Methods 124
6.3.1 Co-culture method I: adhesive biotinylated molecules 124
6.3.2 Co-culture method II: RGD-streptavidin 124
6.3.3 Co-culture of cardiomyocytes and endothelial cells 125
6.3.4 Co-culture of smooth muscle and endothelial cells 126

6.4 Results 127
6.4.1 Co-culture with biotinylated adhesive molecules 127
6.4.2 Co-culture with RGD-streptavidin 130

6.5 Discussion 134

6.6 Figures 137

Chapter 7: Spatially Organized Layers of Cardiomyocytes on Biodegradable Polyurethane Films 152

7.1 Abstract 152

7.2 Introduction 153

7.3 Methods 154

7.3.1 Polyurethane synthesis 154
7.3.2 Polyurethane sample preparation 154
7.3.3 Surface analysis of polyurethane films 156
7.3.4 Micropatterning and cell culture 156
7.3.5 Time course experiments 157
7.3.6 Cell Tracker labeling 158
7.3.7 Serial addition of cardiomyocytes 158

7.4 Results 159
7.4.1 Polymer film analysis 159
7.4.2 Protein pattern stability 160
7.4.3 Cardiomyocyte adhesion to polyurethane films 161
7.4.4 Time course of cardiomyocyte patterns on polyurethane 162
7.4.5 Cardiomyocyte patterns on polyurethane versus polystyrene 163
7.4.6 Cardiomyocyte patterns on polyurethane versus glass 164
7.4.7 Serial addition of cardiomyocytes 165
7.4.8 Cardiomyocyte patterning on polyurethane solvent cast sheets 166

7.5 Discussion 167

7.6 Tables 171

7.7 Figures 173

Chapter 8: Cardiac Grafting of Spatially Organized Sheets of Cardiomyocytes on Biodegradable Polyurethane Films 185

8.1 Abstract 185

8.2 Introduction 185

8.3 Methods 187
8.3.1 Preparation of polyurethane films 187
8.3.2 Cardiomyocyte patterning and culture 187
8.3.3 Fibrin coating of polyurethane implants 187
8.3.4 Fibrin gel coating of cardiomyocytes 188
8.3.5 Cardiac grafting surgery 188
8.3.6 Histology 189

8.4 Results 189
8.4.1 Cardiomyocyte cultures on polyurethane films 189
8.4.2 Fibrin gel coating 190
8.4.3 Macroscopic assessment of cardiac grafting 191
8.4.4 Histological examination of implanted polyurethane films 191

8.5 Discussion 193

8.6 Figures 195

Chapter 9: Conclusions and Future Directions 201

9.1 Conclusions 201

9.2 Future Directions 202
9.2.1 Functional analysis of micropatterned cardiomyocytes 202
9.2.2 Cardiac tissue engineering 203
9.2.3 *In vitro* applications of micropatterned cardiomyocyte cultures 204

References 206

LIST OF FIGURES

Figure Number ..... Page

2.1: Schematic representation of microcontact printing of proteins for patterned cell attachment. 28

3.1: Schematic model of the streptavidin tetramer structure and its relative orientation immobilized on a biotinylated surface 43

3.2: Poly-acrlyamide gel electrophoresis of RGD streptavidin mutants. 44

3.3: Mass spectrometry results of RGD streptavidin mutants. 45

3.4: Concentration dependence of FN-SA and OPN-SA mediated endothelial cell adhesion. 46

3.5: Phase contrast images of rat aortic endothelial cell adhesion. 47

3.6: RGD peptide inhibition of FN-SA and OPN-SA mediated endothelial cell adhesion. 48

3.7: Melanoma cell adhesion to polystyrene dishes coated with FN-SA, OPN-SA and wild-type streptavidin. 49

3.8: Melanoma cell adhesion to mixed self-assembled monolayers (SAMs) containing biotin and poly(ethylene glycol) thiols. 50

3.9: Rat aortic endothelial cell adhesion to RGD-SA/WT SA mixtures immobilized on biotinylated-BSA coated substrates. 51

3.10: Rat aortic endothelial cell adhesion to RGD-SA/WT SA mixtures immobilized on biotinylated-BSA coated substrates at lower concentrations of RGD-SA ($\leq$ 10%). 52

3.11: Nuclear staining of serum-starved endothelial cells on adhesive proteins. 53

3.12: Quantitative analysis of apoptotic endothelial cells on adhesive protein coated surfaces. 54

4.1: Printed patterns of extracellular matrix proteins. 76

4.2: Comparison of printed protein patterns with a new and re-used stamp. 77

4.3: Protein printing onto PDMS substrates. 78

4.4: "Criss-cross" patterning of different protein species. 79

4.5: Stability of protein patterns exposed to serum-containing media. 80

4.6: Patterning of mouse myoblasts and myotubes. 81

4.7: Skeletal myoblast differentiation along micropatterned lanes. 82

4.8: Printed patterns of streptavidin retain biotin binding capability. 83

4.9: ECM protein printing onto adsorbed ECM layers. 84

4.10: Square patterns of osteopontin printed onto fibronectin 85

4.11: Endothelial cells patterned on osteopontin squares 86

4.12: Endothelial cell response to printed patterns of thrombospondin-2 (TSP-2) on fibronectin. 86

5.1: Rat neonatal cardiomyocytes cultured on laminin lane patterns 103

5.2: Time course of cardiomyocyte morphology on micropatterned laminin lanes. 104

5.3: Effect of ara-C treatment on cardiomyocyte patterning. 105

5.4: Individual cardiomyocytes cultured on micropatterned laminin lanes 106

5.5: Measurement of projected cardiomyocyte area on micropatterned laminin lanes. 107

5.6: Measurements of cell length and cell width along the major and minor axis, respectively, of spread cardiomyocytes. 108

5.7: Calculated measurements of the aspect ratio of cardiomyocytes on micropatterned laminin lanes. 109

5.8: Calculated measurements of cardiomyocyte alignment with respect to the direction of the micropatterned laminin lanes. 110

5.9: Hoffman contrast images of cultured cardiomyocytes. 111

5.10: Immunofluorescent staining of myosin heavy chain in patterned cardiomyocytes..... 112

5.11: Transmission electron microscopy characterization of myofibril structure and organization of cardiomyocytes. 113

5.12: Immunofluorescent staining for electrical and mechanical components of intercalated disks. 114

5.13: Transmission electron microscopy characterization of intercalated disk formation. 115

5.14: Effects of adhesive matrix proteins and lane width on contraction rates of cardiomyocytes. 116

5.15: Effects of ara-C treatment on contraction rates of cardiomyocytes. 117

5.16: Synchrony of cardiomyocyte contractions in patterned cultures. 118

5.17: Cardiomyocyte patterning on PLGA. 119

6.1: Schematic of co-culture method I: adhesive biotinylated molecules. 137

6.2: Immobilization of biotinylated proteins between laminin lanes. 138

6.3: Immobilization of biotinylated proteins after exposure to serum-free culture media. 139

6.4: Immobilization of biotinylated proteins after exposure to serum-containing culture media. 140

6.5: Cardiomyocyte patterning on BSA and streptavidin (SA) coated surfaces..... 141

6.6: Spatially directed endothelial cell adhesion to immobilized biotinylated-fibronectin between cardiomyocyte patterns..... 142

6.7: Immunostaining of cardiomyocyte/endothelial cell co-culture utilizing biotinylated-fibronectin..... 143

6.8: Schematic of co-culture method II: RGD-streptavidin..... 144

6.9: Immobilization of RGD-streptavidin to biotinylated-BSA between micropatterned cardiomyocytes. 145

6.10: Spatially directed endothelial cell adhesion to immobilized RGD-streptavidin between cardiomyocyte patterns. 146

6.11: Stability of cardiomyocyte patterns 24 hours after the addition of RGD-streptavidin. 147

6.12: Immunostaining of cardiomyocyte/endothelial cell co-culture utilizing RGD-streptavidin. 148

6.13: Immunostaining for connexin 43 in patterned co-cultures of cardiomyocytes and endothelial cells. 149

6.14: Acetylated-LDL labeling of endothelial cells in co-culture with patterned cardiomyocytes. 150

6.15: Micropatterned co-culture of smooth muscle cells and endothelial cells. 151

7.1: ESEM analysis of polyurethane films. 173

7.2: Stability of laminin patterns exposed to serum-containing media. 174

7.3: Cardiomyocyte adhesion to polyurethane spin-cast films. 175

7.4: Immunostaining of patterned cardiomyocytes on polyurethane films. 176

7.5: Immunostaining for N-cadherin in patterned cardiomyocytes on spin-cast polyurethane films. 177

7.6: Time course of cardiomyocyte patterns on polyurethane spin-coated coverslips. 178

7.7: Comparison of cardiomyocyte patterns on polystyrene dishes and polyurethane spin-cast glass coverslips. 179

7.8: Comparison of cardiomyocyte patterns on native glass and polyurethane spin-cast coverslips. 180

7.9: Schematic representation of seeding additional cardiomyocytes onto patterned cardiomyocyte layers. 181

7.10: Seeding additional cells onto patterned cardiomyocyte cultures on spin-cast polyurethane films. 182

7.11: Successive seeding of cells onto patterned cardiomyocyte cultures. 183

7.12: Still frames of patterned cardiomyocytes contracting polyurethane solvent cast film..... 184

8.1: Spatially organized sheets of cardiomyocytes on thin biodegradable polyurethane films..... 195

8.2: Stereoscope images of grafted polyurethane films with patterned cardiomyocytes..... 196

8.3: Histology of polyurethane implants without patterned cells at 1 week..... 197

8.4: Histology of polyurethane implants + patterned cells at 1 week..... 198

8.5: Histology of polyurethane implants without patterned cells at 4 weeks..... 199

8.6: Histology of polyurethane implants + patterned cells at 4 weeks..... 200

LIST OF TABLES

Table Number ..... Page

2.1: Solution concentrations of proteins used to "ink" PDMS stamps. 27

4.1: Proteins patterned via microcontact printing. 74

4.2: Advancing contact angle values for various substrates used for microcontact printing. 75

7.1: ESCA analysis of polyurethane films 171

7.2: Contact angle measurements 172

ACKNOWLEDGEMENTS

I would like to thank my advisor, Professor Patrick S. Stayton, as well as my co-advisors, Dr. Charles E. Murry and Dr. Stephen D. Hauschka, for their constant support, encouragement and guidance. I would also like to acknowledge several faculty members from the Department of Bioengineering, including Dr. Buddy D. Ratner, Dr. Allan S. Hoffman and Dr. Cecilia M. Giachelli, for the invaluable mentoring they provided during my graduate school experience. I am also grateful to Dr. Kimberly A. Woodhouse, from the University of Toronto, for our fruitful collaborations and discussions. I also thank all of my friends and colleagues in Bioengineering, and various other departments at the University of Washington, whom I've had the opportunity and privilege to work with.

DEDICATION

To my wife, Megan, for her infinite love and patience

Chapter 1: Therapeutic Strategies for Myocardial Tissue Repair

1.1 Overview

Ischemic myocardial tissue lacks the inherent capacity for regeneration since cardiomyocytes are terminally differentiated cells incapable of proliferating in response to injury. Organ transplantation or mechanical assist interventions have traditionally served as the primary means to replace or augment impaired cardiac function in heart failure patients, but such therapies can't actually restore myocardial tissue. Advances in regenerative biology have led to innovative therapeutic strategies to potentially repair injured myocardium. Cell-based therapeutics, such as cellular cardiomyoplasty and cardiac tissue engineering, attempt to introduce new contractile cells to infarcted myocardial tissue in order to restore cardiac function. The clinical success of regenerative approaches to heal cardiac muscle is ultimately dependent on the ability to generate new myocytes for tissue repair. Stem cells can differentiate into cardiomyocytes and thus could serve as a unique source of cells to regenerate ventricular myocardium.

1.2 Myocardial Infarction and Left Ventricular Remodeling

Shortly after an episode of acute myocardial infarction, due to occlusion of the coronary artery, the heart muscle cells (cardiomyocytes) within the ischemic ventricular tissue die. Adult cardiomyocytes are terminally differentiated cells thought to be incapable of proliferating in response to injury, therefore the wounded myocardium lacks

the inherent capacity for regeneration. During the course of wound repair, a series of remodeling events occur leading to structural and functional changes in the left ventricle.[1] These include progressive death of cardiomyocytes leading to a thinning of the ventricle wall, as well as re-organization of cell-cell junctions at the border between the infarct and normal myocardium.[2-4] Surviving cardiomyocytes undergo hypertrophy as a response to functionally compensate for the massive loss of working cardiomyocytes due to the ischemic injury.[5] As a result, the wall of the remaining myocardium dilates and the volume of the ventricular cavity increases.[6, 7] Concomitant with the cellular remodeling events in the heart are changes in the extracellular matrix composition of the myocardium, such as increases in collagen deposition and matrix metalloproteinase activity.[8-11] The lack of new cardiomyocytes combined with the alterations in extracellular matrix structure results in significant fibrous tissue deposition that constitutes the formation of a permanent scar. The scar tissue disrupts the normal propagation of mechanical and electrical signals controlling the rhythmic contractions of the heart, leading to complications such as arrythmias.[12] The progression of these structural changes to the ventricle results in an overall depression in cardiac function, evidenced by a reduced ejection fraction and an increase in the diastolic wall stress,[13, 14] and ultimately leads to heart failure and sudden death.

1.3 "Replacement" Therapies for Myocardial Repair

Current treatments for cardiac failure have focused on limiting the extent of myocardial damage after infarction and restoring cardiac output by augmenting or replacing impaired ventricular function. In general, most of these techniques can be

classified as "replacement" therapies since they attempt to substitute some type of mechanical assistance for the normal function of the heart. However, most replacement therapies suffer from a number of limitations that prevent them from becoming a reliable means of permanently treating heart failure patients.

Several drugs are commonly used to treat infarcted myocardial tissue by limiting ventricular remodeling events and preventing infarct expansion. Compounds such as ACE (angiotensin converting enzyme) inhibitors or beta-blockers can attenuate some of the detrimental remodeling events during the course of myocardial tissue repair and thus prevent further deterioration in cardiac function.[15, 16] While these therapies may be beneficial to preserve or protect surviving myocardium, they are not capable of stimulating myocardial repair or directly enhancing cardiac function.

One of the primary means of restoring cardiac function has been to perform whole heart transplantation, yet the paucity of available organs precludes thousands of potential candidates annually from receiving heart transplants. Estimates are that only 2500 hearts are available annually for transplant surgery, while as many as 40,000-100,000 people could benefit from some type of mechanical assistance.[17, 18] The disparity between the supply and demand for heart transplantation continues to grow annually as the number of available organs remains relatively constant, but the number of eligible recipients steadily increases as heart disease becomes more prevalent. Even the fortunate individuals who receive a new heart require immunosuppressive drug therapy for the remainder of their lives to prevent rejection of the organ. Xenotransplantation has been suggested as a means to fulfill the demand for organ transplantation,[19] but various ethical and safety concerns are associated with the transplantation of tissues from non-human species.

Thus, while allograft or xenograft heart transplantation strategies theoretically remain a viable option, the inadequate supply of organs precludes these approaches from being generally applicable to all patients.

Extracorporeal devices, such as ventricular assist devices and total artificial hearts, have been developed to provide mechanical support for failing hearts. While these devices are mechanically capable of augmenting or replacing cardiac output, they suffer from several problems that limit their use primarily to bridge-to-transplant therapies rather than permanent assist devices. Most do not allow the patients to be ambulatory, and infections and thromboembolism are frequently associated with their use, largely due to their lack of biocompatibility.[20, 21] Despite these concerns and early clinical failures, recently a newly designed totally implantable artificial heart has garnered FDA approval and clinical trials have been initiated.[22-24] Nevertheless, artificial mechanical assist devices do not appear to provide an adequate long-term solution for most individuals suffering from cardiac failure.

As an alternative to synthetic cardiac assist devices, a more biological mechanical substitute has also been derived by wrapping the latisummus dorsi muscle around the failing heart. This procedure, referred to as "cardiomyoplasty" is thought to benefit cardiac function because skeletal muscle is mechanically similar to cardiac tissue and thus can contribute to ventricular contraction.[25] This technique has been used clinically for over 15 years and has been demonstrated to delay or prevent heart failure after myocardial infarction.[25, 26] However, the skeletal muscle tissue requires pacing since it has significantly different electrophysiological properties than cardiac tissue and does not functionally integrate with the heart.

Replacement therapies for heart failure provide mechanical assistance necessary to restore cardiac function and can significantly extend the lives of critically ill heart patients. While such remedies can functionally compensate for depressed cardiac output, they fail to treat the infarcted myocardial tissue responsible for the ventricular dysfunction. Novel interventions designed to actively repair ischemic myocardium could prevent the progressive deterioration in cardiac function normally evidenced after myocardial infarction and eliminate the need for replacement therapies.

1.4 "Regenerative" Therapies for Myocardial Repair

Modern medicine is rapidly entering a new age of "regenerative" therapies based upon discoveries in molecular, cell and developmental biology. Cell transplantation, tissue engineering and *in vivo* stimulation of regenerative processes are related strategies to repair wounded or diseased tissues.[27] These cellular-based approaches signify a shift in medical ideology towards the implementation of more biological therapies for tissue repair and regeneration.[28] Thus, regenerative medicine has the potential to significantly reduce the demand for organ transplantations by restoring tissues that normally do not heal properly, such as the heart. Regenerative approaches for myocardial repair are focused on increasing the number of viable cells capable of functionally integrating with the myocardium in order to improve cardiac performance.

1.4.1 Cellular Cardiomyoplasty. Cellular cardiomyoplasty refers to the injection of viable cells into the wounded heart to repair injured myocardium. Most efforts have focused on the grafting of contractile cell types, such as cardiac and skeletal myocytes,

but various other cells have also been attempted, including fibroblasts, smooth muscle cells and stem cells. Recent reviews of cell transplantation into the heart have detailed the current progress in the field and highlighted some of the remaining challenges.[29-34] Since cardiomyocytes are the native working cells of the normal myocardium, this cell type is generally considered the ideal choice to replace ischemic myocardial tissue. Transplanted cardiomyocytes of various origins survive, form stable grafts and can integrate with normal hearts, based upon the appearance of intercalated disks at the border between host and graft cells.[35-38] In models of myocardial infarction, injected cardiomyocytes have been reported to form neo-myocardium at the site of injury, limit scar formation, and form cell junctions between graft and host,[38-41] but the boundaries of the scar tissue may physically inhibit efficient electromechanical coupling between the graft and host tissue.[38] Successful cardiomyocyte engraftment in wounded myocardial tissue appears to contribute to regional and global improvements in left ventricular cardiac function.[39, 42-44] Unfortunately, the clinical potential of cardiomyocyte grafting is presently limited by the current lack of an appropriate cell source.

Skeletal myocytes are physically similar to cardiomyocytes in a number of ways, but in contrast to the myocardium, skeletal muscle possesses regenerative capacity due to resident satellite cells, which can be easily expanded in culture. Thus skeletal myoblasts are a potential autologous cell source for myocardial repair. Grafted skeletal myoblasts differentiate into mature myotubes in normal and injured cardiac tissue, forming new muscle capable of contractile activity.[45, 46] Although skeletal muscle grafts can convert to a slow twitch fiber phenotype, characteristic of cardiac muscle, the grafts fail to make electromechanical connections with the host tissue.[45-47] Skeletal myotubes can

electrically couple with cardiomyocytes *in vitro*, but generally this is not observed *in vivo*, presumably due to a marked decrease in connexin expression after differentiation.[48] Skeletal muscle grafts are thought to improve cardiac performance because they are mechanically suited for contraction and therefore, myoblast grafts may improve the compliance and diastolic properties of wounded myocardium, as well as attenuate left ventricular remodeling.[49-52] These encouraging results in several animal models have prompted clinical trials of injecting autologous skeletal myoblasts into infarcted myocardium in combination with coronary bypass surgery.[53, 54]

One general conclusion from the myocyte transplantation studies reported to date is that regardless of the particular cell source, cell transplantation into the injured heart may serve to enhance cardiac function. However, it remains largely unclear if the cells grafted into the heart actively contribute to cardiac performance or passively populate the infarcted tissue and inhibit the normal progression of myocardial scar formation following cardiac injury. While contractile and non-contractile cells appear to improve diastolic parameters, contractility and systolic function have reportedly only been improved with contractile cell types, such as cardiac and skeletal myocytes.[55, 56] Morphological characterization studies have demonstrated the functional integration of grafted cells with the host tissue, but there has been no direct evidence that grafted cells contract *in vivo*, either independently or in synchrony with the heart.

Although no grafted cell type has appeared to have a deleterious affect on the host cardiac function or physiology, it remains unclear how different cell types specifically alter ventricular remodeling. One difficulty in interpreting the success of cardiac cell grafting is that the cells may secrete factors or promote secondary events (i.e.

angiogenesis) that can result in observed improvements in cardiac performance, although the cells are not directly contributing to contractile function.

In addition, more recent reports have attempted to address the need for more quantitative studies of engraftment efficiency and graft cell survival.[57] Cellular cardiomyoplasty is performed by injecting suspensions of cells directly into the wall of the heart. Although millions of cells may be initially injected, only a few thousand cells may stably comprise a graft. The role of grafted cells in myocardial repair could be more clearly elucidated by more quantitative studies to correlate morphological attributes with functional assays of grafted cell performance.

1.4.2 Cardiac Tissue Engineering. Cardiac tissue engineering attempts to assemble heart cells into viable and functional tissue constructs for myocardial tissue repair. Thus, organized cardiac tissue constructs could serve as a more efficient and stable means of grafting cells than cell injection methods to form tissue *in vivo*. Engineered tissue constructs can also serve a secondary purpose as *in vitro* models of myocardial tissue.

Cardiomyocytes have been cultured on synthetic biodegradable scaffolds as one approach to cardiac tissue engineering. Cardiomyocytes cultivated on poly-glycolic acid meshes exhibited spontaneous contractile activity in three-dimensional culture and similar structural and functional properties to that of native tissue.[58, 59] These constructs could support macroscopic impulse propagation when electrically stimulated and have been used as *in vitro* models for electrophysiological experiments.[60] Optimization of culture conditions improved the cellularity of the scaffolds, with cardiomyocytes

populating the periphery of the scaffold (120-160 μm thick), but these constructs remained less cellular than normal tissue.[61]

Cardiac tissue engineering constructs have also been developed by incorporating cardiomyocytes into natural gels. Cardiomyocytes have been cultured on or in three-dimensional collagen gels as *in vitro* models of heart tissue.[62-65] Alignment of cardiomyocytes and hypertrophy were induced by stretching collagen gels containing cardiomyocytes.[66] Similarly, fetal cardiomyocytes have been seeded into a biodegradable gelatin mesh and successfully implanted in either myocardial scar tissue or the right ventricular outflow tract of rats.[67, 68] Although the cells within the graft were reported to survive, the cellularized matrices did not appear to morphologically resemble the structure of native myocardial tissue or improve ventricular function.[67, 69] Cardiomyocytes have also been seeded onto a porous alginate scaffold and transplanted into the infarcted myocardium of rats.[70] Despite a relatively low number of cells seeded into the alginate scaffolds, the grafts integrated with the scar tissue and appeared to attenuate post-infarct remodeling events and a deterioration in ventricular function.

One alternative approach to using a scaffold is to create individual layers of myocardial cells, which could be assembled to form a three-dimensional cardiac tissue construct. Cultured sheets of cardiomyocytes were detached intact from thermally sensitive polymer-coated petri dishes by temporarily lowering the temperature of the substrate.[71] The detached cardiomyocyte sheets exhibited an increase in the amplitude of contraction, but the cellular films had to be supported by a membrane since they lacked structural integrity.

Cardiac tissue engineering shares several of the same challenges facing cardiomyoplasty, but also poses some unique problems that need to be resolved. Although most of these constructs incorporate heart cells, it's not clear that the engineered tissues resemble or function similarly to the native myocardium. Most of these engineered tissues containing cardiomyocytes are contractile and electrically coupled to one another, but morphological and histological analysis indicate that such constructs do not appear to be organized similarly to native myocardial tissue. The native myocardium is a complex, heterogeneous tissue composed of different cell types arranged in a spatially distinct fashion. Since the structural organization of cardiac tissue is inherently related to its function, improved methods are required to integrate spatial control into the assembly of the engineered tissue construct.

Another problem common to the engineering of most three-dimensional tissues is supplying sufficient vascularization to keep cells alive within the tissue. Due to the limits of diffusion, only cells within about 100 μm of the surface can survive in avascular tissues. The native myocardium is very metabolically active and thus highly vascularized in order to provide adequate delivery of oxygen and nutrients, as well as removal of waste by-products. Until new methods can be developed to vascularize engineered tissues either *in vitro* or *in vivo*, the size and thickness of functional constructs will be severely limited.

1.4.3 Regenerative Potential of Cardiac Muscle. New insights from cell biology and cardiac wound healing have also led to a re-examination of the potential for cardiac muscle to be regenerated *in vivo*. Recent controversial reports suggest that mammalian

heart muscle may possess a limited number of cardiomyocytes that actively proliferate and that this percentage of cardiomyocytes increases following a myocardial infarct.[72-74] This data seemingly refutes the wealth of evidence supporting the dogma that mature cardiomyocytes are post-mitotic cells incapable of cell division.[75, 76] Even if a small percentage or some sub-population of adult cardiomyocytes remain mitotically active, it still remains to be determined if a clinically significant mass of cardiomyocyte growth could be stimulated to repair a myocardial infarct. Perhaps even more perplexing and critical, though, is identifying what inhibitory cues are present in the injured or normal cardiac environment that would then preclude such cells from normally repairing injured myocardial tissue.

Certain animal models of wound healing indicate that myocardial tissue may have some capacity for regeneration. In contrast to most mammals, amphibians possess an amazing potential to regenerate wounded tissues, including ventricular myocardium.[77] The MRL strain of mice exhibit a similar capacity for tissue regeneration following injury without forming scar tissue.[78] In a recent study, MRL mice were reported to regenerate normal cardiac muscle after being subjected to a cryoablative injury of the right ventricle.[79] Genetic analysis of these species may lead to the identification of molecular factors and pathways that actively participate in ventricular healing and stimulate the growth of new cardiomyocytes. Such information could lead to the development of novel molecular therapeutic interventions to promote myocardial repair.

1.5 Stem Cells for Myocardial Repair

The current limitation impeding most regenerative therapies for myocardial repair is the inability to generate new cardiomyocytes. Stem cells are uniquely poised to serve as a viable source for cardiomyocytes because they are undifferentiated cells capable of self-renewal and have the potential to differentiate into various cell types, including cardiac myocytes. Several lines of investigation have demonstrated that cardiomyocytes can be derived from both embryonic and adult stem cells, thus stem cell technologies may one day provide a reproducible source of cardiomyocytes for myocardial repair.

1.5.1 Embryonic Stem Cells. Embryonic stem (ES) cells are pluripotent progenitors capable of differentiating into cell types from all three germ layers. Murine ES cell lines have been cultured for a number of years and methods have been developed to generate cardiomyocytes *in vitro* from mouse ES cells.[80-82] Purified populations of cardiomyocytes genetically selected from mouse ES cell cultures have been injected into the hearts of mice and form stable grafts.[83] Human ES cell lines have recently been established[84, 85] and cardiomyocytes derived from human ES cell lines exhibit normal structural and functional characteristics.[86] Although human embryonic stem cells have a tremendous therapeutic potential to generate cardiomyocytes and other cell types, the derivation of cells from embryos raises several ethical concerns. The ability to direct cell differentiation along specific lineages and obtain purified cell populations from ES cells also poses a significant technical challenge.

1.5.2 Adult Stem Cells. Adult stem cells, such as those residing in the bone marrow, are also pluripotent cells, but are thought to have a more restricted potential than embryonic cells. Based on a series of recent reports, though, it appears that bone marrow cells can differentiate into cardiomyocytes. In general, *in vitro* methods to induce cardiomyocyte differentiation from bone marrow stem cells have been limited. However in one report, marrow stromal cells cultured in the presence of 5-azacytidine contracted spontaneously and expressed molecular markers of cardiomyocytes.[87] Other recent reports also suggest that stem cells from the bone marrow can engraft the heart and differentiate into cardiomyocytes *in vivo*. In one case, human bone marrow cells were injected into sheep fetuses *in utero* and later identified in cardiac muscle tissue following the development of the organism.[88] Bone marrow cells were also injected into infarcted myocardium and reported to varying extents to differentiate into cardiomyocytes.[89-92]

Bone marrow stem cells were also found to be recruited and differentiate into cardiomyocytes in the heart following myocardial injury in mice.[93-95] Although in one instance the normal level of engraftment by bone-marrow derived cardiomyocytes was very low,[94] another report suggests that mobilization of bone marrow cells with cytokine treatment resulted in a significant number of new cardiomyocytes at the site of injury.[95] While these encouraging results suggest a potentially non-invasive method for self-renewal of myocardial tissue, it remains unclear whether a sufficient quantity of bone marrow-derived cardiomyocytes can be recruited to regenerate a functional mass of cardiac tissue. It is also not apparent what molecular signals recruit bone marrow cells to the heart specifically at the site of injury.

Collectively, these studies suggest two periods of tissue plasticity, development and wound healing, which might allow bone-marrow cells to integrate and differentiate into cardiac muscle. While it appears that some cells from the bone marrow can differentiate into cardiomyocytes, it has not been established if all bone marrow cells possess this potential or if it is restricted to some sub-population of cells. These studies also suggest that the molecular cues present in the microenvironment of the heart can direct tissue-specific differentiation of less differentiated cell types into cardiac muscle cells.

1.6 Conclusions

Traditionally, replacement therapies for myocardial infarction have failed to actively treat the ischemic ventricular myocardium. Now with the advent of regenerative medicine, new cellular-based approaches have the potential to restore and repair injured myocardial tissue. An improved comprehension of cardiac wound healing biology and advances in stem cell technologies are integral to the success of regenerative methods to introduce new cardiomyocytes into wounded myocardium. Regenerative therapies thus have the potential to revolutionize cardiovascular medicine by actually healing damaged heart muscle.

Chapter 2: Materials and Methods

2.1 Materials

2.1.1 Proteins. Bovine plasma fibronectin was purchased from Gibco BRL and Sigma, human plasma fibronectin was obtained from Gibco BRL, mouse laminin (derived from basement membrane of Engelbreth-Holm-Swarm mouse sarcoma) and rat tail type I collagen were obtained from Becton Dickinson. Bovine dermal collagen (>95% type I, remainder type III, Vitrogen) was purchased from Collagen Corporation and endothelin-1 (ET-1) and bovine serum albumin (BSA) were obtained from Sigma. Recombinant rat osteopontin was expressed in a bacterial system and purified by nickel chromatography, as previously described.[96] Thrombospondin-2 was kindly provided by Kurt Hankenson from Dr. Paul Bornstein's laboratory.

2.1.2 Antibodies. Primary antibodies were used to detect the following extracellular matrix proteins: collagen I (rabbit anti-rat, 1:100, Biodesign International), fibronectin (rabbit anti-human, 1;400, Sigma), laminin (rabbit anti-mouse, 1:500, Sigma), osteopontin (OP199, goat anti-rat, 1:1000 Giachelli lab); endothelin-1 (monoclonal, 1:200, Sigma). In addition, primary antibodies were used to identify several cellular proteins including, connexin43 (monoclonal, 1:200, Chemicon), pan-cadherin (monoclonal, 1:200, Sigma), and sarcomeric myosin heavy chain (MF20, 1:20, Hauschka lab). A number of secondary fluorescently labeled antibodies were used including: anti-mouse IgG-FITC and -TRITC (rabbit, 1:20, DAKO), anti-goat IgG-FITC (mouse, 1:100,

Pierce), anti-mouse IgG-FITC (sheep, 1:50, Sigma), and anti-rabbit IgG-TRITC (goat, 1:50-1:80, Sigma).

2.1.3 Substrates. Non-tissue culture polystyrene dishes (35 and 60 mm) were purchased from Falcon and glass slides and glass coverslips were obtained from VWR. Multi-well chamber slides (glass and plastic) were purchased from Nunc.

2.2 Methods

2.2.1 Streptavidin Expression and Purification. Wild type streptavidin and engineered streptavidin mutants were expressed and purified as previously described.[97, 98] BL21 (DE3) cells were transfected with the pET-21a plasmid containing the streptavidin gene and cultured in LB media overnight at 37°C on a shaker at 225 rpm. The cell cultures were used to inoculate flasks of 2x YT medium containing ampicillin (100μg/ml); typically 10 ml of cells per liter of medium was used for inoculation. The cultures were incubated at 37°C on a shaker at 225 rpm until the OD_{600} was between 0.6 and 1.0, and then 0.2 mM isopropyl β-D-thiogalactoside was added to induce protein expression. The cells were cultured an additional 3-4 hours after induction and then centrifuged at 9000 rpm for 20 minutes to harvest the cells. Cell pellets were lysed with lysis buffer (50 mM Tris, 200 mM NaCl, 5 mM EDTA, 8% sucrose, 1 mM PMSF, 1% Triton X-100, pH 8.0) and subjected to at least 3 cycles of sonication/centrifugation to extract the insoluble inclusion bodies containing the expressed protein. The cells were sonicated on ice for 2-3 minutes at full power with a 40% duty cycle and centrifuged at 15,000 rpm for 15 minutes at each cycle. The inclusion bodies were resuspended in the wash buffer (50

mM Tris, 200 mM NaCl, 5 mM EDTA, 8% sucrose, pH 8.0) and subjected to a minimum of 3 cycles of sonication/centrifugation, as described above for cell lysis. Prior to refolding, the isolated inclusion bodies were redissolved in 6 M guanidine hydrochloride and 50 mM Tris, pH 7.5.

The resolubilized protein solution (10 ml, ~ 10 mg/ml) was added dropwise into a 2 L flask of chilled, circulating refolding buffer (50 mM Tris, 100mM NaCl, 5mM EDTA, 0.1mM PMSF) and stirred continuously overnight at 4°C. The diluted protein solution was centrifuged at 9000 rpm for 30 minutes and concentrated to less than 50 ml with an ultrafiltration cell (Amicon). In some cases, the protein solution was filtered with a YM-30 membrane to remove insoluble particulates prior to purification.

The concentrated protein was purified by affinity chromatography with an iminobiotin column (Pierce). The protein solution was centrifuged at 15,000 rpm for 15 minutes prior to loading onto the column to remove insoluble aggregates or particulate matter. The column was equilibrated with binding buffer (50 mM Na_2CO_3, 500 mM NaCl, pH 11.0) and a 5x solution of the binding buffer was added to the concentrated protein solution to equilibrate the pH. The protein was loaded onto the column under gravitational force and washed repeatedly with the binding buffer while immobilized to the column. The protein was eluted from the column with 0.1 M acetic acid and spectrophotometric readings (OD_{280}) were used to determine the collected fractions that contained protein. The protein solution was exchanged into either Tris or phosphate buffered saline and concentrated to > 2 mg/ml with an ultrafiltration cell. Protein aliquots were stored at –80°C for long term storage and –20°C for shorter term storage.

2.2.2 Microfabrication. Micropatterned photoresist features were defined on 3 or 4 inch silicon wafers (Silicon Sense) by standard photolithographic processes in a class 1000 clean room. Hexamethyldisilizane (HMDS) was applied to clean silicon wafers in a vapor priming oven (YES-5) at 10 Torr and 125°C to promote photoresist adhesion. A thin layer of positive photoresist (AZ1512, Clariant Corporation) was spin-coated onto the silicon surfaces at 3000 rpm for 30 seconds, resulting in a photoresist thickness of approximately 1.5 μm. After spin-coating, the wafers were heated at 90°C for 5 minutes before being exposed to UV light through a chromium-plated photomask for 15 seconds with a contact aligner (Kaspar-Quintel 2001). A photomask with linear patterns 5-45 μm wide and spacing distances 10-80 μm apart was purchased from Photosciences. Chrome-plated photomasks with micropatterns of lines and squares were also borrowed from Reto Luginbuhl, Andreas Goessl and Sho Fuji. The wafers were developed in AZ351 developing solution (diluted 1:4 in deionized water) for 60 seconds, gently rinsed with diH_2O and blown dry with an air gun. Patterned wafers were post-baked at 120°C for one hour and silanized ((Tridecafluoro-1,1,2,2-tetrahydrooctyl)-1-trichlorosilane, United Chemical Technologies, Bristol, PA) by vapor treatment under vacuum for 30 minutes at room temperature. Alternatively, thicker photoresist layers were produced with AZ4620 photoresist (~10μm, Clariant Corporation) and required comparable photolithographic processing steps. Patterned silicon wafers, prepared in this manner, were reliably produced with lateral surface features ranging in size from 2-80 μm.

Elastomeric stamps of polydimethylsiloxane (PDMS) were created by casting the polymer against the micropatterned silicon wafers. A 10:1 (W:W) ratio of PDMS and curing agent (Sylgard 184, 1.1 lb kit, Dow), per the manufacturer's recommendation,

were thoroughly mixed together and poured onto the patterned surface of the silicon wafer lying face up in an appropriate size polystyrene petri dish (either 100 or 150 mm) or large polypropylene weigh boat. A sufficient volume of PDMS was added to produce stamps that were about 0.5-1.0 cm thick, allowing them to be easily manipulated by hand. To remove entrapped air bubbles from the viscous polymer solution, the PDMS was degassed under house vacuum within a desiccator prior to curing. The chamber was evacuated multiple times until no bubbles remained at the interface between the silicon wafer and the PDMS. The stamps were cured overnight at 65°C in an oven and the hardened PDMS was then peeled away from the silicon wafer. The polymer was sectioned with a scalpel into smaller blocks containing the different pattern dimensions (based on the original design of the chrome mask) and stored in a petri dish under ambient conditions. Stamps could be stored for several months and individual stamps for protein printing were cut from the larger blocks immediately prior to use (usually 1-2 cm^2). Scotch tape was briefly applied to the patterned surface of PDMS stamps to remove lint and other debris. In some instances, PDMS stamps were treated with an oxygen plasma treatment by a reactive ion etcher (Trion PHANTOM). The "oxidized" PDMS stamps were subjected to 100 watts of RF power for 30-60 seconds in the presence of O_2.

2.2.3 Microcontact Printing of Proteins. Protein micropatterning via microcontact printing was performed similarly to methods previously described.[99-104] A schematic of the microcontact printing of proteins is depicted in Figure 2.1.

For cell culture experiments, the PDMS stamps were sterilized by exposure to UV light for a minimum of 15 minutes. Subsequently, only sterile buffer solutions and reagents were used to prepare the micropatterned surfaces.

In some instances, the substrates to be patterned were pre-coated with a protein solution, most often with 1% bovine serum albumin (BSA, Sigma) in PBS. The protein solution was prepared and incubated on the surface either overnight at 4°C or at room temperature for 1-4 hours before printing. Protein-coated substrates were rinsed with PBS and diH_2O and dried with nitrogen gas immediately prior to printing with the PDMS stamp.

"Inking" solutions of protein were freshly diluted from concentrated stock solutions before adsorbing onto the PDMS stamp. The protein concentrations for adsorption usually ranged between 5-100 μg/ml, corresponding to values reported to provide a monolayer of adsorbed protein (Table 2.1). Protein solutions (with the exception of collagen I) were diluted in phosphate buffered saline (PBS, pH 7.4) and incubated on the patterned surface of the stamp for 30-45 minutes at room temperature. Collagen I solutions (monomeric) were diluted in 0.02 N acetic acid before adsorbing to the stamp. The protein-coated stamp was then rinsed with PBS and diH_2O and dried under a light nitrogen stream before being brought into conformal contact with a clean, dry surface for 2-10 minutes under its own gravitational weight. Additional force was not applied except briefly to the back of the stamp in order to promote rapid sealing of the stamp to the surface. Proper sealing between the PDMS and the substrate appeared necessary for efficient transfer of the protein patterns. After removal of the stamp, the patterned samples were re-solvated with PBS until further use.

2.2.4 Fluorescent Labeling of Proteins. All of the fluorescent labeling reagents were purchased from Molecular Probes. A number of different proteins, including fibronectin, laminin, BSA, and streptavidin were conjugated to fluorescent probes for various studies. Lyophilized proteins (i.e. fibronectin and BSA) were solubilized in 0.1 M sodium bicarbonate, pH 8.3 at a concentration of between 1-10 mg/ml. Solubilized proteins (i.e. laminin and streptavidin) were labeled in the PBS buffer in which they were already dissolved at a concentration of 1-5 mg/ml. The succinimidyl ester amine-reactive probe, either tetramethylrhodamine or Oregon Green 488 (Molecular Probes), was dissolved in 50-100 µl of DMF at a concentration of 10 mg/ml. The fluorescent probe and protein solutions were combined, covered with foil and incubated at room temperature for 1-2 hours on a rotator. The conjugated protein was separated from the unreacted dye by size-exclusion chromatography over a PD-10 column (Pharmacia Biotech) equilibrated with PBS, pH 7.4. Eluted fractions containing labeled protein were detected by spectrophotometric readings (OD_{280nm}) and pooled together. The labeled protein was aliquoted and stored at -20°C until further use.

2.2.5 Biotinylation of Proteins. The protein to be biotinylated (either BSA or fibronectin) was reconstituted in PBS, pH 7.4 at a concentration of 10mg/ml or 2mg/ml, respectively. Sulfo-NHS-LC-biotin was added either directly to the protein solution or first solubilized in distilled, deionized water at a concentration of 2 mg/ml and then added. The amount of the biotinylation reagent added to the protein solution varied depending on the desired labeling ratio (~10-15 molar excess for BSA, ~35 molar excess

for fibronectin). The reaction was allowed to proceed for 60 minutes at room temperature on a rotator. The unconjugated biotin was separated from the biotinylated protein by size exclusion chromatography by passing the protein/biotin reaction solution over a PD-10 column equilibrated with either sterile PBS, pH 7.4 or 0.1 M sodium bicarbonate, pH 8.3 (for subsequent fluorescent labeling). Protein-containing fractions were pooled (OD_{280nm}) and the final protein concentration was determined based upon the extinction coefficient for BSA or the BCA assay (Pierce). The average degree of biotinylation was estimated by performing the HABA assay in order to calculate the approximate labeling ratio (mole biotin:mole protein). Protein aliquots were stored at -20°C until use.

2.2.6 Cell Culture. Various primary cell types and cell lines were used for micropatterning experiments. Unless otherwise noted, all cell culture reagents were purchased from Gibco BRL and the cells were maintained in a humidified incubator at 37°C, 5% CO_2. Cultured cells were routinely passaged by rinsing with either PBS or Versene and enzymatically dissociated with trypsin-EDTA (0.25% trypsin, 1mM EDTA).

Cardiomyocytes were freshly isolated from the ventricles of 1-2 day old Fischer rat pups and cultured as previously described.[38, 105] Briefly, the ventricles were trimmed from the heart, digested with collagenase type II and the resulting single cell suspension was subjected to a series of pre-plating steps to enrich for the population of myocytes (typically 90-95% of the cells). After isolation, the cells were plated onto the culture substrates and allowed to attach overnight (15-17 hours). Culture media consisted of a 3:1 mixture of DMEM and M199 (Sigma) supplemented with 10% horse serum, 5% fetal

bovine serum, L-glutamine, HEPES (17mM) and penicillin-streptomycin. The cultures were rinsed with phosphate buffered saline (PBS, pH 7.4) to remove non-adherent cells, and re-fed with fresh culture media every 2-3 days thereafter. The culture media was often supplemented with 1 μM cytosine arabinofuranoside (ara-C, Sigma) to inhibit the proliferation of non-myocytes (i.e. cardiac fibroblasts) contaminating the culture.

Rat aortic endothelial cells (RAECs) were kindly provided by Dr. Cecilia Giachelli and cultured between passages 16-25 in MCDB131 media supplemented with 10% fetal bovine serum (Hyclone Laboratories), 2 mM L-glutamine, and 10 U/ml penicillin-streptomycin. RAEC cultures were trypsinized and passaged prior to reaching confluence (~90%) in an attempt to maintain the cells in logarithmic growth phase.

Rat smooth muscle cells (WKY3M) were obtained from Dr. Cecilia Giachelli and cultured between passages 12-18 in Waymouth's media supplemented with 10% calf serum and 10 U/ml penicillin-streptomycin.

Mouse NIH 3T3 fibroblasts were obtained from Chuck Cheung and cultured in DMEM media supplemented with 10% fetal bovine serum and 10 U/ml penicillin-streptomycin.

MM14s, a mouse myoblast cell line, were cultured by Steve Hauschka and John Angello. The myoblast growth media consisted of Ham's F10C culture media supplemented with 15% horse serum, 1% antibiotic solution (penicillin & streptomycin) and 2ng/ml basic fibroblast growth factor. The myoblast differentiation media consisted of F10C media with 1.5% horse serum, antibiotics and 1μM insulin.

2.2.7 Immunostaining. Cell cultures were typically fixed with a 2-4% solution of paraformaldehyde in PBS at room temperature for a minimum of 20-30 minutes. Cardiomyocyte cultures were fixed for 2-3 minutes beforehand with 3% paraformaldehyde (PFA) in PBS, pH 7.4, 5 mM EGTA, 0.2% Triton X-100 at room temperature. Fixed samples were stored in PBS at 4°C until staining was performed. The fixed cells (besides cardiomyocytes) were normally permeabilized with a solution of 0.05% Triton X-100 in PBS. The samples were blocked with either a 0.1% solution of BSA or a 2% solution of the appropriate serum of the secondary antibody host species (i.e. rabbit) in PBS for at least 1 hour at room temperature or overnight at 4°C. All subsequent antibody solutions were diluted in the same blocking buffer. Primary antibodies were incubated for 60-120 minutes at room temperature, followed by a secondary antibody at room temperature for 60-90 minutes or overnight at 4°C. Counterstaining of the cells was performed either after antibody staining or immediately after fixation if no antibody staining was used. The cells were counterstained with BODIPY phalloidin 558/568 (1:20 or 1:100, Molecular Probes) to detect actin filaments and DAPI (1:500, Sigma) to visualize cell nuclei. Finally, immunofluorescent samples were mounted with Vectashield media (Vector), coverslipped and stored in the dark at 4°C prior to microscopy.

2.2.8 Microscopy. Fluorescent images were captured with a Nikon Eclipse E800 upright microscope equipped with either a Photometrix SenSys or Coolsnap digital camera (Roper Industries). Phase contrast imaging of live cultures was performed using a Nikon Eclipse TE200 inverted microscope within a plexiglass enclosure heated to 37°C; still

images were captured by a Hamamatsu ORCA II (model C4742-98) digital camera and real-time video microscopy was recorded using a Hamamatsu C2400 CCD camera. Phase and fluorescent images were also acquired by a Spot RT color digital camera (Diagnostic Instruments) mounted to a Nikon Eclipse TE300 inverted microscope. Stereoscope images were captured with a Nikon Coolpix 990 digital camera using a Nikon SMZ 1500 microscope. Time-lapse microscopy was performed with a Nikon Diaphot microscope equipped with a video camera (Series 65, Dage-MTI, Inc.) and a time-lapse recorder (Model TLC 2015R, GYYR Products). Time-lapse cultures on 35 mm plates were enclosed in a T25 flask and gassed with 5% CO_2 to equilibrate the atmosphere.

2.2.9 Image Processing. Digital images were rendered in Adobe Photoshop for aesthetic purposes. Images were typically "sharpened" using a software algorithm, the intensity of the levels was optimized, and fluorescent grayscale images were typically pseudo-colored to reflect their appearance under the appropriate filter settings (i.e. DAPI = blue). Multiple images of the same field acquired under either different light (phase or fluorescence) or filter settings (DAPI, FITC, or rhodamine) were overlaid to form composite images and determine co-localization events.

NIH Image analysis software was used to quantify relative fluorescent intensity levels and acquire two-dimensional measurements. Imported grayscale images were calibrated to the appropriate size scale. Plot profiles were used to determine the signal-to-noise ratio of fluorescent protein patterns. Various spatial parameters including

perimeter, area, length of the major and minor elliptical axis, and angle of the major axis were acquired by tracing objects of interest (i.e. cells).

Real time and time-lapse video data were recorded onto VHS tape and transferred to digital format and edited with Adobe Premiere software. Individual frames were captured from the digitized video.

2.3 Tables

Table 2.1. Solution concentrations of proteins used to "ink" PDMS stamps. The stamps were incubated with the listed concentrations of protein solutions to adsorb at least a monolayer of protein onto the PDMS surface.

Protein	Solution Concentration (μg/ml)
Collagen I	50, 100
Fibronectin	25
Laminin	30, 45
Osteopontin	5, 10
Gelatin	67
Endothelin-1	0.1, 1, 10
Streptavidin	50, 100
Bovine serum albumin	50, 100

2.4 Figures

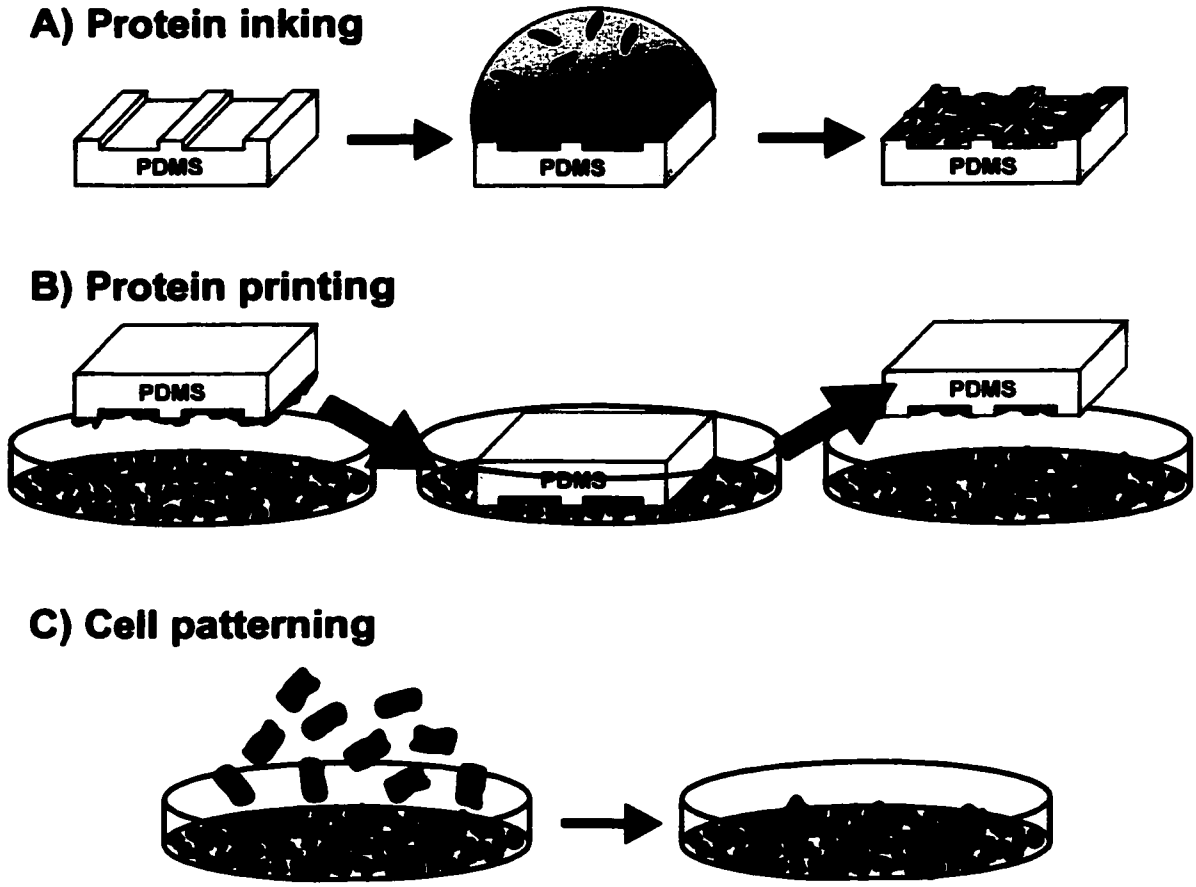

Figure 2.1. Schematic representation of microcontact printing of proteins for patterned cell attachment. A) The microfabricated PDMS stamps were "inked" by adsorbing a layer of protein from solution onto the surface and the stamps were then rinsed and briefly dried. B) The dried stamps were brought into contact with the substrates to be patterned and removed after several minutes, thus depositing protein only in the regions of contact between the stamp and the substrate. In many cases, the substrates were initially pre-coated with a layer of protein prior to printing. C) Cell suspensions were seeded onto the micropatterned surfaces and the cells specifically attached and organized along the adhesive patterned regions.

Chapter 3: Constrained Cell Recognition Peptides Engineered Into Streptavidin

3.1 Abstract

Streptavidin is widely used as an adapter molecule in diagnostics, separations, and laboratory assay applications. We have engineered cell adhesive peptides into the three-dimensional scaffolding of streptavidin that convert streptavidin into a biofunctional protein, while maintaining the biotin binding properties of the protein. The mutations did not alter refolding or tetramer assembly and the native binding affinity of wild-type streptavidin was retained as determined by off-rate measurements. The peptide targets were hexapeptide sequences derived from osteopontin and fibronectin that contain the RGD cell adhesion sequence. Adhesion assays directly demonstrated that rat aortic endothelial cells and human melanoma cells overexpressing the $\alpha_v\beta_3$ integrin adhered to surfaces coated with either of the two RGD streptavidin mutants in a dose dependent fashion, although wild-type streptavidin displayed no significant cell binding activity. Inhibition studies with soluble RGD peptides confirmed that the cell adhesion was RGD mediated. Further inhibition studies with antibodies directed against $\alpha_v\beta_3$ demonstrated that the RGD streptavidin interaction appeared to be integrin specific. These results demonstrate that peptide recognition sequences can be engineered into accessible surface regions of streptavidin without disrupting its biotin binding properties. This approach to introducing secondary functional activities into streptavidin may improve streptavidin's utility in existing applications or provide new technology opportunities.

3.2 Introduction

Streptavidin is a commonly used molecular adaptor in many diagnostic, affinity separations, and drug targeting applications. Its utility arises from the unique biotin binding properties of the four binding sites ($K_a = 10^{13\text{-}15}\ M^{-1}$) and their dyad symmetry that creates oppositely aligned surfaces for binding biotinylated molecules or coatings. The engineering of streptavidin has provided new opportunities to tailor the protein for new or improved technologies. Streptavidin fusion proteins with a variety of proteins such as protein A, metallothionein, single chain antibodies, luciferase, and green fluorescent protein have been created in *E. coli* and baculovirus expression systems.[106-110] These fusion proteins are intended to improve diagnostic and therapeutic biotechnologies which require simultaneous, specific conjugation of multiple proteins or moieties through dual ligand affinities.

We have investigated a complementary approach toward re-engineering streptavidin to contain second functional domains. Specifically we were interested in engineering functional peptide sequences into the streptavidin three-dimensional scaffolding at defined surface locations. We have utilized the Arg-Gly-Asp (RGD) cell adhesive sequence as an initial target, but the peptide sequences could represent a large number of functional activities. This particular motif is a well-characterized peptide sequence responsible for integrin-mediated cell adhesion that is found in fibronectin and many other extracellular matrix and matricellular proteins. Proteins without a native RGD domain have previously been genetically engineered to incorporate an RGD site that confers cell adhesive properties.[111-118] Here we report the design of two streptavidin

mutants that incorporate the RGD sequence and flanking residues from fibronectin (FN-SA) and osteopontin (OPN-SA) (Figure 3.1). These RGD streptavidin mutants are bi-functional proteins that retain wild-type biotin affinity, yet also mediate cell adhesion in an RGD dependent manner. Streptavidin itself may thus be used as both an adaptor and a biological effector, which may provide opportunities for improving diagnostics, separations, and drug targeting applications.

3.3 Methods

3.3.1 Construction and Production of Mutants. 60mer oligonucleotides were initially purchased from Integrated DNA Technologies (IDT) and 5' phosphorylated with T4 kinase (Gibco BRL). The FN-SA cassette was obtained by annealing the following complementary strands: 5' CTAGGTACGTTCTGACCGGTCGTTACGACTCCGCTC-CGGGTCGTGGTGACTCCCCGGGTT 3' and 5' CCGGAACCCGGGGAGTCACCA-CGACCCGGAGCGGAGTCGTAACGACCGGTCAGAACGTAC 3'. The OPN-SA cassette was constructed with the following strands: 5' CTAGGTACGTTCTGACCGG-TCGTTACGACTCCGCTCCGGGTCGTGGTGACTCCGTTGGTT 3' and 5' CCGGA-ACCAACGGAGTCACCACGACCCGGAGCGGAGTCGTAACGACCGGTCAGAAC GTAC 3'. The previously described streptavidin construct in pUC18 was digested with restriction enzymes XbaI and BspEI (New England Biolabs) to create complementary ends for the annealed cassettes, which were subsequently ligated into the plasmid DNA.[97] The ligation products were transformed into NovaBlue competent cells (Novagen). The 60mer oligos contained a single nucleotide mutation that abolished the XbaI site from the streptavidin gene in order to screen for the mutants. Successful production of the mutant

sequences was confirmed by fluorescent dye terminator cycle PCR sequencing. The FN-SA and OPN-SA gene constructs were subsequently subcloned into the pET21a expression plasmid and transformed into BL21(DE3) (Novagen) competent cells in preparation for large scale streptavidin expression. The FN-SA and OPN-SA constructs in pET21a were expressed and purified as previously described.[98]

3.3.2 Protein Analysis. 10-20% Tris-Gly SDS-PAGE gels (Novex) were run with boiled and unboiled samples of the mutants, wild-type streptavidin, and a Kaleidoscope molecular weight marker to characterize the oligomeric state of the proteins. In addition, a native PAGE gel analysis was performed by omitting SDS from the running buffer. Mass spectrometry was performed on samples of the two streptavidin mutants by electron spray ionization mass spectrometry (Micromass Quattro II Tandem Quadrupole Mass Spectrometer). The protein samples were prepared by dialyzing overnight versus distilled water and then boiled for 30 minutes in 25% methanol and 1% formic acid immediately prior to being run on the mass spectrometer. Off-rate measurements were performed at 25°C as previously described to quantitatively compare the biotin binding properties of the mutants to wild-type streptavidin.[98]

3.3.3 Cell Adhesion. Cell adhesion assays were performed as previously described.[119] Briefly, rat aortic endothelial cells were cultured in MDCB131 media with 10% fetal bovine serum and used between passages 20-25. Wild-type and RGD streptavidin mutant proteins were incubated in 96 well polystyrene plates overnight at 4°C at various concentrations and then blocked with 1% BSA in PBS for 1 hour at 37°C prior to the

plating of cells (n=3). Alternatively, biotinylated BSA was incubated in the 96 wells overnight at 4°C, blocked with 1% BSA in PBS for 1 hour at 37°C, and then streptavidin (wild-type or RGD) was incubated in the wells for 1 hour at 37°C. The protein solution was aspirated and the wells were rinsed with sterile PBS. 50,000 cells in serum free media containing 0.1% BSA were plated onto each well and placed in a humidified incubator for 1 hour at 37°C with 5% CO_2. The media was then removed and the wells were rinsed gently twice with warm PBS (37°C) containing Ca+ and Mg+. The adherent cells were fixed with 4% paraformaldehyde (PFA) for 5 minutes and stained with 0.5% toluidine blue in 4% PFA for another 5 minutes at room temperature before the wells were rinsed by immersing the plate into a large bowl of tap water. The plate was dried by blotting the inverted plate onto paper towels and adherent cells were lysed with 1% SDS to release the dye prior to reading the absorbance of the wells with a plate reader at 595 nm. Synthetic hexapeptides GRGDSP, GRGESP, and GRADSP were purchased from Gibco BRL. The inhibition assay was performed with the same protocol as for the cell adhesion assay except that the cells were incubated with the peptides for 15 minutes at room temperature prior to being plated onto the protein-coated wells.

Melanoma cell adhesion assays on streptavidin coated polystyrene dishes were performed as described above for endothelial cell adhesion assays, except that DMEM with 0.1% BSA and 10mM HEPES was used as culture medium and 2 x 10^5 cells were added to each well. Moα_v cells that express high levels of $\alpha_v\beta_3$ integrin were derived from M21 melanoma cells. These cells were generously provided by Dr. Cecilia Giachelli (University of Washington). Adhesion assays were also performed on self-assembled monolayers constructed on 24 well tissue-culture polystyrene dishes. The

dishes were evaporated with ~400Å gold, then incubated with a 0.1 mM ethanolic thiol solution of 20% biotinylated alkylthiol (BAT) and 80% polyethylene glycol (PEG) overnight. The wells were rinsed three times with 100% ethanol, blown dry with nitrogen, then incubated with 0.05 mg/ml of streptavidin in PBS (wild-type or mutant) at 37°C for one hour with side-side rocking. The protein solution was then removed, and the wells were rinsed three times with PBS before the addition of cells. Antibody inhibition assays were performed essentially identically as for the peptide inhibition assays. LM609 and control IgG antibodies were obtained from Chemicon International, Inc. (CA) and were used at 1:1000 dilution (10 μg/ml).

3.3.4 Apoptosis Assay. Adhesive proteins were adsorbed from solution onto 4 well plastic chamber slides (Nunc) overnight at 4°C. The proteins included: poly-D-lysine (100μg/ml), bovine collagen I (5μg/ml), bovine fibronectin (12.5 μg/ml), recombinant rat osteopontin (5 μg/ml), FN-SA (50 μg/ml), and OPN-SA (50μg/ml). Endothelial cells were seeded onto the protein coated chamber slides in serum-free media at a density of 50,000 cells/ml (1 ml volume) and allowed to attach overnight. The cells were maintained under serum-free conditions for 48 hours at which time they were fixed and then stained with DAPI. Cultures in the presence of serum containing media (10%) were used as positive controls. Microscopic images of at least 5 fields per well were acquired and nuclear morphology was assessed for a minimum of 100 cells on each protein-coated surface. Cells with small, bright and in some cases, fragmented nuclei were scored as apoptotic cells. The relative percent of apoptotic cells are reported as the mean ± standard deviation.

3.4 Results

3.4.1 Characterization of Streptavidin Mutants. After purification, the RGD streptavidin mutants were physically characterized to determine if the mutations disrupted the structure or function of native wild-type streptavidin. Wild-type streptavidin runs as a tetramer on denaturing SDS-PAGE gels if the samples are not boiled prior to electrophoresis. Both RGD mutants exhibited faint bands at the tetramer molecular weight under these conditions, with the primary band running at the monomer mass (Figure 3.2). Native PAGE analysis indicated that the mutants proteins did run as tetramers, demonstrating that the proteins existed as tetramers in the absence of high SDS concentrations (Figure 3.2). Mass spectrometry provided accurate mass measurements for both of the streptavidin mutants with calculated molecular weights of 13,554 for FN-SA and 13,556 for OPN-SA. The measured molecular weights of 13,554 for FN-SA and 13,554 for OPN-SA are within experimental error of the predicted masses (Figure 3.3). In order to determine whether the altered sequences affect the biotin binding site, we measured the biotin off-rates, which are very sensitive to structural perturbations. At 25°C, the k_{off} for wild-type is 3.3×10^{-6}/sec compared to 3.28×10^{-6}/sec for FN-SA and 3.13×10^{-6}/sec for OPN-SA. These off-rate determinations thus demonstrate that the mutants retained biotin affinity equivalent to wild-type streptavidin.

3.4.2 Cell Adhesion. Cell attachment assays were conducted in order to assess whether the insertion of RGD sequences into native streptavidin conferred cell adhesive activity on the mutant streptavidin proteins. Adhesion assays with rat aortic endothelial cells and

human melanoma cells were performed with both of the RGD mutants and wild-type streptavidin adsorbed to 96 well polystyrene wells. Wild-type streptavidin did not support cell adhesion, whereas both of the RGD streptavidin mutants displayed high cell binding activities. Endothelial cell adhesion was also supported when the RGD mutants were immobilized via biotinylated BSA that had been preadsorbed onto the polystyrene wells. To assess cell adhesion, the concentration dependence was determined in titration assays where the RGD streptavidin concentration was varied (Figure 3.4). For both the FN-SA and OPN-SA mutants, maximum endothelial cell adhesion was observed at a solution protein concentration of ~100 nM (5 μg/ml). Statistically significant ($p < 0.05$) cell adhesion between the RGD mutants and wild-type streptavidin was achieved at a solution concentration of ~10 μM, but any differences in cell adhesion between the two mutants did not appear statistically significant. Wild-type streptavidin did not support significant cell adhesion above control levels (BSA-coated wells). This was also confirmed by visually inspecting the wells with a phase-contrast microscope prior to introducing the fixative and cell stain. A high number of cells remained adherent to the wells with the RGD streptavidin mutants, whereas very few cells remained in the wells coated with wild-type streptavidin. The morphology of adherent endothelial cells on the RGD streptavidin mutants closely resembled that of cells on a native adhesive matrix protein. For example, sub-confluent endothelial cell morphology on FN-SA was similar to that of cells attached on fibronectin-coated substrates, whereas little cell attachment and spreading were observed on wild-type streptavidin, similar to adhesion on BSA (Figure 3.5). To confirm that the observed cell adhesion was directly RGD dependent, inhibition studies were conducted with GRGDSP, GRGESP, and GRADSP peptides.

The RGE and RAD control peptides had no noticeable inhibitory effect on cell adhesion, but the RGD peptide inhibited cell adhesion in a dose-dependent manner (Figure 3.6).

Comparable cell adhesion and inhibition results were obtained using human melanoma cells. The RGD streptavidin mutants again showed strong cell adhesive activity either physisorbed onto polystyrene wells or immobilized via biotinylated self-assembled monolayer on gold (Figures 3.7 & 3.8). The melanoma cell adhesion was inhibited in a dose-dependent fashion with either a soluble RGD peptide or by an anti-$\alpha_v\beta_3$ integrin monoclonal antibody, but not by a control non-specific antibody (Figures 3.7 & 3.8). These results thus demonstrate that the RGD sequence mediates cell adhesion, and that these sequences interact specifically with the $\alpha_v\beta_3$ integrin present on the melanoma cells.

3.4.3 Modulation of Cell Adhesion. In a separate set of cell adhesion experiments, RGD-SA (FN-SA) was mixed in solution with WT SA and immobilized onto wells pre-coated with biotinylated BSA in order to vary the density of RGD ligands on the surface. Since there was not a significant difference in the off-rates of the streptavidin mutants, it was assumed that the two streptavidin species (RGD-SA & WT SA) had similar affinities for biotinylated BSA and therefore the relative surface concentration of the two molecules should approximately correspond to their ratio in the heterogeneous solution. The total concentration of streptavidin was fixed at 1 μM, since this appeared sufficient to completely saturate the surface binding sites (see Figure 3.4). Similar to the previous results, minimal endothelial cell adhesion was observed on surfaces of WT SA alone (0%

RGD-SA) and maximal adhesion was achieved on the purely RGD-SA surface (100% RGD-SA) (Figure 3.9). At intermediate concentrations of RGD-SA, cell adhesion varied between these two levels, however a significant drop in cell adhesion was not noted until less than 10% RGD-SA was used (Figures 3.9 & 3.10). This value correlates to the same concentration (~100 nM) of the pure RGD-SA solution at which endothelial cell adhesion appeared to decrease in previous experiments (see Figure 3.4). These results indicate that the density of RGD ligands presented on the surface can be rationally controlled by simply varying the molar ratio of RGD streptavidin in solution with wild-type streptavidin. In this fashion, the spatial density of exposed RGD moieties can be varied within a relatively homogeneous monolayer of streptavidin, capable of subsequent biotin binding.

3.4.4 Apoptosis Assays. To determine whether the engineered RGD streptavidin mutants functioned similarly to natural matrix proteins, preliminary experiments examining endothelial cell survival on various protein-coated surfaces were performed. Fibronectin, osteopontin and collagen I were used as positive controls to prevent apoptosis and compared to the two RGD streptavidin mutants. Poly-D-lysine served as a negative control since it promotes non-integrin mediated cell adhesion to surfaces via electrostatic attraction (positive charge of polymer and net negative charge of cell membrane). After 48 hours in serum-free media, endothelial cells remained adherent, spread and exhibited normal nuclear morphology (based on DAPI staining) on matrix proteins such as FN and OPN (Figure 3.11). On the other hand, cells on the PDL-coated surfaces were fewer in number, rounded up and the majority of cells possessed picnotic

nuclei (Figure 3.11). These results are comparable to those reported previously by Scatena et al. using similar methods.[120] Interestingly, the nuclei of serum-starved cells on the RGD streptavidin coated wells appeared similar to those on the native matrix proteins (Figure 3.11). Quantitative analysis (based on the morphology of nuclear condensation) suggested that the RGD streptavidin mutants were able to inhibit endothelial cell apoptosis almost equally as well as normal matrix protein coatings such as fibronectin, osteopontin or collagen (Figure 3.12).

3.5 Discussion

We have here demonstrated that cell adhesive peptides can be incorporated directly into the streptavidin structural scaffolding and that such streptavidin mutants can function similar to native adhesive matrix proteins. RGD sequences are commonly found at the apex of a β–turn loop, such as the type III β-turn for fibronectin.[121] The anti-parallel β strands provide a constrained framework for the RGD loop. Cyclical peptides, which are comparable to loop structures, can demonstrate an enhanced activity over linear peptides of the same amino acid sequence.[122] An exposed loop of the streptavidin molecule between opposing β strands was thus chosen for the site of the RGD mutations (Figure 3.1). This loop lies near the biotin binding site but does not involve any direct contact residues, and is on the symmetry related surface that is maximally exposed to solution when streptavidin is bound to biotinylated surfaces. Our initial design for introducing the RGD sequence into streptavidin substituted an Arg and Gly for residues Ala and Thr (65 and 66) before a naturally occurring Asp residue (67), but this mutant did not promote cell adhesion. Two subsequent mutants based on the original construct

included additional flanking residues mimicking those found in fibronectin and osteopontin. A Gly was inserted between residues 64 and 65 of streptavidin, and a Ser and either Val or Pro (corresponding to fibronectin and osteopontin, respectively) were placed between amino acids 67 and 68.

The additional flanking residues may increase the exposure of the loop and/or sterically optimize the adhesive sequences in a more favorable orientation. The flanking residues surrounding the RGD sequence also play a role in determining the adhesive activity of the peptide, as well as the specificity for individual integrins.[123] Nearly half of the known integrins display an RGD ligand binding dependence, and certain integrins require specific flanking sequences that differ amongst the various extracellular and matricellular proteins.[124] The different flanking residues are believed to alter the conformation of the RGD domain, thus providing a structural basis for integrin specificity. Previous reports have suggested that an RYD site in streptavidin can direct association with Chinese hamster ovary cells, M4 murine melanoma cells, ADP-activated platelets, and CD4+ T lymphocytes cells, and that soluble RGD peptides will compete with the native protein for integrin engagement.[125-128] We did not observe this activity with the endothelial and melanoma cells used in this study, or in other studies with a variety of other cell types. The RYD sequence has limited solvent accessibility in the crystal structure of streptavidin, and is unlikely to be a strong mediator of specific integrin interactions with streptavidin.

In almost all cases, the FN-SA mutant appeared slightly more adhesive than the OPN-SA mutant on an equimolar basis. This may be an interesting observation since in general these two mutants displayed similar adhesive behavior, yet differ in only a single

amino acid in their primary structure. Potentially this phenomenon could have been an artifact of a minor miscalculation in the molar concentration of the two species, but it appeared fairly consistent over the course of all experiments in which the RGD streptavidin mutants were compared. If the difference in adhesivity between the two mutants is indeed real, then this pair of proteins (FN-SA & OPN-SA) serves as an example of the subtle complexity of molecular recognition utilized by cells as they decipher the adhesive cues present within their local environment.

Specifically immobilizing the RGD streptavidin mutants on biotinylated substrates also permits novel methods to control the adhesive ligand density on a surface. The surface density of RGD can be varied within a homogeneous streptavidin monolayer by exposing the substrate to mixed solutions of the RGD and wild-type streptavidin species. Since biotin affinity appears to be equivalent, the two species in solution should compete equally for biotin binding sites on the surface. In addition, the density of RGD could be further controlled by producing chimeras of RGD and wild-type streptavidin by combining the 2 species during protein refolding; methods for producing streptavidin chimeras have been described previously.[129] This approach could be used to reduce the number of RGD motifs per assembled tetramer, but it would be impossible to achieve a homogeneous population since it can be difficult to control the precise stoichiometry of the refolded chimeras.

Streptavidin is used as an adapter in a wide variety of diagnostic, separations, and drug targeting applications. It is thus interesting that streptavidin itself could be used in some applications as both an adapter and as an effector, which could provide opportunities to simplify and improve many of these applications. The cell adhesive

streptavidin derivatives described here are directly useful as tissue culture coatings to immobilize cells. Integrin mediated cell adhesion is closely tied to important signaling pathways that control cell behavior, and these streptavidin derivatives might also be used to stabilize cell phenotype through the incorporation of RGD or related sequences that mediate specific receptor-mediated engagement and biological responses. It is likely that a number of different peptide sequences with a variety of receptor specificities can be incorporated into this loop or other surface locations, which could provide additional opportunities for cell separations and diagnostics applications. The incorporation of receptor specific peptide sequences into streptavidin could also provide opportunities to evaluate streptavidin as both the targeting and capture agent in drug delivery applications utilizing biotinylated biomolecular therapeutics.

3.6 Figures

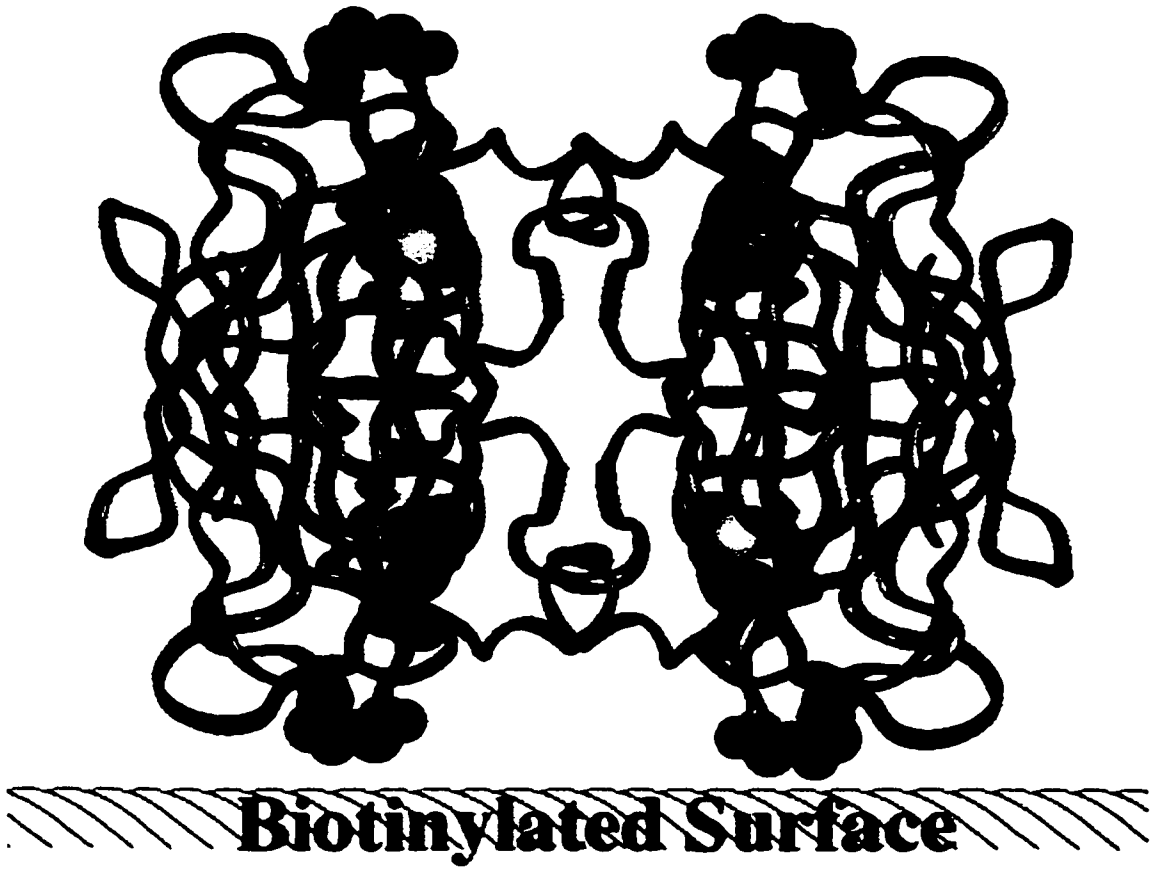

Figure 3.1. Schematic model of the streptavidin tetramer structure and its relative orientation immobilized on a biotinylated surface. The black balls indicate the location of the RGD residues and biotin moieties situated in the binding site are represented as the multi-colored ball-and-stick atoms. Each of the individual streptavidin monomers is identified by the four different colored ribbon structures. The model does not attempt to predict the precise conformation of the mutated loop, but simply to depict the spatial relationships of biotin binding sites and the RGD mutations. The RGD mutation was inserted into a solvent exposed loop on the opposite side from the biotin binding pocket of each individual monomer.

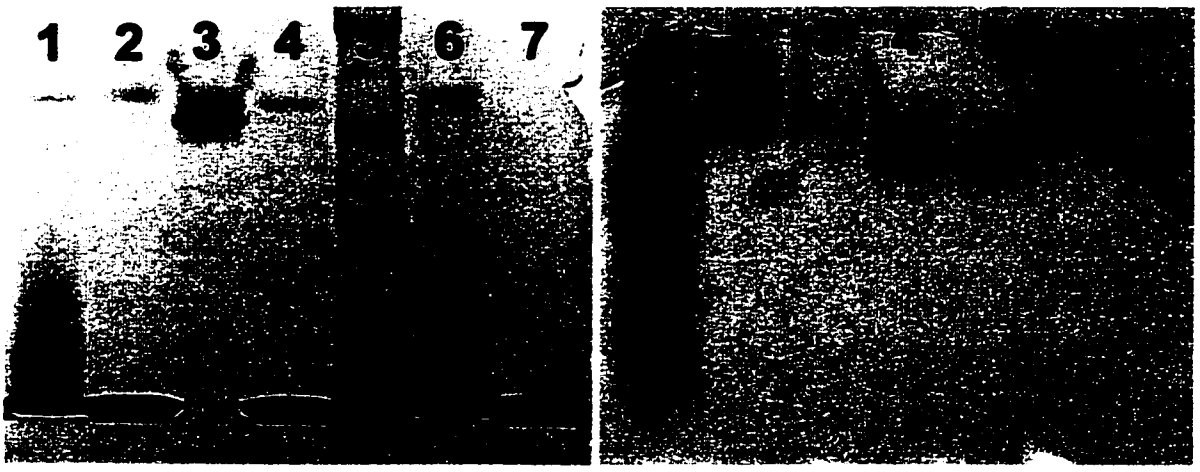

Figure 3.2. Poly-acrlyamide gel electrophoresis of RGD streptavidin mutants. SDS (left) and native gels (right) were run with samples of WT SA, FN-SA and OPN-SA. Left) 1 - OPN-SA unboiled; 2 - OPN-SA boiled; 3 - WT SA unboiled; 4 - WT SA boiled; 5 - MW ladder; 6 - FN-SA unboiled; 7 - FN-SA boiled. Right) 1 - MW ladder; 2 - OPN-SA unboiled; 3 - OPN-SA boiled; 4 - WT SA unboiled; 5 - WT SA boiled; 6 - FN-SA unboiled; 7 - FN-SA boiled. Unboiled samples should run at the tetrameric molecular weight (~52,000 kDa) and boiled samples should run at the monomeric molecular weight (~13,000 kDa). The RGD streptavidin mutants appeared unstable in the presence of SDS (left), indicated by the smeared lanes (1 & 6). However the native gel indicated the RGD streptavidin mutants could stably assemble into tetramers (right, lanes 2 & 6).

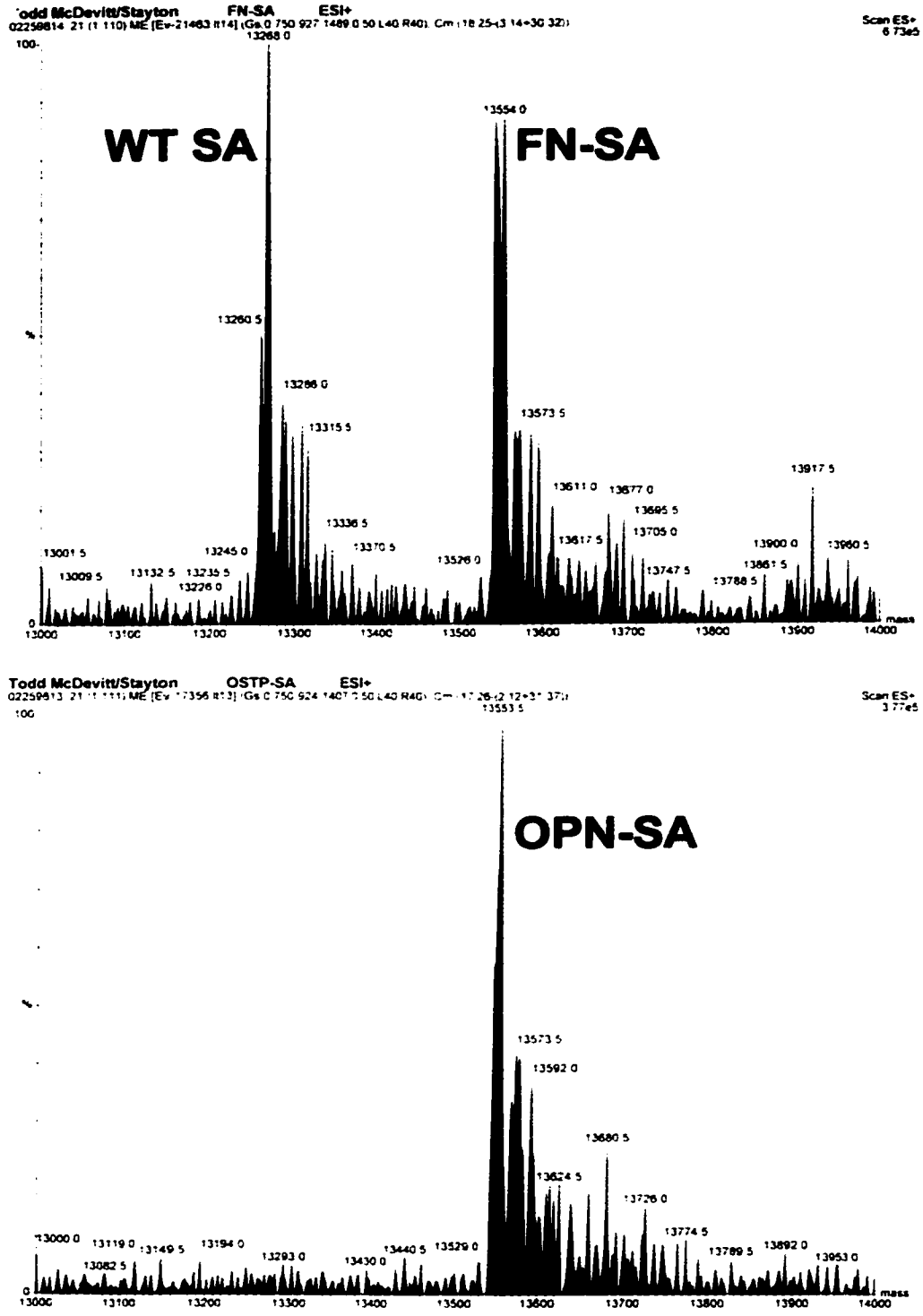

Figure 3.3. Mass spectrometry results of RGD streptavidin mutants. The FN-SA sample was spiked with WT SA as an internal reference.

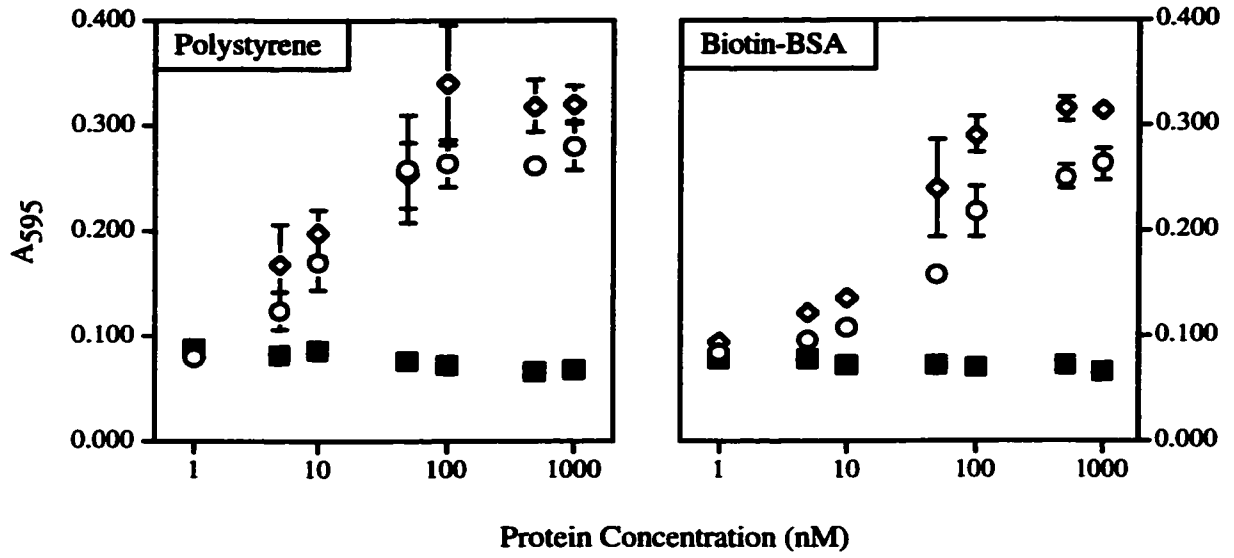

Figure 3.4. Concentration dependence of FN-SA and OPN-SA mediated endothelial cell adhesion. FN-SA (diamonds), OPN-SA (circles) or WT SA (black squares) were coated on either polystyrene wells or immobilized via biotin-BSA adsorbed onto polystyrene wells. Rat aortic endothelial cells were plated onto the wells at a density of 50,000 cells per well and allowed to attach for about one hour at 37°C, 5% CO_2. Non-adherent cells were rinsed from the wells, the cells were fixed and then stained with toluidine blue. Cell membranes were lysed to release the dye and absorbance readings at 595 nm were acquired with a 96-well plate reader. The data are reported as the mean ± standard deviation values (n=3); some standard deviation bars are too small to be depicted. Endothelial cell adhesion increased as the solution concentration of the RGD streptavidin mutants used to coat the wells was increased. Cells did not significantly adhere to WT SA over the same range of concentrations.

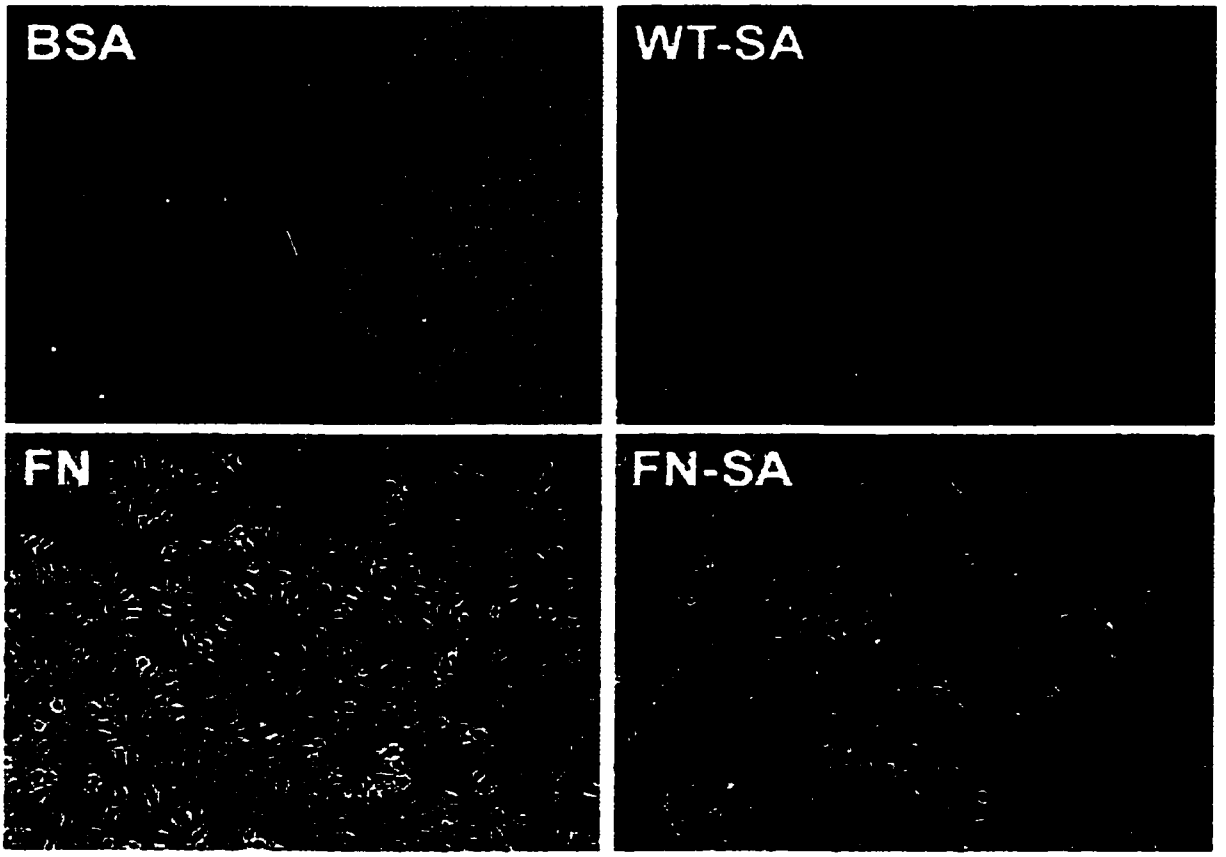

Figure 3.5. Phase contrast images of rat aortic endothelial cell adhesion. Endothelial cells were plated onto protein-coated petri dishes in serum-free media and allowed to adhere for ~24 hours. Adsorbed bovine serum albumin (BSA) and wild-type streptavidin (WT SA) did not support cell attachment and spreading. In contrast, adsorbed fibronectin (FN) and FN-SA facilitated cell adhesion and normal cellular morphology.

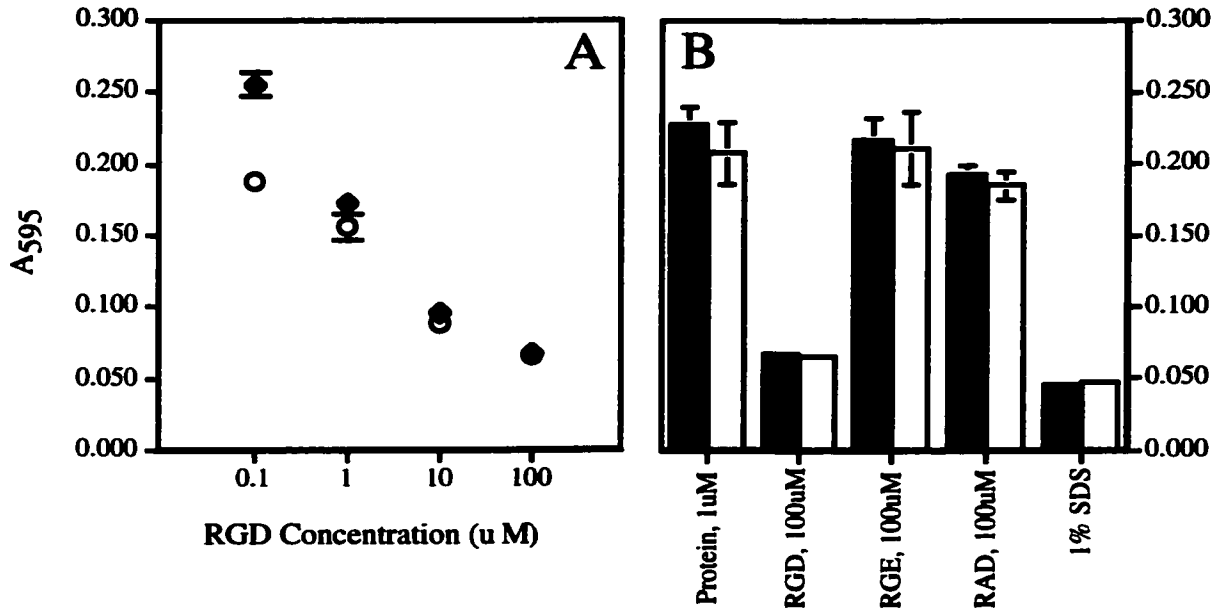

Figure 3.6. RGD peptide inhibition of FN-SA and OPN-SA mediated endothelial cell adhesion. Rat aortic endothelial cells were pretreated with soluble RGD peptides for 15 minutes prior to being plated onto wells pre-adsorbed with RGD streptavidin (1 μM) at a density of 50,000 cells per well and allowed to attach for about one hour at 37°C, 5% CO_2. Non-adherent cells were rinsed from the wells, the cells were fixed and then stained with toluidine blue. Cell membranes were lysed to release the dye and absorbance readings at 595 nm were acquired with a 96-well plate reader. The data are reported as the mean ± standard deviation values (n=3); some standard deviation bars are too small to be depicted. Left) Rat aortic endothelial cell adhesion to FN-SA (black diamonds) or OPN-SA (white circles) was inhibited in a dose-dependent manner by the addition of a soluble GRGDSP peptide. Right) Soluble GRGDSP peptides specifically inhibited cell adhesion to FN-SA (black bars) or OPN-SA (white bars), compared to control peptides, GRGESP and GRADSP. The RGD peptide at 100 μM almost completely inhibited cell adhesion, relative to baseline absorbance levels (1% SDS alone, no cells).

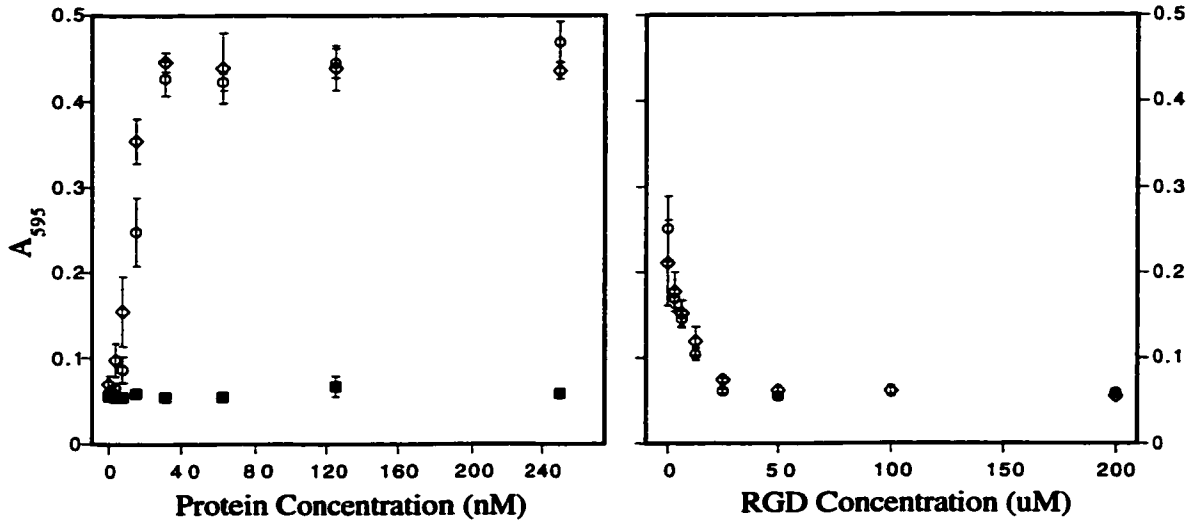

Figure 3.7. Melanoma cell adhesion to polystyrene dishes coated with FN-SA (diamonds), OPN-SA (circles) and wild-type streptavidin (black squares). Left) Dose-dependent cell adhesion at various coating concentrations was observed which could be inhibited in a dose dependent fashion by soluble RGD peptides (right). The streptavidin coating concentration in the peptide inhibition experiment was kept constant at 200 μM (see Materials and Methods). Error bars indicate ± standard deviation (n=3).

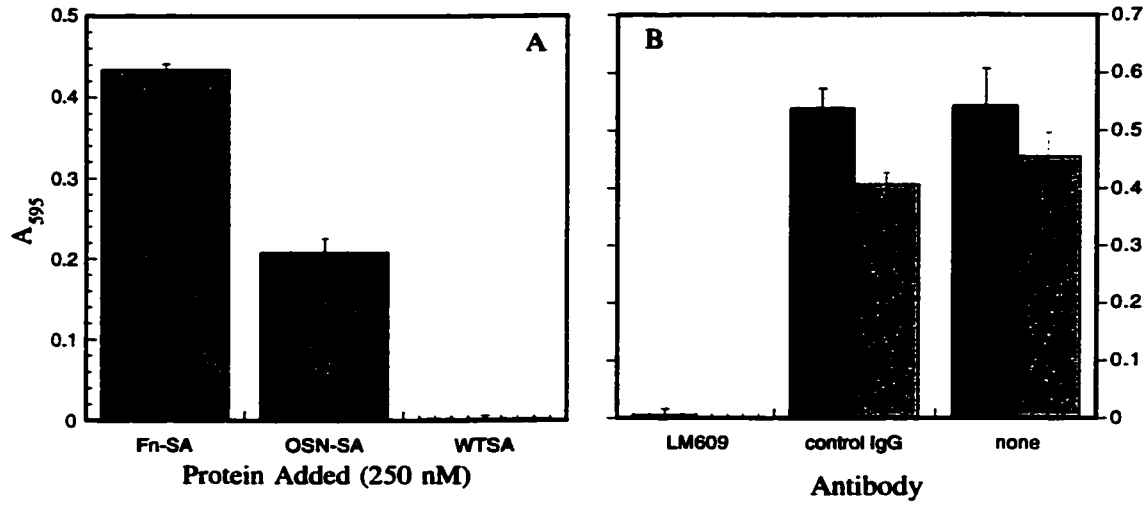

Figure 3.8. Melanoma cell adhesion to mixed self-assembled monolayers (SAMs) containing biotin and poly(ethylene glycol) thiols. Left) Cell adhesion to SAMs coated with FN-SA, OPN-SA, and wild-type streptavidin was compared and right) integrin specificity of melanoma cell adhesion was determined by pre-incubating the cell suspension in the presence of 10 ug/ml anti-$\alpha_v\beta_3$ integrin complex (LM609) or isotype-matched non-immune control antibody, FN-SA (black bars), OPN-SA (grey bars). Error bars indicate ± standard deviation (n=3). Results are representative of at least two independent experiments.

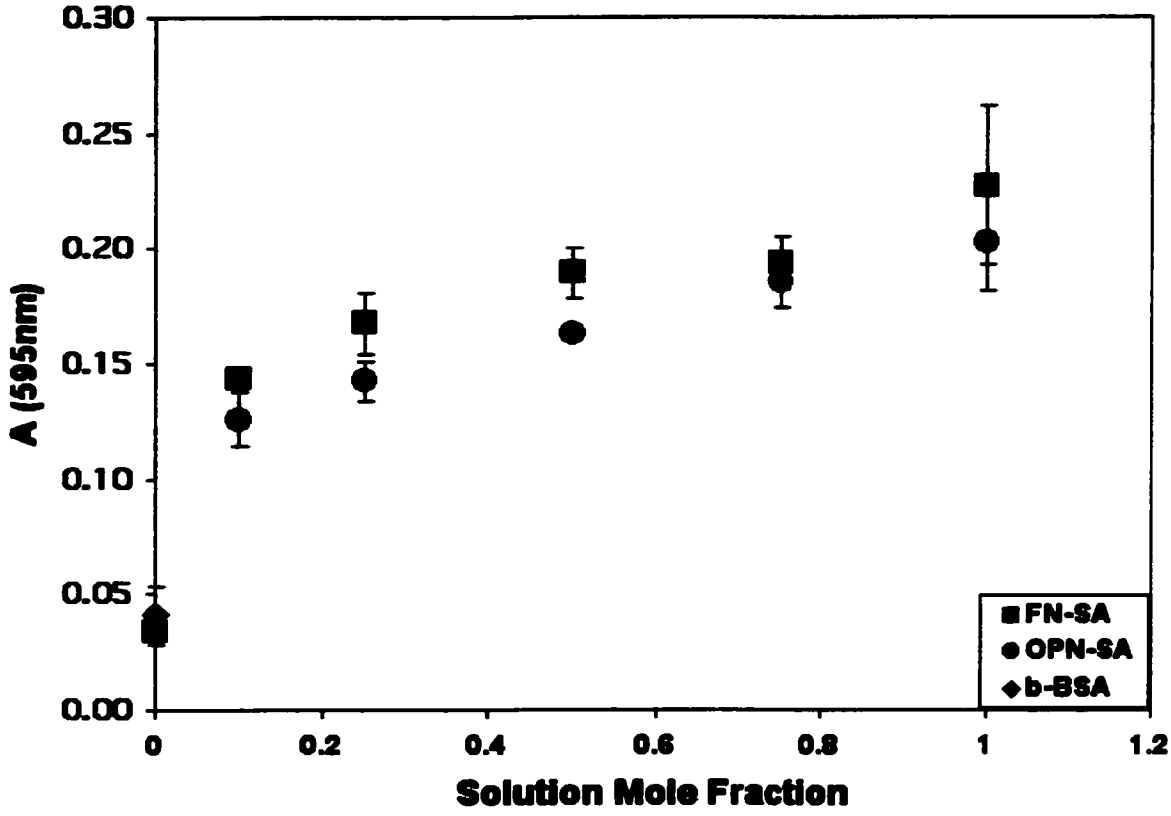

Figure 3.9. Rat aortic endothelial cell adhesion to RGD-SA/WT SA mixtures immobilized on biotinylated-BSA coated substrates. The total streptavidin concentration was fixed at 1 μM while the mole fractions of RGD-SA and WT SA were varied. The cells were allowed to attach for 1 hour and then non-adherent cells were gently rinsed from the wells. Fixed cells were stained with toluidine blue, cell membranes were lysed to release the dye and absorbance readings at 595 nm were acquired with a 96-well plate reader. The data are reported as the mean ± standard deviation values (n=3). Endothelial cell adhesion gradually increased with an increasing molar fraction of either FN-SA (green squares) or OPN-SA (red circles), but remained relatively high even at a mole fraction of 0.1.

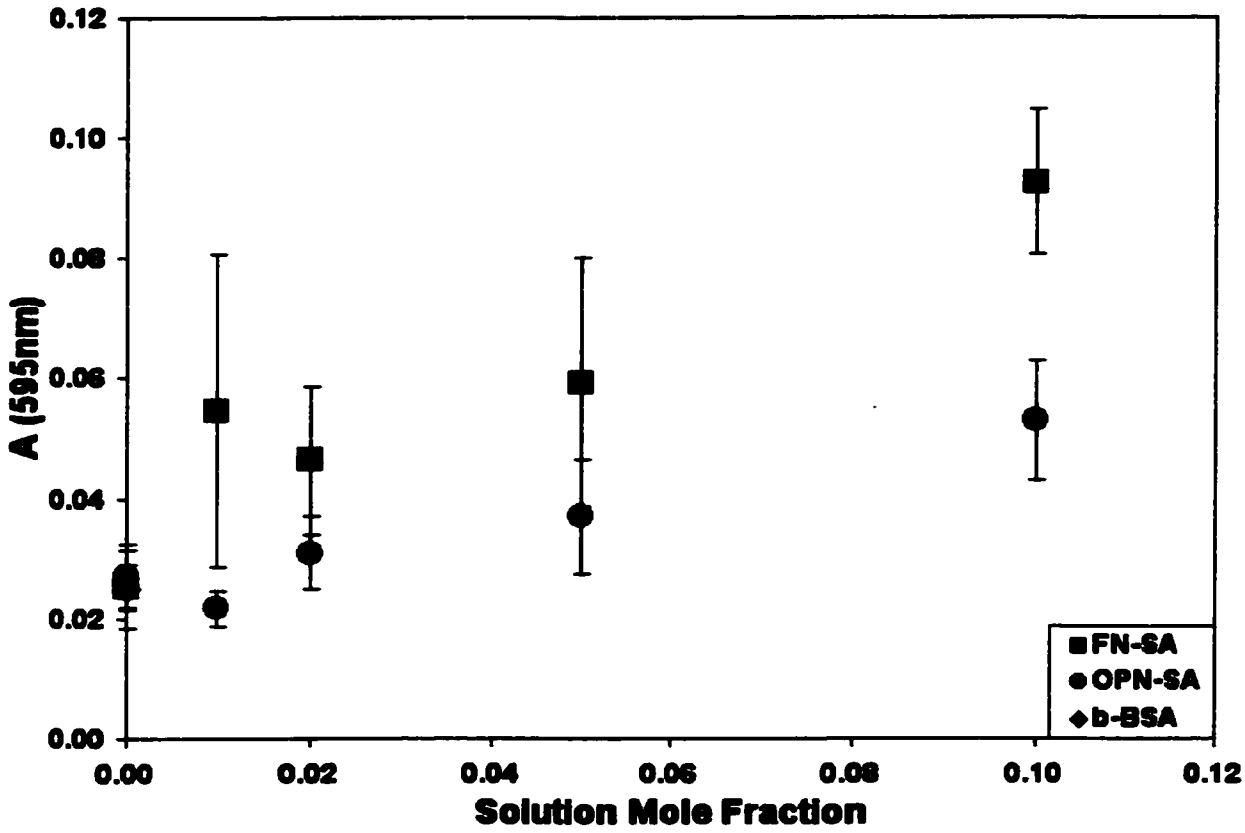

Figure 3.10. Rat aortic endothelial cell adhesion to RGD-SA/WT SA mixtures immobilized on biotinylated-BSA coated substrates at lower concentrations of RGD-SA ($\leq$ 10%). The total streptavidin concentration was fixed at 1 μM while the mole fractions of RGD-SA and WT SA were varied. The cells were allowed to attach for 2 hours and then non-adherent cells were gently rinsed from the wells. Fixed cells were stained with toluidine blue, cell membranes were lysed to release the dye and absorbance readings at 595 nm were acquired with a 96-well plate reader. The data are reported as the mean ± standard deviation values (n=3). Endothelial cell adhesion increased slightly with an increasing molar fraction of either FN-SA (green squares) or OPN-SA (red circles), but not significantly greater than background levels until a mole fraction of 0.05 or 0.1 was used.

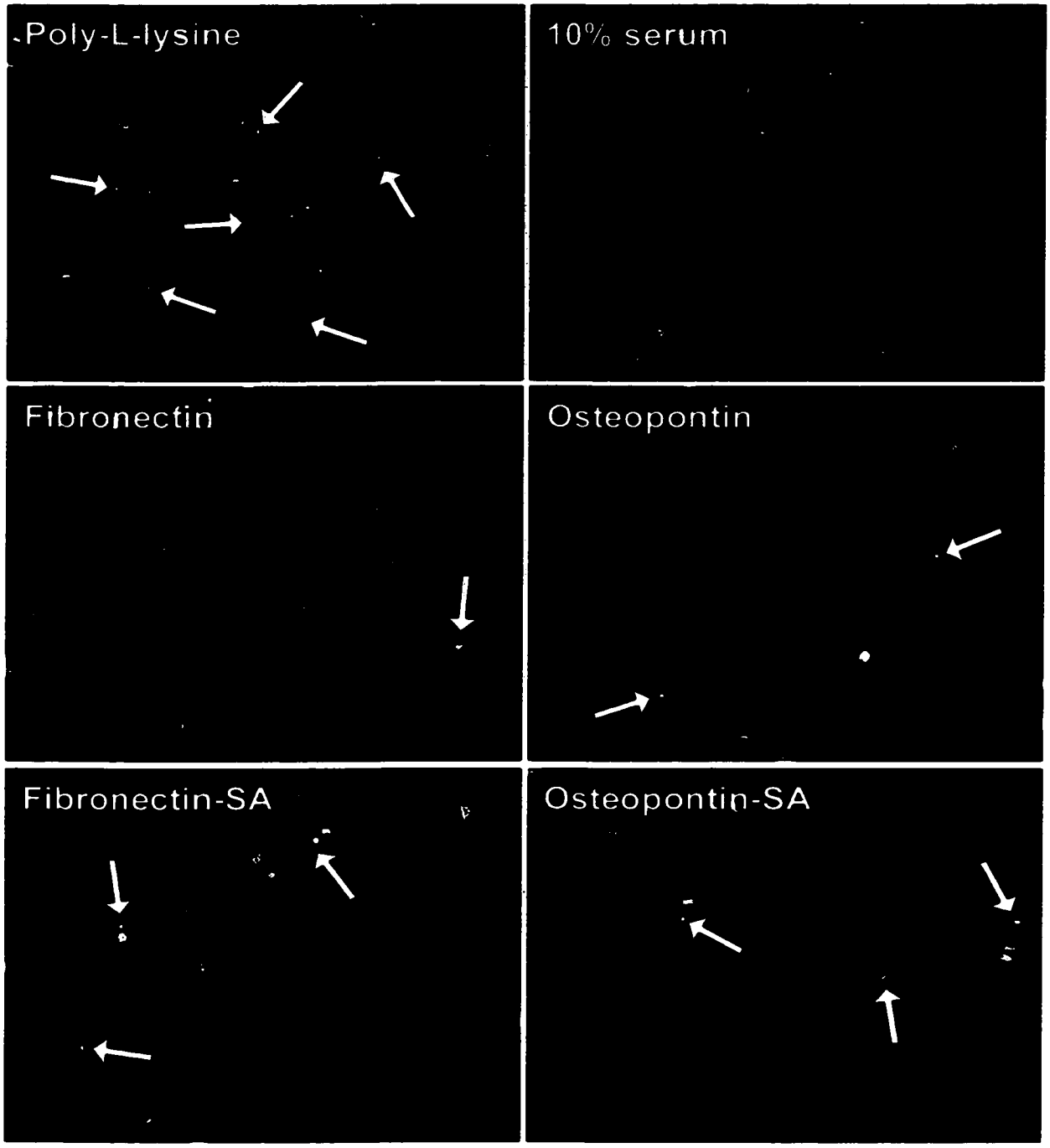

Figure 3.11. Nuclear staining of serum-starved endothelial cells on adhesive proteins. Rat aortic endothelial cells were plated onto protein-coated chamber slides and cultured in serum-free media for 48 hours. The cultures were fixed and stained with DAPI to visualize the morphology of cell nuclei. Arrows highlight small, intensely stained and sometimes fragmented nuclei, indicative of apoptotic cells.

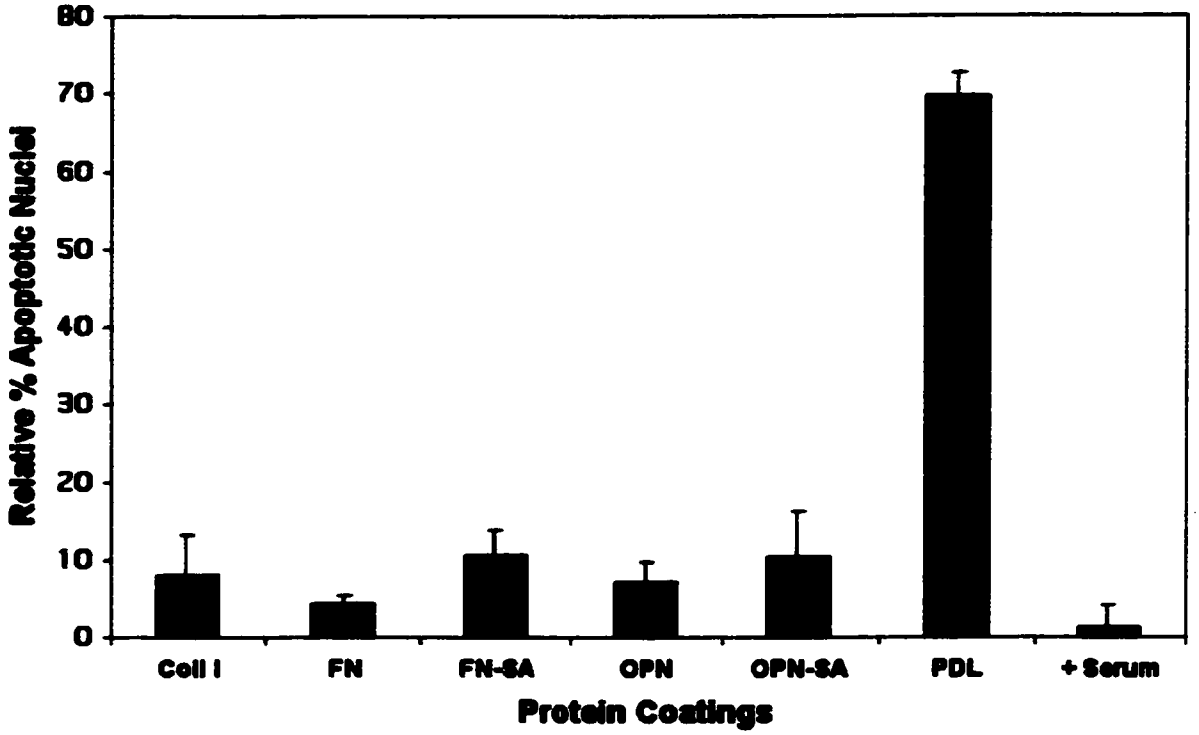

Figure 3.12. Quantitative analysis of apoptotic endothelial cells on adhesive protein coated surfaces. Rat aortic endothelial cells were plated onto protein-coated chamber slides and cultured in serum-free media for 48 hours. The cultures were fixed and stained with DAPI to visualize the morphology of cell nuclei ($n \geq 100$). Apoptotic cells were counted and reported as the % of the total adherent cell population. Endothelial cell apoptosis was inhibited by adhesion to RGD streptavidin mutants, similar to cell attachment to native matrix proteins.

Chapter 4: Spatially Organized Assembly of Extracellular Matrix Proteins on Surfaces to Direct Cellular Response

4.1 Abstract

The precise micro-architecture of the extracellular matrix, consisting of structural and functional proteins, imparts spatiotemporal information to cells that directs macroscopic tissue development and function. Similarly, micropatterning techniques have been developed to control the displacement of proteins and cells at interfaces for investigations of cell biology, biosensor development and tissue engineering applications. Microcontact printing is an attractive micropatterning approach because it affords a relatively simple and rapid method to directly pattern proteins. We have pursued microcontact printing of extracellular matrix and globular proteins to specifically direct cell adhesion and cellular response on a variety of material surfaces. Protein patterns were transferred with approximately 100% efficiency from native PDMS stamps to substrates that were less hydrophobic, based on contact angle measurements. The protein patterns appeared to be stable for several weeks in aqueous buffer or serum-containing media and the printing technique did not appear to significantly inhibit the bioactivity of the protein patterns. Cell adhesion was strictly dictated by the protein patterning dimensions and stable cell patterns could be generated that persisted for several weeks *in vitro*. In addition to patterning onto synthetic materials, protein patterns were also printed onto adsorbed protein layers. Cells could decipher differences in spatial adhesive cues between patterns of different adhesive proteins or subtle spatial variations in the

concentration of a single protein species. The ability to fabricate complex, heterogeneous protein patterned surfaces represents a novel method to spatially control the assembly of proteins in a manner that more accurately resembles the native organization of the extracellular matrix.

4.2 Introduction

The extracellular matrix plays a key role in the development and maintenance of tissue organization and cell phenotype, as well as in wound healing processes. For technologies that rely on controlling biology at surfaces, such as biosensors and tissue engineering[130, 131], there is thus a great interest in developing strategies that direct cell phenotype and tissue development by organizing instructive extracellular matrix cues. This goal poses a significant challenge because the extracellular matrix environment is very complex, with the full information content tied to the structural complexity and dynamic interplay of combinations of multiple soluble and insoluble proteins. For example, matricellular proteins are a subset of matrix proteins that are expressed transiently to control a variety of important cell activities by modulating cell receptor interactions with extracellular matrix proteins, such as collagen.[132] Cell activities are thus dependent on the spatial content of the local extracellular matrix environment mediated by specific interactions with integrins and other receptors on the surface of cells.

Numerous micropatterning methods have been derived using traditional photolithography and soft lithograpy technologies to pattern the displacement of proteins and cells on surfaces. These techniques have been used to study the patterning of a variety of cell types *in vitro*, including macrophages[133], hepatocytes[134], endothelial[135, 136],

bone[137] and neuronal cells[138, 139], as well as cardiac[140] and skeletal muscle cells[141]. A description of major advances in protein patterning and microfabrication technologies to study cellular interactions have been summarized in recent reviews.[142-145]

Microcontact printing has been proven to be a reliable and versatile micropatterning technique for defining spatial patterns of adhesive or non-adhesive surface chemistries.[99, 146] Chemical patterning via microcontact printing of self-assembled monolayers has been used to preferentially direct the adsorption of extracellular matrix proteins from solution, such as fibronectin, thereby creating spatially defined adhesive regions for cell attachment.[100, 147, 148] However, strategies utilizing chemical patterning schemes are often limited to particular substrates, like gold or silicon surfaces, and typically require the synthesis of organic molecules to create the desired surface chemistry.

On the other hand, microcontact printing of proteins directly is a more straightforward approach that is compatible with a variety of surfaces.[101-104] Several studies have described the direct microcontact printing of proteins into spatially defined geometries, including the use of poly-lysine to direct cell adhesion.[102, 103, 149, 150] In the case of poly-lysine though, cell attachment is based solely upon the electrostatic attraction between the cationic polymer and the anionic cell membrane, under aqueous conditions. However, most cell types require receptor-mediated attachment to extracellular matrix (ECM) proteins to promote normal cellular function and long-term survival. Recent reports have described the direct printing of fibronectin[151] or laminin[152-154] to pattern endothelial cells or neuronal cells, respectively, on synthetic substrates.

These reports suggest that this method may be generally applicable to stamp various extracellular matrix proteins to pattern cell attachment.

We have been interested in utilizing matrix proteins at surfaces to instruct cell behavior, but within a more biological context that includes other extracellular matrix components as well. By controlling the spatial organization of extracellular matrix molecules we can systematically investigate the effects of the geometric distribution of these proteins on cellular response. Microcontact printing of proteins can be used to rapidly generate a wide variety of spatially defined combinations of extracellular and matricellular proteins on cell culture substrates or biomaterials by successive stamping with different biomolecules. In addition, spatially organized, heterogeneous mimetics of the natural extracellular matrix can be created by printing protein patterns directly onto adsorbed protein layers. Printed patterns of matrix proteins are stable in the presence of serum-containing cell culture media and a number of different cell types have been patterned to demonstrate the inherent flexibility of this technique to culture anchorage-dependent mammalian cells in this manner. The organized *in vitro* assembly of ECM proteins by microcontact printing provides a new model system to directly investigate the effects of spatially organized matrices on cell adhesion and function.

4.3 Methods

4.3.1 Protein Printing Methods. Protein patterns were fabricated by microcontact printing as described in Chapter 2. In general, protein solutions were incubated on PDMS stamps for 30-45 minutes to allow the proteins to adsorb onto the surface of the elastomer. The stamps were rinsed with deionized water and PBS and dried with a

nitrogen stream immediately before being brought into contact with a dry substrate. It was essential that both the stamp and substrate were macroscopically dry in order to achieve conformal contact between the two materials and thus facilitate protein transfer.

4.3.2 Cell Patterning. The cell types used in patterning experiments were either isolated from tissues or cultured according to the methods described in Chapter 2. Cell suspensions were plated onto the micropatterned substrates and allowed to attach to the protein patterned regions. Typically, after a short period of time, non-adherent cells were rinsed away and cultures were routinely re-fed with fresh media as necessary.

4.3.3. Surface Analysis Techniques. Fluorescent microscopy was used to assess the morphology of protein patterns that were either conjugated to fluorescent probes or detected immunohistochemically. Contact angle measurements of various substrate materials were either measured using a Rame-Hart goniometer, as described in Chapter 7, or taken from the literature. Patterned cell morphology of live cultures was monitored by inverted phase microscopy during the course of experiments.

4.4 Results

4.4.1 Properties of Matrix Protein Printing. The direct microcontact printing of various extracellular matrix proteins (collagen I, laminin, fibronectin, gelatin) was characterized along with small peptides (i.e. endothelin-1) and a set of soluble, globular proteins that included osteopontin and thrombospondin-2, both matricellular proteins, as well as streptavidin and BSA. These proteins varied in their size and structural/physical

properties, ranging from relatively small soluble peptides (~2.5 kDa for endothelin-1) to large extracellular matrix proteins (~900 kDa for laminin) (Table 4.1). The dimensions of the printed protein patterns on the substrates matched precisely with the raised topographic features of the PDMS stamps used. Quality patterns were generated that were mostly free of major defects on the size scale of the patterns themselves (>5 μm), although some small holes or discontinuities (typically < 5 μm) could be observed within patterned features (Figure 4.1). Previous reports have estimated the efficiency of protein transfer at nearly 100%.[101, 104] Based on fluorescent microscopy analysis, it appeared that adsorbed protein layers were completely transferred from the stamp to the substrate selectively in the regions of contact. The relative fluorescent intensity using labeled proteins indicated that uniform surface coverage was adsorbed to the stamps and transferred to the substrate, before and after printing respectively. Although typically the stamps remained in contact with the substrate for a few minutes during the printing procedure, proteins were rapidly transferred after just a few seconds of contact.

The substrates for protein printing encompassed a range of materials with various chemical compositions and surface properties (Table 4.2). Several of the surfaces, such as glass and polystyrene, are commonly used as cell culture substrates and their transparency permits straightforward optical microscopic analysis of protein and cell patterns. Other substrates onto which protein patterns were easily printed included mica, silicon and gold; some of which are frequently employed in the development of microfabricated biosensor devices. Direct printing of extracellular matrix proteins was also studied on several polymeric materials frequently used as biomaterials implants or tissue engineering scaffolds (i.e. PET, PLGA and polyurethanes). Protein patterns were

also printed onto thin films of a non-fouling polymer (tetraglyme) and stably supported the adhesion of cell patterns.[155] These examples demonstrated that microcontact printing of proteins is amenable with most types of surfaces.

Although theoretically PDMS stamps could be cleaned and used repeatedly for protein printing, early experiments indicated that new stamps typically produced better quality patterns than re-used stamps. For example, fibronectin line patterns exhibited fewer defects with a new stamp than one that was re-used after being cleaned by an oxygen plasma treatment (Figure 4.2). To avoid potential complications of using recycled stamps, all of the ensuing protein patterns were printed with a fresh stamp used only once since new stamps provided reproducible results and could be generated rapidly at minimal cost.

4.4.2 Mechanism of Protein Printing. The mechanism for the highly efficient transfer of proteins from PDMS stamps to substrates during microcontact printing has yet to be precisely determined. Although this technique was generally compatible with most surfaces, there were a few instances in which printing was not successful. The sum of these "failed" experiments produced a few consistent trends that could explain the potential mechanism of protein transfer via microcontact printing.

Printing onto PDMS Substrates

The first of these experiments was simply to try to pattern from PDMS onto PDMS. A series of patterned stamps or unpatterned, flat blocks of PDMS were either treated with an oxygen plasma to render them temporarily hydrophilic or left untreated,

thus remaining hydrophobic. The PDMS stamps (oxidized or native) were coated with a BSA protein solution and stamped onto a PDMS block (oxidized or native), for all four possible combinations. Thus, the main difference between the stamp and substrate was in the wettability of the materials, while the other surface chemistry properties remained relatively constant. Protein patterns were transferred from hydrophobic (native) PDMS stamps onto hydrophilic (oxidized) PDMS blocks and weak protein transfer was accomplished by printing with an oxidized stamp onto another hydrophilic PDMS material. In contrast, protein transfer appeared to be almost completely inhibited by printing from either a hydrophobic or hydrophilic stamp onto a native PDMS substrate. The experiment was repeated by printing with native PDMS stamps onto either native or oxidized PDMS substrates, and similar results were again obtained (Figure 4.3).

Criss-cross Patterning

In another series of experiments, line patterns of BSA or biotinylated BSA were printed onto glass slides and the remaining exposed glass surface area was blocked by adsorbing a solution of the other molecule. Thus alternating lanes of biotinylated BSA and BSA differed only in the order of which molecule was either printed or adsorbed. The initial intent of these experiments was to investigate whether secondary patterns of streptavidin printed orthogonal to the direction of the original line patterns were specifically retained on the biotinylated lanes due to streptavidin's affinity for biotin. If so, then squares of streptavidin should coincide with biotinylated BSA regions.

When BSA was printed first and biotinylated BSA was adsorbed to the remaining surface, printed patterns of streptavidin appeared as squares rather than lines and the

streptavidin appeared to co-localize on the biotinylated BSA regions. If the order was reversed and the biotinylated BSA lanes were printed and a BSA solution was then adsorbed, the streptavidin pattern again appeared as squares, but co-localized on the BSA regions between the biotinylated BSA lanes (Figure 4.4). These contrasting results suggested that printed streptavidin was not specifically immobilized to the biotinylated regions. Instead, it appeared that regardless of which molecular species was printed first, the primary patterned regions inhibited the subsequent printing of a secondary protein pattern. However, the surface regions that contained the same molecule passively adsorbed to the substrate and had not been printed onto could be stamped with a secondary protein pattern. This curious phenomenon could be due to the low molecular weight PDMS that transfers with the proteins from the stamp during printing and results in PDMS patterns on the surface. Thus, stamping onto printed patterns would be prevented, similarly to stamping from a native PDMS stamp onto a native PDMS substrate.

Contact Angle Measurements

The relative wettability of surfaces can be assessed on the basis of contact angle measurements of water in air. Based upon measured and reported values, all of the substrates onto which protein patterns were successfully transferred exhibited advancing and receding contact angles that were less than that of native PDMS (Table 4.2). Protein transfer was not achieved from native PDMS stamps to substrates with contact angles that were equal to (i.e. native PDMS ≈ 100-110°) or greater than that of the PDMS (i.e. Teflon ≈ 113°).

These experiments consistently indicated that protein transfer from native PDMS stamps was only achieved with substrates that were less hydrophobic than native PDMS. This suggests that the unidirectional driving force for efficient protein transfer during printing may be related to differences in wettability between the stamp and the substrate.

4.4.3 Protein and Cell Pattern Stability. The durability and integrity of the non-covalently immobilized patterns were assessed by several methods. Protein patterns immersed in PBS appeared unchanged, by fluorescent microscopy inspection, over the course of 2 weeks at 4°C (longest time point assessed) and could be used to pattern cell adhesion with no apparent functional loss of bioactivity. Although this indicates that patterned surfaces could be fabricated and properly stored well in advance of cell patterning experiments, most samples were prepared on the same day cell patterning experiments were initiated for consistency purposes. Samples of printed protein patterns were also incubated with serum-containing media at 37°C and 5%CO_2 to determine the stability of the patterns under typical cell culture conditions. Based upon fluorescent microscopy inspection, patterns in the presence of serum appeared to be unchanged for up to 4 weeks (longest point assessed) (Figure 4.5), suggesting that the original patterns are quite stable for cell culture experiments.

Cell pattern stability was similarly assessed with a variety of cell types. Some cells demonstrated poor spatial confinement to the protein patterns (i.e. fibroblasts, endothelial cells, smooth muscle cells) in the presence of serum-containing media. However, cell pattern integrity was significantly improved by culturing such cell types on

protein patterns in serum-free media conditions for up to several days. These cells, active in extracellular matrix synthesis and remodeling, also appeared capable of re-organizing some of the underlying printed molecules and in some instances, manipulating them into fibrils. In contrast, other cell types less active in synthesizing and remodeling the extracellular matrix, such as cardiac and skeletal myocytes, remained patterned for several weeks in the presence of serum containing (1-10%) cell culture media. Thus depending on the cell type, the integrity of most cell patterns was preserved by controlling soluble factors added to the cell culture media.

The dimensions of the patterning features also contributed to the stability of cell patterning. Cell patterns spaced far apart (≥80 μm) were retained better than patterns spaced close together (i.e. < 20 μm), since the larger non-adhesive regions between the adhesive regions inhibited the degree of cellular bridging and migration between adjacent features, thus preserving the overall integrity of patterning.

4.4.4 Bioactivity of Printed Protein Patterns. The microcontact printing procedure did not appear to significantly affect the activity of the patterned proteins. Functional activity was qualitatively assessed by the ability of extracellular matrix (ECM) molecules to promote cell attachment, spreading, and normal cellular function. Cell adhesion is mediated through adhesive peptide motifs, such as the RGD sequence, within matrix proteins that interact specifically with cell surface receptors (i.e. integrins). Integrin ligation, and in many cases specificity, requires that the appropriate conformation of the peptide sequence be displayed for proper biorecognition by cells. Thus, utilizing cell

adhesion as an indication of the bioactivity of the patterned proteins suggested that native protein functions were preserved for printed matrix proteins.

As one example, mouse myoblasts (MM14) were patterned on microcontact printed laminin, gelatin or fibronectin lanes (15-30 μm wide) on polystyrene culture dishes. The myocytes rapidly attached to the adhesive protein regions within 4 hours and spread in the direction of the lanes (Figure 4.6). The cells proliferated and migrated exclusively along the patterned protein lanes. Differences in myoblast attachment and morphology were detected between patterns using different matrix proteins, but these differences were consistent with characteristics of the myoblasts on unpatterned controls. After switching the culture conditions to promote skeletal myocyte differentiation, the myoblasts fused primarily along individual protein lanes and formed multi-nucleated myotubes oriented with the direction of the patterns (Figure 4.6). The myotubes appeared to be fully differentiated, as assessed by positive immunohistochemical staining with an antibody to myosin heavy chain and the aligned myotubes remained stably patterned for several weeks in culture (Figure 4.7). Similar micropatterning results were also achieved with primary cultures of rat skeletal myoblasts (Figure 4.7). The patterning of skeletal myoblasts also demonstrates the synergy between soluble cytokines and adhesive matrix components to spatiotemporally control cellular differentiation into organized tissue structures.

As another example of preserving protein structure, patterns of streptavidin printed onto glass were capable of specifically immobilizing biotinylated target molecules from a bulk solution (Figure 4.8). Retention of biotin binding is a property of the tetrameric form of streptavidin, thus if the protein had denatured during the

microcontact printing process, it would have irreversibly lost the ability to capture biotinylated molecules. These examples demonstrate that at least for relatively robust biomolecules, such as ECM and other globular proteins, protein function does not appear to be significantly impaired by microcontact printing.

4.4.5 Printing onto Protein Layers. After characterizing the microcontact printing of matrix proteins on various synthetic substrates, we also attempted to pattern matrix proteins on adsorbed protein layers. Successive patterning of proteins or printing onto adsorbed protein layers provides an avenue to spatially organize functional mimics of the extracellular matrix that includes multiple protein signals to instruct cellular behavior. This could be particularly important with matricellular proteins or immobilized growth factors, because their activities are often dependent on the content of the extracellular matrix in which they are presented.

ECM Patterns on Globular Protein Layers

Initially, adhesive matrix proteins were printed onto a non-adhesive protein layer of BSA. BSA is commonly used as a blocking agent because it is not thought to contain any specific peptide motifs to support cell adhesion. Patterns of collagen, laminin, and fibronectin were printed onto BSA-layers adsorbed onto glass slides or polystyrene dishes. The protein patterns were detected by fluorescent microscopy and each printed matrix protein demonstrated the ability to support cell adhesion, as expected. Cell response to a particular protein pattern varied depending on the cell type used and the appropriate choice of the matrix protein to support attachment. For example, cardiac and

skeletal muscle cells attached well to laminin patterned onto BSA-coated polystyrene, although fibroblasts attached poorly to the same laminin patterns. However, every cell type attempted adhered and was easily confined to fibronectin printed patterns on BSA. The observed differences in cell adhesion to distinct matrix protein patterns is likely attributable to the differences in the expression of integrin receptors on the surfaces of the cells. This system proved to be a simple method to specifically direct the adhesion of various cell types by creating adhesive protein domains on a non-adhesive protein background and was used in many future studies (see Chapters 5 & 6).

ECM Patterns on ECM Protein Layers

Based upon differences in cell adhesion to different matrix components, patterns of ECM proteins printed onto adsorbed layers of other matrix molecules could be exploited to direct cell attachment to particular regions of an overall "adhesive" surface. Thus, various ECM proteins were printed onto adsorbed layers of collagen, fibronectin or laminin. For example, line patterns of fibronectin could be stamped onto laminin-coated polystyrene dishes. NIH 3T3 fibroblasts or rat smooth muscle cells were seeded at comparable densities onto the surfaces and allowed to attach for a short period of time in serum-free conditions. The smooth muscle cells easily attached and spread on the adhesive matrix, but displayed no morphological response to the heterogeneous, spatially organized surface (Figure 4.9). On the other hand, the fibroblasts adhered strictly to the fibronectin patterns and spread in the direction of the lines (Figure 4.9). The contrast in adhesion between these two cell types is presumably attributed to inherent differences in the expression of particular receptors on these cells for either fibronectin or laminin.

This strategy can also be employed with a single matrix molecule by varying the concentration of the protein solution adsorbed onto the stamp and the substrate. Thus after printing, an adhesive gradient between higher and lower surface concentrations of the same molecule on a surface could be used to direct cell adhesion and spreading. As one example, patterns of fibronectin (adsorbed onto stamp at 25 μg/ml) were printed onto fibronectin-coated dishes (adsorbed at 2.5 μg/ml) and samples were seeded with either fibroblasts or smooth muscle cells. Fibroblasts attached rather uniformly across the surface, but they appeared to spread more along the line patterns printed with a higher concentration of fibronectin (Figure 4.9). Similarly, the smooth muscle cells appeared to preferentially attach and spread along the higher density fibronectin line patterns than on the intervening regions coated with less fibronectin (Figure 4.9). Differences in the adsorbed protein concentration affect not only ligand density but also structural conformation on the surface, which in turn is reflected by differences in cell adhesion and subsequent signaling events. This method could thus be exploited with a single protein to create organized, heterogeneous surfaces, in terms of ligand density and conformation, in order to convey differential spatial information to cells.

Matricellular Patterns on ECM Protein Layers

Thrombospondin-2 (TSP-2) and osteopontin can be classified as "matricellular" proteins, a class of molecules that modulate cell signaling and function and are distinct from the structural components of the ECM. Many of these matricellular molecules are specifically bound to ECM proteins and are localized to particular regions of a tissue during developmental, pathological or regenerative processes. To investigate whether

complex, spatially controlled interfaces of matricellular proteins could be organized on an ECM background, patterns of osteopontin or TSP-2 were printed onto protein-coated glass substrates. Fluorescent immunohistochemical analysis of osteopontin square patterns indicated that osteopontin islands were clearly defined on an otherwise adhesive background of fibronectin (Figure 4.10). Comparable patterns of osteopontin could also be printed onto BSA-coated glass substrates and rat aortic endothelial cells specifically attached to the osteopontin regions (Figure 4.11).

Thrombospondin has previously been shown to be inhibitor of endothelial cell adhesion and spreading, as noted by reduced focal contact formation.[156-158] Rat aortic endothelial cells were seeded onto TSP-2 square patterns printed onto an adsorbed layer of fibronectin on glass. The endothelial cells attached and spread on regions of the fibronectin, but seemed to largely avoid or spread around the printed islands of TSP-2 (Figure 4.12). The few cells that attached on large printed regions of TSP-2 remained more rounded and less spread than those on fibronectin, as indicated by phalloidin staining of the actin cytoskeleton (Figure 4.12).

4.5 Discussion

Microcontact printing of proteins is a simple and reliable method to rapidly generate protein patterns on most types of material surfaces. Printed patterns of matrix proteins can be used to spatially control the attachment of cells and provide a convenient method to study how cell shape can influence cell function. This has been demonstrated for a number of different extracellular matrix proteins using a variety of cell types to indicate the inherent flexibility of this micropatterning technique.

As described previously, the transfer of protein from the stamp to the substrate appears to be unidirectional and nearly 100% efficient when it works. Although the precise mechanism for the transfer is unknown, it has been suggested that keeping the drying time to a minimum is required for the pattern to be transferred successfully.[104] Proteins at interfaces tend to denature upon drying, and thus become more strongly bound to the surface. By printing immediately after drying the stamp, the proteins may remain only loosely adsorbed to the PDMS and transfer more easily to the substrate. However, these observations still do not necessarily indicate the mechanism for how and why protein transfer efficiency appears to be an "all-or-none" event. Our results suggest that the driving force for protein transfer during printing may be related to differences in wettability between the stamp and substrate since all of the substrates for printing were more hydrophilic than native PDMS. Proteins adsorb to the hydrophobic surface of the stamp presumably through van der Waals interactions, hydrogen bonding and/or electrostatic interactions and these forces appear to be sufficient to retain adsorbed protein species during solvent rinsing steps. However, after the protein-coated stamps are brought into contact with a substrate, all of the protein appears to be transferred within seconds. Although both the stamp and substrate are macroscopically dry during printing, atmospheric water is still present and could remain bound to the substrate and adsorbed protein layer on the stamp. The interaction between the bound water molecules could generate capillary forces that might be sufficient to "pull" the protein from the stamp to the substrate. In addition, low molecular weight PDMS can leach out from the stamps and has been identified within protein patterns stamped by microcontact printing.[159] The

transfer of this oily residue during printing might also facilitate the transfer of proteins, but this has not yet been carefully examined.

Printed protein patterns appeared to be relatively stable under a variety of conditions. Serum proteins did not appear to exchange with the printed molecules on the surface since the protein patterns appeared unchanged in serum-containing cell culture media. By printing onto adsorbed protein layers, protein-protein interactions might have served to stabilize the non-covalently bound patterns. The PDMS transferred with the proteins during printing might have also helped to stabilize the proteins.

For some applications, covalent coupling of micropatterned biomolecules is thought to be important for prolonged patterning integrity. Although the direct microcontact printing of proteins is inherently a non-covalent patterning technique, it can easily be combined with various covalent coupling chemistries to permanently attach molecules to surfaces. This can be done by stamping proteins onto a reactive surface that covalently links the immobilized molecule[160, 161] or by conjugating reactive moieties to the protein beforehand such that it can be crosslinked after printing.[162]

The printing of protein patterns onto adsorbed protein layers represents a novel approach to fabricating more complex molecular interfaces to engineer cell and tissue response. Most methods for the micropatterning of cells *in vitro* rely on depositing adhesive protein patterns juxtaposed with a non-adhesive surface chemistry on synthetic substrates. However, cells in their normal tissue environment don't typically encounter these sorts of synthetic materials or surface chemistries. Instead, cells are tethered to their surroundings through protein-protein interactions of cell surface receptors with extracellular matrix proteins. These specific molecular recognition events not only

mediate cell adhesion, but also initiate signal transduction cascades that ultimately translate into more macroscopic cellular events (i.e. proliferation, migration, apoptosis). Thus studying cells on micropatterned surfaces composed entirely of proteins is perhaps a more relevant model system to examine the native functional activities of ECM proteins.

The ability to pattern different adhesive proteins onto protein layers is also important because the normal extracellular matrix is composed of multiple adhesive biomolecules presented in parallel. Traditionally, cell adhesion studies to different extracellular matrix proteins are performed with separate homogeneous protein-coated surfaces. By simultaneously presenting two or more adhesive proteins on the same substrate, cell response to various matrix components can be more directly assessed. Patterning of matricellular proteins on adhesive matrix components provides another level of sophistication to spatially engineer functional matrices and this concept could be extended to include the patterning of other biomolecules as well, such as growth factors, antibodies or DNA, to further direct cell behavior. Thus by simply printing with different proteins and manipulating the geometric parameters of the patterning, the surface content of multiple protein species can be spatially controlled. This method represents a novel way to create spatially organized, heterogeneous mimetics of the native extracellular matrix in order to study cellular response.

4.6 Tables

Table 4.1. Proteins patterned via microcontact printing. A number of different proteins of various molecular weight, and other properties, were successfully patterned directly by microcontact printing.

Proteins	Molecular weight
Endothelin-1	2500
Osteopontin	32,000
Streptavidin	52,000
Bovine serum albumin	67,000
Thrombospondin	130,000
Collagen I	140,000
Fibronectin	250,000
Laminin	900,000
Gelatin	NA

Table 4.2. Advancing contact angle values for various substrates used for microcontact printing. Advancing contact angles (water in air) are listed for measured or reported values (taken from the literature; denoted by italics). A variety of materials with different surface chemistries were patterned by microcontact printing of proteins. Protein patterns could be printed from native PDMS stamps to surfaces that were less hydrophobic, suggesting a potential mechanism for the unidirectional transfer of proteins from the stamp to the substrate.

Substrate Material	Adv. Contact Angle	Protein Printing
Mica	*0-5°*	+
PDMS (oxidized)	*30°*	+
Glass	35°	+
Silicon	*36°*	+
Protein-layer (BSA)	37°	+
Gold	*60-80°*	+
Tetraglyme film	57°	+
Polystyrene	78°	+
PLGA	68°	+
Polyurethane	72-88°	+
PDMS (native)	100-*110°*	-
Teflon	*113°*	-

4.7 Figures

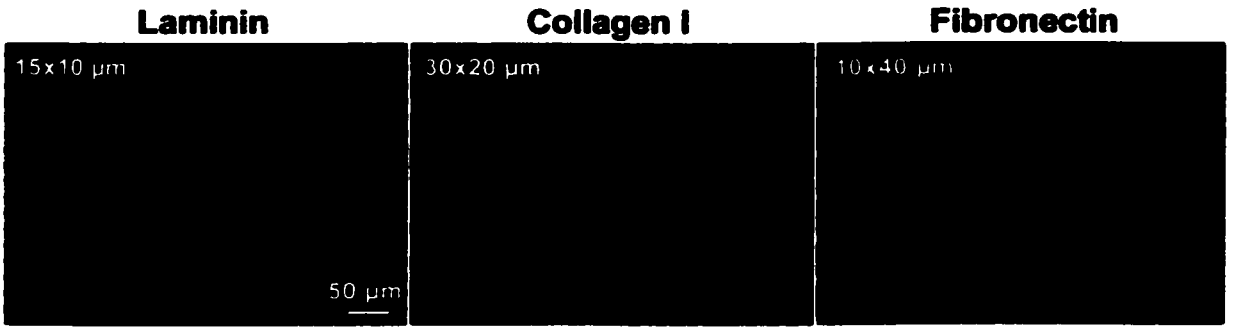

Figure 4.1. Printed patterns of extracellular matrix proteins. Extracellular matrix proteins such as laminin (left), collagen I (center) and fibronectin (right) were patterned directly by microcontact printing. Laminin and fibronectin were conjugated to Oregon Green 488™ before printing and collagen I patterns were immunostained with a primary antibody and a secondary TRITC labeled antibody after printing in order to visualize the patterns by fluorescent microscopy.

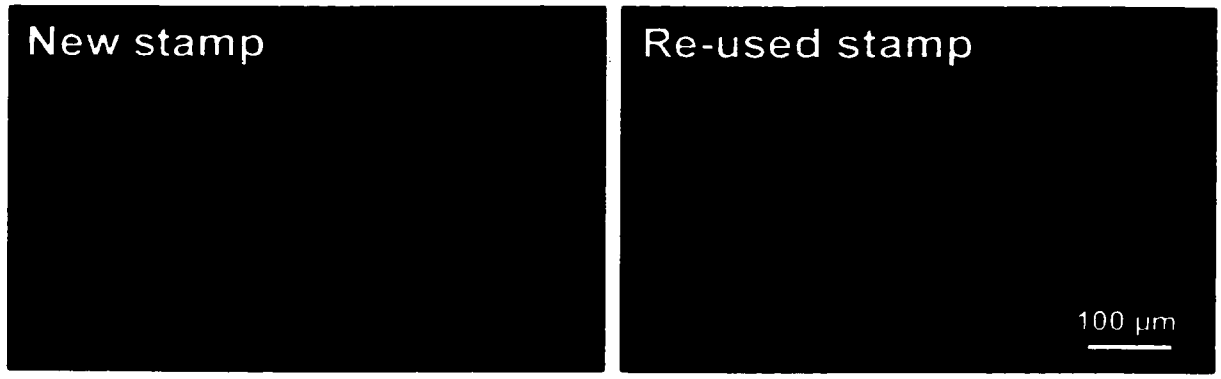

Figure 4.2. Comparison of printed protein patterns with a new and re-used stamp. A new stamp (20x20 μm lanes) and a used stamp (same dimensions), cleaned by an oxygen plasma treatment, were coated with a solution of fibronectin and printed onto glass slides. The resulting fibronectin patterns were detected by immunostaining with a primary fibronectin antibody and secondary antibody conjugated to rhodamine. New stamps produced better quality and more reproducible patterns than used stamps cleaned in this manner.

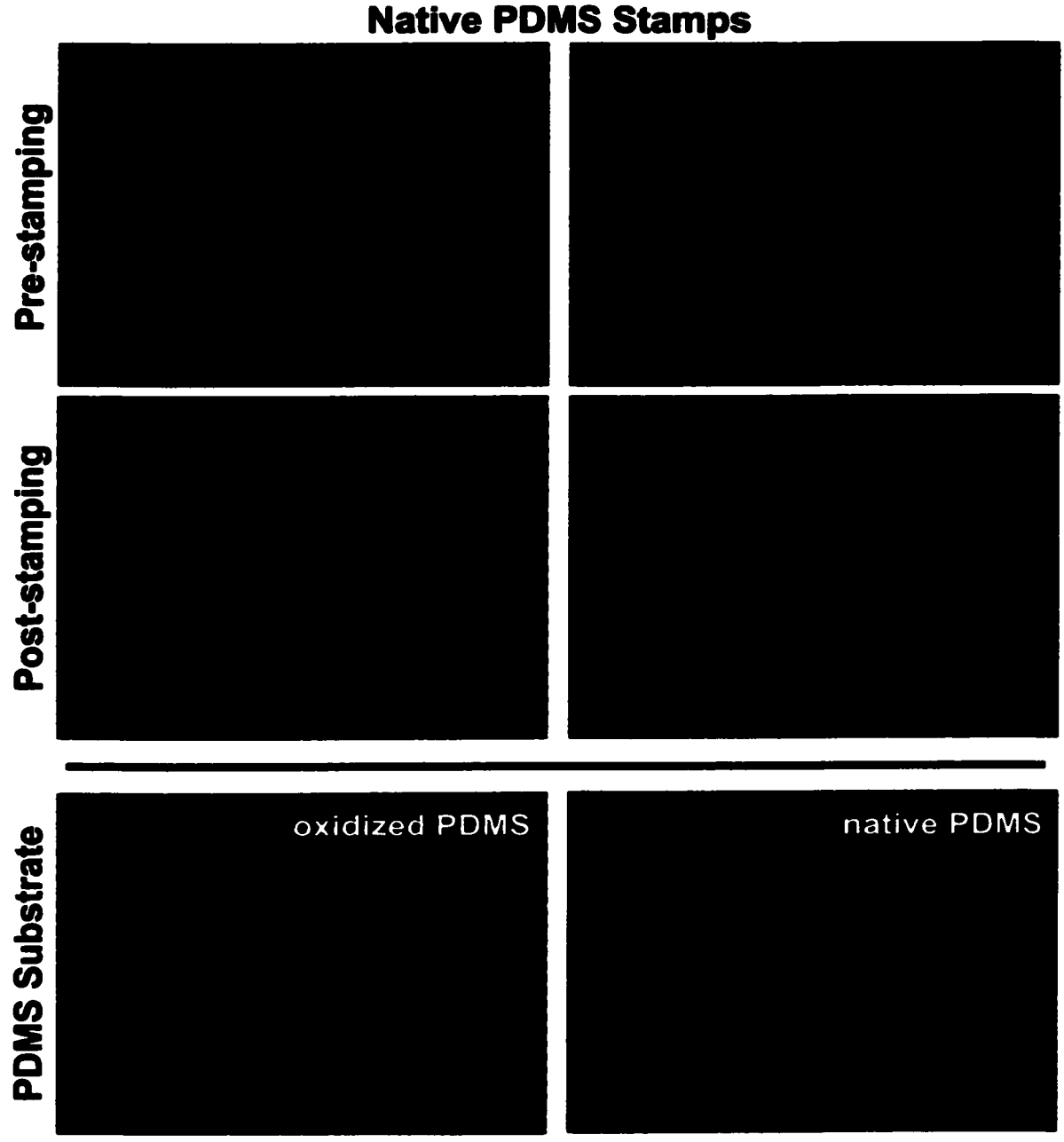

Figure 4.3. Protein printing onto PDMS substrates. Native PDMS stamps (30x20 μm lanes) were coated with rhodamine labeled BSA and printed onto either oxidized (left column) or native PDMS stamps (right column). The surface of the stamp was imaged immediately before (top row) and after printing (middle row), and images of the substrate were acquired after printing (bottom row). Protein patterns were readily transferred to the hydrophilic PDMS (oxidized), but not to the hydrophobic PDMS (native) substrates.

Figure 4.4. "Criss-cross" patterning of different protein species. Patterns of biotinylated BSA (b-BSA, 50x50 μm lanes) were printed onto glass slides (left) and the remaining surface area was blocked by adsorbing BSA from solution. Streptavidin lanes (50x50 μm) were printed orthogonally to the direction of the original protein patterns (center). Biotinylated BSA was rhodamine labeled and the streptavidin was labeled with Oregon Green 488™ (SA-OG) to permit visualization of the patterns by fluorescent microscopy. Rather than producing line patterns, the streptavidin appeared as squares that were localized between the b-BSA lanes (right). This suggested that primary printed regions prevented the secondary stamping of protein patterns.

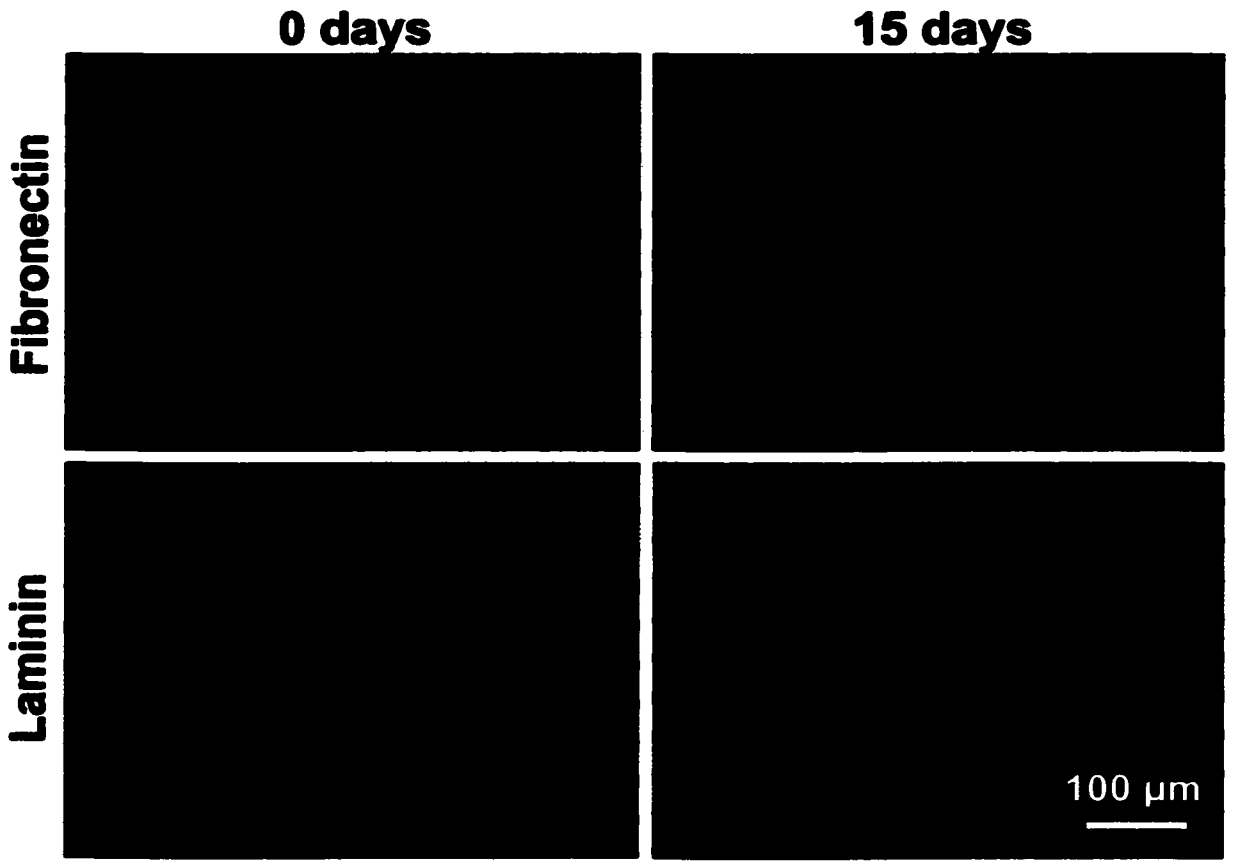

Figure 4.5. Stability of protein patterns exposed to serum-containing media. Printed patterns (30x10 μm lanes) of fluorescently labeled fibronectin (top row) or laminin (bottom row) on polystyrene dishes were incubated for several weeks in serum-containing cell culture media. The printed proteins appear to be stable on the surface since the morphology of the patterns appears unchanged over this period of time.

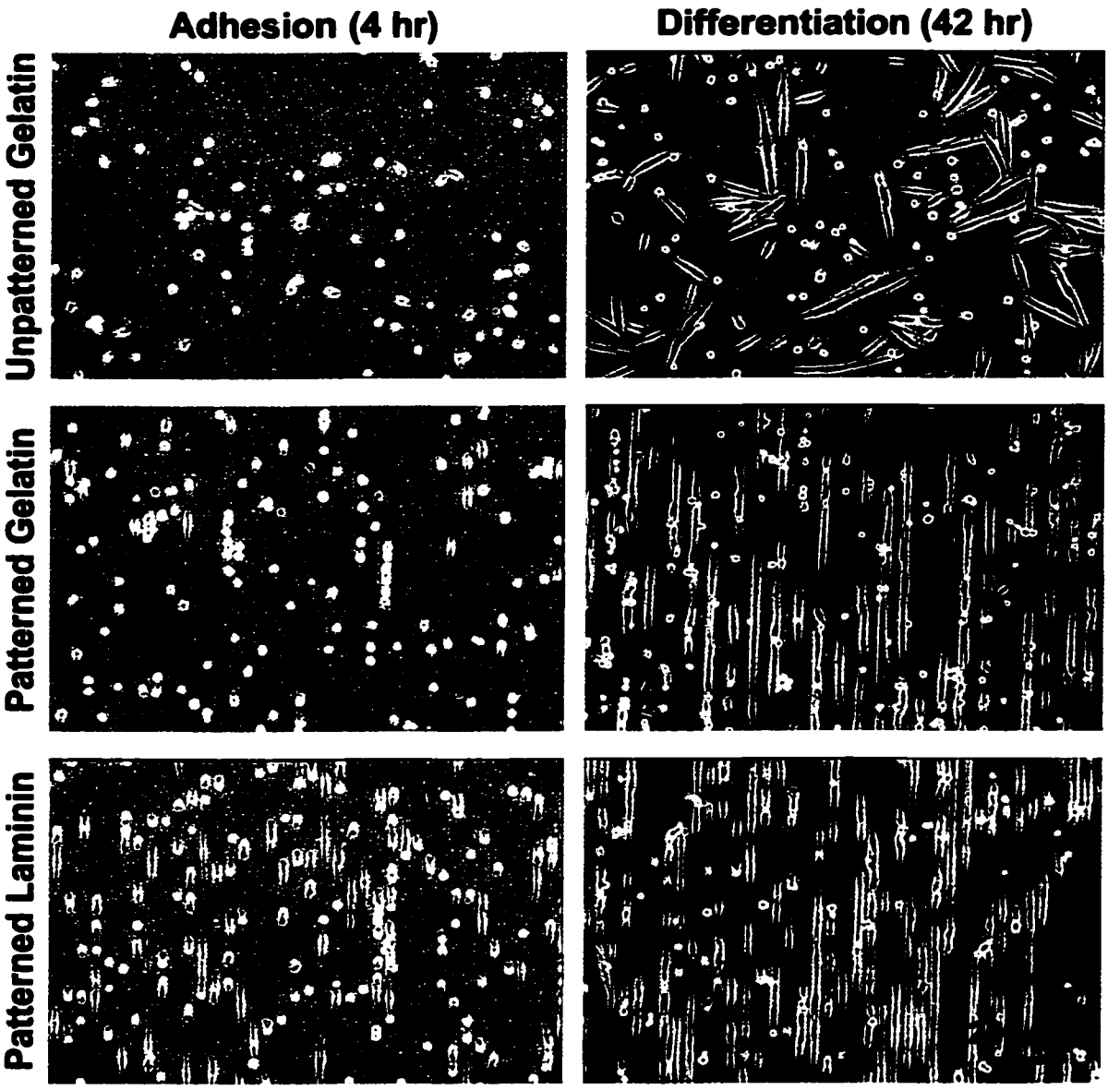

Figure 4.6. Patterning of mouse myoblasts and myotubes. MM14s were seeded onto either unpatterned gelatin polystyrene dishes or patterned gelatin or laminin dishes (15x20 μm lanes) and allowed to adhere for several hours before rinsing off non-adherent cells (left column). After being cultured in differentiation media for several days, the myoblasts fused to form multi-nucleated myotubes, a characteristic of differentiated skeletal myocytes (right column). Myotubes grown on the adhesive protein lanes were clearly elongated with the direction of the patterns, whereas the myotubes on unpatterned substrates displayed no preferred orientation.

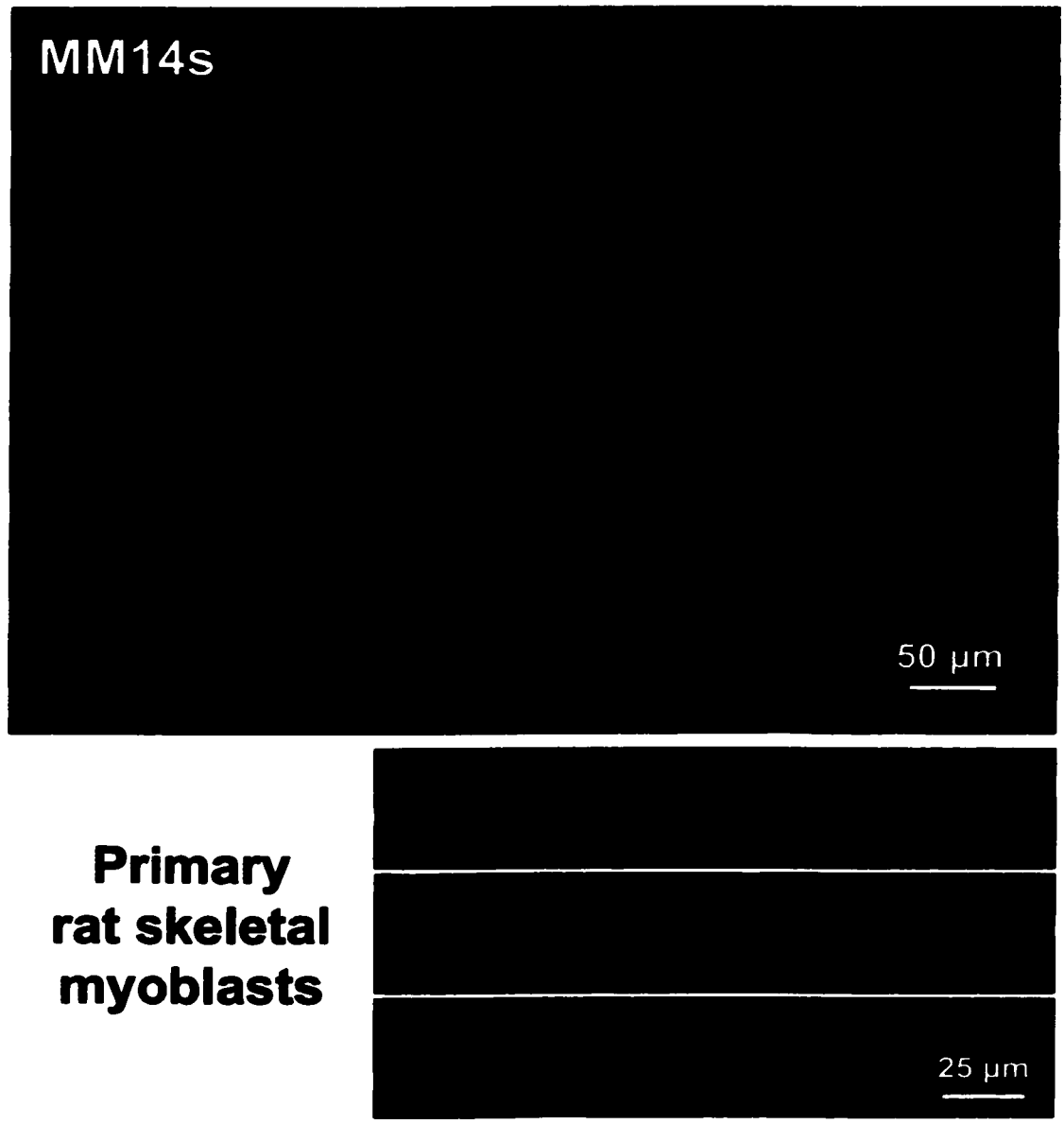

Figure 4.7. Skeletal myoblast differentiation along micropatterned lanes. Differentiation of patterned mouse myoblasts (MM14s, top panel) or primary rat skeletal myoblasts (bottom panels) was confirmed by immunohistochemical staining with an antibody to myosin heavy chain (MF20, green) after 7 days of culture. The MM14s were cultured on 15x40 μm lanes of fibronectin and the primary rat myoblasts were grown on 5x20 μm laminin lanes. The cell nuclei were counterstained with DAPI (blue). The differentiated myocytes formed multi-nucleated myotubes aligned along the protein patterned lanes.

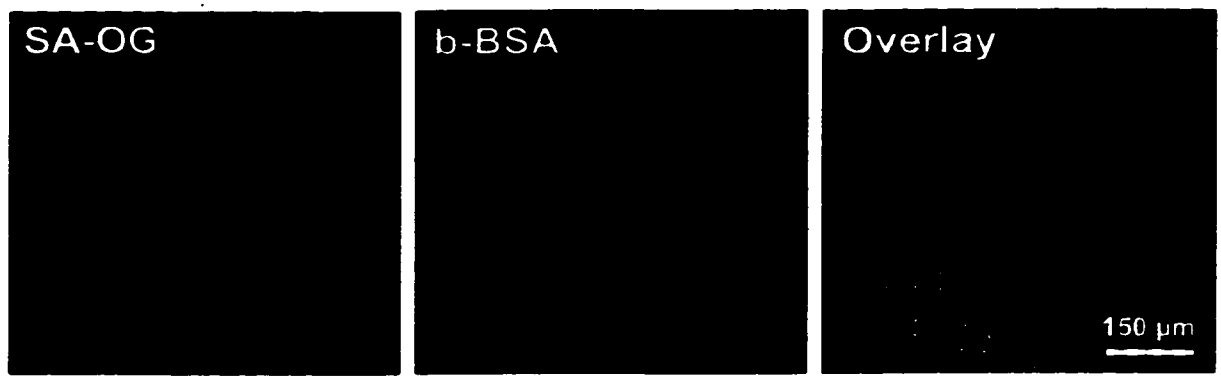

Figure 4.8. Printed patterns of streptavidin retain biotin binding capability. Fluorescently labeled streptavidin was printed onto a glass slide (20x20 µm lanes) and the remaining surface was blocked with a solution of BSA (left panel). A solution of biotinylated BSA, conjugated to rhodamine, was incubated and specifically bound to the surface in a similar pattern as the streptavidin printed lanes (middle panel). The spatial co-localization (yellow, right panel) of the two molecular species indicates that printed streptavidin retains its native ability to specifically bind biotinylated molecules. Therefore microcontact printing does not appear to inhibit the function of the stamped biomolecule.

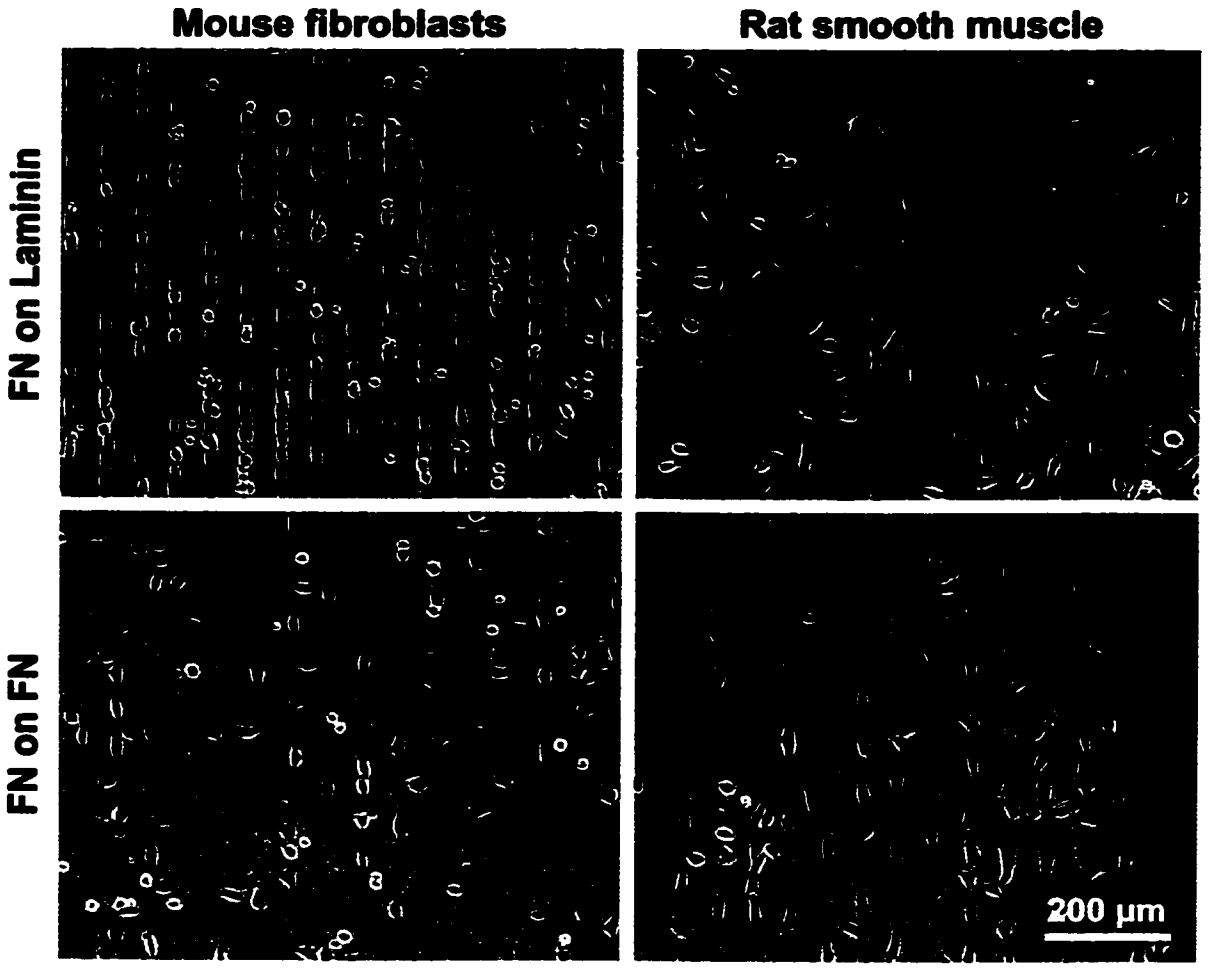

Figure 4.9. ECM protein printing onto adsorbed ECM layers. Fibronectin line patterns (15x40 µm) were printed onto either laminin-coated (top row) or fibronectin-coated polystyrene dishes (bottom row). The patterned fibronectin was adsorbed at 25 µg/ml onto the PDMS stamps and the laminin and fibronectin were pre-adsorbed onto the dishes at a concentration of either 4.5 µg/ml or 2.5 µg/ml, respectively. The patterned samples were seeded with mouse fibroblasts (NIH 3T3s) or rat smooth muscle cells in serum-free media and images were acquired after about 3 hours in culture. Fibroblasts attached and spread exclusively along fibronectin patterns on laminin (top left), whereas the smooth muscle cells exhibited no such preference for fibronectin over laminin (top right). Fibroblasts attached rather uniformly but spread more along higher concentrations of fibronectin printed onto lower concentrations of fibronectin (lower left), while smooth muscle cells adhered primarily along the lanes of fibronectin printed at a higher concentration (lower right). These examples demonstrate the ability of cells to specifically recognize patterns of competing adhesive extracellular matrix proteins.

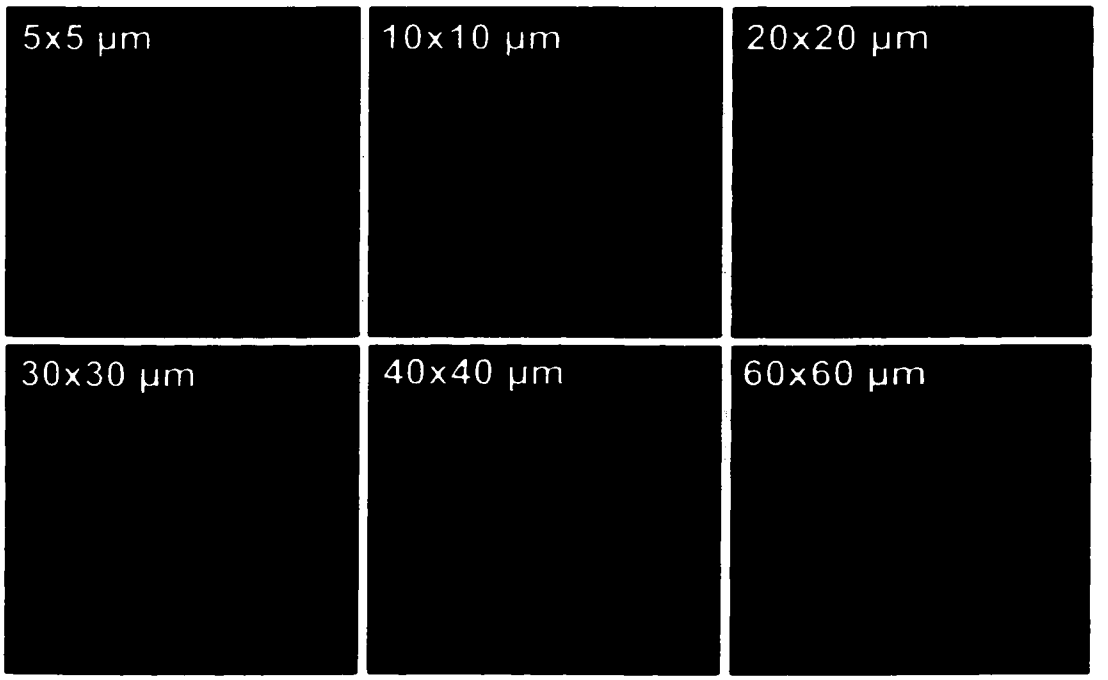

Figure 4.10. Square patterns of osteopontin printed onto fibronectin. Osteopontin square patterns were printed onto a glass slide pre-coated with fibronectin and the osteopontin islands were detected by immunostaining with a primary antibody to osteopontin and a secondary FITC-conjugated antibody. The square patterns ranged in size from sub-cellular dimensions (5x5 μm) to large islands (60x60 μm), much greater than the size of individual cells.

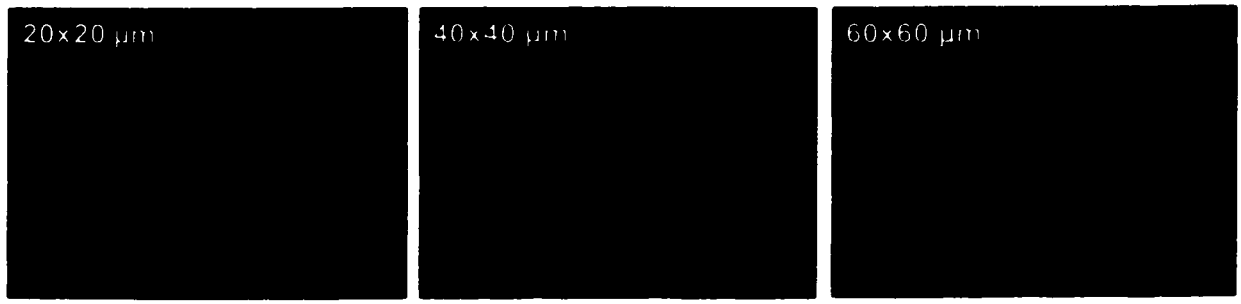

Figure 4.11. Endothelial cells patterned on osteopontin squares. Osteopontin square patterns (like those in Figure 4.10) were printed onto glass slides that were pre-coated with a layer of BSA. Endothelial cells were seeded onto the patterned surfaces and allowed to attach for about 2 hours before rinsing and fixing the adherent cells. The cells were stained with phalloidin to identify actin filaments. The cells were confined to the adhesive osteopontin islands. Smaller squares (20x20 μm & 40x40 μm) typically permitted enough surface area for only a single cell per island, whereas larger patterns (60x60 μm) often contained several cells within a single square.

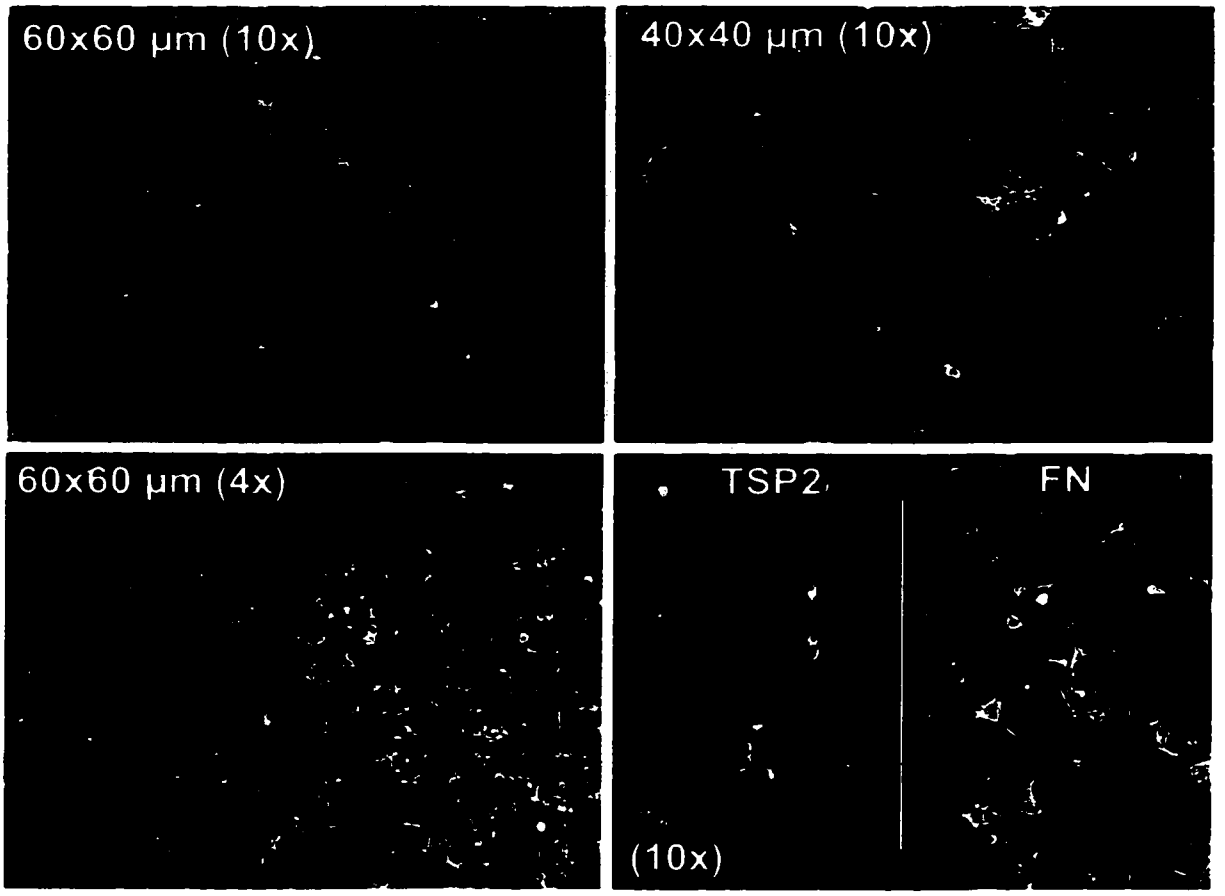

Figure 4.12. Endothelial cell response to printed patterns of thrombospondin-2 (TSP-2) on fibronectin. Square patterns of TSP-2 were printed onto glass slides that were pre-adsorbed with a layer of fibronectin. The cultures were fixed about 3 hours after plating the endothelial cells and stained with phalloidin to visualize actin filaments. The endothelial cells appeared to preferentially attach to the fibronectin regions and largely avoided the printed islands of TSP-2 as they spread (top row & bottom left). Endothelial cells that did adhere on large printed regions of TSP-2 (at the edge of the stamped pattern) did not spread well compared to adjacent cells on fibronectin (bottom right).

Chapter 5: *In vitro* Generation of Differentiated Cardiac Myofibers on Micropatterned Laminin Surfaces

5.1 Abstract

Cardiac muscle fibers consist of highly aligned cardiomyocytes containing myofibrils oriented parallel to the fiber axis and successive cardiomyocytes are interconnected at their ends through specialized junctional complexes (intercalated disks). Cell culture studies of cardiac myofibrils and intercalated disks are complicated by the fact that cardiomyocytes become extremely flattened and exhibit disorganized myofibrils and diffuse intercellular junctions with neighboring cells. In this study we sought to direct the organization of cultured cardiomyocytes to more closely resemble that found *in vivo*. Lanes of laminin 5-50 μm wide were microcontact-printed onto non-adhesive (BSA-coated) surfaces. Adherent cardiomyocytes responded to the spatial constraints by forming elongated, rod-shaped cells whose myofibrils aligned parallel to the laminin lanes. Patterned cardiomyocytes displayed a striking, bipolar localization of the junction molecules N-cadherin and connexin43 that ultrastructurally resembled intercalated disks. When laminin lanes were widely spaced, each lane of cardiomyocytes beat independently, but with narrow spacing, cells bridged between lanes, yielding aligned fields of synchronously beating cardiomyocytes. Similar cardiomyocyte patterns were achieved on the biodegradable polymer PLGA, suggesting that patterned cardiomyocytes could be used in myocardial tissue engineering. Such highly patterned cultures could be

used in cell biology and physiology studies that require accurate reproduction of native myocardial architecture.

5.2 Introduction

Spatially defined adhesive cues play important roles during biological development and later in directing tissue organization and repair in mature tissues. Recent advances in microfabrication have provided new approaches to control the spatial organization of proteins on surfaces in ways that mimic naturally occurring spatial cues.[142, 144, 163] Microfabrication techniques are thus providing important new avenues for investigating fundamental biological questions, including studies designed to define the relationships between cell shape and function.[136, 147, 148, 164] The ability to spatially organize cells into complex and differentiated structures is also providing new opportunities for developing better sensing, drug screening and tissue engineering technologies.[130, 137, 143, 165]

Cardiomyocytes in native myocardial tissue are organized into parallel cardiac muscle fibers with intracellular contractile myofibrils oriented parallel to the long axis of each cell and junctional complexes between abutting cells concentrated at the ends of each cardiomyocyte. This highly oriented cytoarchitecture is critical for the proper electromechanical coupling of cardiomyocytes to stimulate the transmission of directed contraction over long distances. In contrast, cultured cardiomyocytes typically spread to form an epithelioid sheet, with disorganized myofibrils and diffuse intercellular junctions, bearing little similarity to normal myocardial morphology.

Previous attempts to align cardiomyocytes *in vitro* have utilized etching or photolithographic techniques to generate linear surface features to support directed cell adhesion. The earliest studies of linearly oriented embryonic chick cardiomyocytes were performed by cutting channels into collagen films coated with agar or depositing a patterned thin film of palladium onto agar surfaces.[166] Later, more advanced photolithographic techniques permitted two-dimensional patterning of glass coverslips to longitudinally orient neonatal rat or mouse cardiomyocytes.[140, 167] Most of these previous studies have largely focused on engineering isolated strands of cardiac muscle to facilitate electrophysiological studies and are restricted to particular substrates due to the patterning methods.[168-173] These important studies have shown that conduction velocities and action potentials could be engineered by the micropatterning dimensions to recapitulate electrophysiological properties of normal or pathological myocardium, thus serving as model *in vitro* systems.

Here we used microcontact printing of laminin to establish an *in vitro* system in which spatially defined cues from the substrate guide cardiomyocyte alignment and the development of normal cytoarchitecture. Microcontact printing is a simple, versatile method to directly pattern adhesive proteins on a wide variety of surfaces, including common polystyrene dishes.[101, 104] Printed protein patterns provide a high resolution method to study and control how cardiomyocytes respond to spatial adhesion cues. We show that neonatal rat cardiomyocytes cultured on laminin lanes form rod-shaped cells with highly aligned myofibrils and bipolar intercalated disks. Such micropatterned cells form spontaneously beating myofibers that resemble those in native myocardium. This route to organizing cardiomyocytes into more natural structures should provide new

opportunities for studying their cell biology and physiology, and may also be of use for cell array-based screening and tissue engineering applications.

5.3 Methods

5.3.1 Preparation of Micropatterned Substrates. Laminin patterning was performed using microcontact printing as described in Chapter 2. Stamps approximately 1-2 cm^2 in size were coated with laminin at 45 μg/ml in PBS, pH 7.4 for 30-45 minutes at room temperature, and then rinsed and dried under nitrogen. Stamps were printed onto 35 mm polystyrene dishes (Falcon) which had been pre-incubated with 1% BSA in PBS overnight at 4°C, rinsed and then dried under nitrogen immediately prior to printing. Protein patterned dishes were stored in sterile PBS prior to cell plating. Thin PLGA membranes (85:15 composition) spin-coated onto glass coverslips were provided by Dr. Jonathan Mansbridge of Advanced Tissue Sciences, Inc. PLGA-coated coverslips were patterned as described above and secured with double-sided Scotch tape to 35 mm or 60 mm polystyrene dishes. Laminin lane pattern stability was assessed using laminin conjugated to Oregon Green 488™ (Molecular Probes).

5.3.2 Cell Culture. Cardiomyocytes were freshly isolated from the ventricles of 1-2 day old rat pups and cultured at 37°C, 5% CO_2 as described in Chapter 2. After isolation, the cells were plated onto the patterned 35 mm polystyrene dishes and allowed to attach overnight (15-17 hours). The plates were rinsed with Dulbecco's phosphate buffered saline (DPBS, pH 7.4) to remove non-adherent cells, and then re-fed with culture media containing 1 _M cytosine arabinofuranoside (ara-C, Sigma) to prevent fibroblast

overgrowth. Thereafter, cultures were re-fed with ara-C containing media every 2-3 days.

5.3.3 Immunostaining. Cardiomyocyte cultures were fixed for 2-3 minutes with 3% paraformaldehyde (PFA) in PBS, pH 7.4, 5 mM EGTA, 0.2% Triton X-100 at room temperature and then fixed with 3% PFA in PBS for 30 minutes. The samples were blocked with 2% rabbit serum in PBS for 1 hour at room temperature or overnight at 4°C; all subsequent antibodies and stains were diluted in the same blocking buffer. Samples were treated with primary antibodies to sarcomeric myosin heavy chain (MF20), connexin43 (Chemicon), or pan-cadherin (Sigma) as described.[38] Primary antibodies were incubated for 60-90 minutes at room temperature, followed by a secondary rabbit anti-mouse FITC-conjugated antibody (DAKO, 1:20) at room temperature for 60-90 minutes or overnight at 4°C. Lastly, the cells were counterstained with BODIPY phalloidin 558/568 (Molecular Probes, 1:100) to detect actin filaments and DAPI (Sigma, 1:500) to detect nuclei, mounted with Vectashield media (Vector), coverslipped and stored in the dark at 4°C prior to microscopy. Cardiac tissue from adult rats was embedded in OCT (Miles Scientific) and cryosectioned at 5 μm. Sections were dried overnight, fixed and immunostained for connexin43 and N-cadherin as described for the cultured cells.

5.3.4 Morphometric Analysis. Cardiomyocytes were seeded onto either laminin micropatterned or unpatterned dishes at a subconfluent density (~50,000 cells/35 mm dish) in order to clearly assess the borders of individual cells. The cells were fixed after 2

days of culture, allowing sufficient time for full cell spreading following attachment. The cultures were immunostained, as described, and cardiomyocytes were specifically identified as myosin heavy chain positive and contained striated actin filaments visualized by phalloidin staining. Fluorescent images of a number of fields from the different samples were acquired and the sarcolemmal perimeter of individual cells was traced using NIH Image software in order to quantify cell shape parameters such as, 2D projected area, the length of the major and minor axis, and the angle of the major axis. Based on the raw data, calculations of the aspect ratio (defined as the major axis divided by the minor axis) and the alignment of cells with respect to the primary axis of patterned lanes could be obtained. Data was collected for at least 100 cells at each experimental condition and the results are reported as the average mean values ± standard deviations.

5.3.5 Microscopy. Fluorescent, phase and time-lapse microscopy were performed as described in Chapter 2. For electron microscopy, cultures were fixed with Karnovsky solution in 0.1% cacodylate buffer, processed through a graded alcohol series and propylene oxide, and embedded in LR/White plastic (Polyscience, PA) in the tissue culture dishes. Random areas were cut out and thin-sectioned *en face*. Rat heart samples were fixed and processed with the same solutions. Cell culture and tissue thin sections were post-stained with uranyl acetate and lead citrate, and examined with a JEOL electron microscope (JEM-1200EXII).

5.3.6 Quantifying Contraction Rates. Video microscopy of various fields ($n \geq 3$) was acquired for each experimental condition examined (i.e. different lane widths and

spacing, effect of ara-C treatment, different adhesive matrix proteins). The number of "beats" of single lanes of cardiomyocytes were counted over a 30 second period of time by visual inspection of the video data. The contraction rates are reported as the mean beat per minute rate of individual cardiomyocyte lanes.

5.4 Results

5.4.1 Cardiomyocyte Patterning. Spatially defined laminin patterns on a non-adhesive background were constructed by microcontact printing onto a BSA monolayer applied to polystyrene dishes (Figure 5.1 insets). Protein patterns were stable in aqueous buffer or in serum-containing media at 37°C in the absence of cells for at least 4 weeks. Cell adhesion was strictly directed along the micropatterned laminin lanes (Figure 5.1). Rat neonatal cardiomyocytes took 2-6 hours to attach and spread on the laminin lanes as assessed by time-lapse video microscopy, and the cells displayed very little motility along the lanes thereafter. Because most neonatal cardiomyocytes are non-proliferative, cell coverage of the laminin lanes largely depended upon the initial seeding density and subsequent cell spreading. At seeding densities of 250,000-400,000 cells/35 mm dish, there were many gaps between cells along individual lanes at 18-24 hours; by the next day the patterned lanes became almost completely filled due to additional cell spreading (Figure 5.2). After 48 hours, nearly all of the cardiomyocytes had formed cell-cell junctions with adjacent cells in the same lane and were contracting. However, preliminary experiments indicated that by 6 days the patterned cultures appeared largely disrupted and fewer beating cells were observed on the surface (Figure 5.2).

Although cardiac fibroblasts constitute less than 10% of the primary cell population, when permitted to proliferate they comprised 50-60% of the cells within 4 days. Due to their ability to move between lanes and remodel the extracellular environment, fibroblasts eventually degraded the aligned cardiomyocyte patterns. To limit undesirable effects of fibroblasts, cultures were treated with ara-C to kill proliferating cells (cardiomyocytes are relatively unaffected by ara-C because they are post-mitotic). A 1 μM ara-C concentration inhibited fibroblast growth and preserved cardiomyocyte patterning for as long as 10 days (longest time examined) (Figure 5.3). Ara-C did not affect the development of cardiomyocyte cell-cell junctions or contractile activity (discussed further below).

5.4.2 Geometric Dependence of Cardiomyocyte Organization. A systematic study of laminin pattern width and spacing was conducted to establish the optimal adhesive domain geometry for cell alignment, the orientation of contractile myofibrils, and the formation of cell-cell-junctions. On lane widths of 5-15 μm, cells were highly elongated and only single cells spanned the width of each lane, whereas 30 μm lanes could accommodate 1-2 adjacent cells and 45-50 μm lanes contained up to 4 adjacent cells.

The dimensions of typical adult rat ventricular cells *in vivo* are 15-30 μm in diameter by about 100-130 μm long.[174, 175] Ventricular cardiomyocytes in the developing rat heart have cross-sectional diameters of about 6 μm at birth and this dimension increases to about 14 μm by 60 days;[176] cardiomyocyte length undergoes a comparable relative increase during this period. To determine how the dimensions of neonatal rat

cardiomyocytes were affected by culture on laminin lanes, a number of cell shape parameters were calculated for individual cells on various lane widths (Figure 5.4).

A slight increase in 2D projected cell area was observed as the width of the patterned laminin lanes was increased (Figure 5.5). Cell area on the widest lanes ($\geq$ 30 μm) approached that of spatially unrestricted cardiomyocytes on unpatterned laminin substrates, presumably because the wider lanes allowed single cells to spread fully.

Length and width measurements of single patterned cardiomyocytes were calculated as a further measure of cell size (Figure 5.6). As expected, the width of the cells was constrained to the width of the patterned lanes and thus increased as the lane width increased. Elongation of the cells (length along the major axis) decreased slightly as lane width increased, indicating that narrower lanes, especially at the dimensions of individual cells (5-15 μm), induced greater cell extension along the primary axis of the patterned lanes. The length and width measurements were used to calculate the aspect ratio of individual cardiomyocytes, by dividing the length by the width. The mean aspect ratio decreased from approximately 9 to 3 as lane width increased from 5 to 30 μm (Figure 5.7). *In vivo*, cardiomyocytes typically display an aspect ratio of about 3-7, depending upon the maturity of the cells and their location in the heart.

Cardiomyocyte alignment was measured with respect to the primary axis of the patterned lanes in order to reflect how well the cells were linearly oriented by the micropatterning. As lane width increased, the cells were less tightly constrained and thus became slightly less aligned with the direction of the laminin lanes (Figure 5.8). However, even at lane widths (i.e. 30 μm) which did not exert a pronounced influence on the aspect ratio of cardiomyocytes, a high degree of alignment was still observed by the

patterning. In contrast, cardiomyocytes on unpatterned surfaces showed no apparent indication of preferential alignment on the substrate, as expected. In fact, cells with no imposed spatial restraints would be expected to display a random orientation, thus the average "alignment" should be about 45° from the normal with a large standard deviation, which is exactly what was observed (Figure 5.8).

While we were unable to obtain accurate measurements of cell heights, it was evident that cardiomyocytes grown on 5-15 μm laminin lanes had a much more 3-dimensional cell topology compared to those grown on wider lanes (i.e. 30 or 45 μm) or unpatterned laminin (Figure 5.9). However, fewer cells developed end-to-end contact with adjacent cells on 5 μm lanes, whereas most of the cells on 10-20 μm lane widths also contained single cells per lane width, but made bipolar cell-cell contacts and covered most of the lane surface area. Although lane coverage was largely dependent on the cell plating density, these data suggested 5 μm lanes were too narrow to support optimal cell adhesion and junction formation.

5.4.3 Myofibril Alignment. The mechanical work of cardiomyocytes in heart tissue requires myofibril alignment parallel to the long axis of cardiac muscle fibers. Since the myofibrils in cardiomyocytes grown on unpatterned surfaces are randomly aligned, it was of interest to determine whether their orientation would be influenced by growth on laminin patterns. Immunostaining with a myosin heavy chain antibody (Figure 5.10), as well as electron microscopic analysis, indicated that myofibril orientation was strongly aligned by culture on laminin lanes. Patterned cells had a high density of parallel myofibrils, while the myofibrils in cells grown on unpatterned laminin were in disarray

and often branched at acute angles (Figure 5.11). Like normal myocardium, sarcomeres in patterned cultures were often in register across an entire cell width, and the average widths of myofibrils closely resembled those in the neonatal rat heart. In addition, the myofibrils on both sides of junctions between patterned cardiomyocytes were oriented in the same direction, while in unpatterned cultures, myofibrils often occurred at random orientations relative to those in the adjoining cell (Figure 5.11). The elongated shape of mitochondria and their locations between myofibrils in patterned cells were also more similar to that observed in native myocardial tissue. These results demonstrate that cardiomyocytes respond to the imposed adhesive cues by organizing normal myofibril structures over long distances in a manner very similar to that found *in vivo*.

5.4.4 Formation of Intercalated Disks. Cardiomyocytes in heart tissue connect to the abutting cells within cardiac muscle fibers by intercalated disk cell-cell junctions containing N-cadherin and connexin43. These proteins play key roles in adherens and electrochemical gap junctions. If cardiomyocytes on laminin lanes exhibited localized concentrations of N-cadherin and connexin43 and cytoarchitecture resembling intercalated disks, this could potentiate the transmission of cell-to-cell linear electrochemical signals as occurs *in vivo*.

When cardiomyocytes were cultured on lane widths similar to adult cellular diameters, i.e. 15-20 μm, they responded by forming precisely aligned and bipolar cell-cell junctions. Expression of N-cadherin was visible by immunostaining after one day *in vitro* and increased in intensity over the next 48 hours. N-cadherin was concentrated at

the bipolar cell junctions in discrete bands that resembled intercalated disks (Figure 5.12). In contrast, on wider laminin patterns of 30-50μm, which accommodated 2-4 cells per lane-width, some N-cadherin staining was observed along both the short and the long axes of adjacent cardiomyocytes. The gap junction protein connexin43 was also observed predominantly at the bipolar cell junctions (Figure 5.12), and its localization appeared more punctate than the concentrated bands of N-cadherin. In cardiomyocytes grown on unpatterned laminin, a similar time course of N-cadherin and connexin43 appearance was observed, but the staining was not distributed in the bipolar fashion found in native tissue. Instead, it occurred circumferentially around the cell perimeter, wherever there was contact between cells (Figure 5.12). Electron microscopy showed that the junctions between patterned cells resembled normal intercalated disks found *in vivo* (Figure 5.13), and that they contained both desmosomes and intermediate (adherens) junctions.

5.4.5 Contractile Activity. Contraction of individual cells was first detected about 24 hours after plating and by 48 hours, after the formation of intercalated disks, entire lanes of cardiomyocytes were beating in synchrony. Contraction rates of the patterned cardiomyocytes reached maximal levels of ~150 beats/min after 3-4 days in culture. Preliminary experiments indicated that cardiomyocytes patterned on different matrix proteins (either laminin or gelatin lanes) did not exhibit any significant differences in contraction rates (Figure 5.14). The effect of ara-C treatment (10 μM) on contraction rate was also examined for patterned and unpatterned cultures on laminin and no significant differences were observed, suggesting that the ara-C did not adversely affect

cardiomyocyte function (Figure 5.15). In addition, no significant differences in contraction rates were observed for cardiomyocytes cultured on different adhesive lane widths, which suggested that constraining the cells did not appear to affect their inherent contractile behavior (Figures 5.14 & 5.15).

However, the beat synchrony between adjacent lanes was related to the spacing distance between lane patterns. This resulted from the biophysical capability of the cells to extend "bridges" between adjacent lanes. Many cell bridges across lanes were observed with 10 μm separation distances, leading to a high degree of contraction synchrony between adjacent lanes (Figure 5.16). Significantly fewer bridges were observed as the spacing was increased (i.e. 20 and 40μm separation distances) and 80 μm spacing essentially inhibited cardiomyocyte bridging between lanes, thus adjacent lanes beat asynchronously (Figure 5.16).

5.4.6 Organization on PLGA Surfaces. To determine whether microcontact printing and cardiomyocyte patterning could be performed on biodegradable synthetic polymer surfaces, such as those commonly used in tissue engineering scaffolds, laminin lanes were printed onto thin PLGA films. Analysis of laminin persistence beneath cell lanes (Figure 5.17 inset) showed a lower fluorescent intensity and a pitted appearance after 5 days in culture, consistent with the degradation of PLGA in the aqueous culture media. The alignment, cytoarchitecture and contraction of cardiomyocyte patterns on PLGA were comparable to those on polystyrene for at least a week (longest time assessed), suggesting that PLGA could be used as a transient scaffold for patterning cardiomyocytes (Figure 5.17).

5.5 Discussion

These studies indicate that microcontact printing can be used to create patterns of extracellular matrix proteins that organize cardiomyocytes into fibers that resemble those found in native tissue. While multi-cellular strands of cardiomyocytes have been organized on photolithographically patterned chemical surfaces, microcontact printing of matrix proteins is less technically demanding than photolithography and compatible with many substrate materials. Microcontact printing should thus provide a convenient method for studying extracellular matrix-cell interactions, as well as developmental and physiological questions pertaining to the mechanisms of myofibril, sarcoplasmic reticulum, and intercalated disk formation, and the electromechanical coupling of cardiomyocytes.

We have shown that neonatal rat cardiomyocytes form highly organized arrays in response to spatially controlled adhesive cues. The cardiomyocytes assume rod-like geometries comparable to adult cardiomyocytes *in vivo* and develop highly aligned myofibrils with normal diameters and bipolar cell junctions with intercalated disk connections that include spatially localized N-cadherin and connexin43. The resulting cardiomyocyte organization closely resembles that found in native tissue. In addition, by controlling the distances between laminin lanes, cardiomyocytes in adjacent lanes can be engineered to contract independently or in synchrony.

A recent study by Thomas et al.[167] reported on the electrophysiological properties of neonatal mouse cardiomyocytes grown in strands 35-86 μm in diameter, guided by photolithographic patterning of cover slips that directed subsequent serum protein

adsorption. They found that conduction velocities and action potentials were faster and closer to the values of adult mouse myocardium in cardiomyocytes grown in strands versus randomly oriented cultures. These physiological measurements complement our structural and molecular observations, and provide further evidence that spatial organization can direct cardiomyocyte cytoarchitecture to resemble that observed *in vivo*.

In addition to their usefulness for studies of cardiac cell biology and physiology, patterned cardiomyocyte cultures should be well suited to array technologies for screening and diagnostic applications that require better reproduction of myocardial architecture and synchronized contraction. Also, since the micropatterning technique can be readily applied to biodegradable polymeric substrates such as PLGA, micropatterning strategies could be used for controlling the development of oriented muscle for cardiac tissue engineering applications. These strategies complement those of other investigators who have incorporated cardiomyocytes into three-dimensional synthetic and natural polymer matrices.[59, 65, 67] The resulting organization of cardiomyocytes into highly aligned arrays with natural cytoarchitecture and cell junctions could greatly improve engineered tissue function.

5.6 Figures

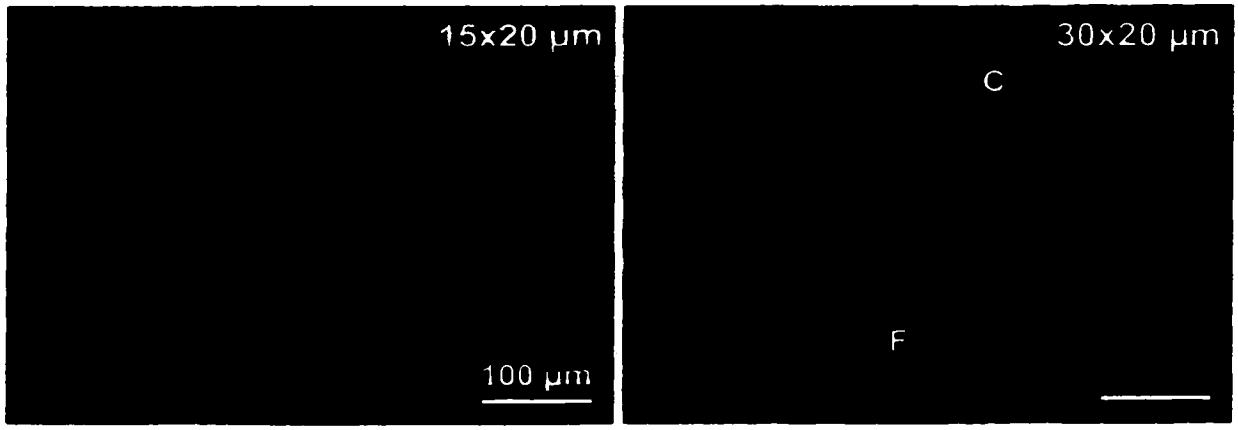

Figure 5.1. Rat neonatal cardiomyocytes cultured on laminin lane patterns either (left) 15 μm laminin lanes spaced 20 μm apart (15x20 μm) or (right) 30 μm laminin lanes spaced 20 μm apart (30x20 μm). Cardiomyocytes were fixed after 4 days in culture and stained with phalloidin (actin filaments, red) and DAPI (nuclei, blue) prior to visualization by fluorescent microscopy. Based on light versus intense phalloidin staining, the bridging cells can be identified as fibroblasts (F) or cardiomyocytes (C), respectively. These fields were selected to illustrate cell bridging between adjacent lanes. Insets show laminin patterns at the corresponding dimensions; laminin was conjugated to Oregon Green 488™.

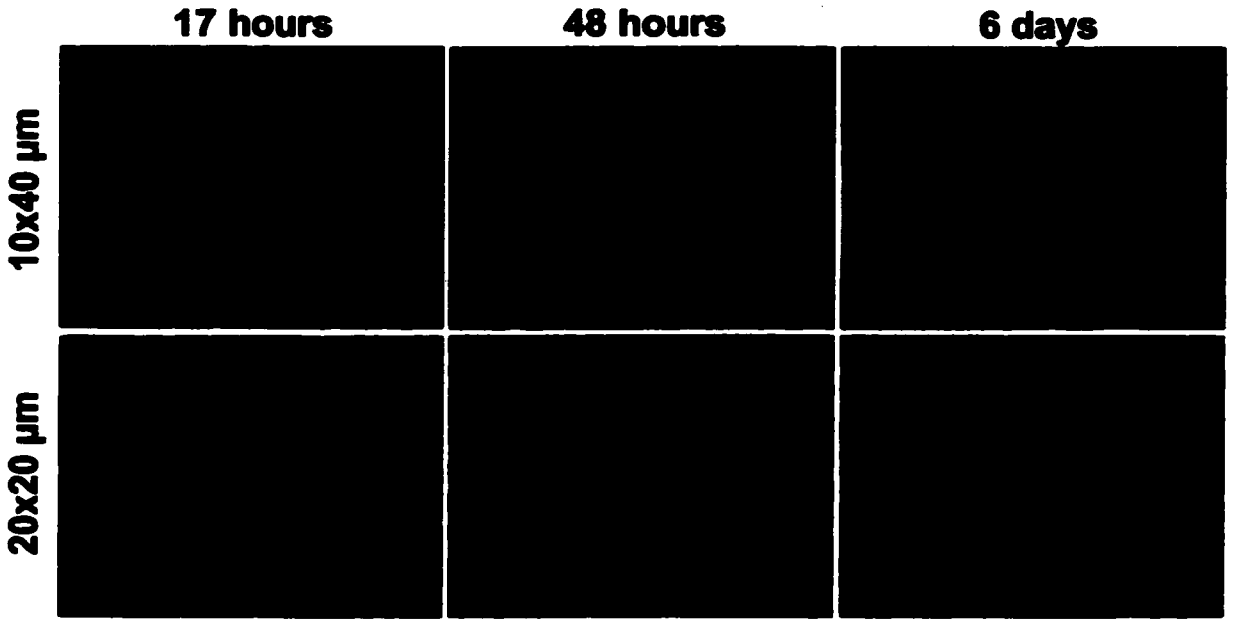

Figure 5.2. Time course of cardiomyocyte morphology on micropatterned laminin lanes. Micropatterned cardiomyocyte cultures (top row:10x40 µm, bottom row: 20x20 µm) were fixed over a series of days and stained with phalloidin (actin filaments, red) and DAPI (cell nuclei, blue) to visualize the cells. The cells attached overnight and took a few days to fully spread along the lanes, but the cell patterning integrity was disrupted by 6 days as the fibroblasts appeared to overgrow the cultures. These cultures were not treated with ara-C.

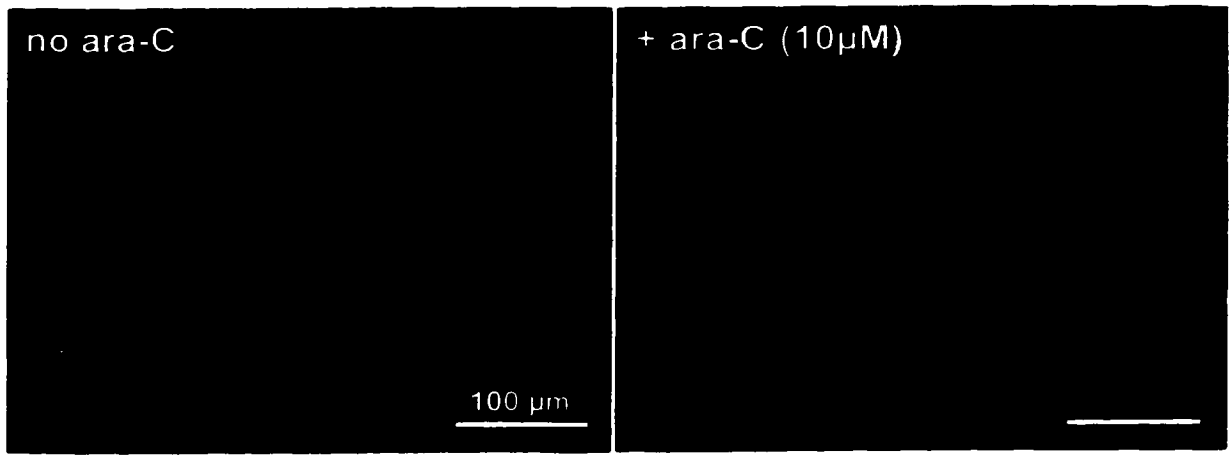

Figure 5.3. Effect of ara-C treatment on cardiomyocyte patterning. Micropatterned cultures (20x20 μm) were fixed after 6 days and stained with phalloidin (actin filaments, red) and DAPI (cell nuclei, blue) to visualize the cells. At a concentration of 10 μM, the ara-C inhibited fibroblast proliferation and the integrity of the patterned cardiomyocyte lanes was retained. Further experiments indicated that a minimum concentration of 1 μM ara-C effectively prevented fibroblast overgrowth of the cultures and thus the lower ara-C concentration (1 μM) was used in most future experiments.

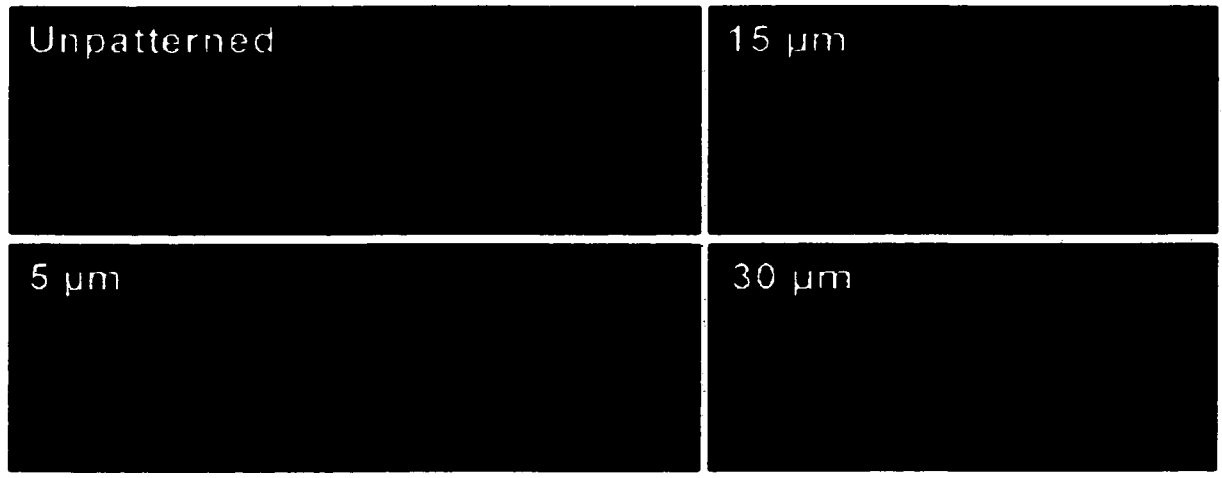

Figure 5.4. Individual cardiomyocytes cultured on micropatterned laminin lanes. Cardiomyocytes were plated at subconfluence, fixed after 3 days in culture, stained with an antibody to myosin heavy chain (MF20, green) and counterstained with phalloidin (actin filaments, red) and DAPI (nuclei, blue). Cardiomyocytes were clearly identified as MHC+ cells and by the striated organization of actin filaments within myofibrils. The perimeter of the cell bodies were traced using NIH Image software in order to acquire measurements of cellular dimensions.

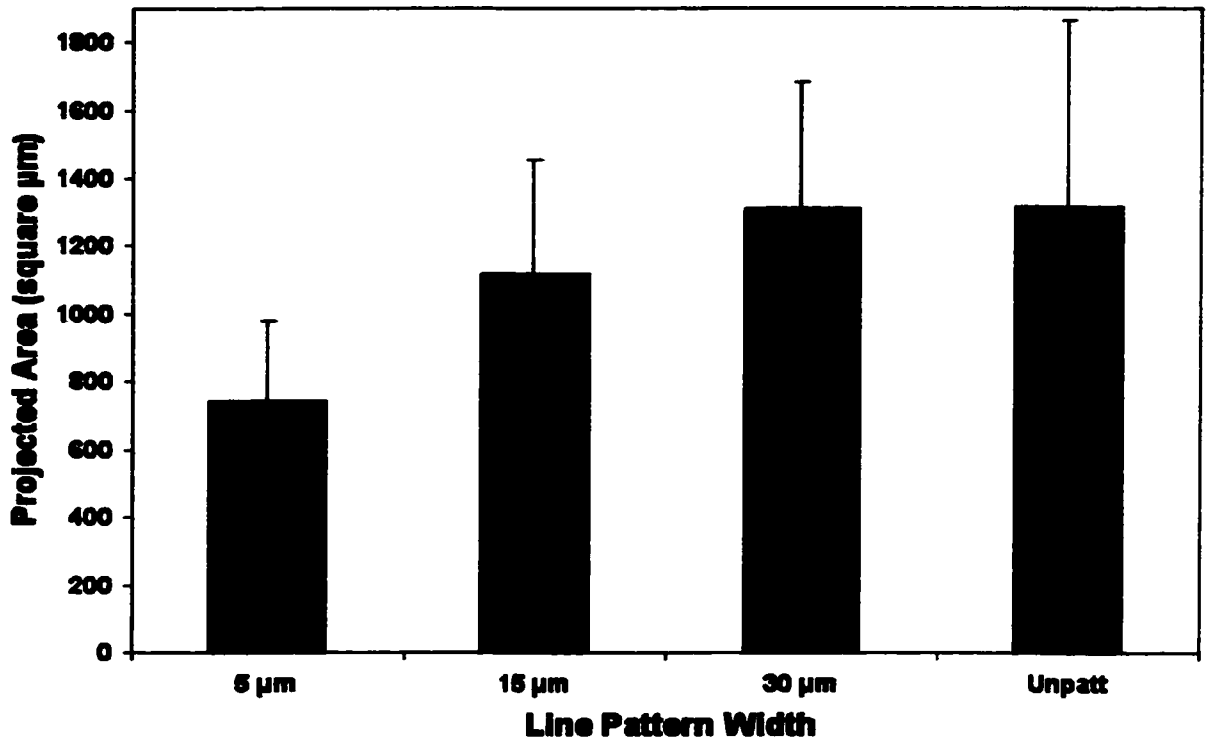

Figure 5.5. Measurement of projected cardiomyocyte area on micropatterned laminin lanes. Cardiomyocytes were plated at subconfluence, fixed after 3 days in culture and traced using NIH Image software to automatically calculate area measurements. A minimum of 100 cells ($n \geq 100$) was measured for each lane width and the mean values ± standard deviations are plotted. Cell area increased with increasing line width up to about 30 µm wide lanes, at which point cardiomyocytes appeared equally spread as on unpatterned laminin surfaces.

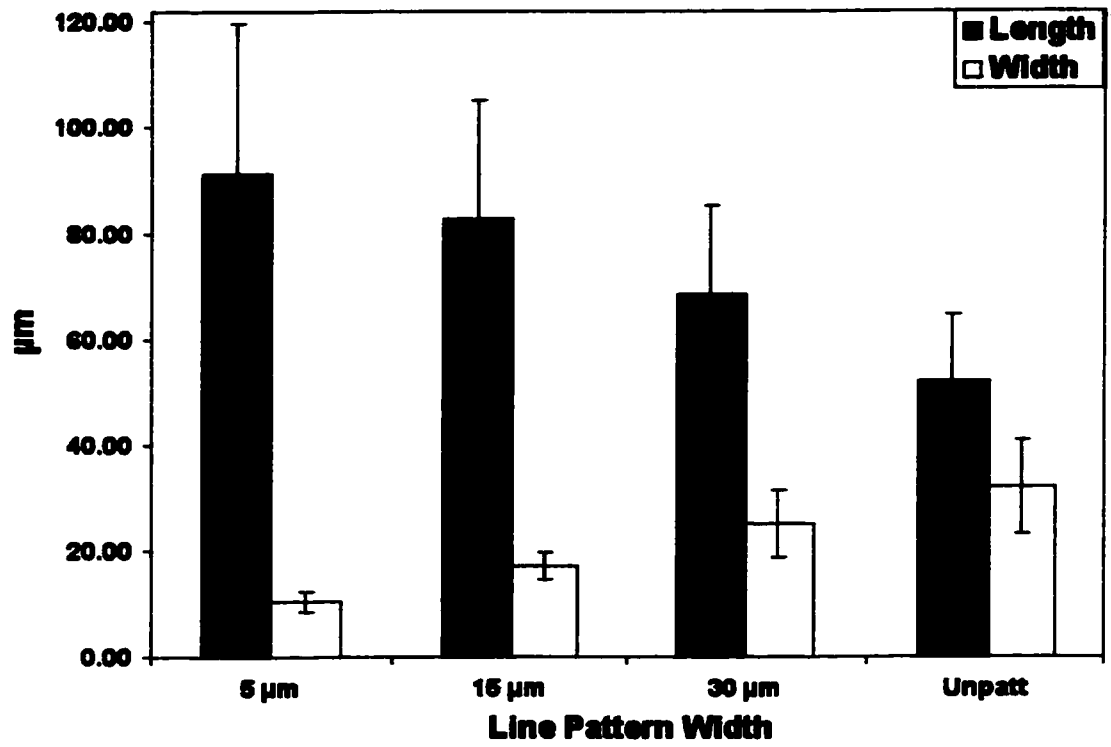

Figure 5.6. Measurements of cell length and cell width along the major and minor axis, respectively, of spread cardiomyocytes. Cardiomyocytes were plated at subconfluence, fixed after 3 days in culture and traced using NIH Image software to automatically calculate cell length and width. A minimum of 100 cells ($n \geq 100$) was measured for each lane width and the mean values ± standard deviations are plotted. Cell width increased with increasing line width, as expected. Cell length decreased slightly as line width increased, indicating that cardiomyocytes were more elongated by the narrower lane patterns. Cellular dimensions on 15 & 30 µm lanes were similar to those of adult cardiomyocytes in native myocardium.

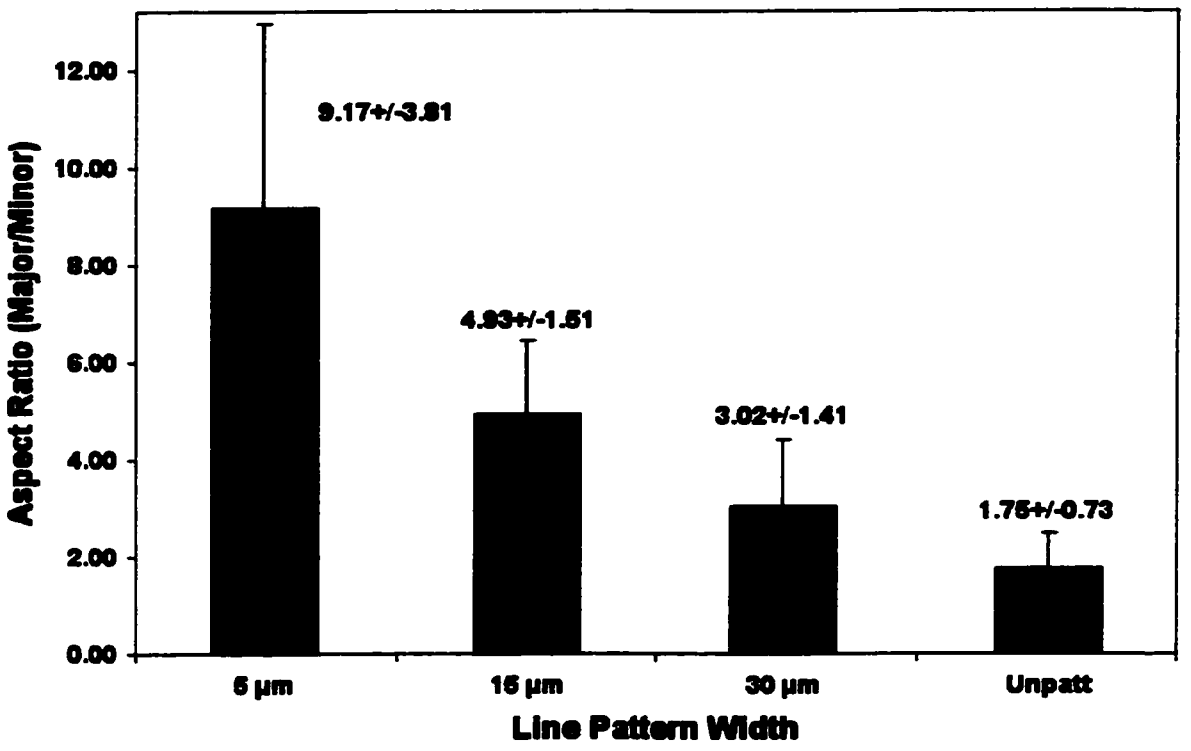

Figure 5.7. Calculated measurements of the aspect ratio of cardiomyocytes on micropatterned laminin lanes. Aspect ratio measurements were obtained by dividing the major axis (length) by the minor axis (width) for each cardiomyocyte traced using NIH Image software. A minimum of 100 cells ($n \geq 100$) was measured for each lane width and the mean values ± standard deviations are plotted. The aspect ratio steadily decreased as lane width increased, indicating that the cells were notably more elongated by narrower line widths. Cardiomyocytes on 15 & 30 µm lanes possessed aspect ratios comparable to those of mature adult cardiomyocytes *in vivo*.

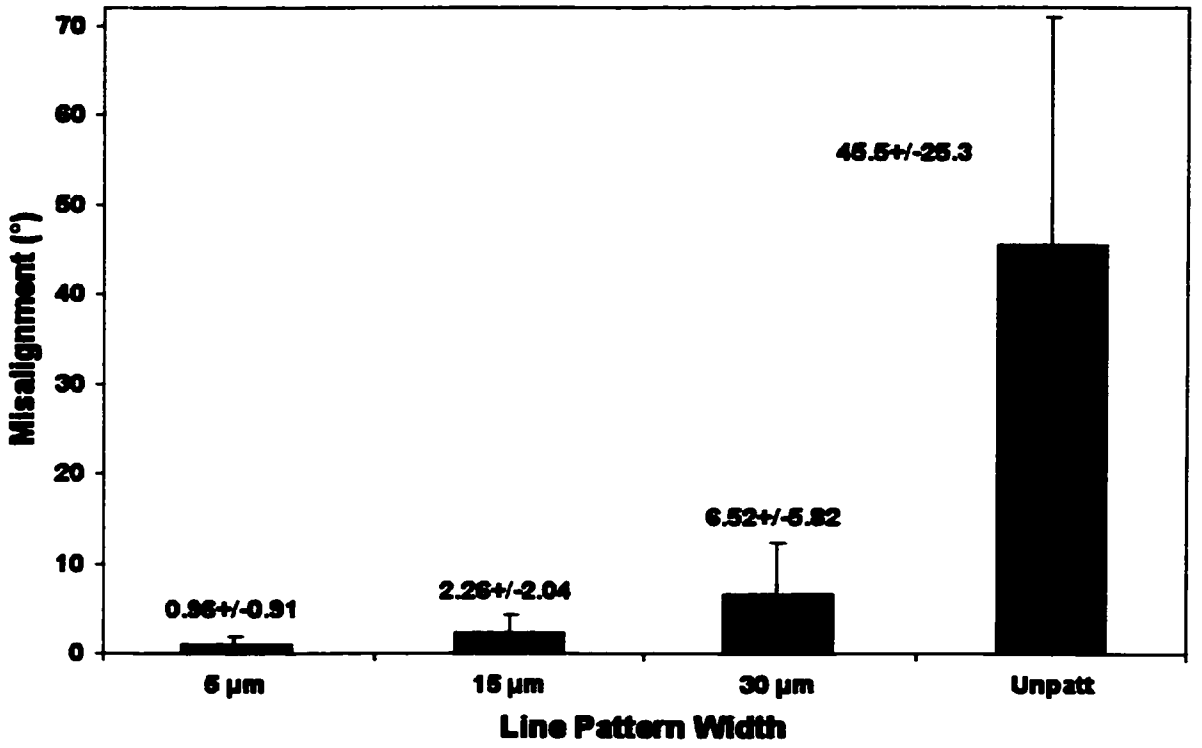

Figure 5.8. Calculated measurements of cardiomyocyte alignment with respect to the direction of the micropatterned laminin lanes. Cardiomyocytes were plated at subconfluence, fixed after 3 days in culture and traced using NIH Image software to obtain a relative angle along the major axis of the cell. The measured angles were normalized with respect to the angle of the micropatterned laminin lanes. A minimum of 100 cells ($n \geq 100$) was measured for each lane width and the mean values ± standard deviations of the difference between the cell axis and the orientation of the patterned lines are plotted. Cardiomyocyte alignment decreased slightly as lane pattern width increased, but even relatively wide lanes still directed the orientation of the cells. In contrast, cells without any spatial constraint imposed (unpatterned) showed no preferred orientation.

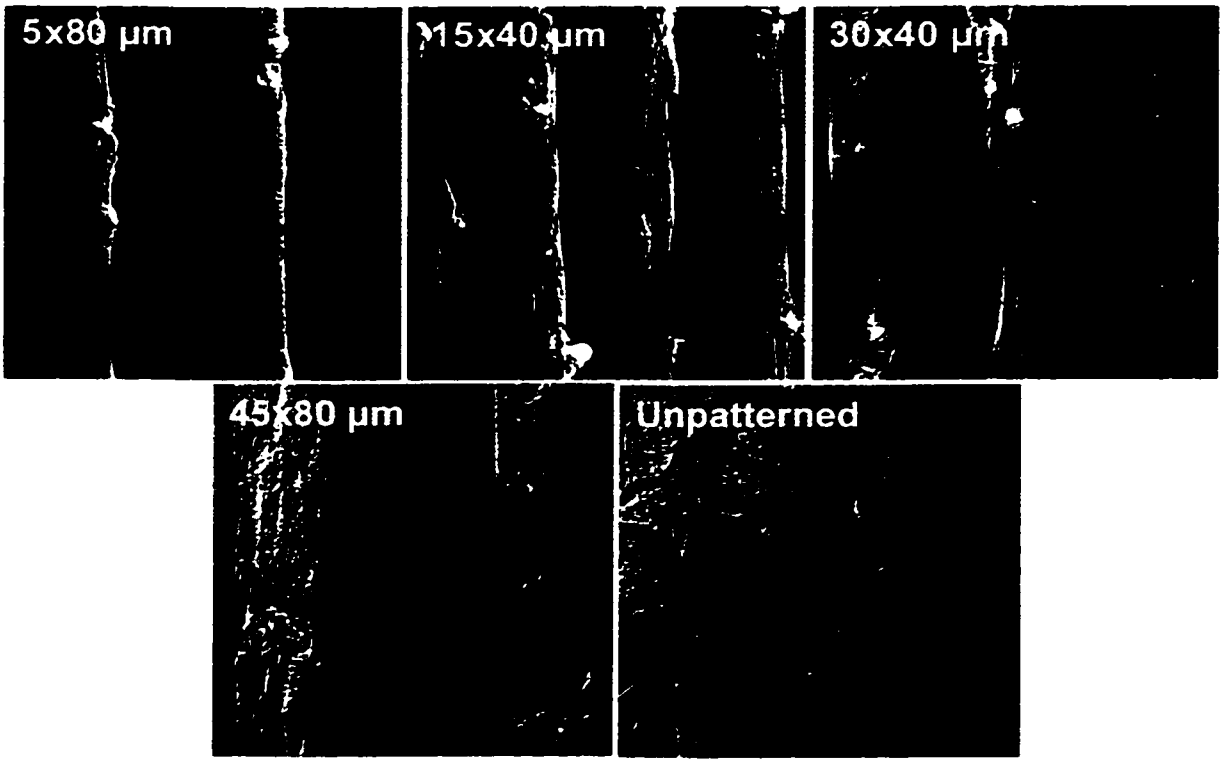

Figure 5.9. Hoffman contrast images of cultured cardiomyocytes. Cardiomyocytes were cultured on micropatterned laminin lanes of various widths and fixed after 4 days. The cultures were visually inspected using Hoffman optics to qualitatively examine the three-dimensional shape of the cells. Cardiomyocytes on the narrower lane widths (5 & 15 µm) appeared to be more rod-like and less flattened on the surface than cells on wider line widths or unpatterned substrates.

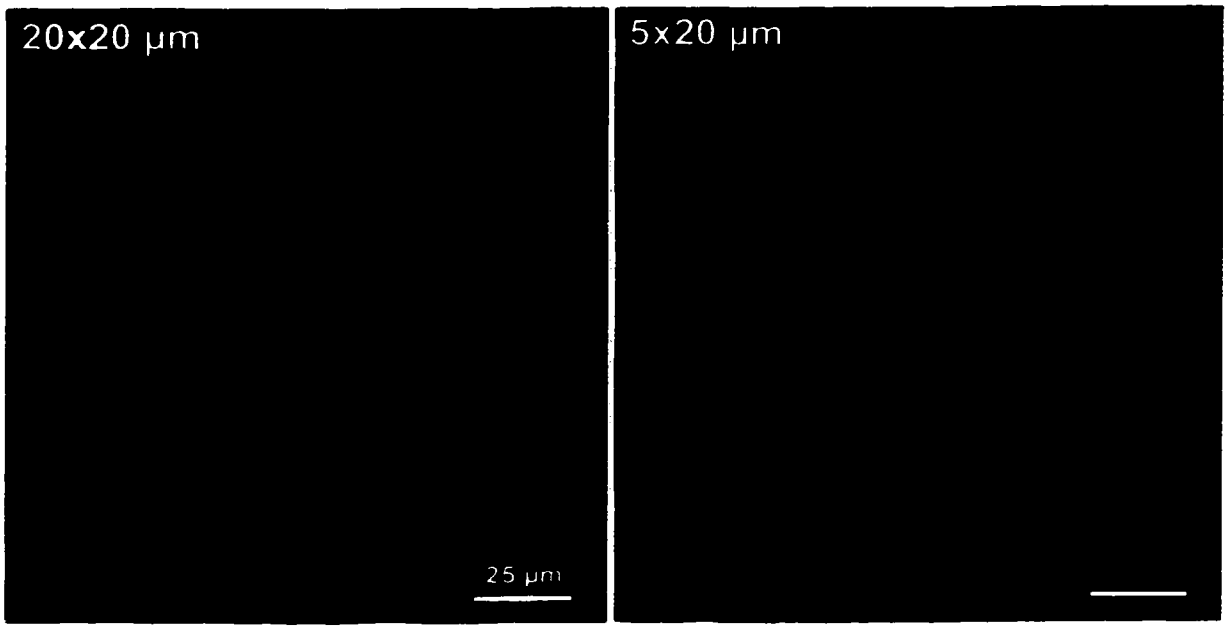

Figure 5.10. Immunofluorescent staining of myosin heavy chain in patterned cardiomyocytes. Cardiomyocytes on laminin patterns of either 20x20 μm or 5x20 μm were fixed after 2 days of culture and immunostained with an antibody to myosin heavy chain (MF20, green). Cell nuclei were counterstained with DAPI (blue). Myofibrils were clearly aligned with the direction of the micropatterned lanes, indicated by the striated sarcomeric bands of myosin expression.

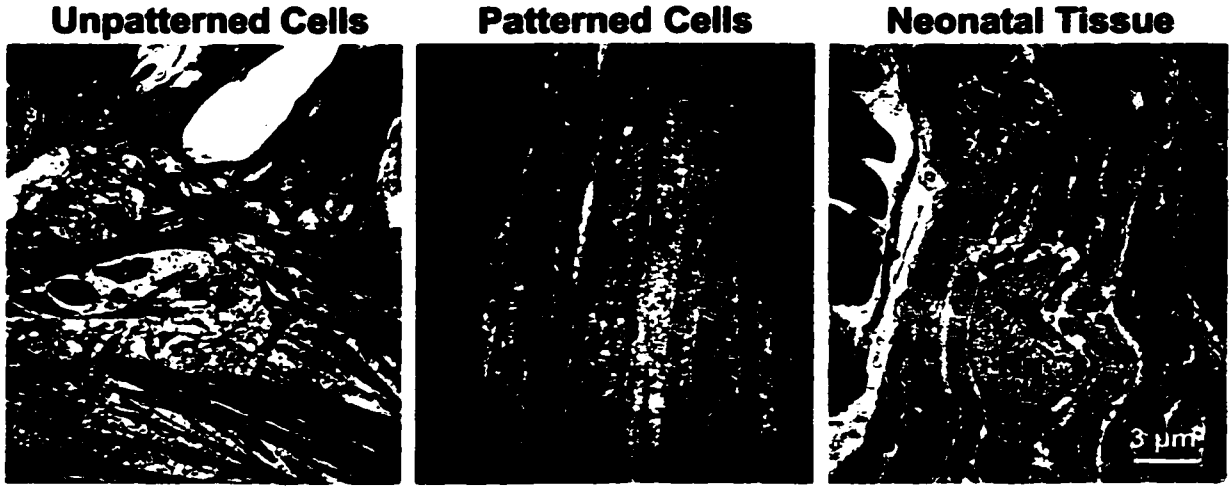

Figure 5.11. Transmission electron microscopy characterization of myofibril structure and organization of cardiomyocytes. Unpatterned (left) and patterned cultures (30x20 µm, middle) of cardiomyocytes after 4 days were compared to rat neonatal cardiac tissue (right). Myofibrils (Mf) and cell nuclei (Nu) are identified and black arrows denote the sarcolemmal boundary of individual cardiomyocytes. Myofibril assembly in patterned cultures was comparable to native tissue, whereas unpatterned cultures exhibited disorganized myofibrils.

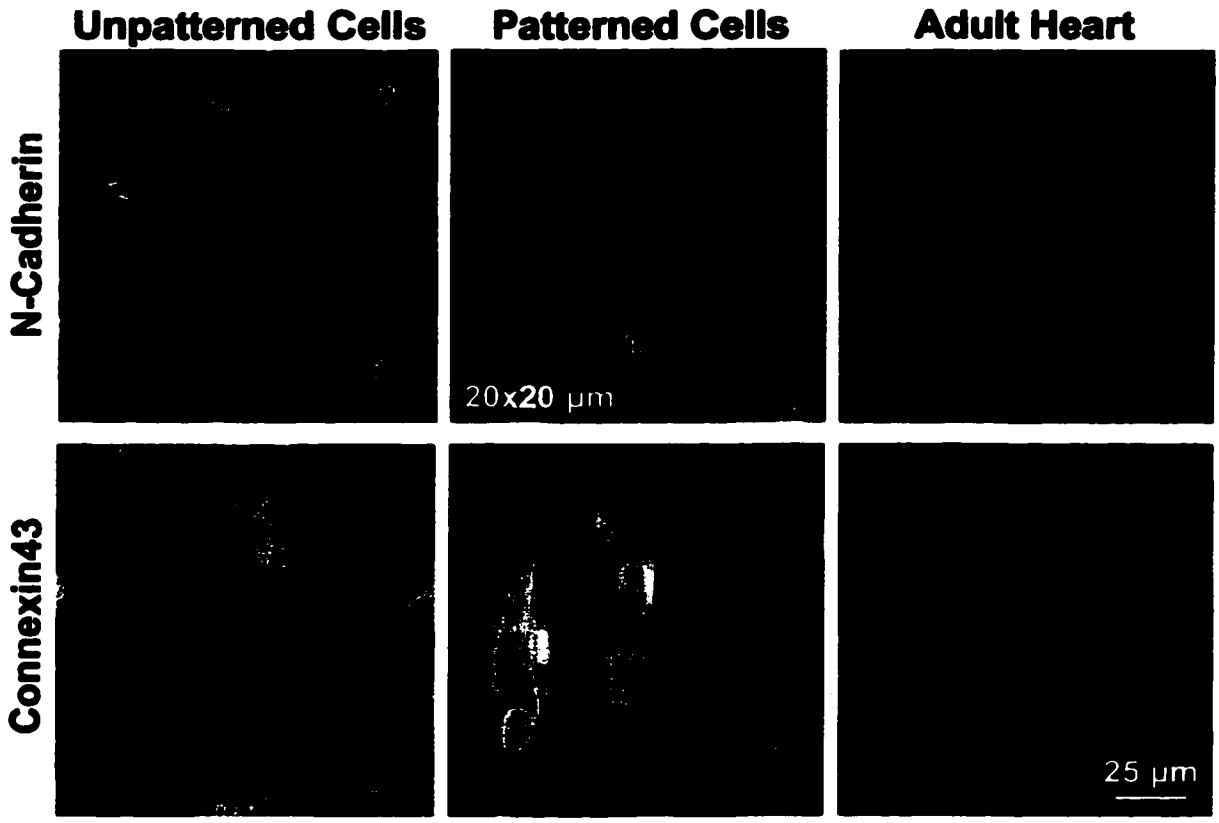

Figure 5.12. Immunofluorescent staining for electrical and mechanical components of intercalated disks. Unpatterned cultures after 7 days (left), patterned cultures after 4 days (20x20 μm, middle), and sections from adult rat heart (right) were immunostained for either N-cadherin (top row, green) or connexin43 (bottom row, green), actin filaments were counterstained with phalloidin (red), and nuclei were stained with DAPI (blue). N-cadherin and connexin43 localization between adjacent cells in patterned cultures resembled that found in the intercalated disks of mature cardiac tissue, while unpatterned cardiomyocytes exhibited circumferential staining. Cell nuclei of non-myocytes appear between the cardiac myofibers of the native tissue.

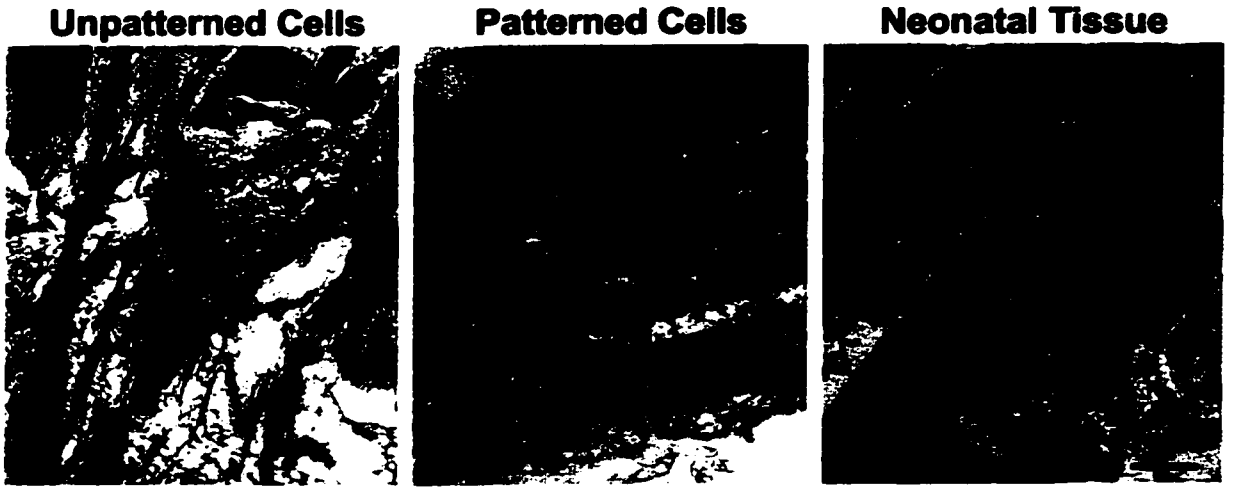

Figure 5.13. Transmission electron microscopy characterization of intercalated disk formation. Unpatterned (left) and patterned cultures (30x20 μm, middle) of cardiomyocytes after 4 days were compared to rat neonatal cardiac tissue (right). Arrows identify the sites of intercellular junctions containing intermediate junctions and desmosomes. Myofibrils inserted perpendicularly into the intercalated disk structures in patterned cultures and native tissue, but abutted each other at oblique angles in unpatterned cultures. Intercalated disk assembly in patterned cultures resembled native tissue, whereas unpatterned cultures did not exhibit similar organization.

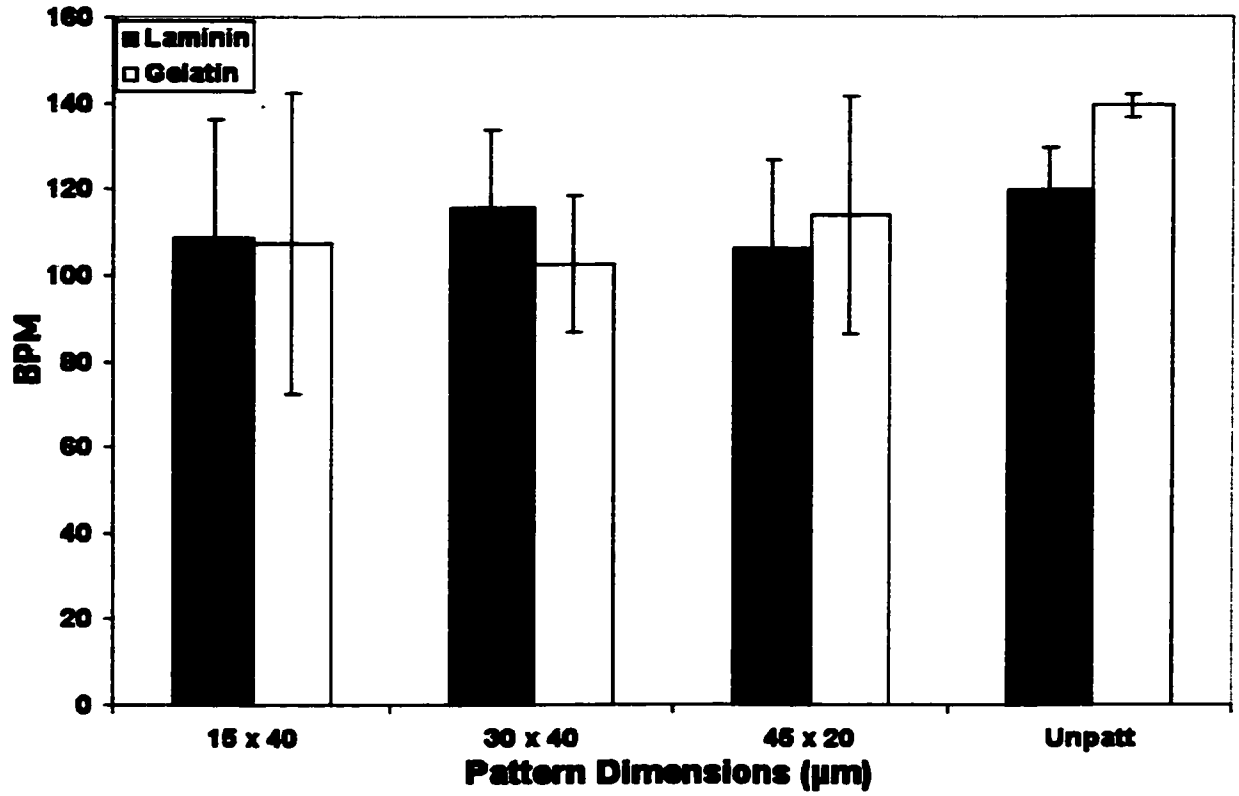

Figure 5.14. Effects of adhesive matrix proteins and lane width on contraction rates of cardiomyocytes. Video microscopy of contracting cardiomyocytes was obtained after 3 days in culture for at least 4 fields per patterned sample and at least 3 fields per unpatterned sample. The number of beats of isolated rows of cardiomyocytes were counted over a 30 second time period for multiple lanes (3 or 4) per field. The rates are reported as the mean beats per minute (BPM) ± standard deviations ($n \geq 16$ for patterned cultures, $n \geq 12$ for unpatterned cultures). No significant differences in contraction rates were apparent between cardiomyocytes on different adhesive matrix proteins or as the width of the patterned lanes was varied.

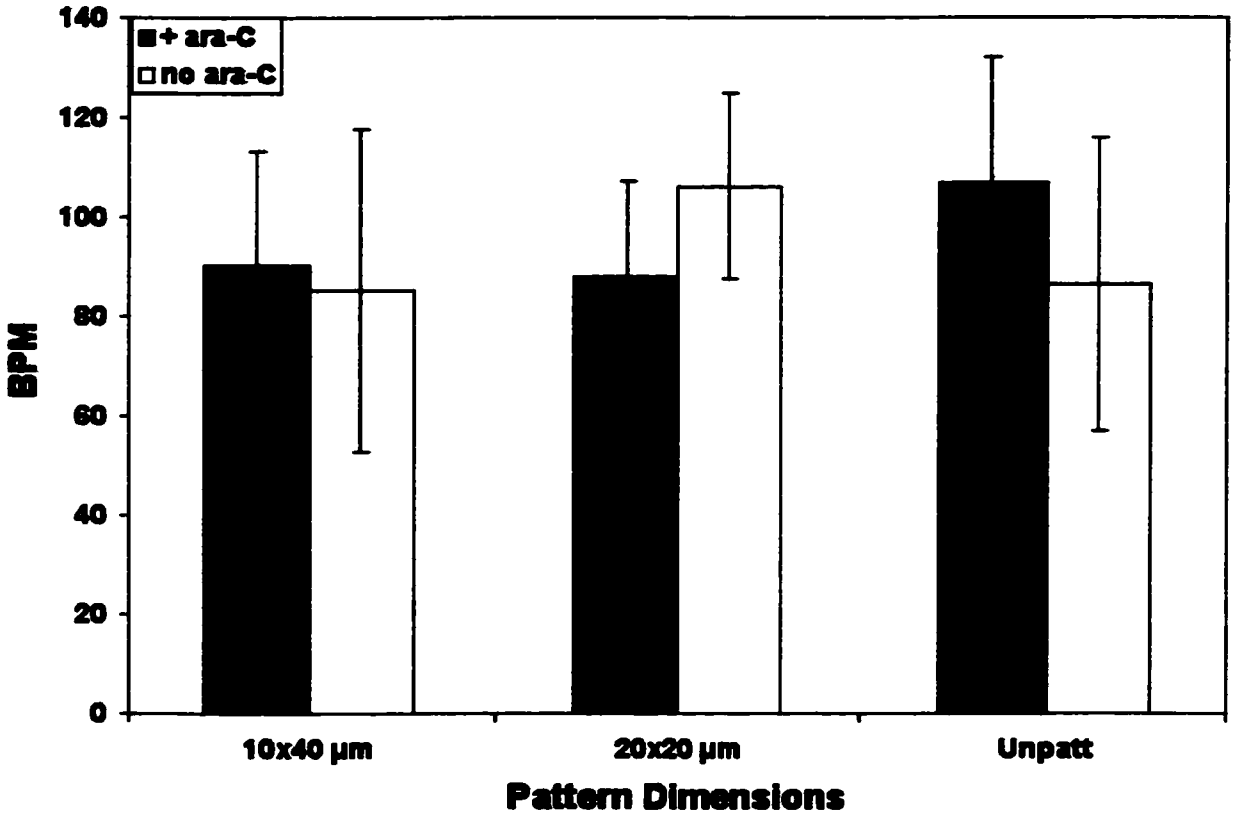

Figure 5.15. Effects of ara-C treatment on contraction rates of cardiomyocytes. Video microscopy of contracting cardiomyocyte cultures after 2 days was obtained for at least 3 fields per sample and the number of beats of isolated rows of cardiomyocytes were counted for a 30 second time period for multiple lanes (3) per field. The rates are reported as the mean beats per minute (BPM) ± standard deviations (n=9). Ara-C treatment (10 µM) did not appear to significantly affect cardiomyocyte contraction rates.

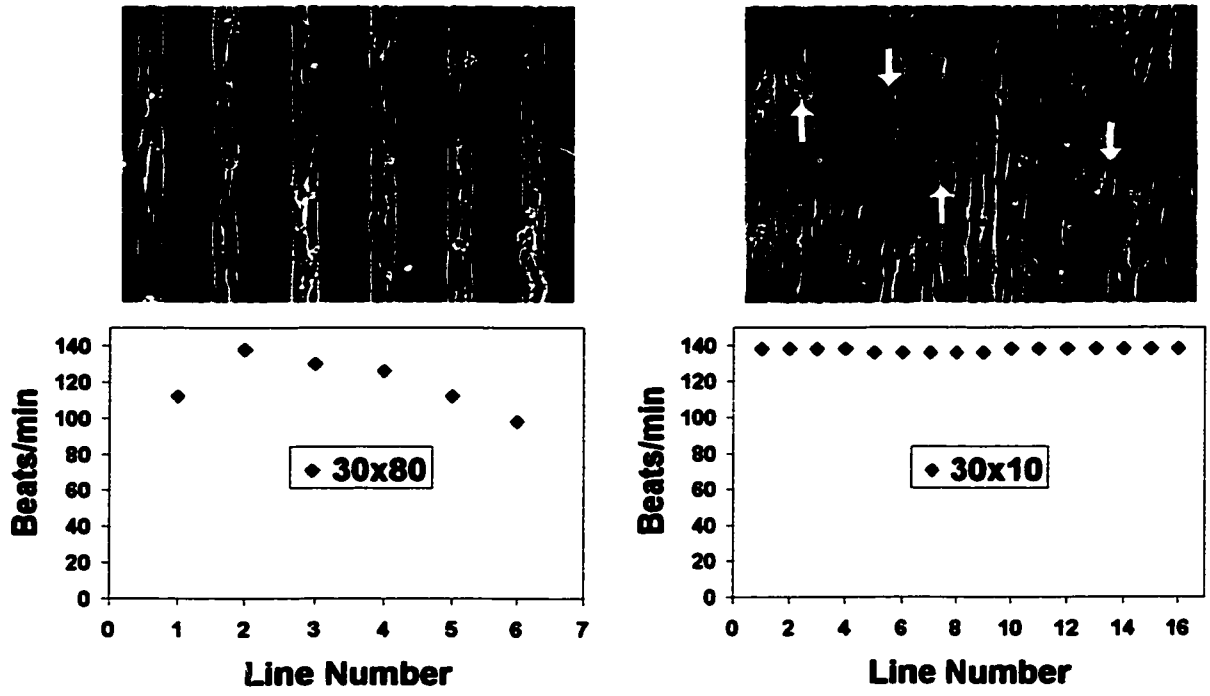

Figure 5.16. Synchrony of cardiomyocyte contractions in patterned cultures. Video microscopy was performed to record the contraction of live cardiomyocyte cultures after 2 days and the rates of individual lanes of beating cells were quantified. Representative phase images are shown for cardiomyocytes on either (left) 30x80 μm or (right) 30x10 μm patterns. The contraction rates within individual lanes are plotted. Adjacent, widely spaced lanes of cardiomyocytes beat asynchronously (left), whereas narrowly spaced lanes of the same width exhibited a high degree of synchronous contraction (right), due to cell bridging between lanes. Some of the cellular bridges are identified with arrows.

Figure 5.17. Cardiomyocyte patterning on PLGA. Cardiomyocytes were cultured for 5 days on thin PLGA membranes with 20x20 µm patterns of laminin conjugated to Oregon Green 488™. Cultures were fixed and stained with phalloidin (red) and DAPI (blue) to permit fluorescent microscopy analysis. The greater number of fibroblasts bridging between lanes is due to a higher percentage of these cells in this particular cardiomyocyte preparation. Laminin lanes underlying the cells were well retained on the PLGA surface during this time course (inset).

Chapter 6: Spatially and Temporally Controlled Generation of Heterotypic Cell Co-cultures

6.1 Abstract

Spatially defined co-cultures provide a controlled method to study the physical interaction between different cell types. Two methods utilizing microcontact printing of proteins and biotin-streptavidin affinity have been developed to create micropatterned co-cultures. The first technique is based on the selective immobilization of biotinylated adhesive molecules and the second approach relies on an engineered streptavidin mutant (RGD-streptavidin) to promote cell adhesion on non-adhesive biotinylated substrates. Adhesive protein patterns were printed onto non-adhesive surfaces that were pre-adsorbed with either streptavidin or biotinylated-BSA to pattern the attachment of a primary cell population (cardiomyocytes or smooth muscle cells). After a desired period of time, the non-adhesive regions were activated to support cell adhesion by the addition of either biotinylated-fibronectin or RGD-streptavidin, respectively, and seeded with a second population of cells (endothelial cells). The secondary proteins and cells specifically attached to the regions between the original cell patterns to create heterogeneous, yet spatially controlled co-cultures. These novel methods provide a route to culturing various combinations of cells on different types of material surfaces for basic cell biology investigations, as well as creating heterogeneous, organized tissues for tissue engineering or biotechnology applications.

6.2 Introduction

Most complex tissues are composed of heterogeneous cell types that are specifically organized in a spatially defined manner. The function of the tissue often relates to the complex and dynamic interplay between these different cell populations. *In vitro* culture of homogeneous cell populations is an established technique to characterize many of the properties of cells in isolation, often reflecting or predicting the *in vivo* biological response of such cells in the host tissue. Although co-cultures of cells may more accurately reflect the heterogeneous composition of tissues, such systems have been less commonly studied *in vitro*.

Many co-culture systems are based on culturing one cell type with media conditioned by another cell type[177] or by culturing different cells within the same shared volume of media, but separated by a membrane that inhibits cell-cell contact.[178-180] These approaches can be used to determine how one cell type is influenced by soluble factors expressed by another cell population, but they do not address how different cell types interact in intimate contact with one another. Heterotypic cell-cell contact can influence cell sorting and tissue organization, as well as direct cell migration and differentiation events. Co-cultures investigating cell-cell contact have been performed by either separating different cell populations with a membrane that allows limited cell contact[181-183] or by culturing different cell types randomly on the same substrate[48, 184], but these methods provide little or no control over how or where the cells contact each other. The variability in cell-cell contact can make it difficult to identify and isolate the individual response of either cell type in a heterogeneous co-culture environment. Thus, while it may be technically challenging to spatially organize cultures of two or more cell

populations in distinct regions, it may more accurately represent their dispersion in the native tissue and therefore provide a more relevant co-culture model.

Micropatterning techniques have been commonly used to control the displacement of cells on surfaces, but to date few methods have been developed to achieve spatially defined co-cultures of more than one cell type. Co-cultures of hepatocytes and fibroblasts were created by photolithographic patterning such that the hepatocytes adhered to islands of collagen and fibroblasts non-specifically attached in the surrounding regions.[185] By varying the spatial dimensions of the patterns, the heterotypic interface between the cells could be varied while the numbers of each cell type remained relatively constant. As the initial heterotypic interface between these cells was increased, the levels of albumin secretion and urea synthesis (both liver-specific functions) increased, indicating that native hepatocyte function was enhanced by the micropatterned co-cultures.[164] Co-cultures of hepatocytes with endothelial cells have also been obtained by culturing hepatocytes on surfaces patterned with a thermally responsive polymer.[186, 187] Adherent cells cultured at 37°C can be selectively detached from the patterned regions by temporarily lowering the culture temperature and a secondary cell type seeded onto the samples can attach to the vacant regions on the surface after returning the temperature to 37°C. Similarly, an electroactive pattern on gold can be created that switches from inhibiting to promoting cell adhesion in order to culture two different cell types on the same substrate.[188] Although all of these methods are capable of creating spatially defined co-cultures, they are either confined to particular substrates and cell types or require specialized surface chemistries. Such restrictions limit the general applicability of these techniques to study various combinations of cells on different types of material surfaces.

Microcontact printing of adhesive extracellular matrix proteins has been utilized to spatially organize a number of different cell-types on a variety of different substrate materials (see Chapter 4). Once the initial cells have been organized, the ability to generate integrin-mediated adhesion in the surrounding areas that were originally non-adhesive could provide many interesting opportunities for fundamental studies of cell biology and technological development. For example, an initial cell type could be organized for a period of time on the printed protein pattern, followed by the conversion of the non-adhesive regions outside this pattern to an adhesive protein composition. This would allow the introduction of a second cell type at a defined timepoint to create co-cultures that remain highly spatially defined.

We have developed two related strategies, based upon biotin-streptavidin affinity, to temporally control the conversion of initially non-adhesive regions to adhesive surfaces that can be used to direct the attachment of a second cell type. In the first approach, streptavidin adsorbed or immobilized on a surface can be used to subsequently capture a biotinylated adhesive molecule of interest. Native streptavidin is a relatively non-adhesive protein for most cell types but can become selectively activated to promote cell adhesion by specifically immobilizing biotinylated adhesive molecules. In the second approach, RGD-streptavidin can be used to activate adhesive regions by binding to a previously non-adhesive biotinylated substrate and mediating cell adhesion. The advantage of this second method is that streptavidin can act as the adhesive moiety directly without having to subsequently add a biotinylated molecule to promote adhesion. To demonstrate the validity and flexibility of these techniques, spatially defined co-

cultures of cardiomyocytes or smooth muscle cells and endothelial cells have been achieved by both methods.

6.3 Methods

6.3.1 Co-culture method I: Adhesive biotinylated molecules. Streptavidin (50 μg/ml in PBS) was adsorbed onto 35 mm polystyrene dishes overnight at 4°C or at room temperature for 2-4 hours. Patterns of laminin were printed onto the adsorbed layer of streptavidin, similarly to the methods described in Chapter 2; in some cases fluorescently labeled laminin (conjugated to Oregon Green™ 488) was used. The samples were stored in PBS at 4°C until further use in cell culture experiments.

In order to confirm the specific immobilization of biotinylated proteins, rhodamine labeled biotinylated-BSA (100 μg/ml in PBS) was briefly incubated on the patterned samples. The biotinylated-BSA was added either immediately after printing or 24 hours after the samples were incubated in F10C culture media with or without 15% horse serum. Based on the reported concentration of biotin in the culture media (~0.024 μg/ml ≈ 100 nM), soluble streptavidin was added at 5, 10, or 20 μg/ml (~100, 200, or 400nM, respectively) to capture the free biotin in solution. In some cases, negative controls were included by pre-coating the surfaces with a 1% solution of BSA in PBS rather than streptavidin.

6.3.2 Co-culture method II: RGD-streptavidin. Biotinylated-BSA (100 μg/ml in PBS) was adsorbed onto 35 mm polystyrene dishes overnight at 4°C and patterns of laminin or fibronectin were printed onto the adsorbed layer of biotinylated-BSA; in some cases

fluorescently labeled laminin (conjugated to Oregon Green™ 488) was used. The samples were stored in PBS at 4°C until further use in cell culture experiments.

RGD-streptavidin conjugated to tetramethyl-rhodamine was used in some experiments in order to confirm the specific immobilization of the protein to the biotinylated regions between primary cell patterns. Cardiomyocytes were cultured on laminin lanes printed onto biotinylated-BSA (see section below) for 2 days and then rinsed with PBS. RGD-streptavidin (50 μg/ml, ~1 μM) was incubated in serum-free DMEM for about 15 minutes at 37°C and then the cultures were rinsed with PBS and immediately fixed with 3% paraformaldehyde. Two negative controls were included to demonstrate the specificity of the streptavidin-biotin immobilization: RGD-streptavidin was added to patterned cardiomyocyte cultures on adsorbed layers of BSA (not biotinylated) or an excess of free biotin (10 μM) was pre-incubated with the RGD-streptavidin solution to prevent immobilization to biotinylated-BSA.

6.3.3. Co-culture of cardiomyocytes and endothelial cells. Micropatterned lanes of laminin (15 or 30 μm wide spaced 80 μm apart) were printed onto polystyrene dishes pre-adsorbed with either streptavidin or biotinylated-BSA. Primary rat neonatal cardiomyocytes were cultured (as described in Chapter 2) on the laminin patterns for 2-3 days in cardiomyocyte plating media supplemented with 1 μM ara-C. Immediately before the start of the co-culture experiments, the cardiomyocyte cultures were rinsed with PBS and incubated with a solution of biotinylated-fibronectin (12.5 μg/ml in DPBS) or RGD-streptavidin (50-100 μg/ml in serum-free DMEM) to specifically immobilize the adhesive molecules to adsorbed regions of streptavidin or biotinylated-BSA, respectively,

between the cardiomyocyte lanes. Rat aortic endothelial cells were then seeded (~500,000 cells per 35 mm dish) in 2 ml of MCDB131 media with 10% serum and allowed to adhere for 2-4 hours. Non-adherent cells were aspirated, the cultures were rinsed with PBS and cardiomyocyte plating media was added to the cultures for the duration of the experiments. At the conclusion of the experiment, the cultures were rinsed, fixed with 3% paraformaldehyde and immunostained as previously described in Chapters 2 and 5. Rhodamine-conjugated acetylated-LDL (Molecular Probes) was added to the live co-cultures at a concentration of 10 μg/ml in serum-free MCDB131 media for 10 minutes at 37°C; the cultures were then rinsed twice with serum-free media and fixed with 3% paraformaldehyde.

6.3.4 Co-culture of smooth muscle and endothelial cells. Square patterns of fibronectin were printed onto polystyrene dishes coated with biotinylated-BSA. Rat aortic smooth muscle cells were seeded (~150,000 cells per 35 mm dish) onto the fibronectin patterns in serum-free Waymouth's media and allowed to attach for about 3 hours. The cultures were then rinsed with PBS and a solution of RGD-streptavidin (FN-SA, 100 μg/ml) in PBS was incubated on the samples for about 15 minutes at 37°C. Endothelial cells, labeled with Cell Tracker Green (see Chapter 7, Methods), were seeded (~250,000 cells per 35 mm dish) onto the samples in serum-free MCDB131 media. After about one hour, the cultures were fixed with 3% paraformaldehyde in PBS and images were acquired by phase and fluorescence microscopy.

6.4 Results

6.4.1 Co-culture with Biotinylated Adhesive Molecules

The original co-culture design was to pattern cells on streptavidin-coated surfaces such that adhesive biotinylated proteins could be added to selectively promote cell adhesion in the regions between the patterns (Figure 6.1). Initial studies were performed with fluorescently labeled proteins to determine whether biotinylated molecules were directed between protein patterns printed onto streptavidin-coated surfaces. Patterns of laminin-Oregon Green™ 488 were printed onto either streptavidin-coated or BSA-coated 35 mm polystyrene dishes and immediately incubated with a solution of rhodamine labeled biotinylated-BSA. Fluorescent microscopy confirmed that the biotinylated-BSA was specifically immobilized between the primary line patterns on streptavidin-coated dishes, but no detectable signal was observed for the BSA-coated samples, as expected (Figure 6.2). This suggested that biotinylated molecules from an aqueous solution were selectively bound to surface-adsorbed streptavidin via the specificity of streptavidin-biotin molecular recognition.

For cell culture studies, it is imperative that the method described above be amenable with the use of cell culture media and serum. This is a concern because most cell culture media contains a number of vitamin supplements, including biotin (Vitamin H), thus endogenous biotin in solution is already present in the cell culture system. Free biotin could likely fill the vacant binding sites of the streptavidin adsorbed to the surfaces, thus impeding the subsequent immobilization of biotinylated molecules. To address this issue, soluble streptavidin was pre-incubated with the culture media to capture free biotin before adding the media to the protein-patterned samples.

Streptavidin is a tetrameric protein possessing 4 biotin binding sites, thus streptavidin added at a 1:1 molar ratio to the reported biotin concentration in the cell culture media provided an excess of 4:1 stoichiometric binding sites. For relatively low biotin concentrations, the addition of streptavidin to the culture media remained experimentally feasible (~5-20 μg/ml). Laminin patterns were printed onto streptavidin adsorbed dishes and incubated with serum-free cell culture media (+/- streptavidin) for approximately 24 hours before attempting to immobilize biotinylated-BSA. Without the addition of streptavidin to the culture media, it did not appear that the fluorescently labeled biotinylated-BSA was directed between the patterned laminin lanes (Figure 6.3). When streptavidin was added to the culture media (1:1 molar ratio = 1x), the biotinylated-BSA was specifically bound to the surface between the laminin regions. As the concentration of streptavidin in the culture media was increased (2x or 4x), the relative fluorescence intensity of the biotinylated-BSA signal remained relatively constant (Figure 6.3). These results clearly demonstrated that adsorbed streptavidin retained the ability to immobilize biotinylated proteins from solution after exposure to cell culture media containing a sufficient concentration of streptavidin to capture the free biotin.

Another complicating factor, though, is that the serum used to supplement the media also contains an unspecified amount of biotin. To address this concern, another series of experiments in which the molar ratio of streptavidin:biotin was incrementally increased (i.e. 1x, 2x, 4x) was performed in cell culture media containing 15% horse serum. Similar to the previous experiments, the laminin patterned samples were exposed to the serum-containing culture media (+/- streptavidin) for 1 day and then incubated briefly with a solution of biotinylated-BSA. The biotinylated protein was not

immobilized on the surface without the addition of streptavidin to the culture media and a weak signal for biotinylated-BSA was obtained, even as the concentration of soluble streptavidin was increased (Figure 6.4). This indicated that the streptavidin concentrations in the media were not sufficient to capture all of the additional free biotin contributed by the serum and therefore some free biotin presumably bound to the surface-adsorbed streptavidin and partially inhibited subsequent immobilization of biotinylated proteins. These results confirmed that biotinylated molecules could be selectively targeted to streptavidin regions between patterned lanes of adhesive protein, even after exposure to serum containing cell culture media. However, an excess of streptavidin to biotin in solution (at least 4:1 molar ratio) was necessary to promote the successful immobilization of biotinylated molecules between the original protein patterned lanes.

Despite the apparently poor immobilization of biotinylated proteins after exposure to serum-containing media, a cell co-culture experiment was attempted to determine the validity of this method. Rat neonatal cardiomyocytes were cultured on laminin lanes printed onto streptavidin-coated petri dishes. Patterns of cardiomyocytes on streptavidin coated surfaces were similar to patterns on BSA-coated substrates (Figure 6.5). During this time, the normal cardiomyocyte culture media was supplemented with ~25 μg/ml of streptavidin to capture the free biotin in solution. After 2 days in culture, the patterned cardiomyocyte cultures were rinsed and briefly incubated with a solution of biotinylated-fibronectin. Rat aortic endothelial cells seeded onto the patterned cultures rapidly attached and spread on the adhesive regions of immobilized fibronectin between the rows of patterned cardiomyocytes (Figure 6.6). Patterned cultures of cardiomyocytes, without the addition of biotinylated-fibronectin and endothelial cells, remained highly aligned and

adherent along the patterns over the same period of time. Based on immunostaining to delineate the different cell types, it was evident that the endothelial cells specifically attached to the regions between the original patterns of cardiomyocytes (Figure 6.7).

6.4.2 Co-culture with RGD-Streptavidin. In order to circumvent some of the technical challenges associated with the first co-culture method, a second, similar approach using biotin-streptavidin affinity was also developed. Instead of a streptavidin-coated non-adhesive surface, protein patterns were printed onto a layer of adsorbed biotinylated-BSA. Since streptavidin is not a normal constituent of cell culture media, surface-immobilized biotin moieties remain accessible in the presence of serum-containing media. The non-adhesive biotinylated-BSA regions can then become selectively activated to promote cell adhesion by the specific immobilization of RGD-streptavidin, a streptavidin mutant engineered to contain a cell adhesive domain (RGD) capable of supporting integrin-mediated cell adhesion (Figure 6.8).

To examine whether RGD-streptavidin could be specifically immobilized between patterned rows of cells, fluorescently labeled RGD-streptavidin was incubated on patterned cardiomyocyte cultures on dishes coated with biotinylated-BSA. After 3 days in culture, the patterned cardiomyocyte samples were rinsed with PBS and incubated with a solution of rhodamine-labeled RGD-streptavidin. Inspection by fluorescent microscopy indicated that the RGD streptavidin was clearly bound to the biotinylated surface between the patterned rows of cells (Figure 6.9). The specificity of biotin-mediated surface immobilization was confirmed by two negative controls. No fluorescent signal for the RGD streptavidin was observed for dishes pre-coated with BSA

rather than biotinylated-BSA, suggesting that the RGD-streptavidin did not passively adsorb to the surface (Figure 6.9). Similarly, when an excess of free biotin was pre-incubated with the RGD streptavidin solution to fill the binding sites, no fluorescent signal was detected on the surface coated with biotinylated-BSA (Figure 6.9). Together these controls indicated that RGD streptavidin immobilization to the surface was specifically mediated via the biotin moieties on the surface.

Co-culture of Rat Neonatal Cardiomyocytes and Aortic Endothelial Cells

After confirming the immobilization of RGD-streptavidin, co-culture experiments were attempted with cardiomyocytes and endothelial cells. The cardiomyocytes attached and spread along the micropatterned lanes of laminin and exhibited contractile activity after 2-3 days in culture. The cardiomyocytes beat in synchrony along individual lanes, but separate lanes beat asynchronously due to the relatively wide spacing that prevented adjacent rows of cardiomyocytes from making cellular connections. Cell patterns were retained equally well on protein patterns printed onto biotinylated-BSA layers as they were on protein lanes stamped onto BSA-coated surfaces, as previously described. Following the addition of the RGD-streptavidin, the endothelial cells attached between the original cardiomyocyte patterned lines within 1-2 hours and appeared to be well spread by 3-4 hours after plating (Figure 6.10). During this same period of time, cardiomyocytes on laminin lanes without the addition of RGD-streptavidin and endothelial cells remained well aligned along the original patterns.

Several control samples were included as well to demonstrate that the addition of the RGD-streptavidin was necessary to direct the adhesion of the secondary cell type.

With the addition of RGD-streptavidin, but no endothelial cells, the initial cardiomyocyte patterned lines were well retained for as long as 24 hours (longest time point assessed) and few cells were observed between the rows of cardiomyocytes (Figure 6.11). This is likely due to the fact that the cardiomyocytes are largely non-proliferative and non-motile cells, especially after they have formed cell-cell junctions with neighboring cells and are contracting. Any cells that did migrate onto the immobilized RGD-streptavidin regions appeared to be fibroblasts since they stained negative with a sarcomeric myosin heavy chain antibody specific for striated muscle cells.

Endothelial cells were also plated onto patterned cardiomyocyte cultures to which RGD-streptavidin was not added, thus the regions between the lines were still largely non-adhesive. Significantly more endothelial cells remained in suspension after 2 hours of incubation than when RGD-streptavidin was added first, indicating fewer cells were capable of attaching to the surface. Of those cells that did attach, most adhered to regions of the patterned lines not covered by cardiomyocytes or on top of the cardiomyocytes.

The localization of the cardiomyocytes to the original patterned lanes of laminin and endothelial cells to the activated surface regions between was detected by several means. The cardiomyocytes remained highly elongated on the relatively narrow lane widths and continued to beat in culture, in stark contrast to the neighboring endothelial cells which spread randomly on the wide adhesive regions of RGD-streptavidin and did not beat. Furthermore, immunofluorescent staining with an antibody towards myosin heavy chain (Figure 6.12) or connexin43 (Figure 6.13) confirmed the identity of the cardiomyocytes along the original micropatterned lanes. In addition, the endothelial cells

were specifically identified by acetylated-LDL uptake (Figure 6.14) and found to be localized primarily between the cardiomyocyte lanes.

In some instances, after the endothelial cells attached between the cardiomyocyte lines, all of the rows of cardiomyocytes beat synchronously. This behavior was recorded by video microscopy and found to be consistent across the entire surface of such samples. In previous experiments, synchronous contraction between lanes of cardiomyocytes separated by 80 μm was not observed unless cardiomyocytes somehow physically bridged this distance and made cell-cell contacts. However, even with a relatively low density of endothelial cells in some cases, the contraction appeared to become synchronous between adjacent lines. This behavior was transient - first appearing about 3-4 hours after the plating of the endothelial cells and continuing for several hours, but it was not evident after the cultures were continued overnight. After 12-24 hours, the endothelial cells overgrew the cultures and disrupted the patterns of cardiomyocytes. This phenomena was not consistently reproduced during the course of all co-culture experiments, and thus attempts to characterize the potential mechanism responsible for synchronous contraction were unsuccessful.

Co-cultures of smooth muscle and endothelial cells.

Co-cultures of smooth muscle and endothelial cells were also established using RGD-streptavidin on biotinylated surfaces. The smooth muscle cells were cultured on micropatterned square islands of fibronectin printed onto dishes pre-adsorbed with biotinylated-BSA. After the immobilization of RGD-streptavidin, endothelial cells were seeded onto the patterned cultures and attached primarily to the regions outside of the

square islands (Figure 6.15). Some of the endothelial cells also attached either on top of some smooth muscle cells or to regions of the fibronectin squares not completely covered by smooth muscle cells.

6.5 Discussion

Two methods for creating spatially controlled heterotypic co-cultures have been developed utilizing biotin-streptavidin affinity to activate non-adhesive regions of surfaces to become selectively adhesive for cell attachment. Both of these methods provide novel techniques based on relatively simple protein-ligand interactions to fabricate co-culture systems compatible with a variety of surfaces and cell types. Integrating different cell types together in a spatially controlled fashion begins to more accurately reflect the composition, and perhaps, function of complex heterogeneous tissues. For example, micropatterned co-cultures of endothelial cells with cardiomyocytes could possibly serve as a means to incorporate a pre-vascular network within a sheet of cardiac muscle tissue or spatially organized co-cultures of endothelial cells and smooth muscle could be used in the design of vascular conduits. In addition to tissue engineering applications such as these, spatially defined co-cultures also provide the means to examine the heterotypic interface between different cell types for relevant investigations in cell and developmental biology.

One of the major limitations of these methods, though, is the long-term stability of culturing different cell types in spatially distinct regions. Often 8-12 hours after the addition of a second cell type to the patterned cultures, the secondary cells began to disrupt the primary cell patterns and quickly overgrew the cultures. This resembled the

behavior of cardiac fibroblasts that contaminate the primary isolations of cardiomyocytes and overgrow the cultures if left uninhibited. Thus, in order to improve the utility of the described co-culture models it would be beneficial to prolong the spatial separation of the micropatterned cells. The integrity of the micropatterned co-cultures could potentially be preserved by inhibiting cell proliferation and migration.

Another problem that apparently compromised these methods is the presence of endogenous or free biotin that competes for biotin-binding sites in streptavidin. Free biotin is present in most types of culture media and serum and therefore could inhibit RGD-streptavidin binding to biotinylated substrates or immobilizing adhesive biotinylated molecules to streptavidin-coated surfaces. This problem was resolved by using biotin-free media or removing biotin from the cell culture media to enhance the immobilization efficiency of adhesive molecules.

Although both of these comparable systems were effective means to create spatially defined co-cultures, each method possessed certain advantages and disadvantages. Biotinylation can be used to modify virtually any adhesive molecule of interest to be implemented in the co-culture system, but conjugation of small molecules can potentially inhibit protein activity. On the other hand, RGD-streptavidin can be used in its native state because it already contains cell-adhesive capability and molecular recognition via biotin-binding, but it may only support the adhesion of a limited number of cell types. Streptavidin-coated substrates may be occupied by free biotin present in the cell culture media before the addition of biotinylated proteins, but stable biotinylated surfaces are not prone to being similarly blocked since streptavidin is not a normal constituent of culture media formulations. Hence, free biotin in solution is more likely to

inhibit the immobilization of biotinylated adhesive molecules to streptavidin-coated surfaces than the binding of RGD-streptavidin to biotinylated substrates. The different attributes of these two co-culture systems suggest instances in which one method may be preferred over the other depending on the particular cell types and culture conditions being used.

6.6 Figures

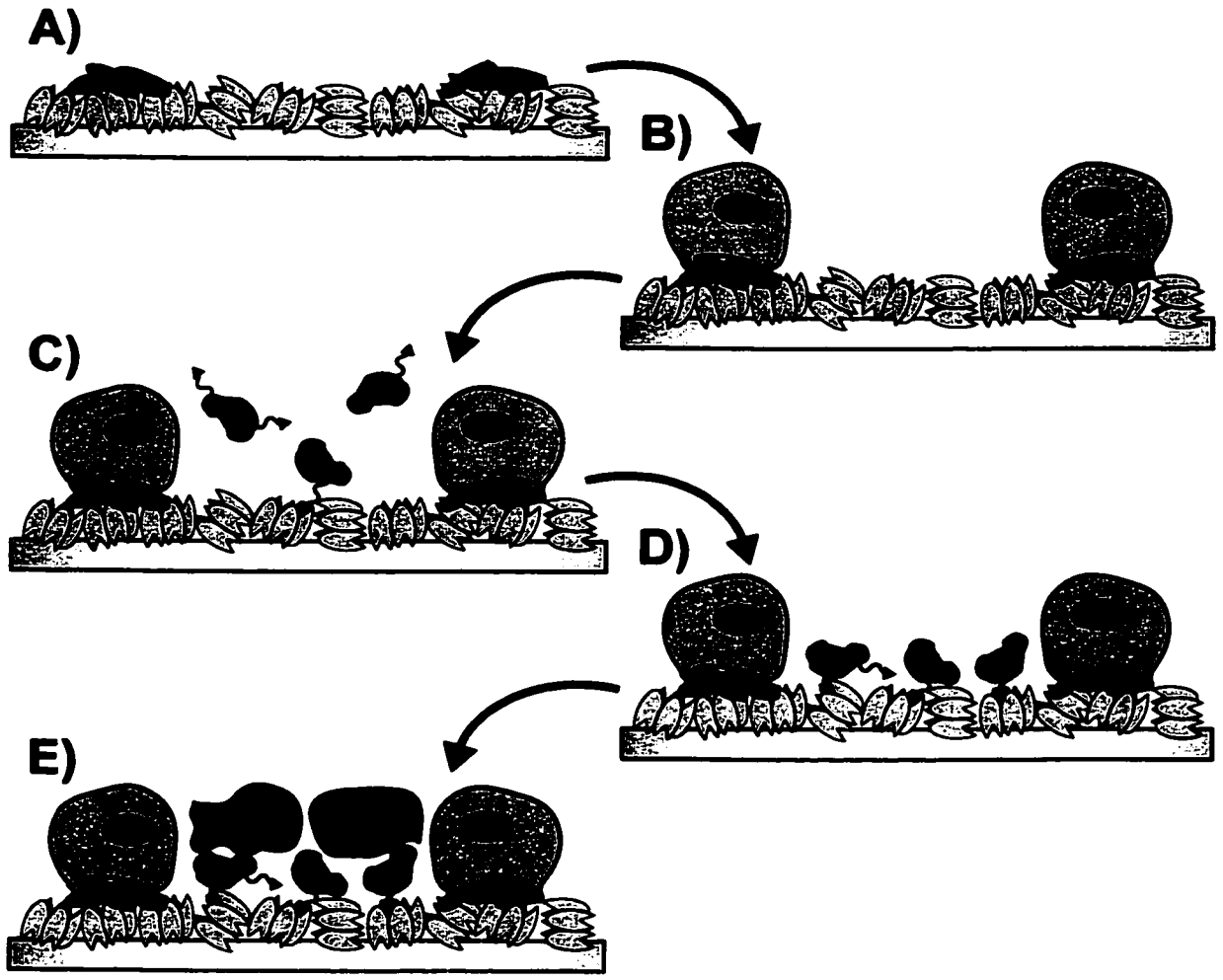

Figure 6.1. Schematic of co-culture method I: adhesive biotinylated molecules. A) An adhesive protein pattern was printed onto a streptavidin-coated surface and B) cell adhesion was strictly directed along the micropatterned features. C) Biotinylated adhesive molecules were incubated in solution with the cultures and D) immobilized specifically to the non-adhesive regions of streptavidin between the patterned cells. E) The attachment of a secondary cell type was directed to the newly adhesive regions between the primary cell patterns.

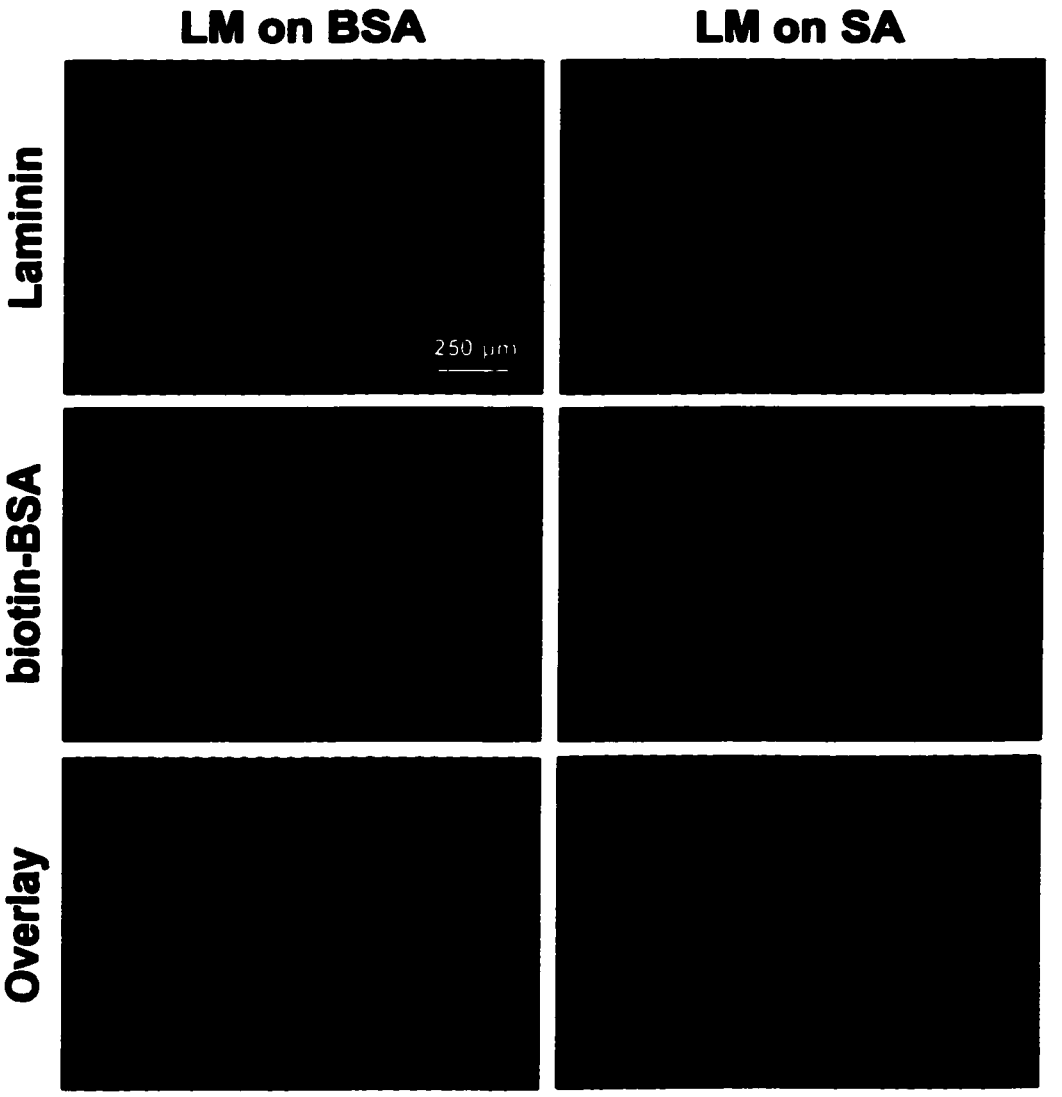

Figure 6.2. Immobilization of biotinylated proteins between laminin lanes. Patterns of fluorescently labeled laminin conjugated to Oregon Green 488 (30x20 µm lanes) were printed onto either BSA-coated (left column) or streptavidin-coated polystyrene dishes (right column) and incubated with a solution of rhodamine-labeled biotinylated-BSA in PBS. Biotinylated-BSA was not immobilized to the BSA-coated substrate, but was specifically bound to the streptavidin-coated surface between the printed lanes of laminin.

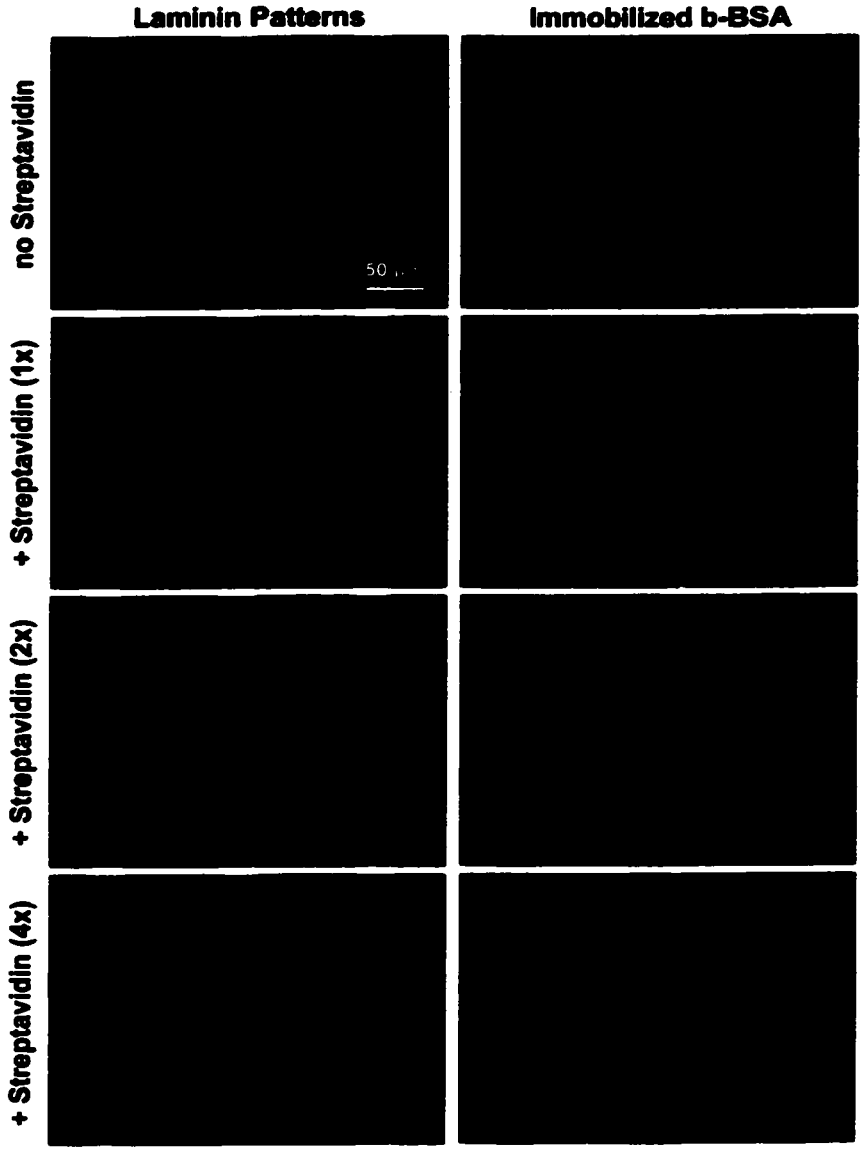

Figure 6.3. Immobilization of biotinylated proteins after exposure to serum-free culture media. Lanes of fluorescently labeled laminin (30x80 μm) were printed onto dishes pre-adsorbed with streptavidin and incubated at 37°C with F10C culture media. Soluble streptavidin was added to the culture media at 1x, 2x, or 4x molar equivalents to that of the reported free biotin concentration in the media. After 24 hours, the samples were incubated with a solution of biotinylated-BSA in PBS and visualized by fluorescent microscopy. Without the addition of streptavidin to the culture media, biotinylated-BSA was not immobilized to the surface. On the other hand, the addition of soluble streptavidin to the media captured the free biotin in solution and permitted the immobilization of biotinylated-BSA. No significant differences in biotinylated-BSA immobilization were observed for increasing concentrations of soluble streptavidin.

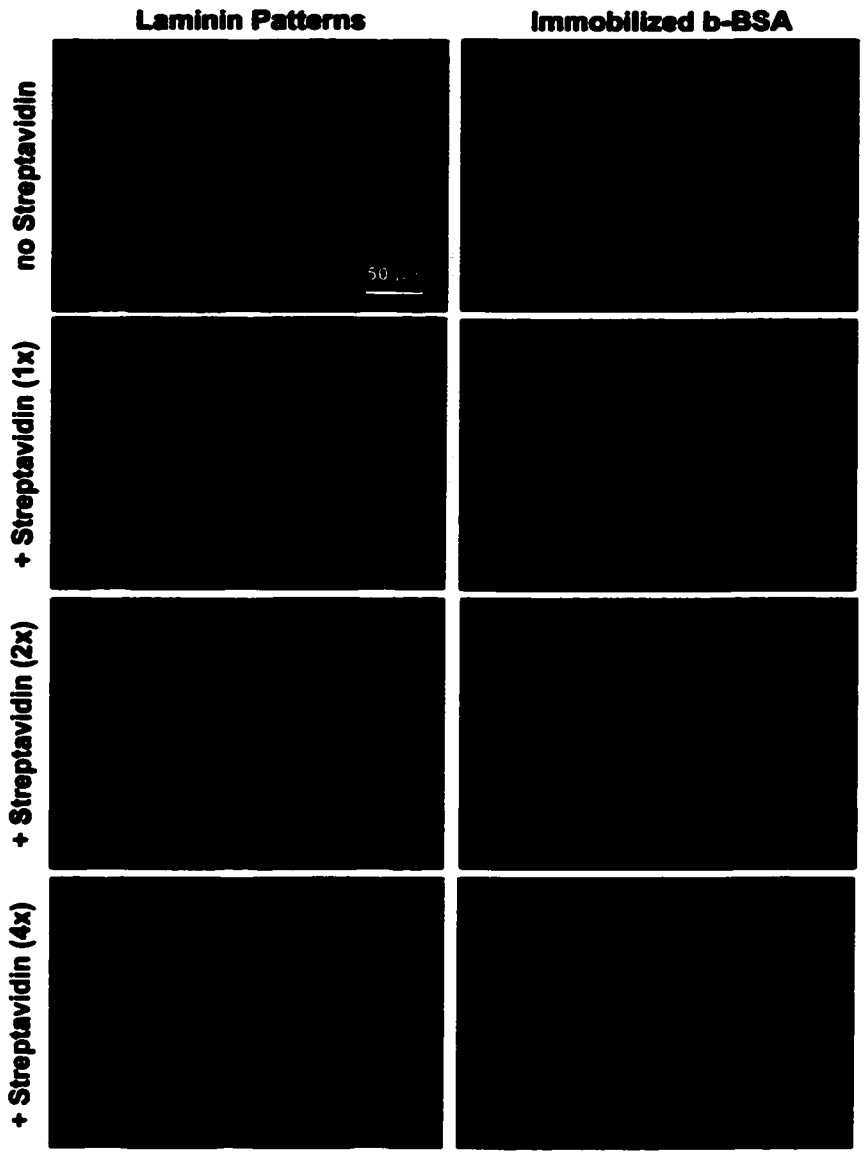

Figure 6.4. Immobilization of biotinylated proteins after exposure to serum-containing culture media. Lanes of fluorescently labeled laminin (30x80 μm) were printed onto dishes pre-adsorbed with streptavidin and incubated at 37°C with F10C culture media containing 15% horse serum. Soluble streptavidin was added to the culture media at 1x, 2x, or 4x molar equivalents to that of the reported free biotin concentration in the media. After 24 hours, the samples were incubated with a solution of biotinylated-BSA in PBS and visualized by fluorescent microscopy. Without the addition of streptavidin to the culture media, biotinylated-BSA was not immobilized to the surface. An increasing amount of biotinylated-BSA appeared to be immobilized as the concentration of soluble streptavidin was increased, but overall a much weaker fluorescent signal was observed than for samples exposed to serum-free media. This suggested that additional free biotin contributed by the serum inhibited efficient immobilization of biotinylated proteins.

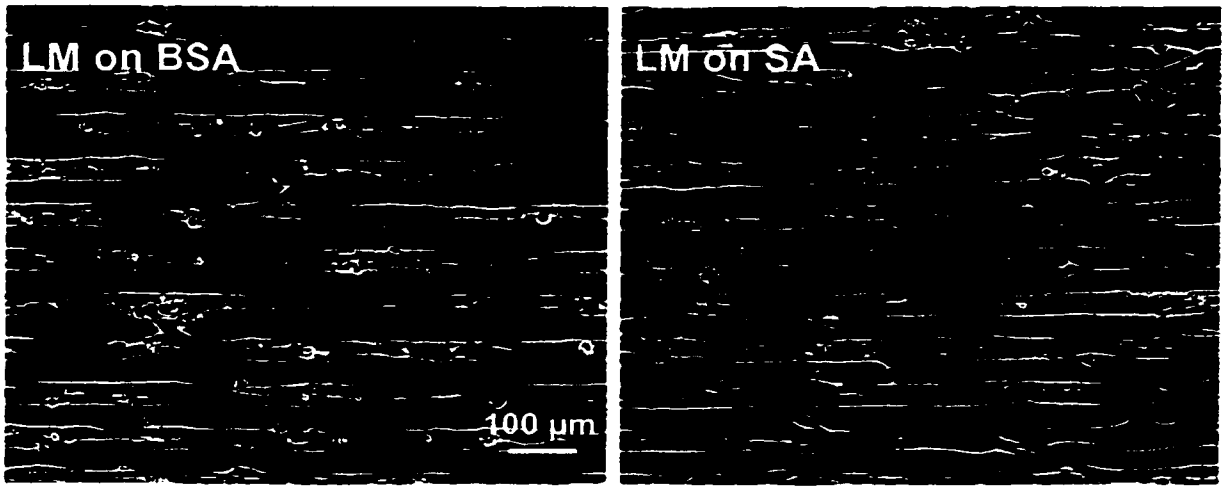

Figure 6.5. Cardiomyocyte patterning on BSA and streptavidin (SA) coated surfaces. Laminin lanes (30x40 µm) were printed onto polystyrene dishes coated with either BSA (left) or streptavidin (SA, right) and the samples were seeded with cardiomyocytes. After 2-3 days in culture, cell patterns on the two different types of protein-coated surfaces were comparable, indicating that streptavidin inhibited cell adhesion similarly to BSA.

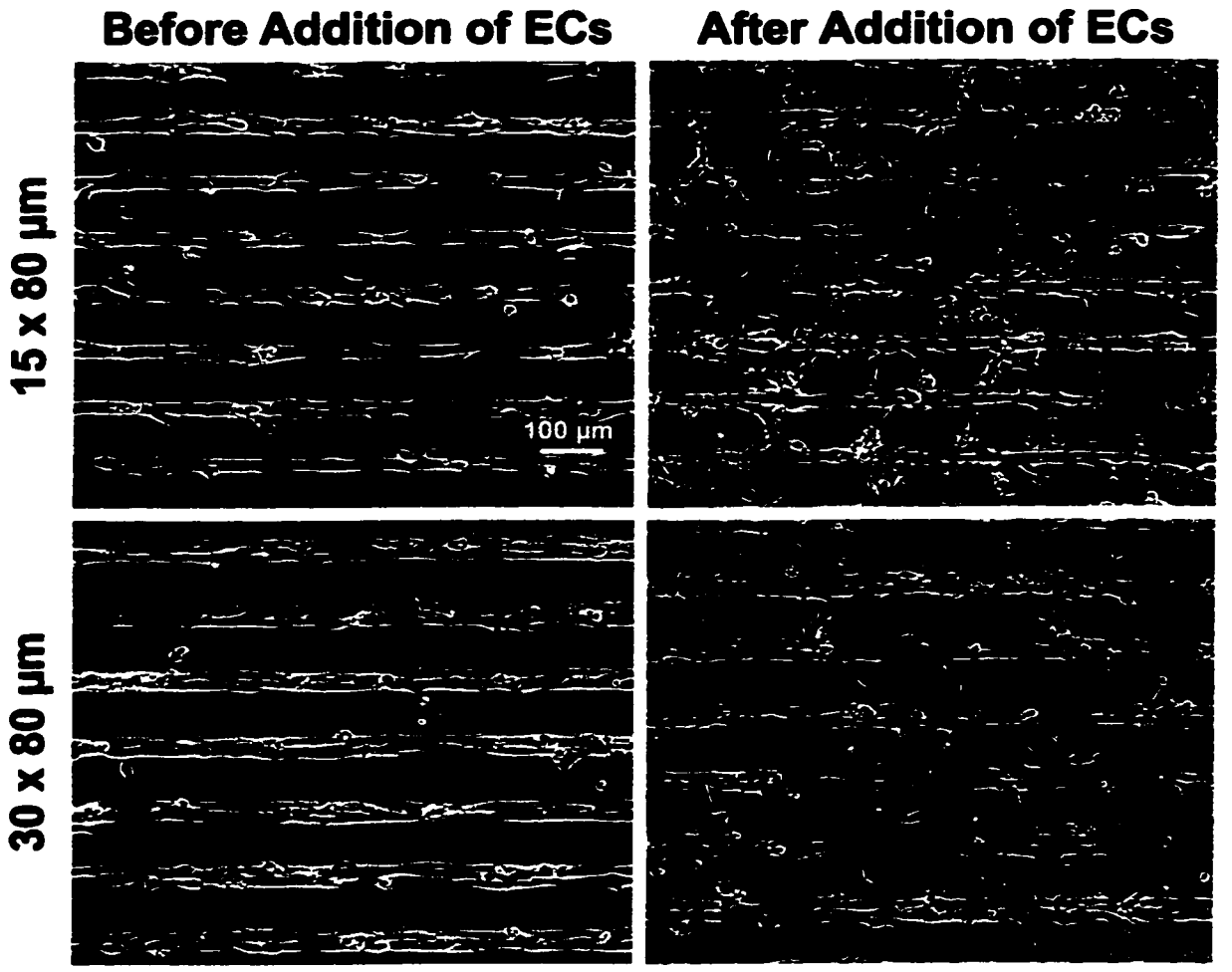

Figure 6.6. Spatially directed endothelial cell adhesion to immobilized biotinylated-fibronectin between cardiomyocyte patterns. Cardiomyocytes were cultured for 2 days on laminin lanes either 15x80 µm (top row) or 30x80 µm (bottom row) printed onto streptavidin-coated polystyrene dishes. The cultures were rinsed with PBS, incubated with a solution of biotinylated-fibronectin (12.5 µg/ml in PBS) and seeded with endothelial cells. The endothelial cells attached and spread in the regions between the rows of cardiomyocytes on the immobilized fibronectin.

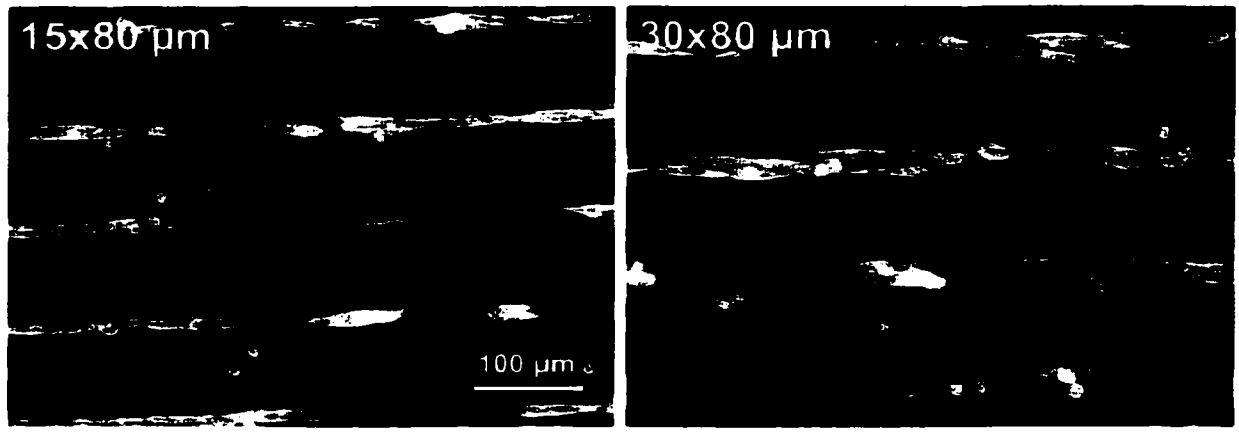

Figure 6.7. Immunostaining of cardiomyocyte/endothelial cell co-culture utilizing biotinylated-fibronectin. Cardiomyocytes were cultured on patterned lanes of laminin either 15x80 µm (left) or 30x80 µm (right) printed onto streptavidin-coated polystyrene dishes and endothelial cells were seeded onto the patterned cultures after the addition of biotinylated-fibronectin. The cultures were fixed several hours after the addition of endothelial cells and stained for myosin heavy chain (green/gold) and counterstained with phalloidin (actin filaments, red) and DAPI (cell nuclei, blue). The cardiomyocytes (green/gold) remained adherent along the original laminin patterns, whereas the endothelial cells (red) attached and spread primarily in the regions between the patterned lanes.

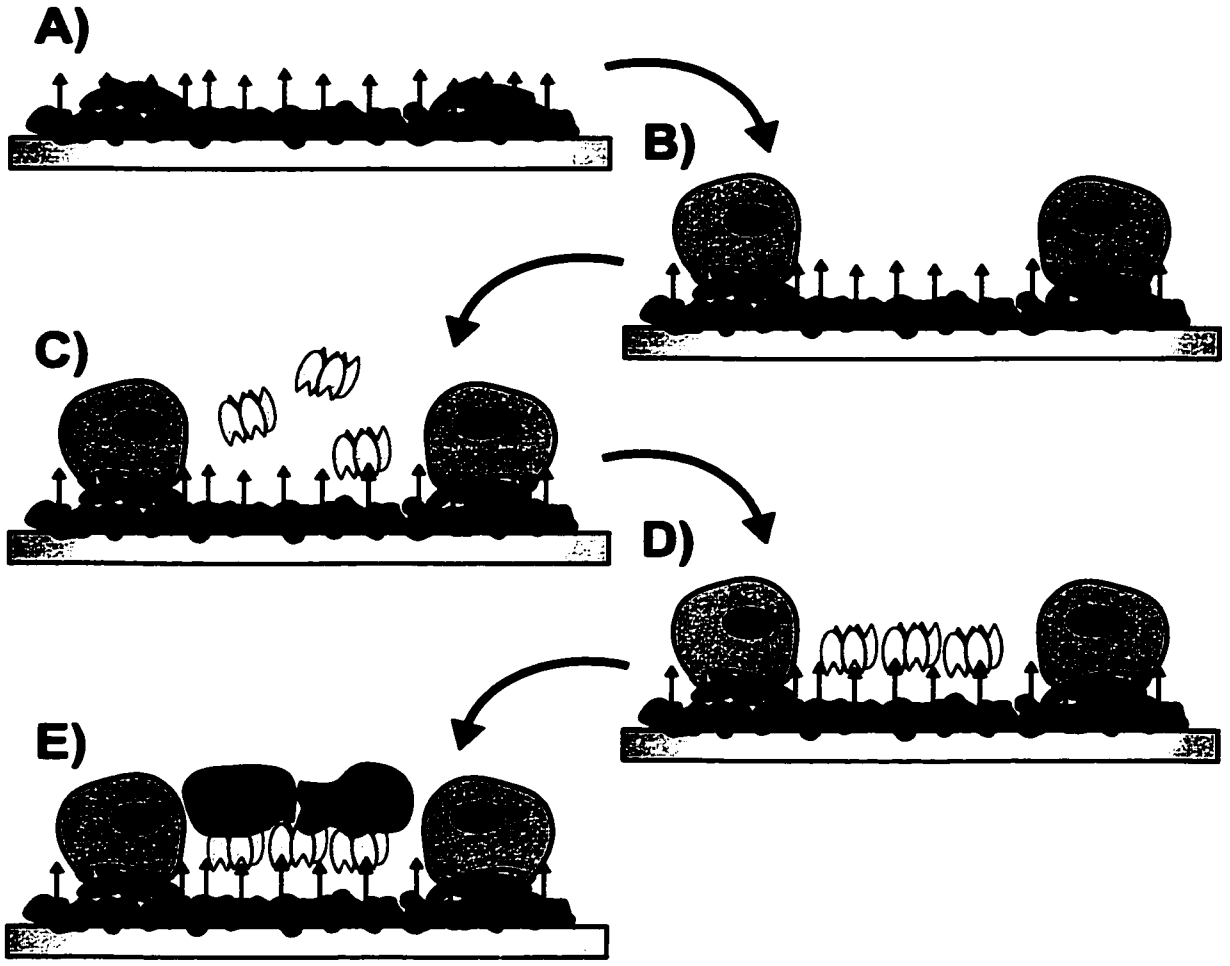

Figure 6.8. Schematic of co-culture method II: RGD-streptavidin. A) An adhesive protein pattern was printed onto a surface coated with biotinylated-BSA and B) cell adhesion was strictly directed along the micropatterned features. C) A solution of RGD-streptavidin was incubated with the cultures and D) bound specifically to the non-adhesive regions of biotinylated-BSA between the patterned cells. E) The attachment of a secondary cell type was directed to the newly adhesive regions of RGD-streptavidin between the primary cell patterns.

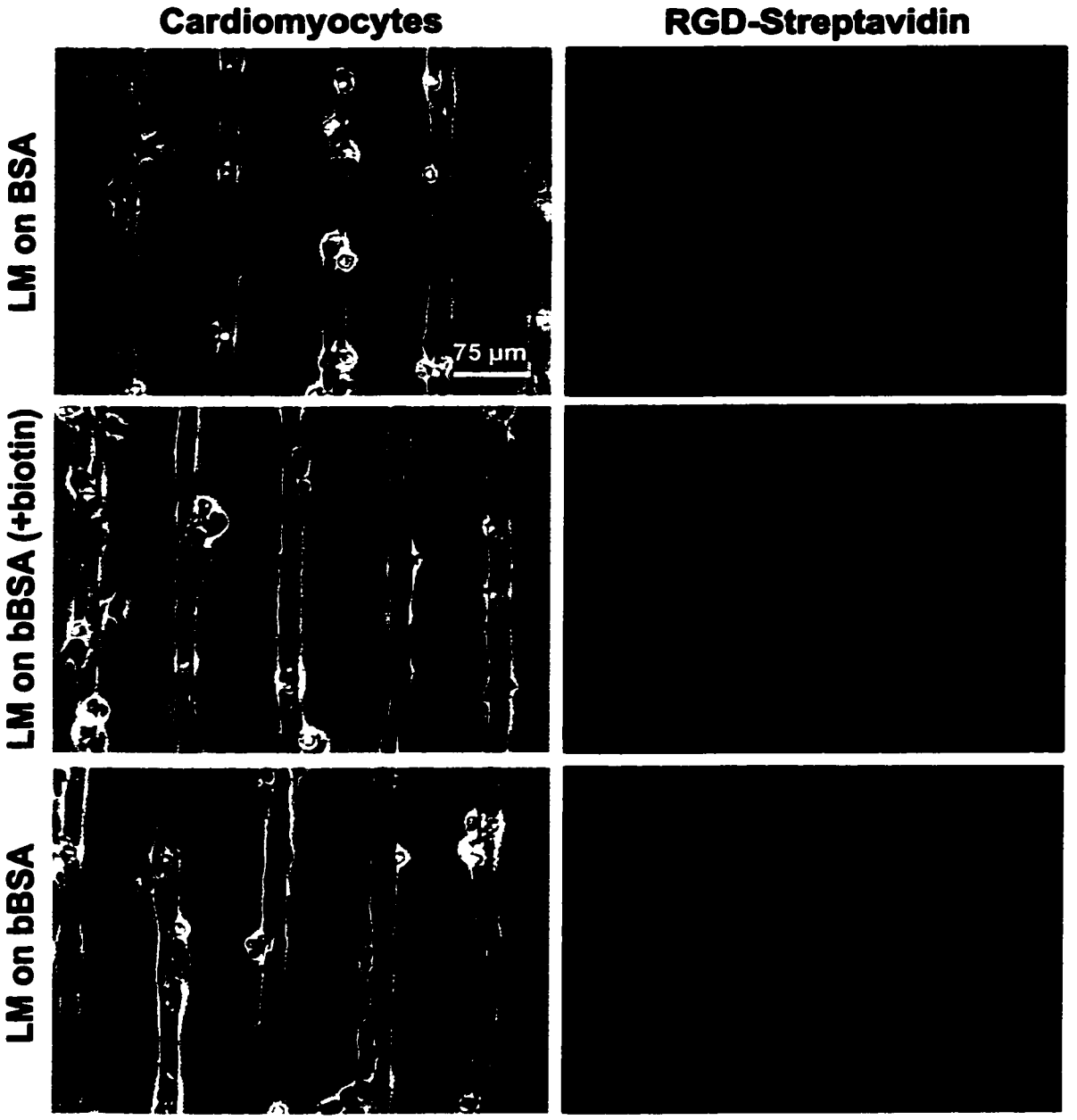

Figure 6.9. Immobilization of RGD-streptavidin to biotinylated-BSA between micropatterned cardiomyocytes. Cardiomyocytes were cultured for 2 days on patterned lanes of laminin (30x80 µm) printed onto either BSA-coated or biotinylated-BSA-coated polystyrene. The cultures were rinsed with PBS and incubated with a solution of rhodamine-labeled RGD-streptavidin (50 µg/ml in serum-free DMEM). The RGD-streptavidin was specifically immobilized on biotinylated-BSA surfaces (bottom row) but not on BSA-coated substrates (top row). The immobilization of RGD-streptavidin to the biotinylated BSA was inhibited by adding an excess of free biotin to the RGD-streptavidin solution (middle row).

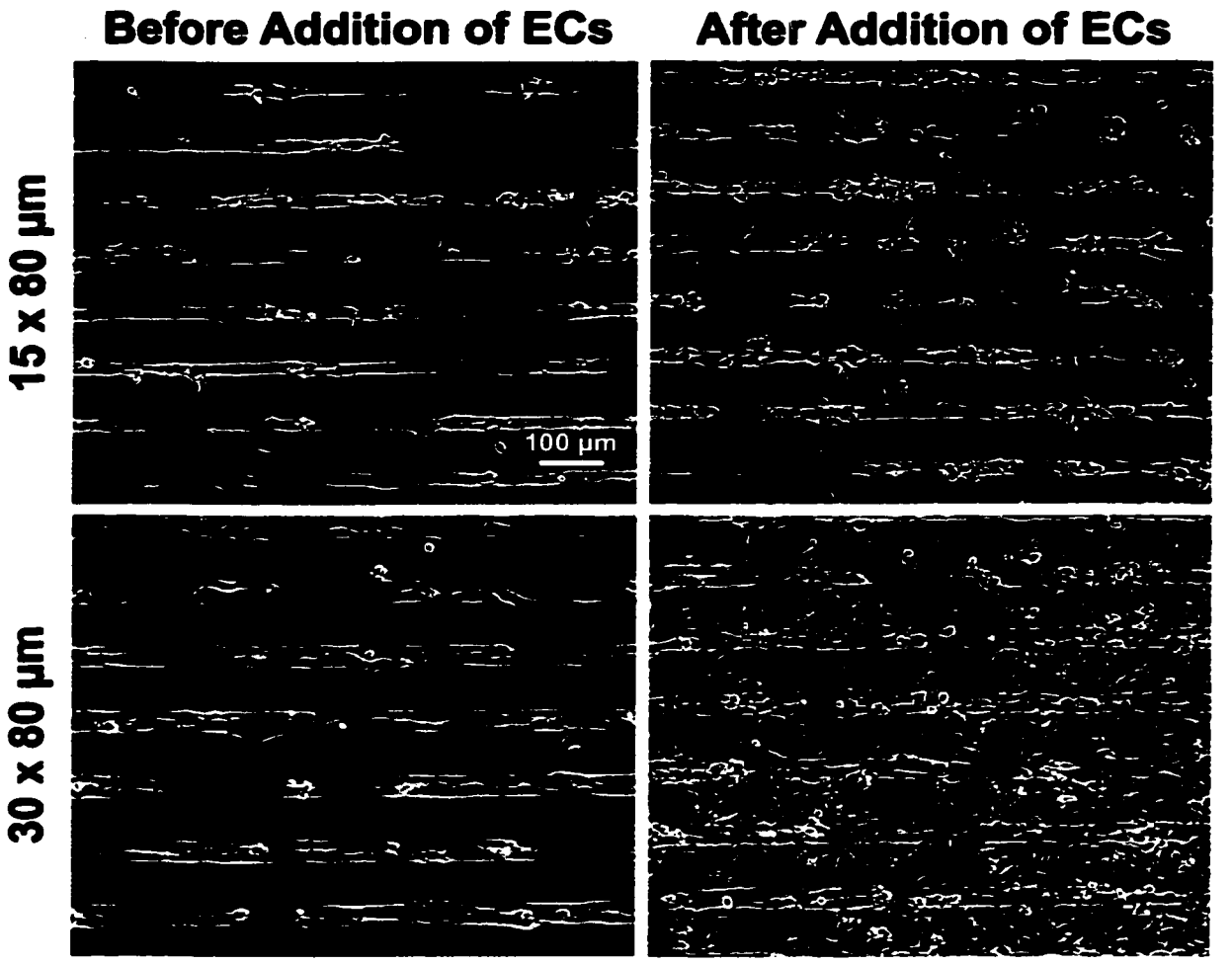

Figure 6.10. Spatially directed endothelial cell adhesion to immobilized RGD-streptavidin between cardiomyocyte patterns. Cardiomyocytes were cultured for 2 days on laminin lanes either 15x80 µm (top row) or 30x80 µm (bottom row) printed onto polystyrene dishes adsorbed with biotinylated-BSA. The cultures were rinsed with PBS, incubated with a solution of RGD-streptavidin (100 µg/ml in PBS) and seeded with endothelial cells. The endothelial cells adhered in the regions between the rows of cardiomyocytes on the immobilized RGD-streptavidin.

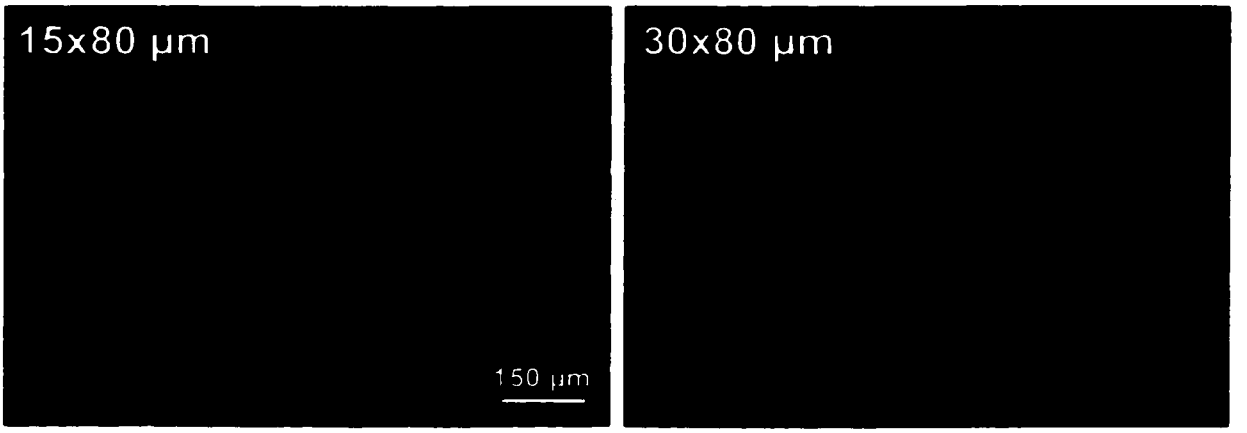

Figure 6.11. Stability of cardiomyocyte patterns 24 hours after the addition of RGD-streptavidin. Cardiomyocytes were cultured for 2 days on patterned lanes of laminin either 15x80 μm (left) or 30x80 μm (right) printed onto adsorbed layers of biotinylated-BSA. The cultures were rinsed with PBS and incubated briefly with a solution of RGD-streptavidin (50 μg/ml in PBS). The cells were then cultured an additional 24 hours before being fixed and stained for myosin heavy chain (green) and counterstained with DAPI (cell nuclei, blue). Despite the immobilization of adhesive RGD-streptavidin between the patterned rows of cardiomyocytes, the cells remained adherent along the original laminin lanes.

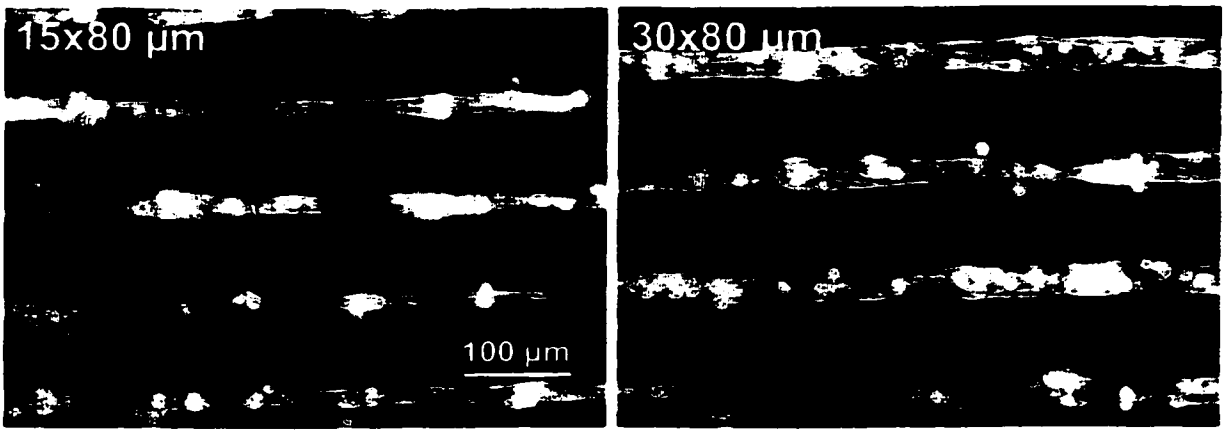

Figure 6.12. Immunostaining of cardiomyocyte/endothelial cell co-culture utilizing RGD-streptavidin. Cardiomyocytes were cultured on patterned lanes of laminin either 15x80 μm (left) or 30x80 μm (right) printed onto dishes pre-adsorbed with biotinylated-BSA and endothelial cells were seeded onto the patterned cultures after the addition of RGD-streptavidin. The cultures were fixed several hours after the addition of endothelial cells and stained for myosin heavy chain (green/gold) and counterstained with phalloidin (actin filaments, red) and DAPI (cell nuclei, blue). The cardiomyocytes (green/gold) remained organized along the original laminin lanes, whereas the endothelial cells (red) attached and spread primarily in the regions between the cardiomyocyte patterns.

Figure 6.13. Immunostaining for connexin 43 in patterned co-cultures of cardiomyocytes and endothelial cells. Cardiomyocytes were cultured for 3 days on patterned lanes of laminin (30x80 µm) printed onto polystyrene dishes coated with biotinylated-BSA and endothelial cells were seeded onto the patterned cultures after the addition of RGD-streptavidin (50 µg/ml in serum-free DMEM). The cultures were fixed several hours after the addition of endothelial cells and stained for connexin43 (green) and counterstained with phalloidin (actin filaments, red) and DAPI (cell nuclei, blue). Connexin43 expression was only observed in the cardiomyocytes and not in the endothelial cells.

Figure 6.14. Acetylated-LDL labeling of endothelial cells in co-culture with patterned cardiomyocytes. Cardiomyocytes were cultured for 3 days on patterned lanes of laminin (15x80 µm) printed onto polystyrene dishes coated with biotinylated-BSA and endothelial cells were seeded onto the patterned cultures after the addition of RGD-streptavidin (50 µg/ml in serum-free DMEM). A solution of acetylated-LDL (red) was incubated with the cultures 3 hours after the addition of the endothelial cells and the cultures were then fixed and counterstained with DAPI (cell nuclei, blue). Acetylated-LDL uptake was restricted to the endothelial cells, which were primarily adherent between the patterned rows of cardiomyocytes.

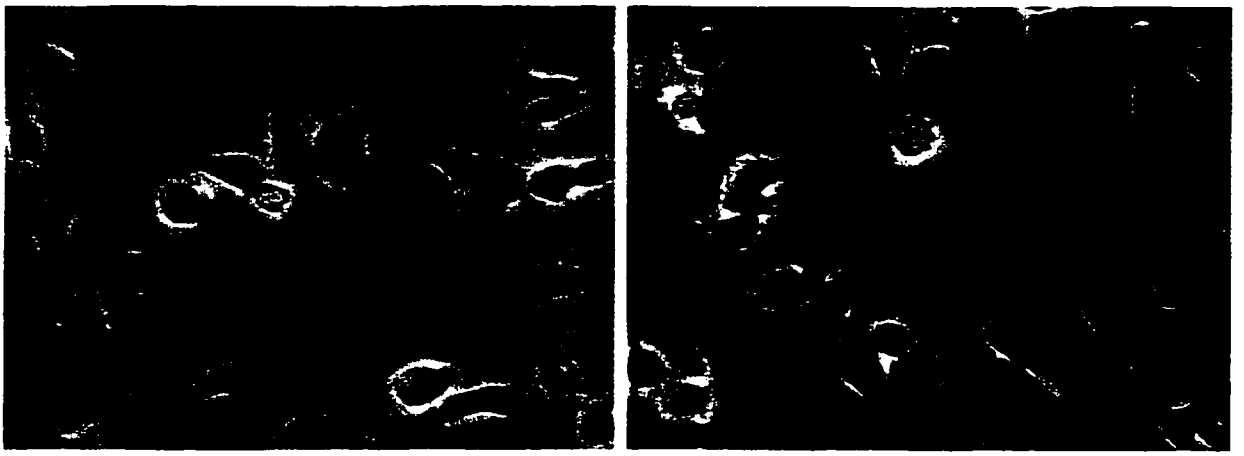

Figure 6.15. Micropatterned co-culture of smooth muscle cells and endothelial cells. Smooth muscle cells were cultured in serum-free Waymouth's media for 3 hours on micropatterned squares of fibronectin (60x60 μm) printed onto dishes coated with biotinylated-BSA. Endothelial cells were labeled with Cell Tracker Green and seeded onto the cultures after the addition of RGD-streptavidin (100 μg/ml in serum-free DMEM). The endothelial cells adhered mostly between the islands of patterned cells, although some also attached to portions of the original fibronectin patterns not covered by smooth muscle cells.

Chapter 7: Spatially Organized Layers of Cardiomyocytes on Biodegradable Polyurethane Films

7.1 Abstract

Ideally, tissue engineering constructs should match the physical and mechanical properties of the native tissue. This implies that pliable scaffolds might be better suited for soft tissue applications than rigid polymeric materials. In this study, we examined spatially organized cardiomyocyte cultures on biodegradable, elastomeric polyurethane films. The films were patterned by microcontact printing of laminin lanes and the resulting cell patterns on polyurethane displayed a similar morphology to those that were previously achieved on other substrates, such as polystyrene dishes. However, the integrity of the cardiomyocyte patterns on polyurethane films was retained for longer periods of time than on either polystyrene dishes or glass coverslips. When additional cardiomyocytes were seeded onto the patterned cultures, secondary and tertiary cell populations were aligned by the organization of the primary patterned cells. Dense, highly aligned layers of patterned cardiomyocytes were able to contract thin solvent cast polyurethane films. These results indicate that elastomeric, biodegradable polyurethane films can serve as an appropriate scaffold material to stably support the engineering of spatially organized layers of cardiomyocytes *in vitro*.

7.2 Introduction

Tissue engineering constructs frequently require the use of cells seeded into or onto polymeric scaffolds.[189, 190] Interest in reconstruction and regeneration of soft and connective tissues has resulted in a number of new degradable materials however there are few with mechanical properties required for cardiovascular applications. Poly-lactic/glycolic acid, one of the most widely used biodegradable polymers, is a relatively rigid, brittle material that may not be optimally suited for engineering of soft tissue constructs, such as cardiac tissue.[191] In order to better meet the mechanical demands of such a contractile tissue and allow adequate force generation, an elastomeric polymeric material may serve as a more appropriate scaffold. Recently a new class of biodegradable, segmented polyurethane elastomers has been synthesized using a lysine-based diisocyanate, polycaprolactone and a novel phenylalanine chain extender.[192] Materials produced using these polyurethanes are elastomeric and have tunable degradation rates.[193]

Having previously demonstrated that cardiomyocyte cultures could be spatially organized on polystyrene dishes and thin PLGA films (see Chapter 5), we sought to transfer this patterning method to other materials that could potentially serve as more appropriate scaffolds for cardiac tissue engineering constructs. In this study, we evaluated patterned cardiomyocyte morphology and contractile function on biodegradable polyurethane thin films, for up to four weeks *in vitro*. The morphology and stability of the patterned cardiomyocytes on polyurethane were compared to similar cultures on polystyrene or glass coverslips. Most of the experiments designed to characterize the cell interaction with the material were performed with spin-cast

polyurethane films on glass coverslips. However, several experiments were also conducted using solvent cast films, in order to determine if the cells could contract the elastomeric polymer films.

7.3 Methods

7.3.1 Polyurethane Synthesis. The polyurethanes were synthesized in the laboratory of Dr. Kim Woodhouse at the University of Toronto, using the methods of Skarja and Woodhouse.[192] Briefly, the chain extender was synthesized using a Fischer esterification reaction between L-phenylalanine and 1,4 cyclohexane dimethanol. The segmented polyurethane was then synthesized using a standard two step condensation reaction with a 2:1:1 stoichiometry of di-isocyanate:soft segment:chain extender. In the first step, 2,6 di-isocyanato methyl caproate (LDI: Kyowa Hakko Kogyo Co. Ltd Japan) was reacted with polycaprolactone (PCL 1250)(MW 1250: Aldrich Milwaukee, WI) in the presence of stannous 2-ethylhexanoate (Sigma, St. Louis, MO). This pre-polymer was subsequently reacted with the phenylalanine chain extender (Phe). The segmented polyurethane was then washed extensively to remove all traces of catalyst and leachables, evaluated using GPC and elemental analysis and cast into films for transport to the University of Washington. The PU had a M_w of 140,770 and a poly-dispersity index of 1.59. These materials have previously been extensively characterized[192, 193] and can be synthesized with good reproducibility.

7.3.2 Polyurethane Sample Preparation. A 2% solution (W/V) of the polyurethane (PU) was dissolved in anhydrous tetrahydrofuran (THF, Sigma) and passed through a

0.45μm PTFE membrane filter (Millipore) to remove small particulates. Round 25 mm glass coverslips were cleaned by soaking in 100% ethanol for a minimum of 30 minutes followed by a subsequent rinse in distilled, deionized water for an additional 30 minutes. Thin films of the polyurethane were deposited on the glass coverslips by a spin-coating device (Headway Research, Inc., Garland, TX), which was housed within a plexiglass chamber equilibrated with a nitrogen environment. Based upon preliminary optimization experiments, 50 μl of the polymer solution was applied to the center of the coverslips at the start of a 30 second spin cycle at 3000 rpm. The PU-coated coverslips were stored in a desiccator at room temperature until further use in surface analysis or cell culture experiments.

Alternatively, thin films of the PU were solvent cast in 10 ml Teflon beakers. The Teflon beakers were cleaned before each use by soaking in acetone for several hours followed by several rinses in distilled, deionized water and then air-dried. 300-600 μl of the 2% PU solution in THF was added to each beaker and a large petri dish lid was placed above the beakers to deter dust and debris from settling in the polymer films. The solvent was allowed to evaporate slowly from the covered beaker for at least 24 hours within a fume hood and then the cast films were removed from the bottoms of the beakers with forceps. A range of volumes was initially explored to determine the minimal amount of the polymer solution necessary to cast the PU films. It appeared that a minimum volume of ~450-500 μl was necessary to obtain continuous, thin PU sheets free of holes and similar defects. After determining the minimal necessary volume, all subsequent films were cast using this amount. The free-standing polymer films were

placed in 100 mm polystyrene dishes and stored in a desiccator at room temperature until further use.

7.3.3 Surface Analysis of Polyurethane Films. The quality and clarity of PU spin-coated coverslips and PU solvent cast films were visually inspected with an inverted microscope (Nikon Eclipse TE-300). The morphology and film thickness of the PU samples were examined with an environmental scanning electron microscope (ESEM, FEI 2020) with an accelerating voltage of 15kV at a pressure of 5 Torr. The samples were viewed transverse to the surface and in cross-section. The surfaces of the PU samples were analyzed by ESCA (S-probe) at a take-off angle of 55°; low resolution spectra and high resolution of the carbon 1s peak were acquired. ESCA analysis was performed on samples from separate 2% PU solutions and prepared on different days to ensure the consistency of sample preparation. Sessile bubble contact angle measurements of water in air were taken with a goniometer (Rame Hart) for 3 individual samples (3 spots per sample, n=9 total). Advancing contact angle measurements were taken after delivering five consecutive drops of distilled, deionized water (7 µl each) to the surface of the materials, and receding contact angle measurements were taken after the removal of the fifth and final drop.

7.3.4 Micropatterning and Cell Culture. The coverslip samples were affixed to the bottom of 35 mm polystyrene dishes with double-sided scotch tape. Individual solvent cast films were placed in 35 mm polystyrene dishes, but not secured to the dish. Despite the initial hydrophobicity of the PU solvent cast samples, their mass kept them weighted

down sufficiently to avoid floating during cell culture. The samples were sterilized by 10 minutes of UV light irradiation in a cell culture hood prior to cell culture experiments.

The samples were patterned by microcontact printing of laminin lines (15 or 30 μm wide spaced 10 or 20 μm apart) and seeded with freshly isolated rat neonatal cardiomyocytes (1-2 days old), as previously described (see Chapter 2). A 30 μg/ml laminin solution in PBS was adsorbed onto the surface of the stamps which were printed onto the native PU materials and the patterned films were then blocked with a 0.1% solution of BSA in PBS. The cells were plated at a density of ~400,000-500,000 cells/dish for coverslip samples in 2.5 ml of media. Solvent cast samples were seeded with 500,000-700,000 cells/sample at a density of $1x10^6$ cells/ml overnight and additional media was added the following day to bring the final volume in the dish to ~2.5 ml. A 1 μM concentration of cytosine arabinofuranoside (ara-C, Sigma) was supplemented to the culture media to prevent fibroblast proliferation and overgrowth of the cultures. The ara-C containing media was added at the first and all subsequent re-feedings.

7.3.5 Time Course Experiments. Fluorescently labeled laminin, conjugated to Oregon Green 488™ as described in Chapter 2, was patterned onto the PU spin-cast glass coverslips. Laminin-Oregon Green patterns were monitored by fluorescent microscopy over the course of 4 weeks *in vitro* both with and without adherent cardiomyocytes on the protein patterns. Fresh cardiomyocyte culture media was added to the protein patterns without cells at least twice a week and patterned cardiomyocyte cultures were re-fed 2-3 times per week during the course of the experiments. The signal-to-noise ratio of the

fluorescence intensity of the laminin lanes was quantified using NIH Image software to assess the relative stability of the protein patterns.

7.3.6 Cell Tracker Labeling. Unpatterned cardiomyocytes were cultured on gelatin-coated 100 mm dishes in the presence of 1 μM ara-C prior to labeling with Cell Tracker (Molecular Probes). The cells were rinsed twice with PBS and labeled with either Cell Tracker Green (13.4 μM) or Orange (12.5μM) in serum-free DMEM solution. The cells were incubated with the Cell Tracker solution for 15 minutes at 37°C, 5%CO2 and rinsed twice for 5 minutes with serum-free DMEM. The Cell Tracker labeling efficiency of adherent cultures (visualized by fluorescent microscopy) appeared to be 100% prior to the trypsinization of the cells and the dye remained visible in the cytoplasm of viable cells for at least 7 days in culture.

7.3.7 Serial Addition of Cardiomyocytes. Patterned cardiomyocyte cultures on PU spin-coated coverslips were rinsed with PBS and 400,000-500,000 cells labeled with Cell Tracker were added per sample. The cardiomyocytes labeled with Cell Tracker were seeded onto patterned cultures after 3 or 5 days with Green or Orange labeled cells, respectively, and allowed to attach overnight. The cultures were rinsed the following day and re-fed with fresh media containing 1 μM ara-C. The cultures were monitored by phase and fluorescent microscopy to distinguish between the different populations of cardiomyocytes. Fluorescently marked cells were also seeded onto gelatin-coated 35 mm polystyrene dishes as an unpatterned control.

7.4 Results

7.4.1 Polymer Film Analysis. The PU spin-coated films were very thin and optically clear when viewed by light microscopy. The PU solvent cast films were slightly opaque, but remained sufficiently transparent to permit visualization through the material. A concentric ring pattern on the solvent cast samples was observed by light microscopy on the bottom surface of the polymer films. The topological ring pattern originated from the surface morphology of the Teflon beakers used to cast the PU films and thus partially obscured subsequent light microscopy inspection of cells on the opposing surface of the film. The free-standing solvent cast PU films were quite flexible, allowing them to be easily folded or stretched.

ESEM analysis of the PU films provided more detailed inspection of the surface morphology and facilitated a rough estimate of the thickness of the films (Figure 7.1). The PU spin-coated films on glass coverslips, viewed transverse to the surface, appeared very smooth and uniform. The films were so smooth, in fact, it was necessary to scratch defects into the film in order to clearly locate the surface and provide some contrast for image acquisition. The solvent cast PU films had a slightly greater surface roughness when viewed transversely, but exhibited a comparable morphology (spherolites) to previous solvent casting results with this material (Fromstein & Woodhouse, personal communication). The surface topology did not affect the quality of protein or cell patterning in subsequent experiments. Cross-section or tilted views of the edge of the PU samples were used to estimate film thickness. By this technique, it appeared that the PU spin-coated films were less than a micron thick and the PU solvent cast samples were on the order of 10-15 μm thick.

ESCA surface analysis of the PU coverslips and solvent cast films (Table 7.1) was in good general agreement with previously reported results for this material.[193] The spin-cast PU films appeared to be free from any surface contamination, but the solvent cast films contained a small amount of silicone contamination. Micropatterning and cell culture experiments did not appear to be affected by the trace amount of silicone detected on the solvent cast films by ESCA analysis.

The PU films were relatively hydrophobic, as indicated by contact angle measurements (Table 7.2), however the advancing and receding values were less than that of native PDMS. This fact was important because previous protein printing experiments with native PDMS stamps and materials of varying wettability suggested that the substrate must be less hydrophobic than PDMS in order to facilitate protein transfer from the stamp to the surface (see Chapter 4). The increase in hydrophobicity of the solvent cast films, compared to the spin-cast, could have been due to the silicone contamination detected by ESCA. Although the films were initially hydrophobic, they became more wettable after pre-adsorbing protein solutions or subjecting the samples to cell culture media containing serum.

7.4.2 Protein Pattern Stability. Patterns of laminin conjugated to Oregon Green 488™ permitted *in situ* visualization and temporal analysis of the proteins on the surface. The laminin patterns were reproducibly achieved on the PU films and remained stable for as long as 28 days on the spin-cast films (Figure 7.2). Although the relative fluorescence intensity of the laminin-Oregon Green patterns on PU-spin-coated films decreased slightly over the course of 2-3 weeks in the serum-containing media, the signal-to-noise

ratio (SNR) remained relatively constant. Notably however, in the absence of cells, no appreciable defects in the patterns were detected over this time course, such as "holes" or "pits" within single lines (sub-micron) or larger-sized defects (10-100 μm scale) that disrupted one or several adjacent lines. These results suggest that the laminin patterns alone, prepared in this manner, are relatively stable in serum-containing cell culture media.

7.4.3 Cardiomyocyte Adhesion to Polyurethane Films. Cardiomyocytes did not attach well to any of the native substrates (i.e. glass, polystyrene, or PU), but they did attach and spread if the samples were pre-coated with matrix proteins beforehand (Figure 7.3). Cardiomyocyte adhesion, morphology, and contractile behavior on unpatterned samples prepared in this way resembled cardiomyocytes cultured on polystyrene dishes with pre-adsorbed protein coatings, such as laminin or gelatin.

Micropatterned cardiomyocytes on PU films exhibited similar morphological features to comparable cultures on polystyrene dishes described previously (see Chapter 5). The cardiomyocytes specifically attached and spread on the printed laminin lanes of the micropatterned samples. Although cardiomyocytes did not readily adhere to the native PU material, blocking with a BSA solution immediately following the protein printing appeared to improve the initial confinement of cardiomyocytes to the laminin lanes, indicated by fewer cells bridging between adjacent rows of cardiomyocytes. The addition of ara-C to the culture medium resulted in highly pure cardiomyocyte cultures. Cardiomyocytes were distinguished from non-myocytes by positive immunohistochemical staining with an antibody to myosin heavy chain (MHC) (Figure

7.4). MHC and phalloidin staining indicated that intercellular myofibrils were primarily aligned with the orientation of the major axis of the cells spread along the laminin patterns. Immunostaining for N-cadherin and connexin43, components of intercalated disks, exhibited localized bands of expression at the bipolar ends of neighboring cells (Figure 7.5). This expression pattern closely resembles that found in mature adult tissue, as previously demonstrated (see Chapter 5).

7.4.4. Time Course of Cardiomyocyte Patterns on Polyurethane. To assess the stability of the laminin patterns and associated cell patterns, cardiomyocyte cultures on patterned PU spin-coated samples were followed by fluorescent and phase microscopy for up to 28 days. Laminin-Oregon Green patterns printed onto PU spin-cast samples were seeded with cardiomyocytes. After 2 days with adherent cardiomyocytes, the laminin patterns appeared to be unchanged, but the cells began to reorganize the patterned matrix after about 7 days in culture. Over the course of the next several weeks, the cells degraded some regions of the patterned laminin, however the protein patterns were still largely retained for as long as 4 weeks while supporting cardiomyocyte adhesion (Figure 7.6). In addition to some of the laminin apparently being degraded, after about 10-14 days the fluorescently labeled laminin was re-organized into fibrils by the cells. The laminin fibrils were clearly attached to the surface of the cardiomyocytes since the fibrils were observed to move in unison with the contractions of the cells.

The cardiomyocytes were highly aligned by the initial protein patterns for 4 weeks in culture. After about 1 week, dense cardiomyocyte cultures on line patterns with narrow spacing (i.e. 15x10 μm) coalesced into a highly aligned sheet of synchronously

beating cells (Figure 7.6). This patterned cardiomyocyte morphology and contractile behavior on the PU film persisted for the duration of the experiment (up to 4 weeks). Under high-powered magnification, striated myofibrils aligned with the direction of the patterned lines were observed within the cells. After about 3 weeks in culture, some portions of the PU film appeared to be detaching from the glass coverslips, however most regions with a high-density of patterned cardiomyocytes remained intact and stable.

7.4.5 Cardiomyocyte Patterns on PU versus Polystyrene. Previously we demonstrated that cardiomyocyte patterns on microcontact printed laminin lanes on polystyrene dishes were relatively stable for 7-10 days. As an initial comparison, protein and cell patterns of the same dimension were compared on polystyrene dishes and spin-cast PU films on glass coverslips. After 2 days, the cells had attached and spread along the patterned laminin lanes. The laminin patterns on PU exhibited fewer defects than the printed patterns on the polystyrene; this difference may be attributed to the contrast between the surface roughness of the two substrates (Figure 7.7). Although the PDMS can conform to general surface features, the polystyrene is not as smooth as the PU films on coverslips and thus minor topological features of the polystyrene may translate to minor defects in the protein patterns. The cell patterns after 2 days were comparable on both types of surfaces, but the cell density appeared to be slightly higher on the PU films, although the initial seeding density was the same for both (Figure 7.7). After about 6 days in culture, the cardiomyocyte patterns on polystyrene began to deteriorate. While most of the cells were still aligned with the laminin lanes, many began to apparently detach from the polystyrene dish and aggregate into beating clusters. In contrast, the cardiomyocytes

patterned on PU films remained firmly adherent to the surface and well aligned by the laminin lanes. The differences in cardiomyocyte morphology on laminin patterns on polystyrene and PU films suggested that differences in the intrinsic mechanical properties of the two materials might influence cell behavior.

7.4.6 Cardiomyocyte Patterns on Polyurethane versus Glass. In order to more accurately assess the effect of the PU polymer on cardiomyocyte patterning, the PU spin-coated coverslips were compared to the native glass coverslips. Thus the major difference between these two substrates was the presence or absence of the PU polymer film beneath the organized cardiomyocyte cultures. Laminin patterns were fabricated on both types of surfaces successfully by microcontact printing and the quality of the protein patterns was similar on PU films and the glass coverslips. The cell patterning was also similar on both materials after 2 days in culture, although the cardiomyocytes on PU were more highly confined to the patterned laminin lanes (Figure 7.8). After about 5-6 days in culture, the cardiomyocytes on the glass coverslips began to detach and aggregate into beating clusters, similar to the behavior observed on polystyrene dishes. By 7-10 days, the cell patterns on the glass alone were largely disrupted and only hints of some aligned cells indicated the original influence of the protein patterns (Figure 7.8). In contrast, the cardiomyocyte patterns on the PU spin-coated films were retained for as long as 13 days (longest time assessed in this experiment) and the cells remained adherent to the film without forming the beating clusters observed on the glass coverslips. This difference in cardiomyocyte morphology on the PU films, suggested that the elastomeric polymer provided a more suitable substrate for stable cardiomyocyte patterning.

7.4.7 Serial Addition of Cardiomyocytes. Having achieved stably patterned sheets of cardiomyocytes on the PU films, we investigated whether we could begin to create more three-dimensional organized constructs by seeding additional cells onto the patterned cell monolayers. The cells added to the patterned cultures were first labeled with Cell Tracker reagents (Green or Orange) to mark their identity (Figure 7.9). Upon the first addition, cells adhered between and on top of the original patterned rows of cardiomyocytes to produce a much denser layer of cells (1-2 cells thick), in contrast to patterned cultures without additional cells (Figure 7.10). The labeled cells aligned with the direction of the original cell and protein line patterns and took 2-3 days to fully spread after being added to the cultures. The second population of cardiomyocytes (Green) integrated with the originally patterned cell layer to form a synchronously beating sheet of cells that persisted for up to 10 days in culture (longest time point assessed).

A second addition of labeled cardiomyocytes (Cell Tracker Orange), representing a third cell population, was also performed with some samples. These cells were added 2 days after the addition of Cell Tracker Green labeled cells and 5 days since the original, unlabeled population of cardiomyocytes were initially seeded onto the PU films patterned with laminin. The "Orange" cells attached and spread on top of the dense layer of cardiomyocytes, although they did not appear to spread as much as the "Green" cells (Figure 7.11). After the second addition of cells, the culture layer was even denser than before and appeared to consist of 2-3 layers of cells. These results suggest that successive addition of more cells onto patterned cardiomyocyte layers can be performed

for several iterations to build up a more three-dimensional organized sheet of cardiomyocytes.

7.4.8 Cardiomyocyte Patterning on Polyurethane Solvent Cast Sheets. The PU spin-coated films were rapidly prepared and convenient substrates to characterize many of the properties of the patterned cardiomyocyte layers on the PU polymer. However, the ultrathin PU films spin-coated on glass did not readily detach from the coverslips, thus we also examined cardiomyocyte patterning on thin solvent cast PU films to determine whether the cardiomyocytes could contract the elastomeric material.

Laminin patterns were successfully printed onto the solvent-cast PU films and remained stable for as long as 21 days under cell culture conditions (longest time assessed). Often patterns with narrow spacing (i.e. 10 μm) were used to achieve high-density cultures of organized cardiomyocyte layers on the PU films.

The morphology of the cardiomyocyte patterns on the solvent cast PU samples resembled those achieved on the thinner PU spin-coated films. One noticeable difference, however, was the ability of the cells to contract the PU solvent cast films. During the first few days in culture, the cells beat normally, but they did not appear to contract the film. After 5-6 days in culture, many of the PU films were observed to contract in unison with the contraction of the cells. This resulted in cardiomyocyte contractions that were visually greater in magnitude than any beating activity previously observed on any other type of substrate. In some cases, the force of contraction was great enough to lift the entire polymer sheet, as it could be seen shifting in the culture dish with each "beat" (Figure 7.12). The primary direction of the cardiomyocyte contractions were

aligned with the orientation of the original protein patterns and persistent contraction of the films over several days induced wrinkles in the polymer film perpendicular to the direction of the patterns. The appearance of more and larger wrinkles in the films coincided with longer periods of time in culture (several weeks). Although this behavior was not observed for every one of the solvent cast PU films with patterned cardiomyocytes, about one half of the samples exhibited this phenomenon. On the other hand, although unpatterned cell cultures beat synchronously on the solvent cast films, none of the unpatterned samples ever appeared to contract the material. This suggests that an elastomeric scaffold material, like PU, may possess more appropriate mechanical properties for the engineering of sheets of organized cardiomyocytes to permit greater magnitude of contractile force.

7.5 Discussion

Cardiomyocyte patterns on PU films exhibited similar morphological attributes to cell patterns achieved on polystyrene dishes or PLGA films, as previously described (see Chapter 5). When cell patterning was compared between rigid substrates, such as polystyrene or glass, and the elastomeric polyurethane films, the integrity and longevity of cardiomyocyte patterns were improved on the polyurethane films. Organized multi-layered cell constructs could be generated on the polyurethane films by seeding additional cells onto the original cardiomyocyte patterns to form more three-dimensional tissue constructs. In addition, dense, highly aligned layers of cardiomyocytes on the solvent cast polyurethane films were able to contract the elastomeric film, in contrast to any other substrate material used. Based on these criteria, the elastomeric, biodegradable

polyurethane used here seems to be a desirable scaffold material for fabricating spatially organized cardiac tissue engineering constructs *in vitro*.

The quality and stability of the cardiomyocyte patterns were greatly improved on thin PU spin-cast films compared to either polystyrene dishes or glass coverslips. Initially, protein and cell patterns on the different materials were similar, but after several days in culture (5-6 typically) the cardiomyocytes on polystyrene or glass often formed beating aggregates of cells tethered to the substrate, as if the cardiomyocytes were pulling themselves off of the surface. In contrast, the cardiomyocytes on the thin PU films remained adherent to the surface along the protein patterned lanes. However, fluorescent microscopy inspection of the protein patterns on the different materials indicated that the laminin lanes remained largely unchanged during this time course. This suggested that the difference in cell morphology was not attributable to differences in the quality of the protein patterns, but perhaps to the intrinsic mechanical properties of the materials. Since the polyurethane is elastomeric, it could allow the contracting cardiomyocytes to pull on the thin film as they beat, whereas the force exerted by the contracting cells on more rigid substrates might cause them to eventually detach. Thus, the difference in the mechanical environment of the adherent cells appeared to influence the stability of cardiomyocyte patterning.

One problem with the patterned cardiomyocytes on spin-cast PU films was that they were unable to visibly contract the material because it was deposited as a thin layer on the rigid glass coverslips. On the rigid substrates, the adherent cardiomyocytes could only perform isometric contractions, thus although cells "beat", they weren't actually contracting. The cardiomyocytes patterned on solvent cast PU films were able to shorten

and thereby contract the films as they beat synchronously because they were attached to an elastomeric substrate. An interesting observation was that contraction of the elastomeric polymer was only observed with patterned cells and not unpatterned samples. The patterning aligned the cells such that their myofibrils were predominantly oriented in the direction of the patterned lines and thus the contractions of the cells were aligned. Presumably the alignment of the contracting cells resulted in a linear force vector such that the sum of the forces of the individual cells were able to contract the material. The unpatterned samples contained a similar density of cardiomyocytes, but since they were randomly arranged the sum of the contractile forces would cancel each other out. These results clearly demonstrated that by providing an elastomeric substrate, organized sheets of cardiomyocytes were able to produce visible contractions with a net force aligned with the direction of the patterned cells.

One of the biggest challenges of spatially controlled tissue engineering is to try and transform two-dimensional cell patterning methods into more relevant three-dimensional organized tissue constructs. Based on our results, one approach could be to seed additional cells onto patterned cell layers, such that the added cells organize according to the original cell patterns. This suggests that cells respond not only to spatial adhesive cues such as protein patterns, but also to topographical patterns of cells, with a monolayer of patterned cells serving as a template upon which to grow spatially organized tissue. Although this cellular self-assembly approach was only investigated to build up a few cell layers, conceptually it lends itself to becoming an iterative process whereby thicker tissue constructs could be generated. While successive seeding of cells is not an efficient procedure to develop very thick tissue constructs, it could be used to

generate relatively thin organized sheets of tissue (< 1mm). Separate sheets could then potentially be combined to form thicker multi-layered tissue structures.

7.6 Tables

Table 7.1. ESCA analysis of polyurethane films. The data presented are for samples prepared from different batches of the PU and cast on separate days. The relative atomic compositions of the samples match well with the expected percentages of carbon (C), oxygen (O), and nitrogen (N). No silicone (Si) contamination was detected on the spin-cast films, but a small amount of silicone was present on the solvent cast films.

	Atomic Composition (%)			
Samples	**C**	**O**	**N**	**Si**
PU spin-cast #1	81.1	16.5	2.4	nd
PU spin-cast #2	76.9	20.6	2.5	nd
PU solvent cast #1	79.5	13.8	1.4	5.3
PU solvent cast #2	79.9	13.8	1.4	4.9

Table 7.2. Contact angle measurements. Advancing and receding contact angles were measured for water droplets on the surface of the materials in air. The PU materials are relatively hydrophobic compared to the other substrates, but are less hydrophobic than the native PDMS stamps.

Sample	Adv. Contact Angle	Rec. Contact Angle
Glass coverslip	35 ± 3°	17 ± 3°
Polystyrene	78 ± 1°	69 ± 4°
PU coverslip	72 ± 3°	50 ± 1°
PU solvent cast	88 ± 2°	54 ± 4°
PDMS (native)	100 ± 2°	97 ± 1°

7.7 Figures

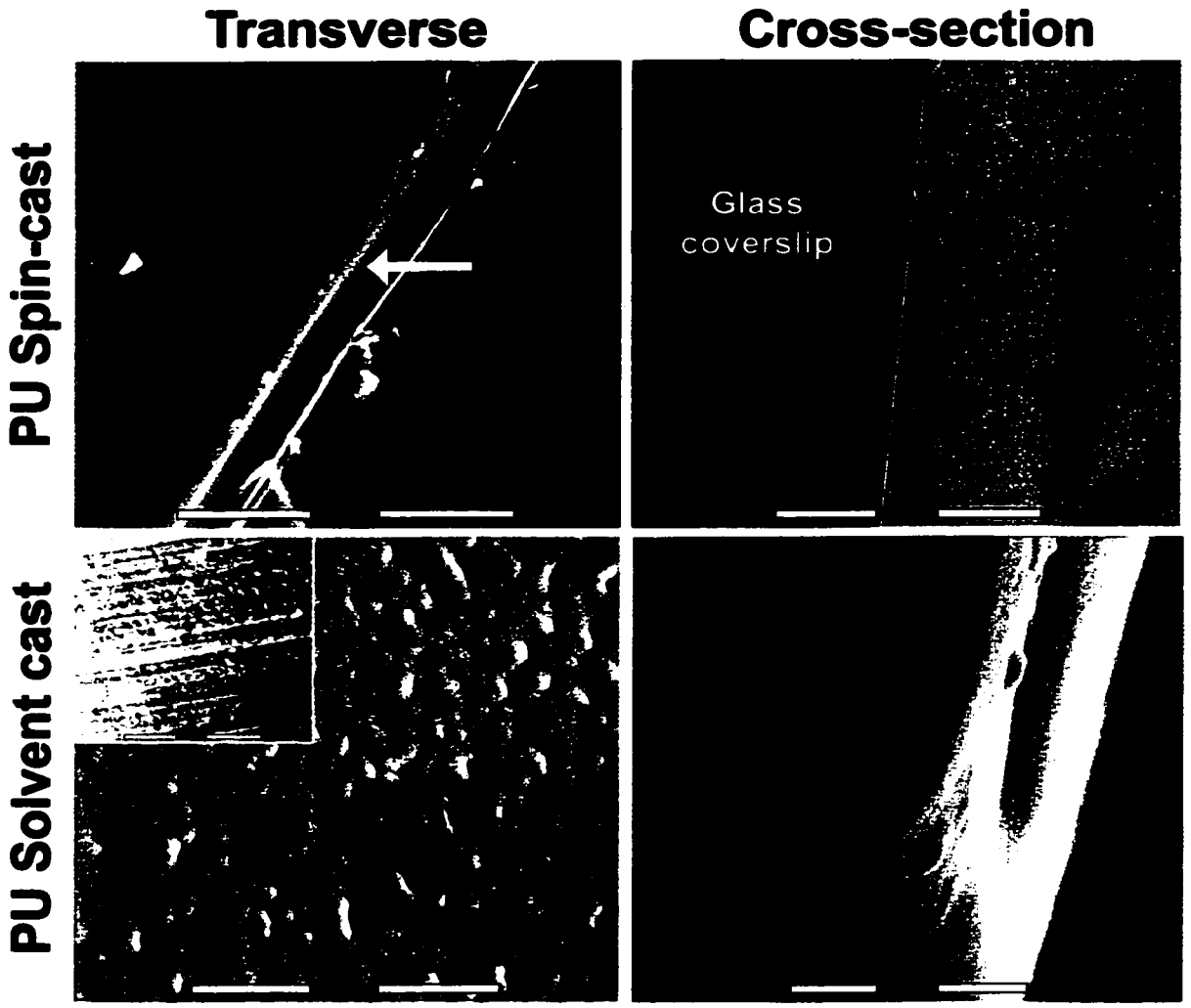

Figure 7.1. ESEM analysis of polyurethane films. The surfaces of spin-cast (top row) and solvent cast PU films (bottom row) were analyzed transversely to the surface and in cross-section. The PU spin-cast films were very smooth (the white arrow denotes a scratch intentionally made in the film to create contrast for imaging). The surface of the PU solvent cast films were relatively smooth, but displayed more of a spherolite morphology; the inset shows the back side of the film cast against the Teflon beaker. Cross-sectional analysis indicated that the spin-cast films were less than a micron thick and the solvent cast films were about 10-15 μm thick.

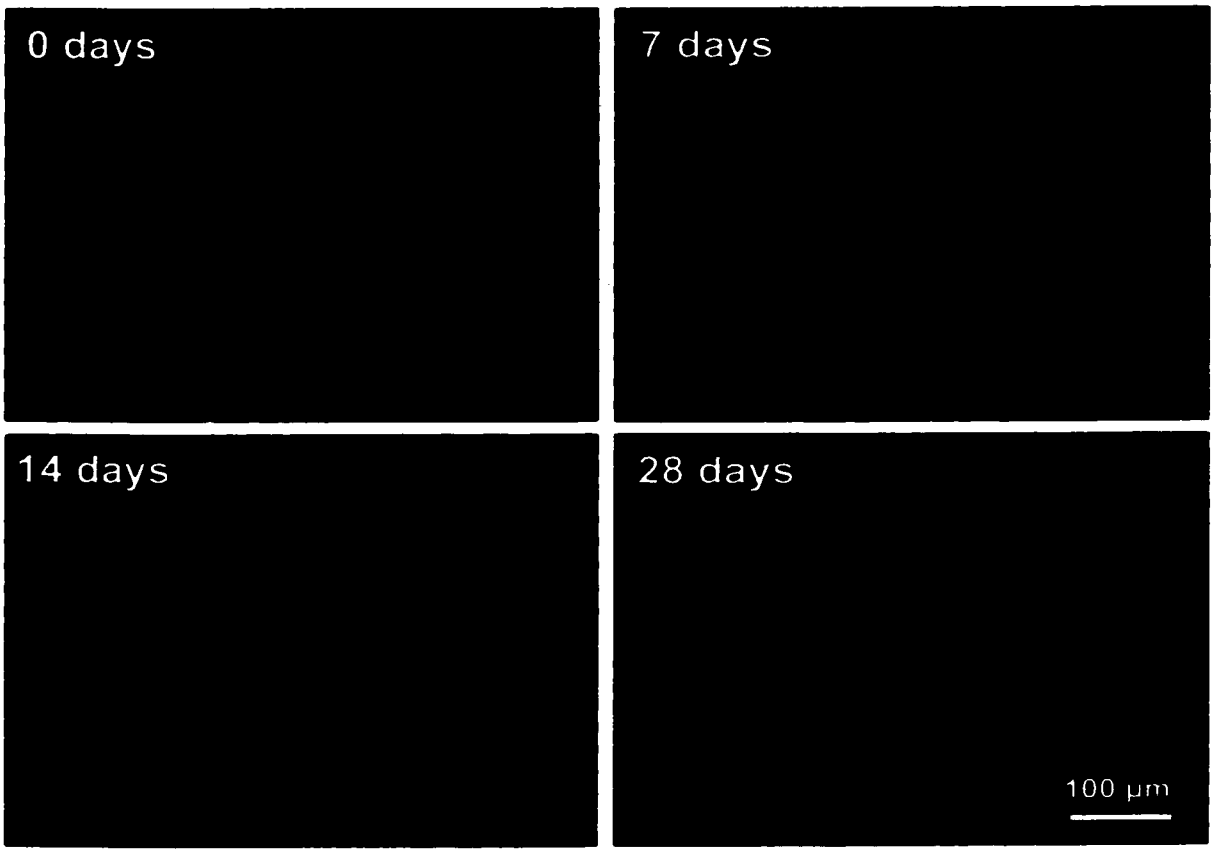

Figure 7.2. Stability of laminin patterns exposed to serum-containing media. Patterns of laminin conjugated to Oregon Green 488™ (15x10 µm lanes) were printed onto PU spin-coated glass coverslips and exposed to serum-containing cardiomyocyte culture media for up to 28 days under standard cell culture conditions (37°C, 5% CO_2). Although the fluorescence intensity decreased slightly over the course of 4 weeks, the morphology of the protein patterns remained unchanged over this period of time.

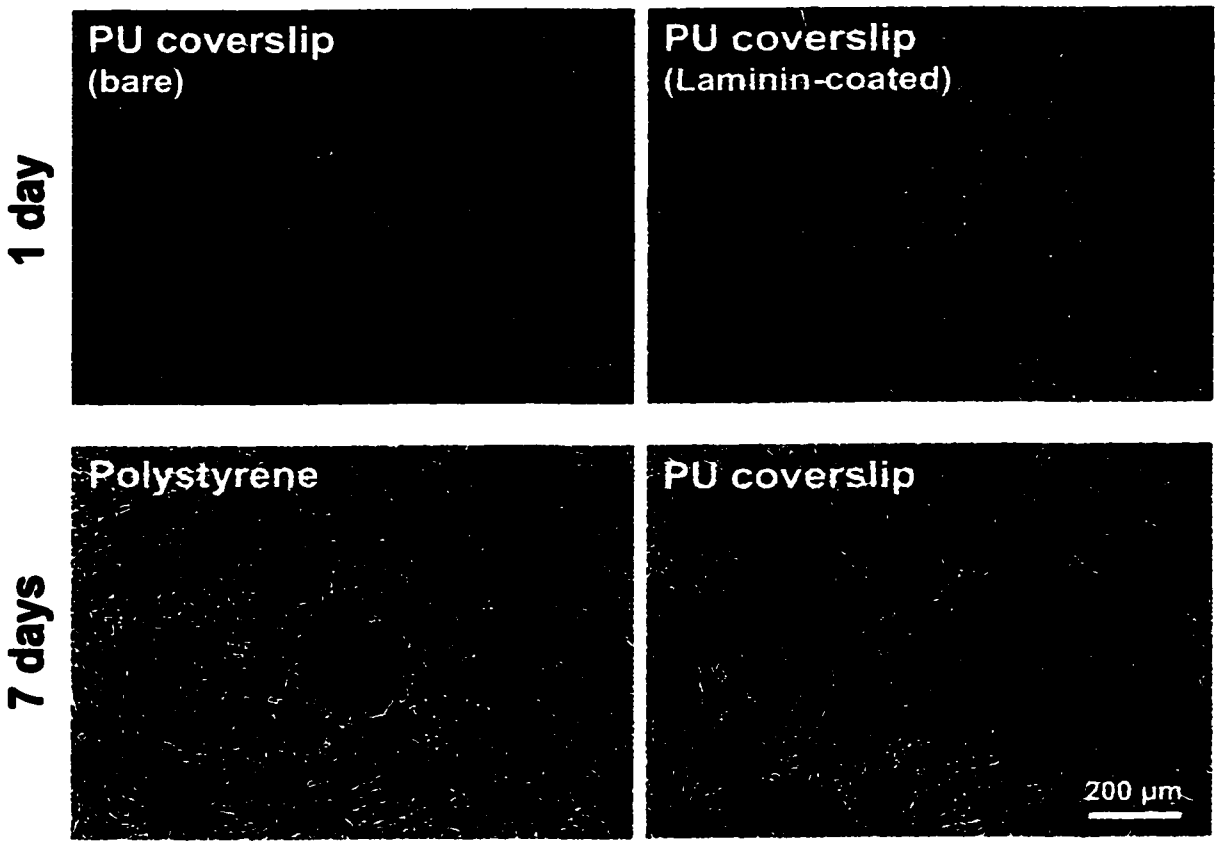

Figure 7.3. Cardiomyocyte adhesion to polyurethane spin-cast films. Cardiomyocytes did not readily attach to the native PU material, but did adhere and spread if laminin was pre-adsorbed onto the surface (top row). The morphology and contractile activity of the cardiomyocytes on the laminin-coated PU films were comparable to cultures on gelatin-coated polystyrene dishes (bottom row).

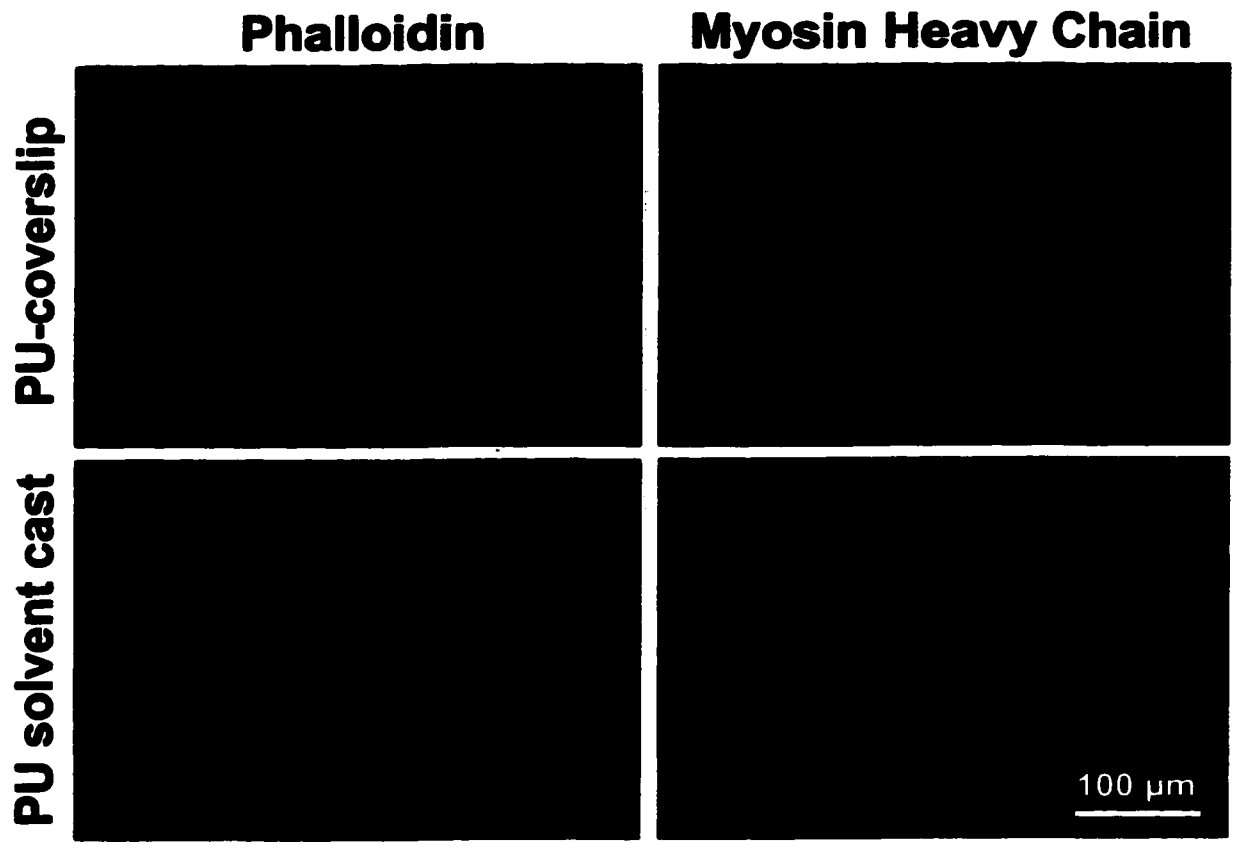

Figure 7.4. Immunostaining of patterned cardiomyocytes on polyurethane films. Cardiomyocyte patterns (15x20 µm lanes) on spin-cast or solvent cast PU films were fixed after 4 days, stained with an antibody to myosin heavy chain and counterstained with phalloidin (actin filaments). With ara-C present in the culture media, dense, highly aligned layers of cardiomyocytes were generated.

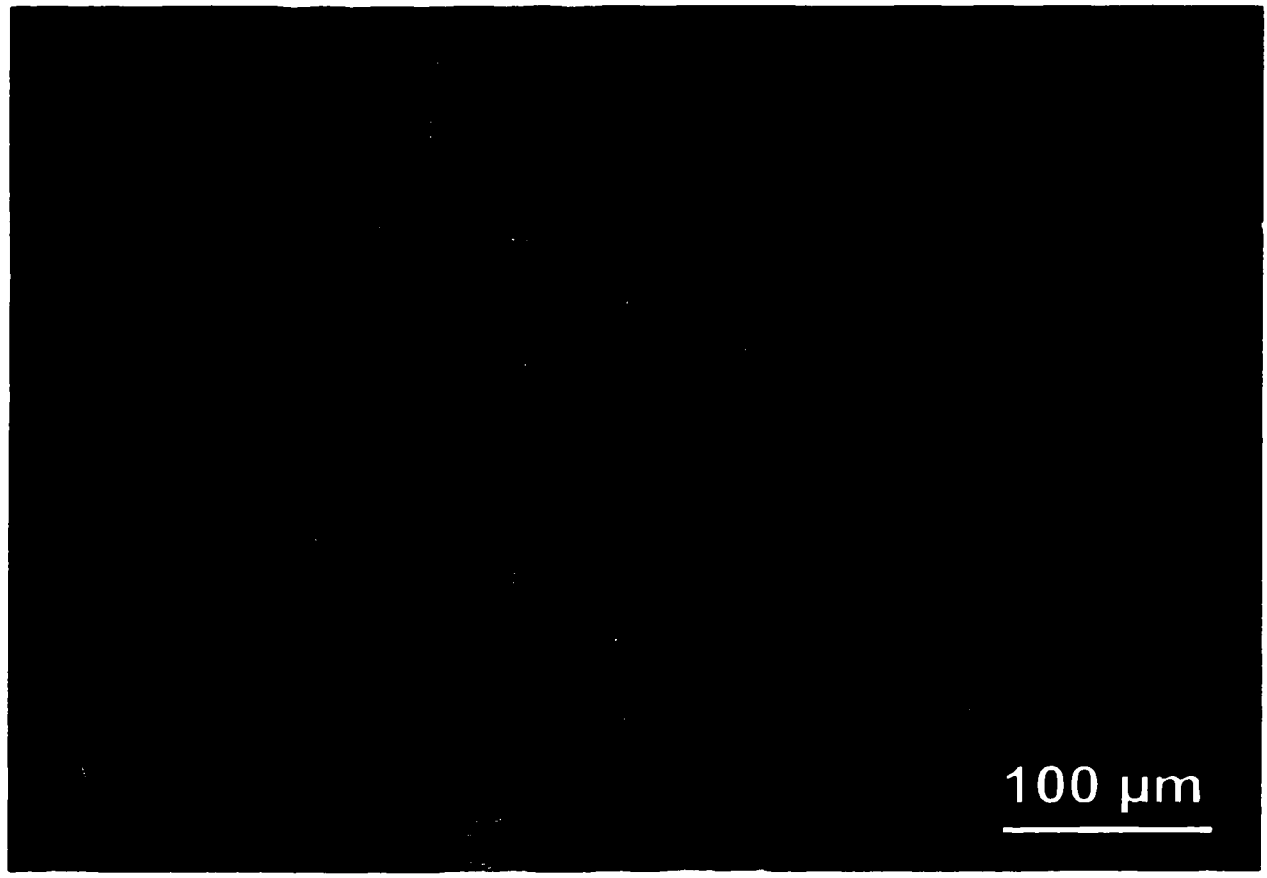

Figure 7.5. Immunostaining for N-cadherin in patterned cardiomyocytes on spin-cast polyurethane films. Cardiomyocyte patterns (15x20 μm lanes) were fixed after 4 days in culture, stained with an antibody to N-cadherin (green) and counterstained with phalloidin (actin filaments, red). N-cadherin was concentrated in localized bands of expression at the bipolar ends of adjacent cells, similar to native myocardial tissue.

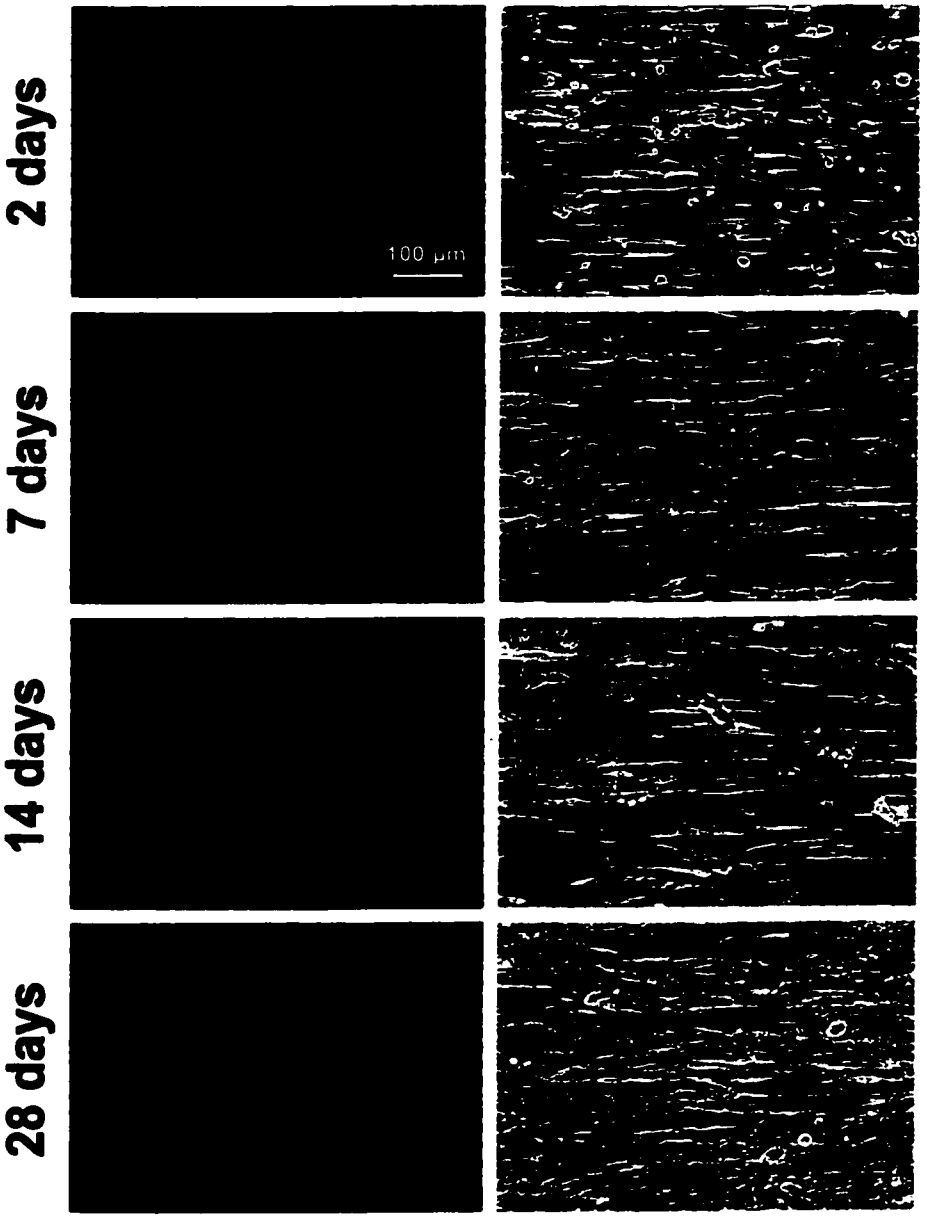

Figure 7.6. Time course of cardiomyocyte patterns on polyurethane spin-coated coverslips. Patterns of laminin conjugated to Oregon Green 488™ (15x10 µm lanes) were printed onto PU spin-coated glass coverslips, seeded with cardiomyocytes and cultured for up to 28 days. The laminin patterns (left column) were partially resorbed and re-organized by the cells during this time course, but remained clearly visible for up to 4 weeks. The cells remained highly aligned with the direction of the protein patterns during the course of the experiment (right column).

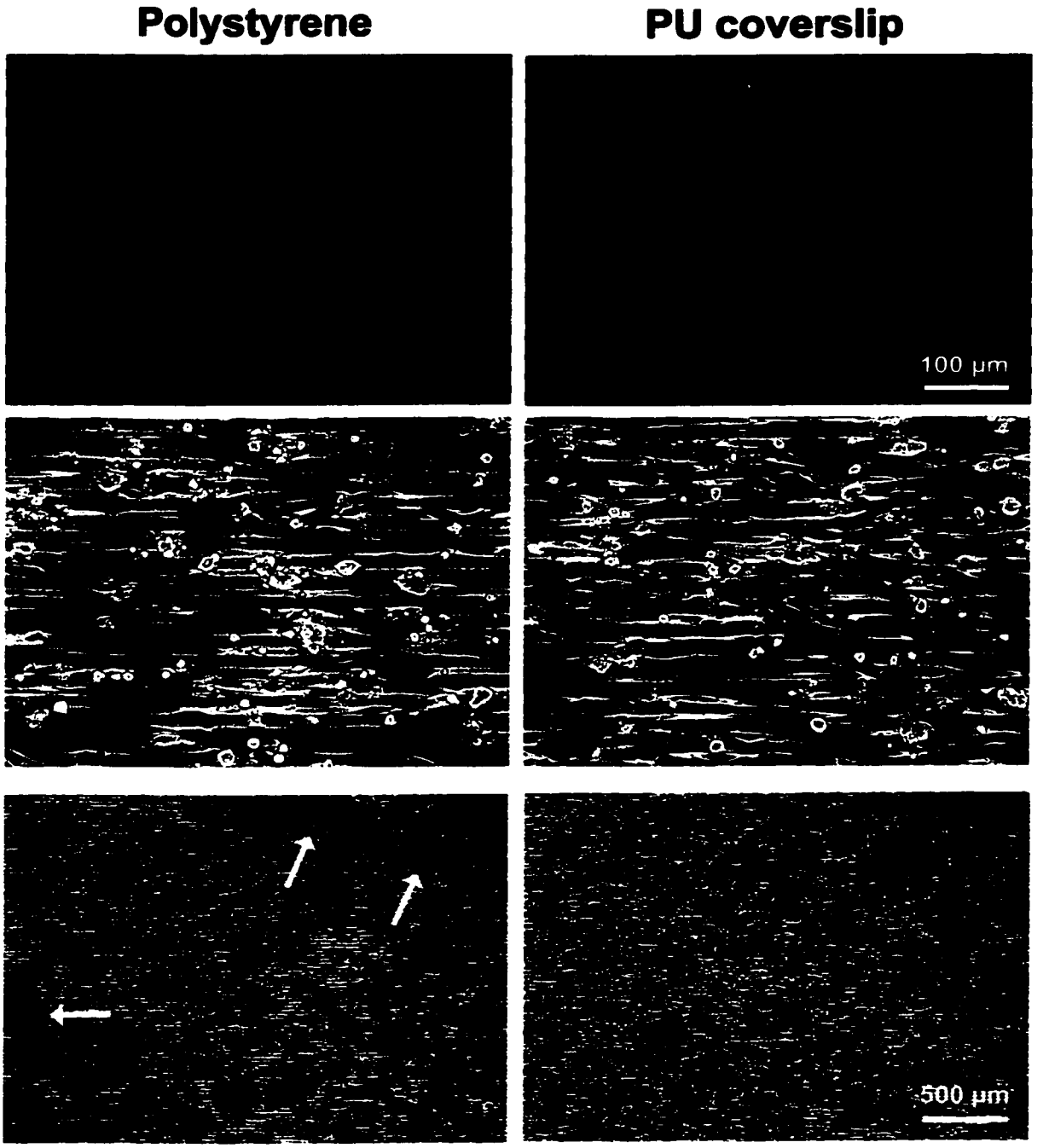

Figure 7.7. Comparison of cardiomyocyte patterns on polystyrene dishes and polyurethane spin-cast glass coverslips. After 2 days of culture, laminin (top row) and cardiomyocyte patterns (15x10 µm lanes) on polystyrene and PU were similar, but the overall patterning fidelity appeared to be better on the PU films. Arrows denote regions of interrupted cell patterning observed on polystyrene dishes. By 6-7 days, the cell patterns on polystyrene deteriorated whereas the patterns on PU films were retained.

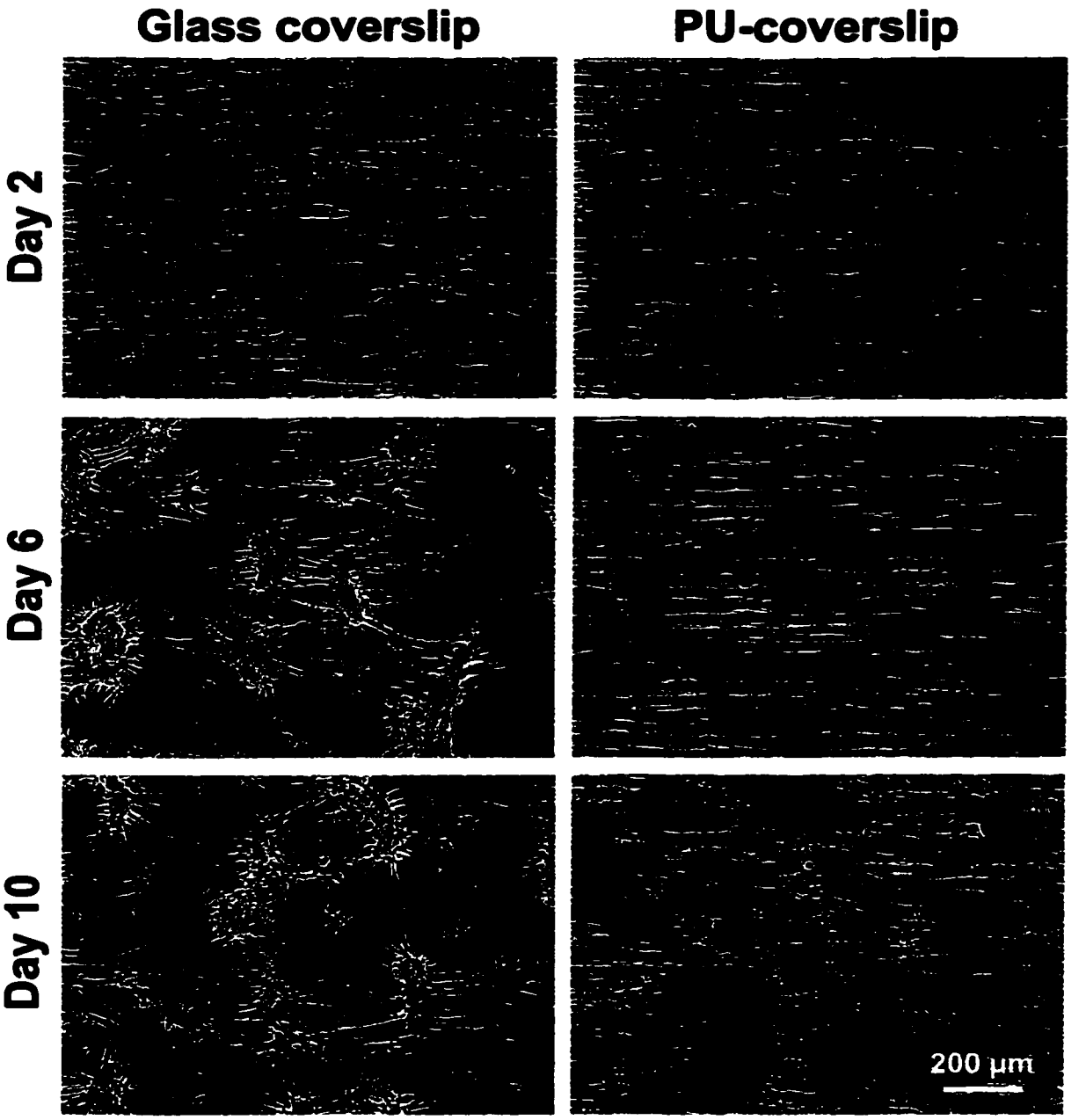

Figure 7.8. Comparison of cardiomyocyte patterns on native glass and polyurethane spin-cast coverslips. Initially, cardiomyocyte patterns (15x20 µm lanes) on the glass and PU films appeared similar, although the cells were better confined to the laminin patterns on the PU films. Over time, the cardiomyocytes on glass formed beating aggregates of cells, whereas the cells on the PU films remained adherent and highly aligned by the patterns.

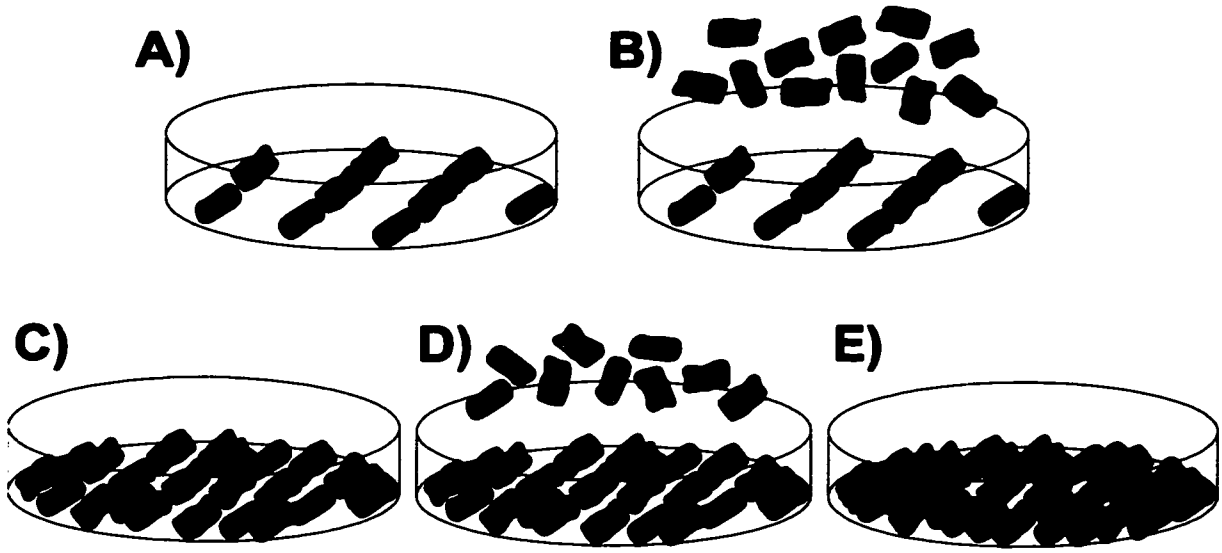

Figure 7.9. Schematic representation of seeding additional cardiomyocytes onto patterned cardiomyocyte layers. A) Cardiomyocytes were patterned on printed lanes of laminin on PU spin-cast films. B) After 3 days in culture, additional cardiomyocytes labeled with Cell Tracker Green were seeded onto the patterned cell cultures and C) adhered between and on top of the primary cell patterns. D) An additional 2 days later (5 days in culture total), cardiomyocytes labeled with Cell Tracker Orange were seeded onto the cultures and E) adhered onto the dense layer of cells.

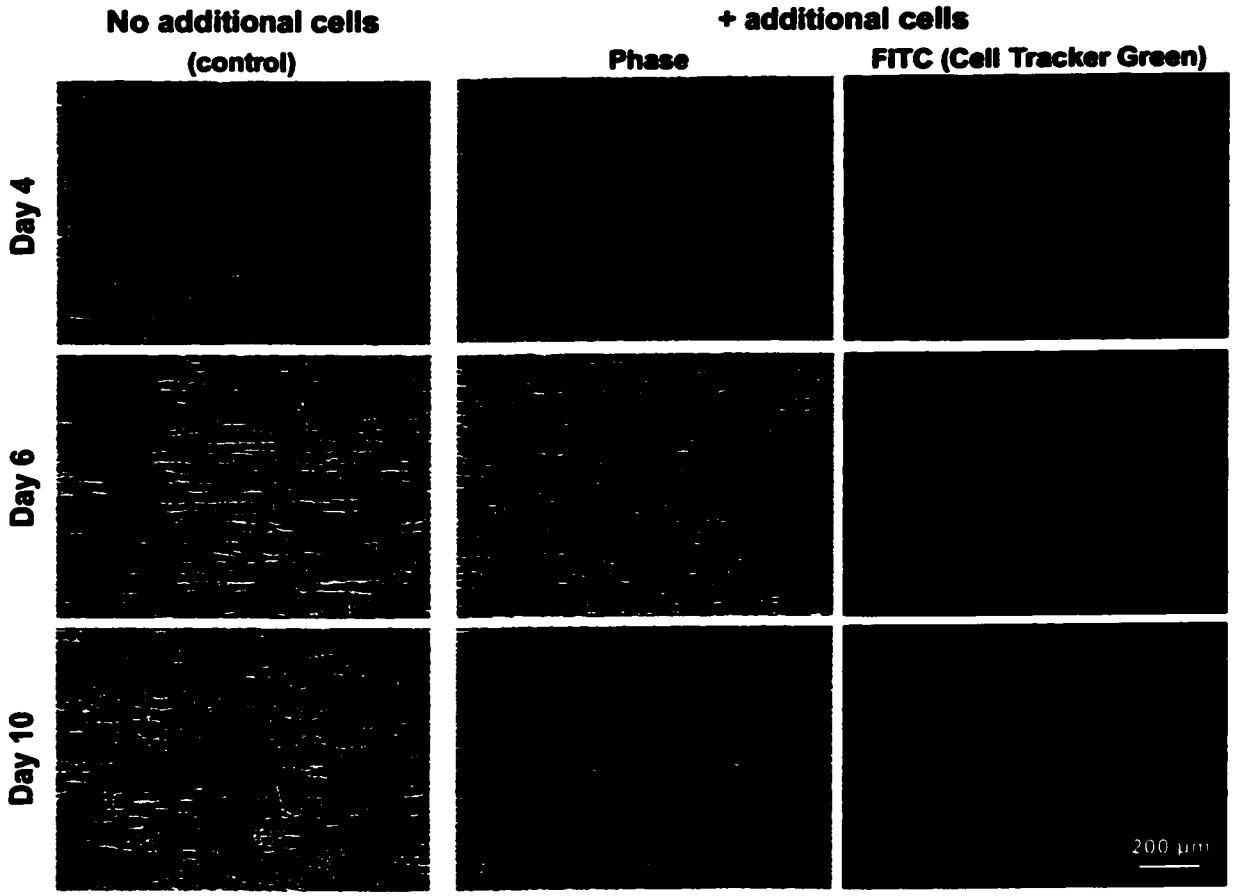

Figure 7.10. Seeding additional cells onto patterned cardiomyocyte cultures on spin-cast polyurethane films. Patterns of cardiomyocytes on laminin lanes (15x20 µm) were seeded with additional cardiomyocytes labeled with Cell Tracker Green after 3 days in culture. The added cells (right column, green) initially attached between and on top of the patterned cardiomyocytes to form a dense layer of cells and spread in the direction of the original patterned lines. Patterned cultures without additional cells served as a control.

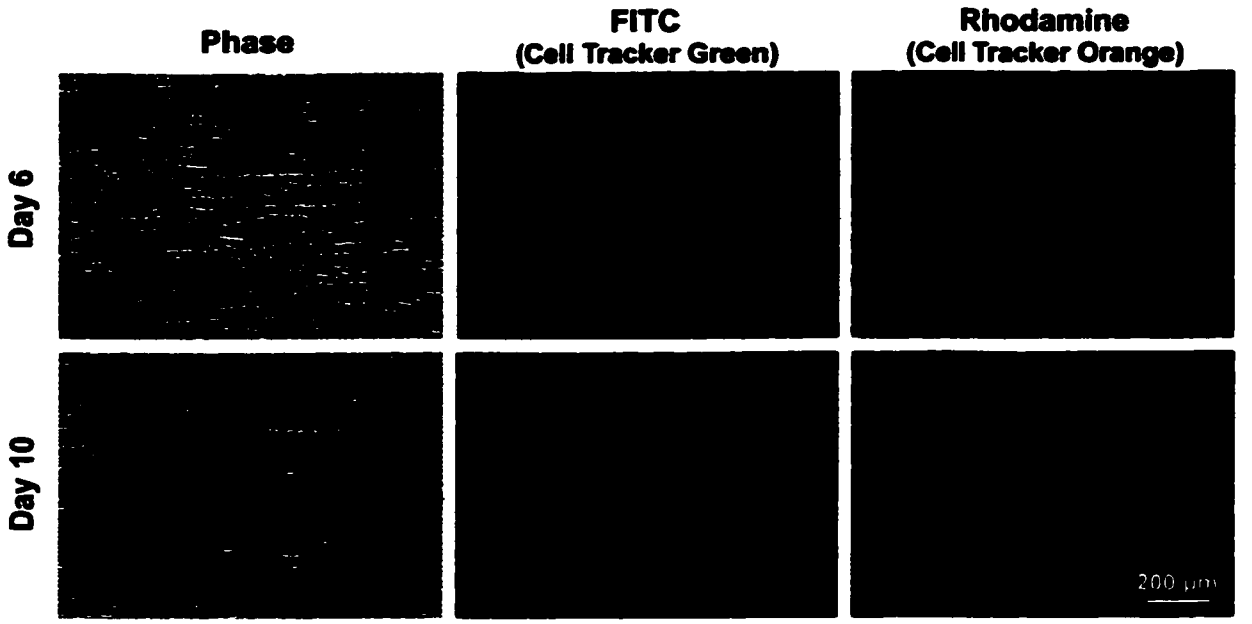

Figure 7.11. Successive seeding of cells onto patterned cardiomyocyte cultures. Patterns of cardiomyocytes on laminin lanes (15x20 μm) were seeded with additional cardiomyocytes labeled with Cell Tracker Green after 3 days in culture and again with cardiomyocytes labeled with Cell Tracker Orange 2 days later (5 days total). The third population of cells (right column, orange) adhered onto the dense layer of cells and spread in the direction of the primary patterns of cardiomyocytes (horizontally), but not as much as the second population of cells (middle column, green).

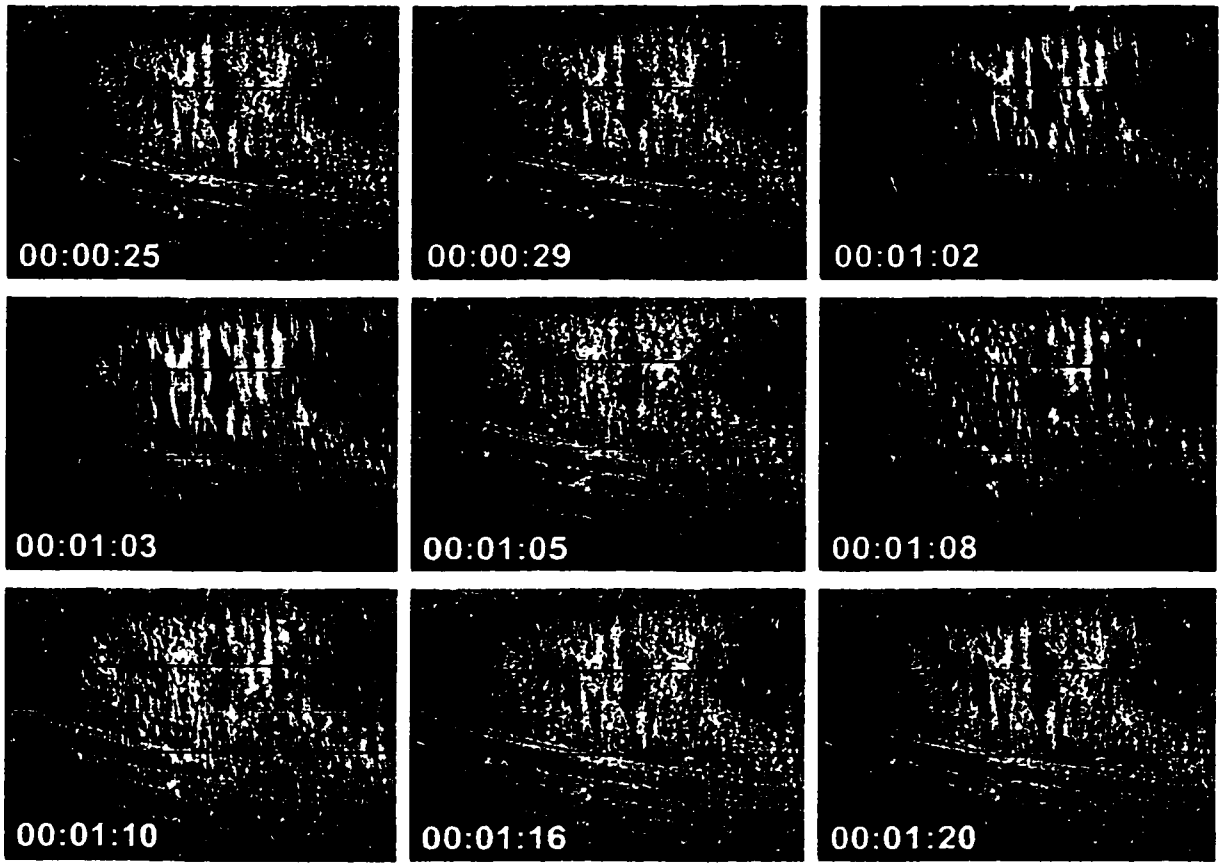

Figure 7.12. Still frames of patterned cardiomyocytes contracting polyurethane solvent cast film. Real time video of cardiomyocytes on solvent cast PU films was acquired, digitized and selected frames were captured. This series of images was taken from a sample of patterned cardiomyocytes (15x20 μm lanes) after 8 days of culture; the patterned cells are aligned vertically. The yellow line is a fixed reference point and the red lines track the movement of the cells and PU film during one contraction cycle. The time stamp on each frame is minutes:seconds:frames per second. A significant magnitude of contraction was observed for the patterned cardiomyocytes on the solvent cast PU films in the direction of the aligned cells.

Chapter 8: Cardiac Grafting of Spatially Organized Sheets of Cardiomyocytes on Biodegradable Polyurethane Films

8.1 Abstract

In this study we examined the response of cardiac tissue to implanted films of a biodegradable polyurethane material and the feasibility of using this approach to graft spatially organized sheets of cardiomyocytes onto the heart. Thin polyurethane films (with or without a patterned layer of cardiomyocytes) were attached to the left ventricle of normal hearts of nude mice and examined histologically 1 and 4 weeks after implantation. The grafted polyurethane films induced a pronounced inflammatory response on the surface of the heart with all of the characteristics of a classic foreign body response. Implantation of the materials did not appear to adversely affect the viability of the adjacent myocardium and a low mortality rate was associated with the surgical procedure.

8.2 Introduction

Biomaterials are frequently used in various cardiovascular applications to replace failing heart valves, open occluded blood vessels, and as implantable electrode leads for cardiac assist devices. Based on the frequency of such procedures, the foreign body response to these implanted materials has been relatively well characterized. On the other hand, the host response to biomaterials surgically implanted in the myocardium is less well known because it is not a common surgical intervention. One instance in which

biomaterials have been used in myocardial repair is to repair or prevent ventricular free wall rupture following myocardial infarction - an uncommon, but lethal condition requiring immediate repair.[194] A number of different materials, including fibrin glue[195, 196], gelatin films[197], fixed pericardium[198, 199] and Dacron[200] or Teflon[201], have been used clinically to "patch" infarcted tissue susceptible to rupture. Although these efforts can mechanically stabilize the structure of the ventricular wall, these acellular techniques fail to actively restore depressed cardiac function following myocardial infarction and ventricular remodeling. However, transplantation of viable, contractile cardiac cells to the wounded myocardial tissue is thought to be necessary to functionally improve cardiac output. Recently, various biomaterials have been examined as suitable substrates for the cultivation of differentiated cardiomyocytes *in vitro*[202-204], but few cell-seeded materials have been examined in implantation studies.[67, 68, 70]

We have previously demonstrated that sheets of cardiomyocytes can be spatially organized on biodegradable polyurethane films *in vitro* and exhibit a greater magnitude of contraction on the elastomeric polymer than on rigid, non-flexible substrates (see Chapter 7). These results suggested that this polyurethane might serve as an appropriate carrier for cardiomyocyte transplantation onto the heart, thus we grafted polyurethane films, either with or without adherent cardiomyocytes, onto the surface of the left ventricle of mouse hearts. The hearts were examined 1 and 4 weeks after surgery in order to assess the host response to the implanted material.

8.3 Methods

8.3.1 Preparation of Polyurethane Films. Thin films of biodegradable polyurethane (PU) were solvent cast in 10 ml Teflon beakers from a 2% solution in THF, as previously described in Chapter 7 (Figure 8.1). After solvent evaporation in a fume hood for several days, the films were placed under vacuum in a desiccator to removal any residual organic solvents. The films were sterilized by UV exposure for 10 minutes in a cell culture hood prior to micropatterning and cell culture.

8.3.2 Cardiomyocyte Patterning and Culture. Primary rat neonatal cardiomyocytes (1-2 days old) were freshly isolated and seeded onto PU films that had been micropatterned with laminin lane patterns (15x10 m), as previously described (Chapter 7). Individual samples were placed in 35 mm polystyrene dishes and initially seeded with a high density of cells ($1x10^6$/ml) in a small volume (500-700 µl) (Figure 8.1). The cells were allowed to attach overnight before additional culture media (~2 ml) was added to the dishes. After 24 hours in culture, a 1 µM concentration of ara-C was added to the media to inhibit fibroblast proliferation and the cultures were re-fed every 2-3 days thereafter with ara-C containing media. For cardiac grafting studies, the cardiomyocytes were cultured for 8 days on the PU films prior to being implanted.

8.3.3 Fibrin Coating of Polyurethane Implants. Just prior to implantation, the surface of the PU films were coated with a thin fibrin gel to promote the adhesion of the implant to tissue. For PU samples with cells, the fibrin gel also served to cushion the adherent layer of patterned cardiomyocytes against the surface of the heart. Bovine plasma

fibrinogen (CalBiochem) was diluted to ~15-20 mg/ml in serum-free DMEM media supplemented with 2.5 μM of $CaCl_2$ and kept on ice. Thrombin protease (2 units, Amersham Pharmacia) was added to ~300-400 μl of the fibrinogen solution, mixed and applied immediately to the surface of the PU film. In most cases, 100-200 μl/sample was sufficient to cover most of the PU film surface with a thin fibrin gel. The samples were then placed at 37°C for at least 15 minutes to allow the fibrin gel to form.

8.3.4 Fibrin Gel Coating of Cardiomyocytes. In order to optimize the fibrin gel formulation, a range of fibrinogen concentrations were attempted and applied to unpatterned cultures of cardiomyocytes on the thin PU films. Fibrinogen was diluted in serum-free DMEM to a concentration of 2, 10 or 56 mg/ml and about 200 μl of the fibrin gel solution was applied to the cardiomyocyte samples after 4 days in culture. The gels formed within 10-15 minutes at 37°C and after 30 minutes of incubation, additional serum-free DMEM was added to the cultures. The viability and activity of cardiomyocytes within the fibrin gel was monitored for 2 days in culture.

8.3.5 Cardiac Grafting Surgery. After gelation occurred, a 6 mm biopsy punch was used to remove a portion of the larger PU film; this allowed 2 or 3 samples to be obtained from a single solvent cast film. Adult nude mice (Charles River) were anesthetized with 20μl/mg body weight Avertin (20mg/ml), and placed on a ventilator (model RS232, Columbus Instruments, Columbus, OH), during the surgical procedure. The thoracic cavity of the mice was held open with a pediatric ophthalmic speculum to expose the heart. The 6 mm diameter PU samples were placed against the epicardial surface of the

left ventricle with the fibrin gel side of the PU film in contact with the heart. A single 8-0 suture (polypropylene monofilament suture, SurgiPro, USS DG Sutures, CT) near the apex of the heart was used to affix the PU implant. The mice were closed with 6-0 (polypropylene monofilament suture, SurgiPro, USS DG Sutures, CT) sutures and allowed to recover in a warming chamber. Three mice were used in preliminary studies to establish the surgical technique and nine mice were used for the remainder of the study (n = 4 without cells, n = 5 with patterned cardiomyocytes).

8.3.6 Histology. After either 1 or 4 weeks, the mice were anesthetized with Pentobarbital (0.2 ml/ 15g) and sacrificed. The hearts were excised, briefly rinsed in saline solution and fixed in 4% paraformaldehyde. Stereoscopic images of the implant material on the heart were captured prior to tissue sectioning and processing. Hearts were transversely cut into 4 equal slabs and subsequent tissue processing, paraffin embedding, sectioning (4 microns) and hematoxylin and eosin staining were carried out according to routine procedures.

8.4 Results

8.4.1 Cardiomyocyte Cultures on Polyurethane Films. Dense, highly aligned cultures of cardiomyocytes were achieved on the thin solvent cast PU films and the cells could visibly contract the elastomeric polymer substrate (Figure 8.1). Contraction of the film by the cardiomyocytes became apparent after about 4-6 days in culture and eventually caused wrinkles in the film after 10-14 days of culture. Thus it appeared that it took the cells several days to modify or condition the elastomeric scaffold such that they could

generate force, but prolonged contraction of the films resulted in permanent distortions of the material. Based on these results, patterned cardiomyocyte sheets were cultured for about a week *in vitro* before being implanted.

8.4.2 Fibrin Gel Coating. During preliminary attempts to implant the PU materials it appeared necessary to coat the films with a thin fibrin gel before grafting onto the heart. Smaller pieces of the polymer (6 mm diameter) sectioned from the larger film (20 mm diameter) tended to collapse on themselves and thus could not be easily handled or transferred to the surface of the heart. The fibrin gel served to mechanically stabilize the samples once they were cut from the solvent cast films such that they could be laid flat on the heart. The adhesive gel also stabilized the placement of the films situated on the left ventricle.

In vitro experiments were conducted to optimize the fibrin gel formulation and assess the viability of cardiomyocytes covered by fibrin gels. A series of gels at different concentrations were cast on PU films with adherent unpatterned cardiomyocytes. Gels quickly formed for each of the formulations within a few minutes at 37°C. Gels with the highest fibrinogen concentrations (56 mg/ml) were highly viscous and turbid in appearance, but stable, relatively clear gels were formed with 2 and 10 mg/ml of fibrinogen. Cardiomyocytes continued to beat within all of the fibrin gel coatings for several days, similarly to their contractile behavior prior to the introduction of the fibrin gel. This evidence suggested that a minimum of 10 mg/ml of the fibrinogen solution produced good fibrin gels and that the fibrin coating did not adversely affect the function of the cardiomyocytes on the PU film.

8.4.3 Macroscopic Assessment of Cardiac Grafting. In preliminary experiments, 2 out of 3 mice survived only 5 days and the third was sacrificed 6 days after surgery. Histological results indicated that some of these mice suffered minor transmural myocardial infarcts, possibly related to the surgical attachment of the PU film to the heart. After refining the surgical technique for implantation of the films, all of the successive mice (n=9), except one, survived the experiment until sacrifice with no signs of myocardial infarction. The lone mortality occurred within the first day after surgery, suggesting it was likely due to trauma related to the surgical procedure.

The PU films remained attached and fairly well spread across the surface of the heart after both 1 and 4 weeks *in vivo*. In some cases the PU material formed a lesion with the chest wall on the opposing side of the film. After 1 week, the morphology of the PU film did not appear significantly different, however after 4 weeks *in vivo*, the PU material was significantly degraded (Figure 8.2). In addition, numerous blood vessels were observed on the surface of the heart at the site of the implant. These observations suggested that there was no macroscopic aberrant reaction to the PU material implanted in the hearts of mice that resulted in either cardiotoxicity or mortality.

8.4.4 Histological Examination of Implanted Polyurethane Films. The PU films were in direct contact with the mesothelial lining on the left ventricle of the heart and in some instances, a portion of the film also partially covered the right ventricle. The myocardium adjacent to the PU material appeared healthy and there were no indications of significant cardiomyocyte death in the wall of heart (Figures 8.3-8.6). However, the

implantation of the PU films resulted in an acute and chronic inflammatory response on the surface of the heart that persisted for up to four weeks from the time of surgery.

In some cases the inflammatory response surrounded the entire surface of the heart, even on the opposite side from the PU material. A capsule began to form around the PU material after one week *in vivo*. The majority of inflammatory cells appeared to be neutrophils and macrophages and while the formation of foreign body giant cells was not apparent after one week, many were present after four weeks (Figures 8.5 & 8.6). Under higher magnification, the cytoplasm of large cells resembling macrophages were observed to be full of cellular or foreign debris, indicative of phagocytosis. The inflammatory response seemed most pronounced near the apex of the heart, where the suture was also placed to fasten the PU film. These results indicated that the cardiac tissue response had all of the classic hallmarks of the foreign body reaction to an implanted synthetic material.

After one week *in vivo*, some cells began to invade the PU material and a few blood vessels were observed, but the film remained completely intact. The surface of the polymer in contact with the heart remained relatively flat, but the opposite side of the film appeared rippled (Figure 8.3). After four weeks, the PU films appeared thinner and broken up into smaller pieces of material. Some of the smaller portions of PU were surrounded by foreign body giant cells and several vacant clefts suggested regions the polymer use to occupy in the tissue (Figures 8.5 & 8.6). More cells had invaded the material after four weeks and some neovascularization within the material was observed. Based on these two time points, it appeared that an increase in the cellularity of the material correlated with the enhanced degradation of the material over time.

No significant differences were detected between the grafted PU samples with or without a patterned layer of cardiomyocytes. After one week, it appeared that perhaps a more dense layer of cells was adherent to the surface of the film in contact with the heart, but these cells could not be identified morphologically as cardiomyocytes (Figure 8.4). The PU films with cells exhibited a thinner capsule formation on the basal side of the material facing away from the heart after one week than films without cells. By four weeks though, no differences in cellularity or the foreign body response were apparent for samples with or without adherent cardiomyocytes.

8.5 Discussion

Thin films of biodegradable polyurethane were successfully grafted onto the hearts of mice, suggesting this method could potentially be used to transplant layers of adherent cardiomyocytes. The implanted polymer did not appear to induce cardiomyocyte death in the adjacent myocardial tissue or mortality of the mice, based on preliminary survival data. However, the polymer did provoke an inflammatory reaction characteristic of a foreign body response on the surface of the heart that persisted for at least 4 weeks after implantation. During this time, a significant portion of the polymer degraded, but a large fraction of the material was still present. This suggests perhaps that a different formulation of the polyurethane with an accelerated degradation rate might reduce the chronic inflammatory response associated with the material. Alternatively, a longer period of *in vitro* culture with the cells on the material could be used to degrade more of the material prior to being implanted or thinner films of the material could be fabricated that might degrade faster.

Initially the patterned cardiomyocytes were labeled with Cell Tracker Green prior to grafting to try and clearly mark their identity. Unfortunately, after removing and fixing the hearts, auto-fluorescence from the host tissue made it difficult to distinguish the thin layer of transplanted cells on the surface of the heart. Although a denser layer of cells was observed *in vivo* along the surface of PU films with adherent cardiomyocytes after a week, it was impossible to differentiate on a morphological basis whether these cells were transplanted cardiomyocytes or simply inflammatory cells invading the material. Even if some of the cells are transplanted cardiomyocytes, it remains unclear whether the cells survive *in vivo* and if so, for how long. Grafted cell survival could be addressed by examining the implants only one or two days after surgery to discern the initial rate of cell death and then followed over a longer time course by methods similar to those previously described.[57]

In addition to assessing the survival of grafted sheets of cardiomyocytes, it would also be interesting to determine whether the patterned cells remain aligned *in vivo*. Cells grafted into the heart by injection typically align similarly to the neighboring myocardial cells, suggesting that spatial cues in the granulation tissue, as well as local contractile mechanical forces of the heart are sufficient to induce cellular alignment. However, it takes time for injected cells to become oriented and properly organized *in vivo*, thus delaying their functional integration with the host tissue. One of the primary objectives of patterning the alignment of the cells *in vitro* beforehand is to generate large patches of myocardial tissue with functional, differentiated cardiomyocytes that could be grafted and rapidly integrate with the host tissue.

8.6 Figures

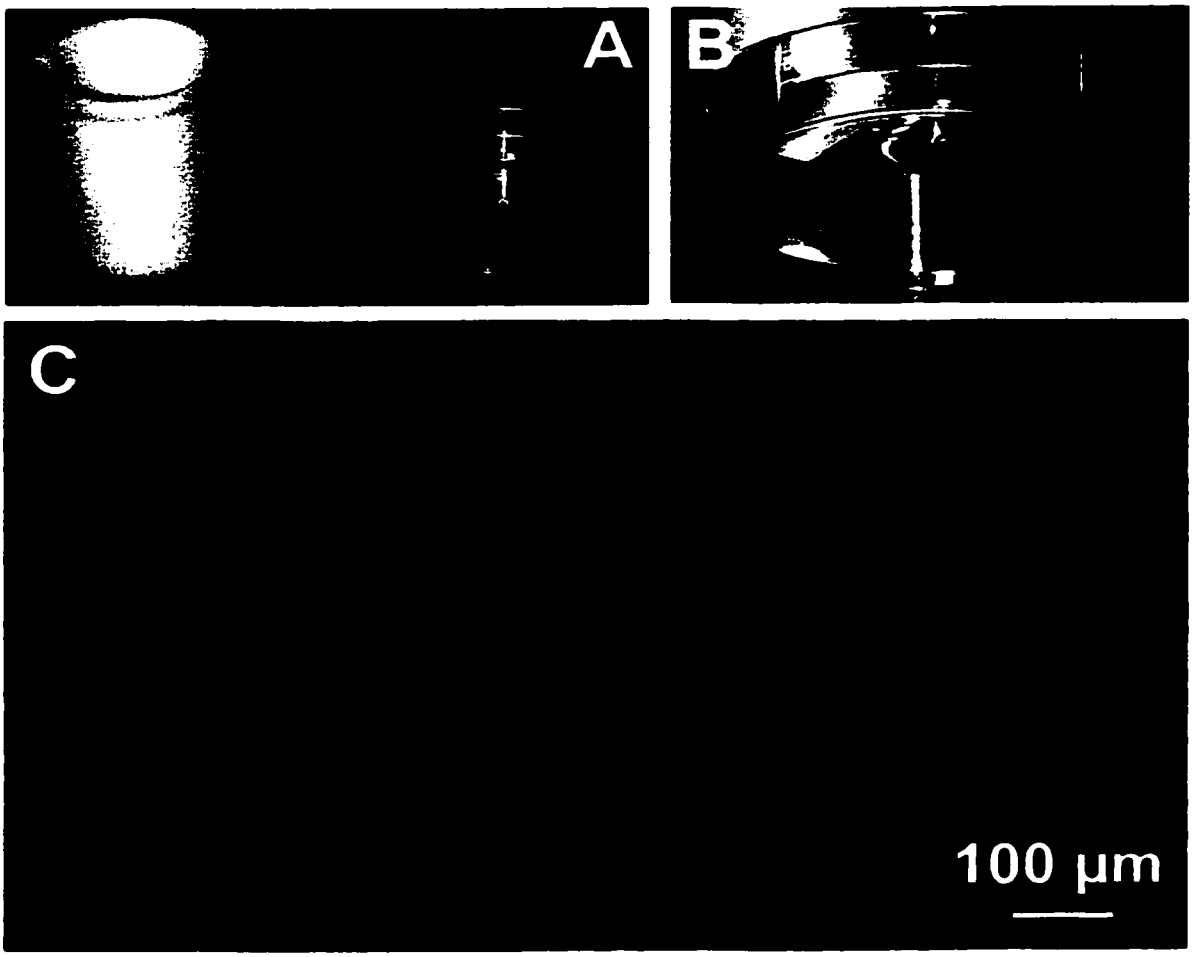

Figure 8.1. Spatially organized sheets of cardiomyocytes on thin biodegradable polyurethane films. A) Thin films of biodegradable polyurethane are solvent cast in 10 ml Teflon beakers, micropatterned by microcontact printing of laminin lanes and B) seeded with a high density of cardiomyocytes. C) A dense, highly aligned layer of cells is cultured on the thin films, consisting mostly of cardiomyocytes (stained with an antibody for sarcomeric myosin heavy chain; shown after 4 days in culture; 15x10 µm lanes).

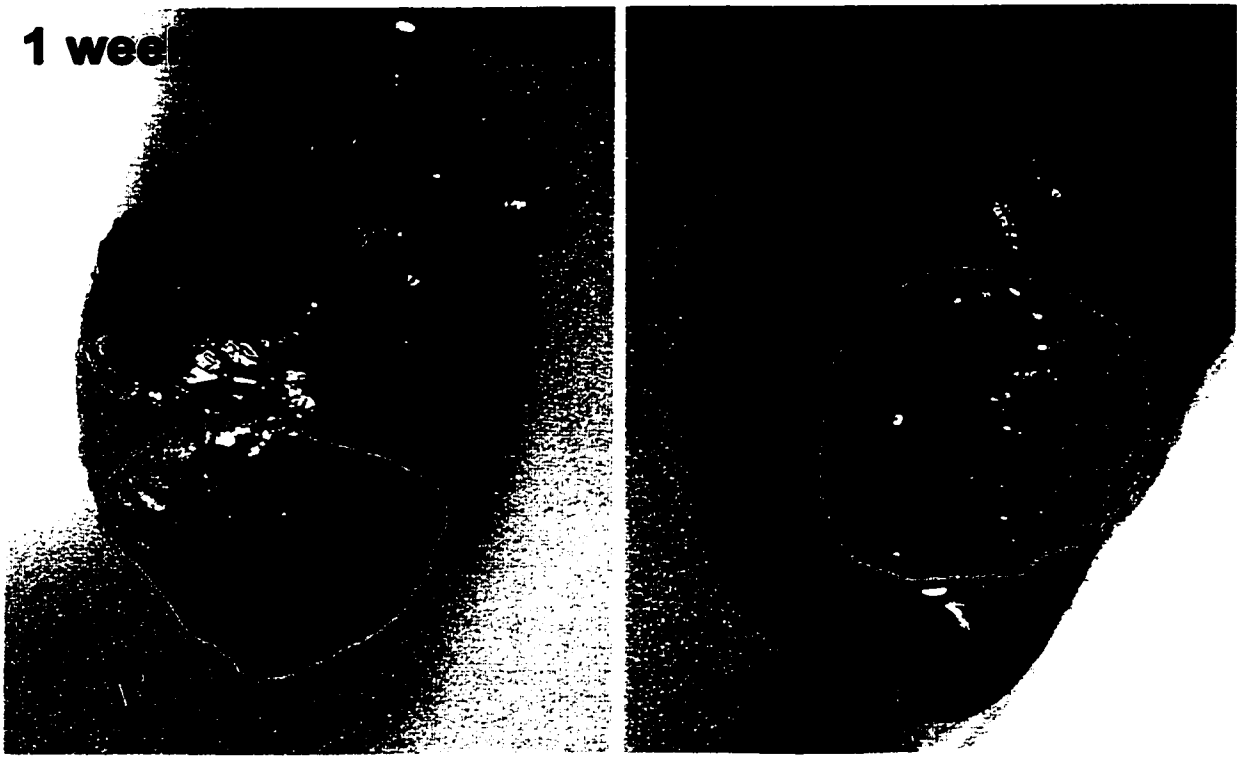

Figure 8.2. Stereoscope images of grafted polyurethane films with patterned cardiomyocytes. The mouse hearts were retrieved 1 or 4 weeks after grafting the PU films onto the surface of the heart. The area covered by the PU implants is traced in yellow and the suture is located near the apex of the heart (blue). The PU films remained adherent to the surface of the heart and did not appear different after 1 week *in vivo* (left). After 4 weeks, though, the PU material was significantly degraded and some blood vessels were apparent at the site of the implant (right).

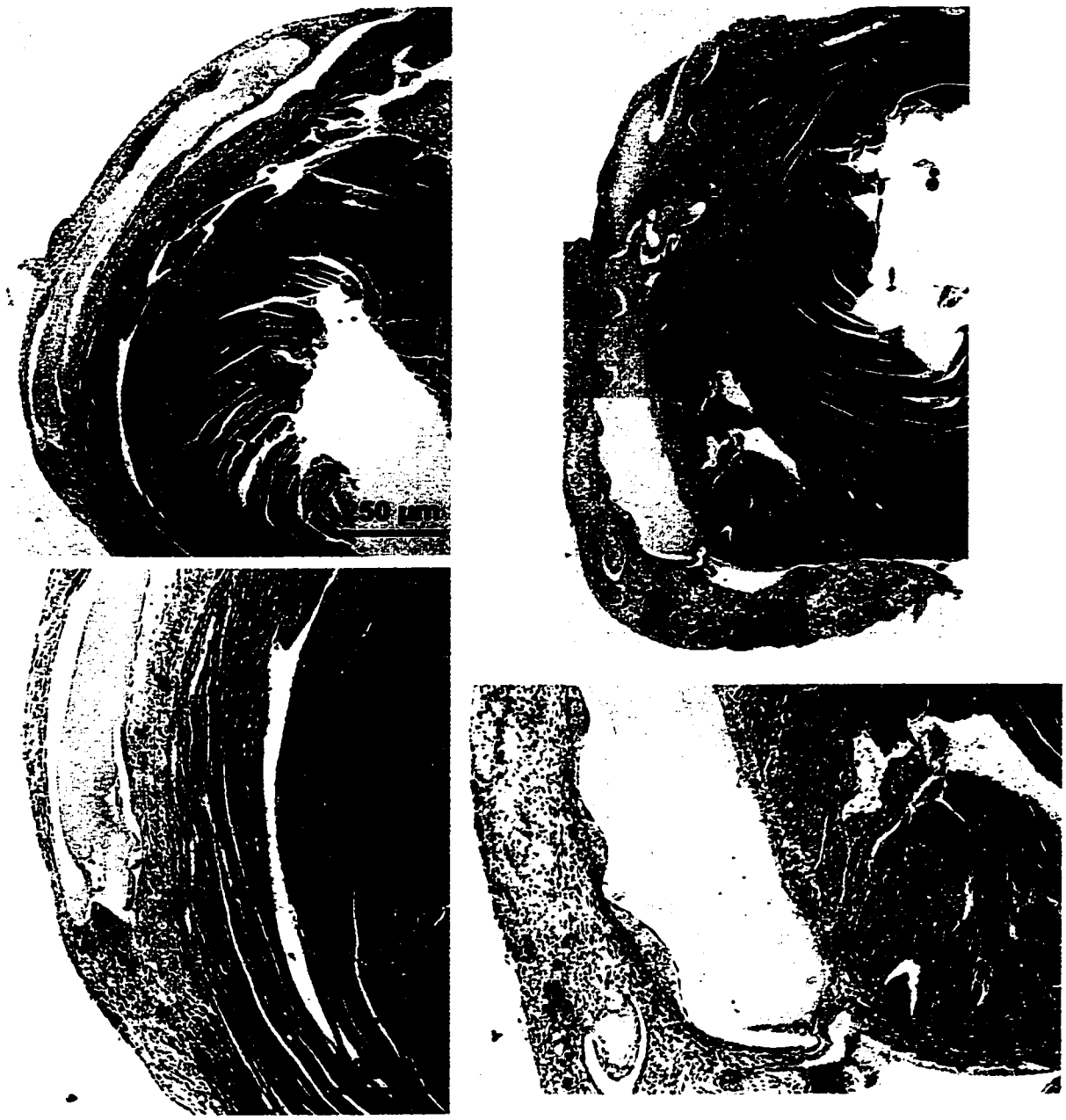

Figure 8.3. Histology of polyurethane implants without patterned cells at 1 week. Sections of the heart were stained with hematoxylin and eosin and viewed under low power (4x, top) and higher power magnification (10x, bottom). The PU films induced a significant inflammatory response at the surface of the heart, but adjacent myocardium appeared healthy and viable. A composite image (top right) was formed to show the extent of the inflammatory response encompassing the implant.

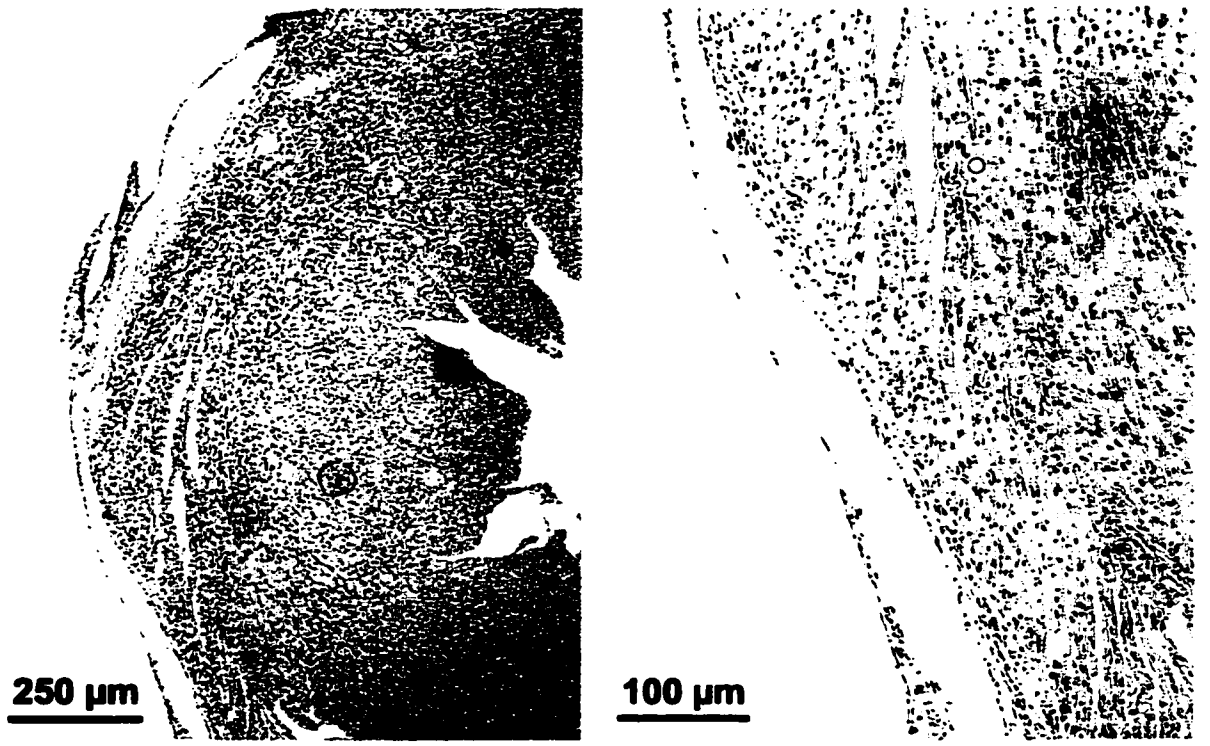

Figure 8.4. Histology of polyurethane implants + patterned cells at 1 week. Sections of the heart were stained with hematoxylin and eosin and viewed under low power (4x, left) and higher power magnification (10x, right). The inflammatory response due to the PU films appeared to be reduced, especially on the basal side of the material. A dense layer of cells were adherent to the surface of the material in contact with the heart, but it was unclear if these cells were grafted cardiomyocytes or host inflammatory cells.

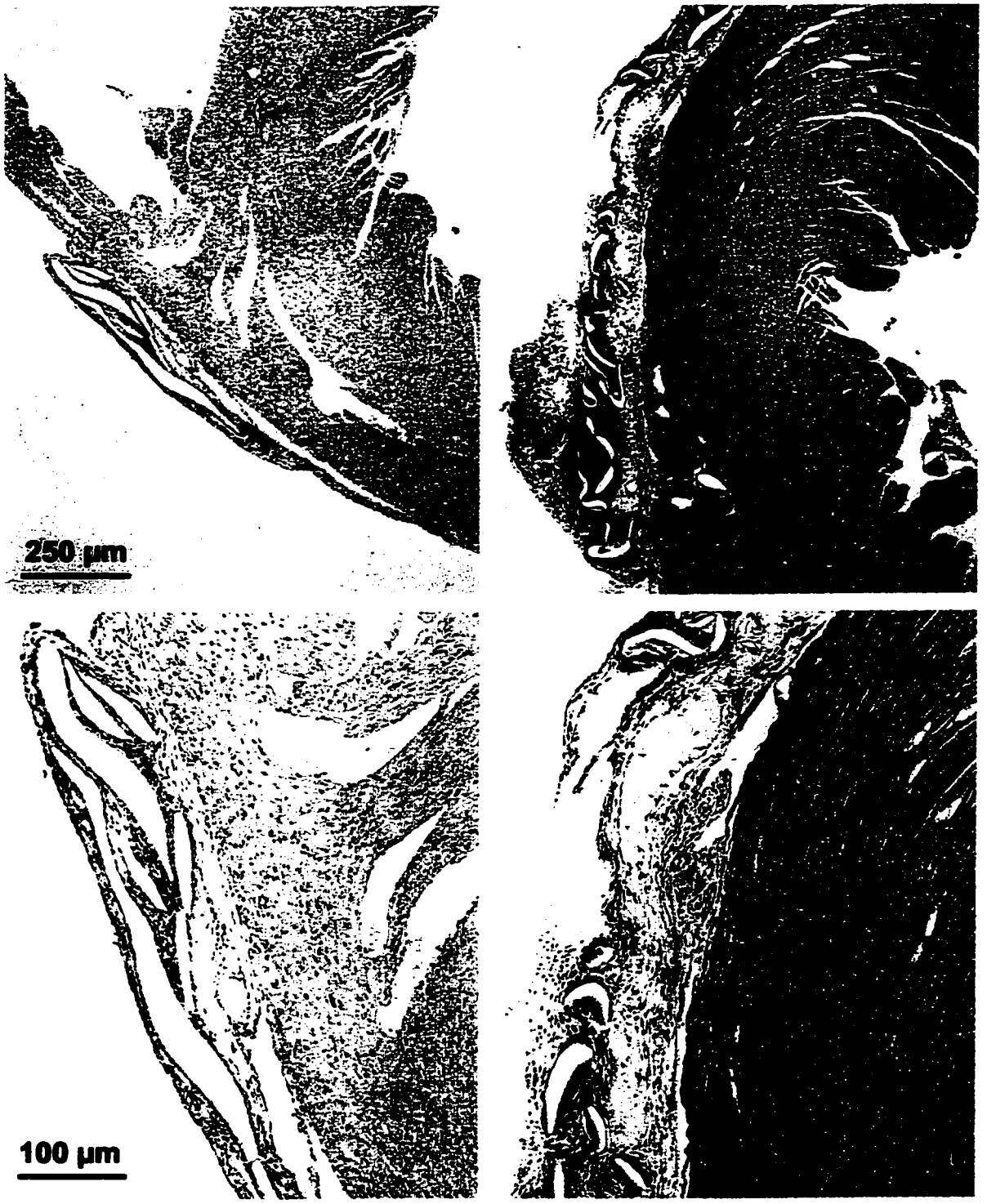

Figure 8.5. Histology of polyurethane implants without patterned cells at 4 weeks. Sections of the heart were stained with hematoxylin and eosin and viewed under low power (4x, top) and higher power magnification (10x, bottom). Although a large portion of the polymer had degraded, a chronic inflammatory response persisted after 4 weeks.

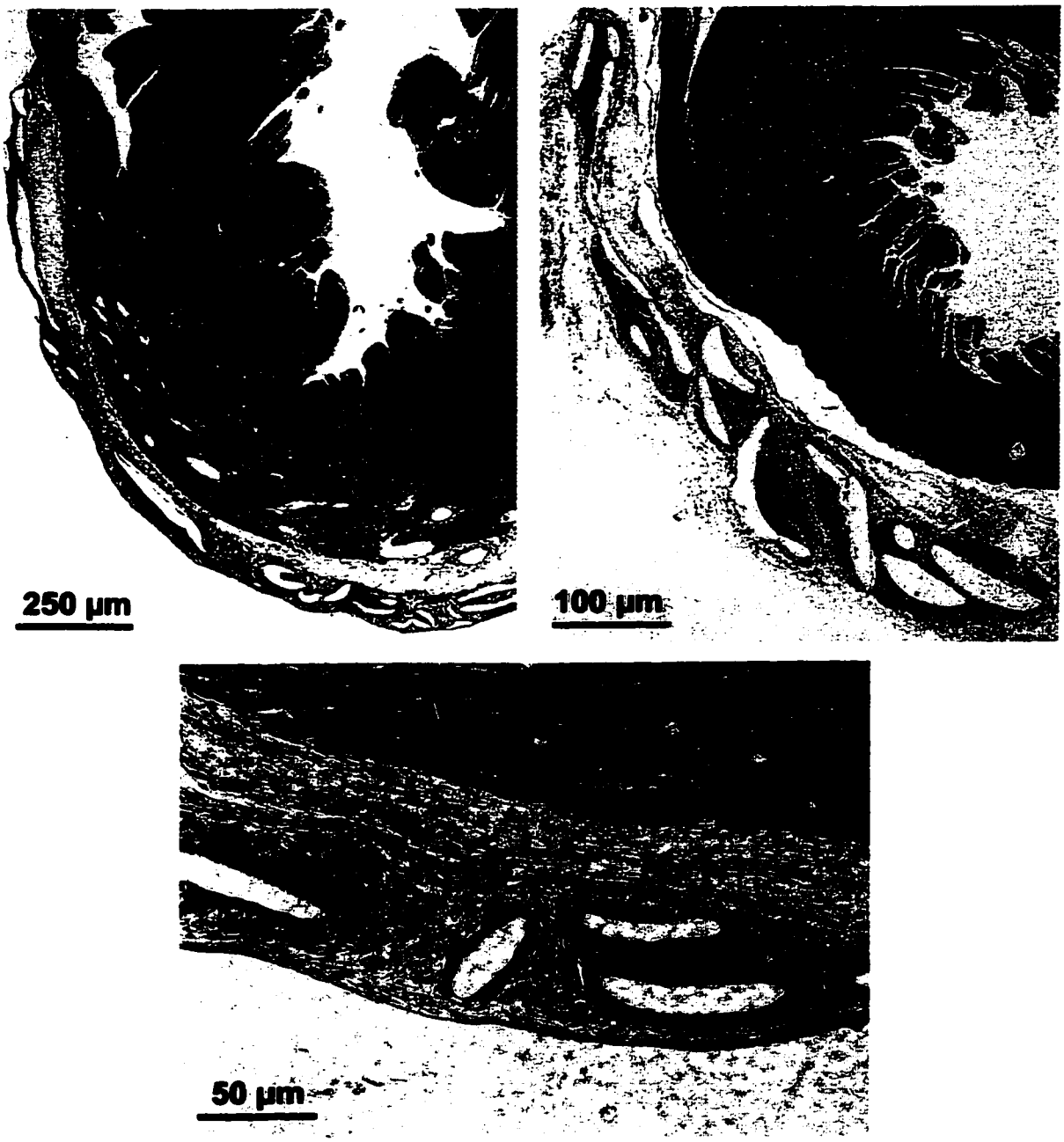

Figure 8.6. Histology of polyurethane implants + patterned cells at 4 weeks. Sections of the heart were stained with hematoxylin and eosin and viewed under low power (4x, top left) and higher power magnification (10x, top right; 20x, bottom). Much of the polymer had degraded and several regions devoid of material were apparently surrounded by foreign body giant cells (bottom).

Chapter 9: Conclusions and Future Directions

9.1 Conclusions

Several key advances have been made in the molecular design of materials to spatially control the assembly of cells for tissue engineering constructs. Although these efforts have primarily focused on the engineering of myocardial tissue, the general principles derived from these studies can be applied to the design of other structurally complex tissues as well.

Microcontact printing of proteins is a versatile micropatterning technique that facilitates the engineering of spatially complex extracellular matrices on surfaces. Adhesive protein patterns direct cell attachment and control cellular dimensions, and dictate inter- and intracellular organization. For instance, cardiomyocytes patterned on parallel lanes exhibit longitudinally oriented myofibrils and localized expression of molecular components of intercalated disks at the bipolar ends of adjacent cells. Additional cell types can be integrated with micropatterned cultures of cells by activating non-adhesive regions to support cell attachment. This allows the creation of spatially organized co-cultures that begin to more closely resemble the true composition of complex, heterogeneous tissues, such as the myocardium.

The microcontact printing of proteins is compatible with a variety of substrate materials allowing patterned cardiomyocytes to be cultured on thin films of biodegradable scaffold materials as well as petri dishes. Organized sheets of cardiomyocytes on elastomeric biodegradable polymeric films created by this method are

more stable and exhibit a greater magnitude of contraction than on rigid substrates. This suggests that the mechanical properties of the scaffold material play an important role in the function of engineered tissues. These thin layers of patterned cardiomyocytes can be transplanted directly onto the surface of the heart. Thus, thin constructs of organized myocardial tissue can be engineered *in vitro* and might be useful as a stable and efficient means of cell transplantation to the heart for cardiac repair.

9.2 Future Directions

9.2.1 Functional Analysis of Micropatterned Cardiomyocytes. Since micropatterned cultures of cardiomyocytes appear to morphologically resemble the structure of the native myocardium, it is also important to determine if and how micropatterning influences cardiomyocyte function. Cardiomyocytes are electrically coupled to one another through gap junctions to form an excitable network of cells. Electrophysiological measurements of cardiac activity, such as action potential propagation and conduction velocities, could be acquired and compared to the properties of unpatterned cardiomyocyte cultures and native myocardial tissue. The effect of spatial parameters on the electrophysiological properties of myocardial tissue could be examined by fabricating micropatterned cardiomyocyte cultures with different geometries. Such experiments could examine how morphological attributes controlled by micropatterning, such as cellular dimensions and restricted gap junction expression, could translate into functional differences in cardiac electrophysiology.

In addition to their electrical activity, contractile cardiomyocytes are capable of generating mechanical force and performing work. Micropatterned cultures possess

aligned myofibrils that direct the primary orientation of cardiomyocyte contraction. Quantitative mechanical analysis of organized cardiac layers could be performed to assess the magnitude and precise orientation of contractile forces generated by the patterned cells on elastomeric substrates. The degree of cardiomyocyte alignment can be controlled by the micropatterning dimensions and could be varied as an experimental parameter while measuring the forces produced by the cells. These studies could thus relate the mechanical properties of micropatterned cardiomyocytes with the organization of contractile myofibril elements.

The response to agonists and antagonists of cardiomyocyte contraction could also be investigated to evaluate how faithfully the response of micropatterned cultures recapitulates the response of native myocardium in comparison to unpatterned cultures. A combination of these types of quantitative analyses could provide a more thorough functional characterization of micropatterned cardiomyocyte cultures and correlate some of the morphological attributes with physiologically relevant measures of activity.

9.2.2 Cardiac Tissue Engineering. After the functional performance of spatially organized constructs has been better characterized *in vitro*, further *in vivo* experiments could be conducted to determine if this approach will lead to a viable method for cardiac tissue engineering. Although preliminary studies established the surgical implantation procedure and demonstrated the feasibility of grafting thin layers of cells onto the heart, several larger issues remain unresolved. Cell survival and functional integration of the transplanted tissue constructs need to be examined to ascertain the fate of the grafted cardiomyocytes. Initially, organized cardiomyocyte sheets were grafted onto normal

hearts, but future studies could examine transplanting the tissue constructs onto ischemic myocardium created by experimental infarct models. This would represent a more appropriate model to determine the ability of engineered tissues to heal wounded myocardium and contribute to ventricular function. The efficiency, stability and function of transplanted cardiomyocyte sheets could be compared to cardiac grafts formed by cell injection methods. In addition, a comparison of implanted sheets of patterned and unpatterned cardiomyocytes could determine whether the organization of the engineered tissue is retained *in vivo* and the functional necessity of incorporating spatial control into the design of the tissue construct.

9.2.3 *In vitro* Applications of Micropatterned Cardiomyocyte Cultures. Spatially organized layers of cardiomyocytes that recapitulate morphological and functional characteristics of native myocardial tissue provide improved *in vitro* models for diagnostic applications. Cardiomyocyte cultures are frequently used in assays, such as pharmacological screening, as models of the myocardium.[205-207] The fact that organized cultures of cardiomyocytes more closely resemble the architecture of myocardial tissue suggests that they may serve as a more accurate and predictive model system than unpatterned cell cultures.

Micropatterned cardiomyocyte cultures can be integrated with silicon devices in the development of cell-based biosensors. Excitable cells, like cardiomyocytes and neurons, have been cultured on electrode arrays capable of stimulating and recording electrical signals,[208-211] and alignment strategies have been designed to properly position micropatterned cells over individual electrode features.[150, 152] Micropatterning of

cardiomyocytes on biosensor surfaces could thus simultaneously control the positioning of the cells and their morphological phenotype in order to obtain more accurate physiological measures of activity.

References

1. Maisch B. Ventricular remodeling. *Cardiology* 1996. **87**(Suppl 1): 2-10.

2. Colucci WS. Molecular and cellular mechanisms of myocardial failure. *Am J Cardiol* 1997. **80**(11A): 15L-25L.

3. Sam F, Sawyer DB, Chang DL, Eberli FR, Ngoy S, Jain M, Amin J, Apstein CS, Colucci WS. Progressive left ventricular remodeling and apoptosis late after myocardial infarction in mouse heart. *Am J Physiol Heart Circ Physiol* 2000. **279**(1): H422-428.

4. Matsushita T, Oyamada M, Fujimoto K, Yasuda Y, Masuda S, Wada Y, Oka T, Takamatsu T. Remodeling of cell-cell and cell-extracellular matrix interactions at the border zone of rat myocardial infarcts. *Circ Res* 1999. **85**(11): 1046-1055.

5. Olivetti G, Capasso JM, Meggs LG, Sonnenblick EH, Anversa P. Cellular basis of chronic ventricular remodeling after myocardial infarction in rats. *Circ Res* 1991. **68**(3): 856-869.

6. Pfeffer JM, Pfeffer MA, Fletcher PJ, Braunwald E. Progressive ventricular remodeling in rat with myocardial infarction. *Am J Physiol* 1991. **260**(5 Pt 2): H1406-1414.

7. Kurrelmeyer K, *et al.* Cardiac remodeling as a consequence and cause of progressive heart failure. *Clin Cardiol* 1998. **21**(12 Suppl 1): I14-19.

8. Cleutjens JP, Verluyten MJ, Smiths JF, Daemen MJ. Collagen remodeling after myocardial infarction in the rat heart. *Am J Pathol* 1995. **147**(2): 325-338.

9. Jugdutt BI, Joljart MJ, Khan MI. Rate of collagen deposition during healing and ventricular remodeling after myocardial infarction in rat and dog models. *Circulation* 1996. **94**(1): 94-101.

10. Tyagi SC, Campbell SE, Reddy HK, Tjahja E, Voelker DJ. Matrix metalloproteinase activity expression in infarcted, noninfarcted and dilated cardiomyopathic human hearts. *Mol Cell Biochem* 1996. **155**(1): 13-21.

11. Etoh T, *et al.* Myocardial and interstitial matrix metalloproteinase activity after acute myocardial infarction in pigs. *Am J Physiol Heart Circ Physiol* 2001. **281**(3): H987-994.

12. Josephson ME, Zimetbaum P, Huang D, Sauberman R, Monahan KM, Callans DS. Pathophysiologic substrate for sustained ventricular tachycardia in coronary artery disease. *Jpn Circ J* 1997. **61**(6): 459-466.

13. Gaudron P, Eilles C, Kugler I, Ertl G. Progressive left ventricular dysfunction and remodeling after myocardial infarction. Potential mechanisms and early predictors. *Circulation* 1993. **87**(3): 755-763.

14. Patten RD, Aronovitz MJ, Deras-Mejia L, Pandian NG, Hanak GG, Smith JJ, Mendelsohn ME, Konstam MA. Ventricular remodeling in a mouse model of myocardial infarction. *Am J Physiol* 1998. **274**(5 Pt 2): H1812-1820.

15. Goldstein S, Sabbah H. Ventricular remodeling and angiotensin-converting enzyme inhibitors. *J Cardiovasc Pharmacol* 1994. **24**(Suppl 3): S27-31.

16. Khalil ME, Basher AW, Brown EJ, Jr., Alhaddad IA. A remarkable medical story: benefits of angiotensin-converting enzyme inhibitors in cardiac patients. *J Am Coll Cardiol* 2001. **37**(7): 1757-1764.

17. American-Heart-Association. 2000 heart and stroke statistical update. In.: American Heart Association; 1999.

18. Willman VL. Expert panel review of the NHLBI total artificial heart (TAH) program, June 1998-November 1999. 1999.

19. Cooper DK, Keogh AM, Brink J, Corris PA, Klepetko W, Pierson RN, Schmoeckel M, Shirakura R, Warner Stevenson L. Report of the Xenotransplantation Advisory Committee of the International Society for Heart and Lung Transplantation: the present status of xenotransplantation and its potential role in the treatment of end-stage cardiac and pulmonary diseases. *J Heart Lung Transplant* 2000. **19**(12): 1125-1165.

20. Borovetz HS, Kormos RL, Griffith BP, Hung TC. Clinical utilization of the artificial heart. *Crit Rev Biomed Eng* 1989. **17**(2): 179-201.

21. Coumbe A, Graham TR. The pathology of artificial hearts and ventricular assist devices. *Curr Top Pathol* 1994. **86**161-197.

22. Josefson D. US surgeons implant new artificial heart. *BMJ* 2001. **323**(7304): 66.

23. Nose Y. Implantable total artificial heart developed by abiomed gets fda approval for clinical trials. *Artif Organs* 2001. **25**(6): 429.

24. SoRelle R. Cardiovascular news. Totally contained AbioCor artificial heart implanted July 3, 2001. *Circulation* 2001. **104**(3): E9005-9006.

25. Chachques JC, Marino JP, Lajos P, Zegdi R, D'Attellis N, Fornes P, Fabiani JN, Carpentier A. Dynamic cardiomyoplasty: clinical follow-up at 12 years. *Eur J Cardiothorac Surg* 1997. **12**(4): 560-567; discussion 567-568.

26. Carpentier A, Chachques JC. Myocardial substitution with a stimulated skeletal muscle: first successful clinical case. *Lancet* 1985. **1**(8440): 1267.

27. Stocum DL. Regenerative biology and engineering: strategies for tissue restoration. *Wound Repair Regen* 1998. **6**(4): 276-290.

28. Suh H. Tissue restoration, tissue engineering and regenerative medicine. *Yonsei Med J* 2000. **41**(6): 681-684.

29. Koh GY, Soonpaa MH, Klug MG, Field LJ. Strategies for myocardial repair. *J Interv Cardiol* 1995. **8**(4): 387-393.

30. Soonpaa MH, Daud AI, Koh GY, Klug MG, Kim KK, Wang H, Field LJ. Potential approaches for myocardial regeneration. *Ann N Y Acad Sci* 1995. **752**: 446-454.

31. Kessler PD, Byrne BJ. Myoblast cell grafting into heart muscle: cellular biology and potential applications. *Annu Rev Physiol* 1999. **61**: 219-242.

32. Papadaki M, Langer R. Cardiomyoplasty: cellular and tissue engineering approaches. *Basic Appl Myol* 1999. **9**(4): 151-159.

33. El Oakley RM, Ooi OC, Bongso A, Yacoub MH. Myocyte transplantation for myocardial repair: a few good cells can mend a broken heart. *Ann Thorac Surg* 2001. **71**(5): 1724-1733.

34. Weisel RD, Li RK, Mickle DA, Yau TM. Cell transplantation comes of age. *J Thorac Cardiovasc Surg* 2001. **121**(5): 835-836.

35. Koh GY, Soonpaa MH, Klug MG, Field LJ. Long-term survival of AT-1 cardiomyocyte grafts in syngeneic myocardium. *Am J Physiol* 1993. **264**(5 Pt 2): H1727-1733.

36. Soonpaa MH, Koh GY, Klug MG, Field LJ. Formation of nascent intercalated disks between grafted fetal cardiomyocytes and host myocardium. *Science* 1994. **264**(5155): 98-101.

37. Koh GY, Soonpaa MH, Klug MG, Pride HP, Cooper BJ, Zipes DP, Field LJ. Stable fetal cardiomyocyte grafts in the hearts of dystrophic mice and dogs. *J Clin Invest* 1995. **96**(4): 2034-2042.

38. Reinecke H, Zhang M, Bartosek T, Murry CE. Survival, integration, and differentiation of cardiomyocyte grafts: a study in normal and injured rat hearts. *Circulation* 1999. **100**(2): 193-202.

39. Li RK, Jia ZQ, Weisel RD, Mickle DA, Zhang J, Mohabeer MK, Rao V, Ivanov J. Cardiomyocyte transplantation improves heart function. *Ann Thorac Surg* 1996. **62**(3): 654-660; discussion 660-651.

40. Matsushita T, *et al.* Formation of cell junctions between grafted and host cardiomyocytes at the border zone of rat myocardial infarction. *Circulation* 1999. **100**(19 Suppl): II262-268.

41. Scorsin M, Marotte F, Sabri A, Le Dref O, Demirag M, Samuel JL, Rappaport L, Menasche P. Can grafted cardiomyocytes colonize peri-infarct myocardial areas? *Circulation* 1996. **94**(9 Suppl): II337-340.

42. Jia ZQ, Mickle DA, Weisel RD, Mohabeer MK, Merante F, Rao V, Li G, Li RK. Transplanted cardiomyocytes survive in scar tissue and improve heart function. *Transplant Proc* 1997. **29**(4): 2093-2094.

43. Scorsin M, *et al.* Does transplantation of cardiomyocytes improve function of infarcted myocardium? *Circulation* 1997. **96**(9 Suppl): II-188-193.

44. Scorsin M, *et al.* Can cellular transplantation improve function in doxorubicin-induced heart failure? *Circulation* 1998. **98**(19 Suppl): II151-155; discussion II155-156.

45. Koh GY, Klug MG, Soonpaa MH, Field LJ. Differentiation and long-term survival of C2C12 myoblast grafts in heart. *J Clin Invest* 1993. **92**(3): 1548-1554.

46. Murry CE, Wiseman RW, Schwartz SM, Hauschka SD. Skeletal myoblast transplantation for repair of myocardial necrosis. *J Clin Invest* 1996. **98**(11): 2512-2523.

47. Scorsin M, Hagege A, Vilquin JT, Fiszman M, Marotte F, Samuel JL, Rappaport L, Schwartz K, Menasche P. Comparison of the effects of fetal cardiomyocyte and skeletal myoblast transplantation on postinfarction left ventricular function. *J Thorac Cardiovasc Surg* 2000. **119**(6): 1169-1175.

48. Reinecke H, MacDonald GH, Hauschka SD, Murry CE. Electromechanical coupling between skeletal and cardiac muscle. Implications for infarct repair. *J Cell Biol* 2000. **149**(3): 731-740.

49. Taylor DA, Atkins BZ, Hungspreugs P, Jones TR, Reedy MC, Hutcheson KA, Glower DD, Kraus WE. Regenerating functional myocardium: improved

performance after skeletal myoblast transplantation [published erratum appears in Nat Med 1998 Oct;4(10):1200]. *Nat Med* 1998. **4**(8): 929-933.

50. Atkins BZ, Hueman MT, Meuchel JM, Cottman MJ, Hutcheson KA, Taylor DA. Myogenic cell transplantation improves in vivo regional performance in infarcted rabbit myocardium. *J Heart Lung Transplant* 1999. **18**(12): 1173-1180.

51. Atkins BZ, Hueman MT, Meuchel J, Hutcheson KA, Glower DD, Taylor DA. Cellular cardiomyoplasty improves diastolic properties of injured heart. *J Surg Res* 1999. **85**(2): 234-242.

52. Jain M, *et al.* Cell therapy attenuates deleterious ventricular remodeling and improves cardiac performance after myocardial infarction. *Circulation* 2001. **103**(14): 1920-1927.

53. Menasche P, Hagege AA, Scorsin M, Pouzet B, Desnos M, Duboc D, Schwartz K, Vilquin JT, Marolleau JP. Myoblast transplantation for heart failure. *Lancet* 2001. **357**(9252): 279-280.

54. Menasche P, Hagege A, Scorsin M, Pouzet B, Desnos M, Duboc D, Schwartz K, Vilquin JT, Marolleau JP. [Autologous skeletal myoblast transplantation for cardiac insufficiency. First clinical case]. *Arch Mal Coeur Vaiss* 2001. **94**(3): 180-182.

55. Sakai T, Li RK, Weisel RD, Mickle DA, Jia ZQ, Tomita S, Kim EJ, Yau TM. Fetal cell transplantation: a comparison of three cell types. *J Thorac Cardiovasc Surg* 1999. **118**(4): 715-724.

56. Hutcheson KA, Atkins BZ, Hueman MT, Hopkins MB, Glower DD, Taylor DA. Comparison of benefits on myocardial performance of cellular cardiomyoplasty with skeletal myoblasts and fibroblasts. *Cell Transplant* 2000. **9**(3): 359-368.

57. Zhang M, Methot D, Poppa V, Fujio Y, Walsh K, Murry CE. Cardiomyocyte grafting for cardiac repair: graft cell death and anti- death strategies. *J Mol Cell Cardiol* 2001. **33**(5): 907-921.

58. Freed LE, Vunjak-Novakovic G. Microgravity tissue engineering. *In Vitro Cell Dev Biol Anim* 1997. **33**(5): 381-385.

59. Carrier RL, Papadaki M, Rupnick M, Schoen FJ, Bursac N, Langer R, Freed LE, Vunjak-Novakovic G. Cardiac tissue engineering: cell seeding, cultivation parameters, and tissue construct characterization. *Biotechnol Bioeng* 1999. **64**(5): 580-589.

60. Bursac N, Papadaki M, Cohen RJ, Schoen FJ, Eisenberg SR, Carrier R, Vunjak-Novakovic G, Freed LE. Cardiac muscle tissue engineering: toward an in vitro model for electrophysiological studies. *Am J Physiol* 1999. **277**(2 Pt 2): H433-444.

61. Papadaki M, Bursac N, Langer R, Merok J, Vunjak-Novakovic G, Freed LE. Tissue engineering of functional cardiac muscle: molecular, structural, and electrophysiological studies. *Am J Physiol Heart Circ Physiol* 2001. **280**(1): H168-178.

62. Souren JE, Schneijdenberg C, Verkleij AJ, Van Wijk R. Factors controlling the rhythmic contraction of collagen gels by neonatal heart cells. *In Vitro Cell Dev Biol* 1992. **28A**(3 Pt 1): 199-204.

63. Souren JE, Peters RC, Van Wijk R. Collagen gels populated with rat neonatal heart cells can be used for optical recording of rhythmic contractions which also show ECG-like potentials. *Experientia* 1994. **50**(8): 712-716.

64. Eschenhagen T, *et al.* Three-dimensional reconstitution of embryonic cardiomyocytes in a collagen matrix: a new heart muscle model system. *FASEB J* 1997. **11**(8): 683-694.

65. Zimmermann WH, Fink C, Kralisch D, Remmers U, Weil J, Eschenhagen T. Three-dimensional engineered heart tissue from neonatal rat cardiac myocytes. *Biotechnol Bioeng* 2000. **68**(1): 106-114.

66. Fink C, Ergun S, Kralisch D, Remmers U, Weil J, Eschenhagen T. Chronic stretch of engineered heart tissue induces hypertrophy and functional improvement. *FASEB J* 2000. **14**(5): 669-679.

67. Li RK, Jia ZQ, Weisel RD, Mickle DA, Choi A, Yau TM. Survival and function of bioengineered cardiac grafts. *Circulation* 1999. **100**(19 Suppl): II63-69.

68. Sakai T, Li RK, Weisel RD, Mickle DA, Kim ET, Jia ZQ, Yau TM. The fate of a tissue-engineered cardiac graft in the right ventricular outflow tract of the rat. *J Thorac Cardiovasc Surg* 2001. **121**(5): 932-942.

69. Li RK, Yau TM, Weisel RD, Mickle DA, Sakai T, Choi A, Jia ZQ. Construction of a bioengineered cardiac graft. *J Thorac Cardiovasc Surg* 2000. **119**(2): 368-375.

70. Leor J, Aboulafia-Etzion S, Dar A, Shapiro L, Barbash IM, Battler A, Granot Y, Cohen S. Bioengineered cardiac grafts: A new approach to repair the infarcted myocardium? *Circulation* 2000. **102**(19 Suppl 3): III56-61.

71. Shimizu T, Yamato M, Kikuchi A, Okano T. Two-dimensional manipulation of cardiac myocyte sheets utilizing temperature-responsive culture dishes augments the pulsatile amplitude. *Tissue Eng* 2001. **7**(2): 141-151.

72. Kajstura J, Leri A, Finato N, Di Loreto C, Beltrami CA, Anversa P. Myocyte proliferation in end-stage cardiac failure in humans. *Proc Natl Acad Sci U S A* 1998. **95**(15): 8801-8805.

73. Beltrami AP, *et al.* Evidence that human cardiac myocytes divide after myocardial infarction. *N Engl J Med* 2001. **344**(23): 1750-1757.

74. Leri A, Barlucchi L, Limana F, Deptala A, Darzynkiewicz Z, Hintze TH, Kajstura J, Nadal-Ginard B, Anversa P. Telomerase expression and activity are coupled with myocyte proliferation and preservation of telomeric length in the failing heart. *Proc Natl Acad Sci U S A* 2001. **98**(15): 8626-8631.

75. Soonpaa MH, Field LJ. Assessment of cardiomyocyte DNA synthesis in normal and injured adult mouse hearts. *Am J Physiol* 1997. **272**(1 Pt 2): H220-226.

76. Soonpaa MH, Field LJ. Survey of studies examining mammalian cardiomyocyte DNA synthesis. *Circ Res* 1998. **83**(1): 15-26.

77. Becker RO, Chapin S, Sherry R. Regeneration of the ventricular myocardium in amphibians. *Nature* 1974. **248**(444): 145-147.

78. Clark LD, Clark RK, Heber-Katz E. A new murine model for mammalian wound repair and regeneration. *Clin Immunol Immunopathol* 1998. **88**(1): 35-45.

79. Leferovich JM, Bedelbaeva K, Samulewicz S, Zhang XM, Zwas D, Lankford EB, Heber-Katz E. Heart regeneration in adult MRL mice. *Proc Natl Acad Sci U S A* 2001. **98**(17): 9830-9835.

80. Maltsev VA, Rohwedel J, Hescheler J, Wobus AM. Embryonic stem cells differentiate in vitro into cardiomyocytes representing sinusnodal, atrial and ventricular cell types. *Mech Dev* 1993. **44**(1): 41-50.

81. Maltsev VA, Wobus AM, Rohwedel J, Bader M, Hescheler J. Cardiomyocytes differentiated in vitro from embryonic stem cells developmentally express cardiac-specific genes and ionic currents. *Circ Res* 1994. **75**(2): 233-244.

82. Muller M, *et al.* Selection of ventricular-like cardiomyocytes from ES cells in vitro. *FASEB J* 2000. **14**(15): 2540-2548.

83. Klug MG, Soonpaa MH, Koh GY, Field LJ. Genetically selected cardiomyocytes from differentiating embronic stem cells form stable intracardiac grafts. *J Clin Invest* 1996. **98**(1): 216-224.

84. Thomson JA, Itskovitz-Eldor J, Shapiro SS, Waknitz MA, Swiergiel JJ, Marshall VS, Jones JM. Embryonic stem cell lines derived from human blastocysts. *Science* 1998. **282**(5391): 1145-1147.

85. Shamblott MJ, Axelman J, Wang S, Bugg EM, Littlefield JW, Donovan PJ, Blumenthal PD, Huggins GR, Gearhart JD. Derivation of pluripotent stem cells from cultured human primordial germ cells. *Proc Natl Acad Sci U S A* 1998. **95**(23): 13726-13731.

86. Kehat I, *et al.* Human embryonic stem cells can differentiate into myocytes with structural and functional properties of cardiomyocytes. *J Clin Invest* 2001. **108**(3): 407-414.

87. Makino S, *et al.* Cardiomyocytes can be generated from marrow stromal cells in vitro. *J Clin Invest* 1999. **103**(5): 697-705.

88. Liechty KW, MacKenzie TC, Shaaban AF, Radu A, Moseley AM, Deans R, Marshak DR, Flake AW. Human mesenchymal stem cells engraft and demonstrate site-specific differentiation after in utero transplantation in sheep. *Nat Med* 2000. **6**(11): 1282-1286.

89. Tomita S, Li RK, Weisel RD, Mickle DA, Kim EJ, Sakai T, Jia ZQ. Autologous transplantation of bone marrow cells improves damaged heart function. *Circulation* 1999. **100**(19 Suppl): II247-256.

90. Orlic D, Kajstura J, Chimenti S, Bodine DM, Leri A, Anversa P. Transplanted adult bone marrow cells repair myocardial infarcts in mice. *Ann N Y Acad Sci* 2001. **938**: 221-229; discussion 229-230.

91. Orlic D, *et al.* Bone marrow cells regenerate infarcted myocardium. *Nature* 2001. **410**(6829): 701-705.

92. Strauer BE, Brehm M, Zeus T, Gattermann N, Hernandez A, Sorg RV, Kogler G, Wernet P. [Intracoronary, human autologous stem cell transplantation for myocardial regeneration following myocardial infarction]. *Dtsch Med Wochenschr* 2001. **126**(34-35): 932-938.

93. Bittner RE, *et al.* Recruitment of bone-marrow-derived cells by skeletal and cardiac muscle in adult dystrophic mdx mice. *Anat Embryol (Berl)* 1999. **199**(5): 391-396.

94. Jackson KA, *et al.* Regeneration of ischemic cardiac muscle and vascular endothelium by adult stem cells. *J Clin Invest* 2001. **107**(11): 1395-1402.

95. Orlic D, *et al.* Mobilized bone marrow cells repair the infarcted heart, improving function and survival. *Proc Natl Acad Sci U S A* 2001. **98**(18): 10344-10349.

96. Jono S, Peinado C, Giachelli CM. Phosphorylation of osteopontin is required for inhibition of vascular smooth muscle cell calcification. *J Biol Chem* 2000. **275**(26): 20197-20203.

97. Chilkoti A, Tan PH, Stayton PS. Site-directed mutagenesis studies of the high-affinity streptavidin- biotin complex: contributions of tryptophan residues 79, 108, and 120. *Proc Natl Acad Sci U S A* 1995. **92**(5): 1754-1758.

98. Klumb LA, Chu V, Stayton PS. Energetic roles of hydrogen bonds at the ureido oxygen binding pocket in the streptavidin-biotin complex. *Biochemistry* 1998. **37**(21): 7657-7663.

99. Kumar A, Biebuyck HA, Whitesides GM. Patterning self-assembled monolayers: applications in materials science. *Langmuir* 1994. **10**(5): 1498-1511.

100. Mrksich M, Dike LE, Tien J, Ingber DE, Whitesides GM. Using microcontact printing to pattern the attachment of mammalian cells to self-assembled monolayers of alkanethiolates on transparent films of gold and silver. *Exp Cell Res* 1997. **235**(2): 305-313.

101. Bernard A, Delamarche E, Schmid H, Michel B, Bosshard HR, Biebuyck H. Printing patterns of proteins. *Langmuir* 1998. **14**(9): 2225-2229.

102. Branch DW, Corey JM, Weyhenmeyer JA, Brewer GJ, Wheeler BC. Microstamp patterns of biomolecules for high-resolution neuronal networks. *Med Biol Eng Comput* 1998. **36**(1): 135-141.

103. James CD, Davis RC, Kam L, Craighead HG, Isaacson M, Turner JN, Shain W. Patterned protein layers on solid substrates by thin stamp microcontact printing. *Langmuir* 1998. **14**(4): 741-744.

104. Bernard A, Renault JP, Michel B, Bosshard HR, Delamarche E. Microcontact printing of proteins. *Adv Mater* 2000. **12**(14): 1067-1070.

105. Iwaki K, Sukhatme VP, Shubeita HE, Chien KR. Alpha- and beta-adrenergic stimulation induces distinct patterns of immediate early gene expression in neonatal rat myocardial cells. fos/jun expression is associated with sarcomere assembly; Egr-1 induction is primarily an alpha 1-mediated response. *J Biol Chem* 1990. **265**(23): 13809-13817.

106. Sano T, Cantor CR. A streptavidin-protein A chimera that allows one-step production of a variety of specific antibody conjugates. *Biotechnology (N Y)* 1991. **9**(12): 1378-1381.

107. Sano T, Glazer AN, Cantor CR. A streptavidin-metallothionein chimera that allows specific labeling of biological materials with many different heavy metal ions. *Proc Natl Acad Sci U S A* 1992. **89**(5): 1534-1538.

108. Dubel S, Breitling F, Kontermann R, Schmidt T, Skerra A, Little M. Bifunctional and multimeric complexes of streptavidin fused to single chain antibodies (scFv). *J Immunol Methods* 1995. **178**(2): 201-209.

109. Karp M, Lindqvist C, Nissinen R, Wahlbeck S, Akerman K, Oker-Blom C. Identification of biotinylated molecules using a baculovirus-expressed luciferase-streptavidin fusion protein. *Biotechniques* 1996. **20**(3): 452-456, 458-459.

110. Oker-Blom C, Orellana A, Keinanen K. Highly efficient production of GFP and its derivatives in insect cells for visual in vitro applications. *FEBS Lett* 1996. **389**(3): 238-243.

111. Maeda T, Oyama R, Ichihara-Tanaka K, Kimizuka F, Kato I, Titani K, Sekiguchi K. A novel cell adhesive protein engineered by insertion of the Arg-Gly- Asp-Ser tetrapeptide. *J Biol Chem* 1989. **264**(26): 15165-15168.

112. Hashino K, Shimojo T, Kimizuka F, Kato I, Maeda T, Sekiguchi K, Titani K. Engineering of artificial cell adhesion proteins by grafting the Arg- Gly-Asp cell adhesive signal to a calpastatin segment. *J Biochem (Tokyo)* 1992. **112**(4): 547-551.

113. Barbas CF, 3rd, Languino LR, Smith JW. High-affinity self-reactive human antibodies by design and selection: targeting the integrin ligand binding site. *Proc Natl Acad Sci U S A* 1993. **90**(21): 10003-10007.

114. Yamada T, Matsushima M, Inaka K, Ohkubo T, Uyeda A, Maeda T, Titani K, Sekiguchi K, Kikuchi M. Structural and functional analyses of the Arg-Gly-Asp sequence introduced into human lysozyme. *J Biol Chem* 1993. **268**(14): 10588-10592.

115. Rossi F, Billetta R, Ruggeri Z, Zanetti M. Engineered idiotypes. Immunochemical analysis of antigenized antibodies expressing a conformationally constrained Arg-Gly-Asp motif. *Mol Immunol* 1995. **32**(5): 341-346.

116. Smith JW, Tachias K, Madison EL. Protein loop grafting to construct a variant of tissue-type plasminogen activator that binds platelet integrin alpha IIb beta 3. *J Biol Chem* 1995. **270**(51): 30486-30490.

117. Yamada T, Shimada Y, Uyeda A, Sugiyama S, Kikuchi M. Construction of a divalent cell adhesive lysozyme by introducing the Arg-Gly-Asp sequence at two sites. *FEBS Lett* 1995. **374**(2): 262-264.

118. Yamada T, Shimada Y, Kikuchi M. Integrin-specific tissue-type plasminogen activator engineered by introduction of the Arg-Gly-Asp sequence. *Biochem Biophys Res Commun* 1996. **228**(2): 306-311.

119. Liaw L, Almeida M, Hart CE, Schwartz SM, Giachelli CM. Osteopontin promotes vascular cell adhesion and spreading and is chemotactic for smooth muscle cells in vitro. *Circ Res* 1994. **74**(2): 214-224.

120. Scatena M, Almeida M, Chaisson ML, Fausto N, Nicosia RF, Giachelli CM. NF-kappaB mediates alphavbeta3 integrin-induced endothelial cell survival. *J Cell Biol* 1998. **141**(4): 1083-1093.

121. Main AL, Harvey TS, Baron M, Boyd J, Campbell ID. The three-dimensional structure of the tenth type III module of fibronectin: an insight into RGD-mediated interactions. *Cell* 1992. **71**(4): 671-678.

122. Pierschbacher MD, Ruoslahti E. Influence of stereochemistry of the sequence Arg-Gly-Asp-Xaa on binding specificity in cell adhesion. *J Biol Chem* 1987. **262**(36): 17294-17298.

123. Maeda T, Hashino K, Oyama R, Titani K, Sekiguchi K. Artificial cell adhesive proteins engineered by grafting the Arg-Gly- Asp cell recognition signal: factors modulating the cell adhesive activity of the grafted signal. *J Biochem (Tokyo)* 1991. **110**(3): 381-387.

124. D'Souza SE, Ginsberg MH, Plow EF. Arginyl-glycyl-aspartic acid (RGD): a cell adhesion motif. *Trends Biochem Sci* 1991. **16**(7): 246-250.

125. Alon R, Bayer EA, Wilchek M. Streptavidin contains an RYD sequence which mimics the RGD receptor domain of fibronectin. *Biochem Biophys Res Commun* 1990. **170**(3): 1236-1241.

126. Alon R, Bayer EA, Wilchek M. Cell-adhesive properties of streptavidin are mediated by the exposure of an RGD-like RYD site. *Eur J Cell Biol* 1992. **58**(2): 271-279.

127. Alon R, Bayer EA, Wilchek M. Cell adhesion to streptavidin via RGD-dependent integrins. *Eur J Cell Biol* 1993. **60**(1): 1-11.

128. Alon R, Hershkoviz R, Bayer EA, Wilchek M, Lider O. Streptavidin blocks immune reactions mediated by fibronectin-VLA-5 recognition through an Arg-Gly-Asp mimicking site. *Eur J Immunol* 1993. **23**(4): 893-898.

129. Chilkoti A, Schwartz BL, Smith RD, Long CJ, Stayton PS. Engineered chimeric streptavidin tetramers as novel tools for bioseparations and drug delivery. *Biotechnology (N Y)* 1995. **13**(11): 1198-1204.

130. Patel N, *et al.* Spatially controlled cell engineering on biodegradable polymer surfaces. *FASEB J* 1998. **12**(14): 1447-1454.

131. Scholl M, Sprossler C, Denyer M, Krause M, Nakajima K, Maelicke A, Knoll W, Offenhausser A. Ordered networks of rat hippocampal neurons attached to silicon oxide surfaces. *J Neurosci Methods* 2000. **104**(1): 65-75.

132. Bornstein P. Matricellular proteins: an overview. *Matrix Biol* 2000. **19**(7): 555-556.

133. Collier TO, Thomas CH, Anderson JM, Healy KE. Surface chemistry control of monocyte and macrophage adhesion, morphology, and fusion. *J Biomed Mater Res* 2000. **49**(1): 141-145.

134. Bhatia SN, Toner M, Tompkins RG, Yarmush ML. Selective adhesion of hepatocytes on patterned surfaces. *Ann N Y Acad Sci* 1994. **745**: 187-209.

135. Spargo BJ, Testoff MA, Nielsen TB, Stenger DA, Hickman JJ, Rudolph AS. Spatially controlled adhesion, spreading, and differentiation of endothelial cells on self-assembled molecular monolayers. *Proc Natl Acad Sci U S A* 1994. **91**(23): 11070-11074.

136. Dike LE, Chen CS, Mrksich M, Tien J, Whitesides GM, Ingber DE. Geometric control of switching between growth, apoptosis, and differentiation during angiogenesis using micropatterned substrates. *In Vitro Cell Dev Biol Anim* 1999. **35**(8): 441-448.

137. Healy KE, Thomas CH, Rezania A, Kim JE, McKeown PJ, Lom B, Hockberger PE. Kinetics of bone cell organization and mineralization on materials with patterned surface chemistry. *Biomaterials* 1996. **17**(2): 195-208.

138. Kleinfeld D, Kahler KH, Hockberger PE. Controlled outgrowth of dissociated neurons on patterned substrates. *J-Neurosci* 1988. **8**(11): 4098-4120.

139. Stenger DA, *et al.* Microlithographic determination of axonal/dendritic polarity in cultured hippocampal neurons. *J Neurosci Methods* 1998. **82**(2): 167-173.

140. Rohr S, Scholly DM, Kleber AG. Patterned growth of neonatal rat heart cells in culture. Morphological and electrophysiological characterization. *Circ Res* 1991. **68**(1): 114-130.

141. Clark P, Coles D, Peckham M. Preferential adhesion to and survival on patterned laminin organizes myogenesis in vitro. *Exp Cell Res* 1997. **230**(2): 275-283.

142. Blawas AS, Reichert WM. Protein patterning. *Biomaterials* 1998. **19**(7-9): 595-609.

143. Kane RS, Takayama S, Ostuni E, Ingber DE, Whitesides GM. Patterning proteins and cells using soft lithography. *Biomaterials* 1999. **20**(23-24): 2363-2376.

144. Folch A, Toner M. Microengineering of cellular interactions. *Ann Rev Biomed Eng* 2000. **2**: 227-256.

145. Jung DR, Kapur R, Adams T, Giuliano KA, Mrksich M, Craighead HG, Taylor DL. Topographical and physicochemical modification of material surface to enable patterning of living cells. *Crit Rev Biotechnol* 2001. **21**(2): 111-154.

146. Zhang S, Yan L, Altman M, Lassle M, Nugent H, Frankel F, Lauffenburger DA, Whitesides GM, Rich A. Biological surface engineering: a simple system for cell pattern formation. *Biomaterials* 1999. **20**(13): 1213-1220.

147. Singhvi R, Kumar A, Lopez GP, Stephanopoulos GN, Wang DI, Whitesides GM, Ingber DE. Engineering cell shape and function. *Science* 1994. **264**(5159): 696-698.

148. Chen CS, Mrksich M, Huang S, Whitesides GM, Ingber DE. Geometric control of cell life and death. *Science* 1997. **276**(5317): 1425-1428.

149. Branch DW, Wheeler BC, Brewer GJ, Leckband DE. Long-term maintenance of patterns of hippocampal pyramidal cells on substrates of polyethylene glycol and microstamped polylysine. *IEEE Trans Biomed Eng* 2000. **47**(3): 290-300.

150. James CD, *et al.* Aligned microcontact printing of micrometer-scale poly-L-lysine structures for controlled growth of cultured neurons on planar microelectrode arrays. *IEEE Trans Biomed Eng* 2000. **47**(1): 17-21.

151. Kam L, Boxer SG. Cell adhesion to protein-micropatterned-supported lipid bilayer membranes. *J Biomed Mater Res* 2001. **55**(4): 487-495.

152. Lauer L, Ingebrandt S, Scholl M, Offenhausser A. Aligned microcontact printing of biomolecules on microelectronic device surfaces. *IEEE Trans Biomed Eng* 2001. **48**(7): 838-842.

153. Lauer L, Klein C, Offenhausser A. Spot compliant neuronal networks by structure optimized micro-contact printing. *Biomaterials* 2001. **22**(13): 1925-1932.

154. Yeung CK, Lauer L, Offenhausser A, Knoll W. Modulation of the growth and guidance of rat brain stem neurons using patterned extracellular matrix proteins. *Neurosci Lett* 2001. **301**(2): 147-150.

155. Pan YV, McDevitt TC, Kim TK, Leach-Scampavia D, Stayton PS, Denton DD, Ratner BD. Micro-scale cell patterning on non-fouling plasma polymerized tetraglyme coatings by protein microcontact printing. *Plasmas & Polymers* 2001. **in press**.

156. Lahav J. Thrombospondin inhibits adhesion of endothelial cells. *Exp Cell Res* 1988. **177**(1): 199-204.

157. Murphy-Ullrich JE, Hook M. Thrombospondin modulates focal adhesions in endothelial cells. *J Cell Biol* 1989. **109**(3): 1309-1319.

158. Berge N, Loganadane LD, Vassy J, Monnet E, Legrand C, Fauvel-Lafeve F. Adhesion-induced intracellular signalling in endothelial cells depends on the nature of the matrix. *Cell Adhes Commun* 1999. **7**(1): 29-41.

159. Yang ZP, Belu AM, Liebmann-Vinson A, Sugg H, Chilkoti A. Molecular imaging of a micropatterned biological ligand on an activated polymer surface. *Langmuir* 2000. **16**(19): 7482-7492.

160. Patel N, Bhandari R, Shakesheff KM, Cannizzaro SM, Davies MC, Langer R, Roberts CJ, Tendler SJB, Williams PM. Printing patterns of biospecifically-adsorbed protein. *J Biomat Polym Sci Ed* 2000. **11**(3): 319-331.

161. Yang ZP, Chilkoti A. Microstamping of a biological ligand onto an activated polymer surface. *Adv Mater* 2000. **12**(413).

162. Duong JL, McDevitt TC, Stayton PS. Covalent protein patterning on polymer surfaces by microcontact printing. *J Undergrad Res Bioeng* 2001. **in press**.

163. Pins GD, Toner M, Morgan JR. Microfabrication of an analog of the basal lamina: biocompatible membranes with complex topographies. *FASEB J* 2000. **14**(3): 593-602.

164. Bhatia SN, Balis UJ, Yarmush ML, Toner M. Probing heterotypic cell interactions: hepatocyte function in microfabricated co-cultures. *J Biomater Sci Polym Ed* 1998. **9**(11): 1137-1160.

165. Rowe CA, Scruggs SB, Feldstein MJ, Golden JP, Ligler FS. An array immunosensor for simultaneous detection of clinical analytes. *Anal Chem* 1999. **71**(2): 433-439.

166. Lieberman M, Roggeveen AE, Purdy JE, Johnson EA. Synthetic strands of cardiac muscle: growth and physiological implication. *Science* 1972. **175**(24): 909-911.

167. Thomas SP, Bircher-Lehmann L, Thomas SA, Zhuang J, Saffitz JE, Kleber AG. Synthetic strands of neonatal mouse cardiac myocytes: structural and electrophysiological properties. *Circ Res* 2000. **87**(6): 467-473.

168. Lieberman M. Electrophysiological studies of a synthetic strand of cardiac muscle. *Physiologist* 1973. **16**(4): 551-563.

169. Lieberman M, Sawanobori T, Kootsey JM, Johnson EA. A synthetic strand of cardiac muscle: its passive electrical properties. *J Gen Physiol* 1975. **65**(4): 527-550.

170. Fast VG, Kleber AG. Cardiac tissue geometry as a determinant of unidirectional conduction block: assessment of microscopic excitation spread by optical mapping in patterned cell cultures and in a computer model. *Cardiovasc Res* 1995. **29**(5): 697-707.

171. Fast VG, Darrow BJ, Saffitz JE, Kleber AG. Anisotropic activation spread in heart cell monolayers assessed by high-resolution optical mapping. Role of tissue discontinuities. *Circ Res* 1996. **79**(1): 115-127.

172. Kucera JP, Kleber AG, Rohr S. Slow conduction in cardiac tissue, II: effects of branching tissue geometry. *Circ Res* 1998. **83**(8): 795-805.

173. Rohr S, Kucera JP, Kleber AG. Slow conduction in cardiac tissue, I: effects of a reduction of excitability versus a reduction of electrical coupling on microconduction. *Circ Res* 1998. **83**(8): 781-794.

174. Gerdes AM, Moore JA, Hines JM, Kirkland PA, Bishop SP. Regional differences in myocyte size in normal rat heart. *Anat Rec* 1986. **215**(4): 420-426.

175. Capasso JM, Fitzpatrick D, Anversa P. Cellular mechanisms of ventricular failure: myocyte kinetics and geometry with age. *Am J Physiol* 1992. **262**(6 Pt 2): H1770-1781.

176. Hirakow R, Gotoh T, Watanabe T. Quantitative studies on the ultrastructural differentiation and growth of mammalian cardiac muscle cells. I. The atria and ventricles of the rat. *Acta Anat* 1980. **108**(2): 144-152.

177. Dodson MV, Vierck JL, Hossner KL, Byrne K, McNamara JP. The development and utility of a defined muscle and fat co-culture system. *Tissue Cell* 1997. **29**(5): 517-524.

178. Cirillo P, Golino P, Ragni M, Battaglia C, Pacifico F, Formisano S, Buono C, Condorelli M, Chiariello M. Activated platelets and leucocytes cooperatively stimulate smooth muscle cell proliferation and proto-oncogene expression via release of soluble growth factors. *Cardiovasc Res* 1999. **43**(1): 210-218.

179. He Q, Cahill CJ, Spiro MJ. Suspension culture of differentiated rat heart myocytes on non-adhesive surfaces. *J Mol Cell Cardiol* 1996. **28**(5): 1177-1186.

180. Powell RJ, Cronenwett JL, Fillinger MF, Wagner RJ, Sampson LN. Endothelial cell modulation of smooth muscle cell morphology and organizational growth pattern. *Ann Vasc Surg* 1996. **10**(1): 4-10.

181. Saunders KB, D'Amore PA. An in vitro model for cell-cell interactions. *In Vitro Cell Dev Biol* 1992. **28A**(7-8): 521-528.

182. Fillinger MF, Sampson LN, Cronenwett JL, Powell RJ, Wagner RJ. Coculture of endothelial cells and smooth muscle cells in bilayer and conditioned media models. *J Surg Res* 1997. **67**(2): 169-178.

183. Maurin AC, Chavassieux PM, Frappart L, Delmas PD, Serre CM, Meunier PJ. Influence of mature adipocytes on osteoblast proliferation in human primary cocultures. *Bone* 2000. **26**(5): 485-489.

184. Nishida M, Springhorn JP, Kelly RA, Smith TW. Cell-cell signaling between adult rat ventricular myocytes and cardiac microvascular endothelial cells in heterotypic primary culture. *J Clin Invest* 1993. **91**(5): 1934-1941.

185. Bhatia SN, Yarmush ML, Toner M. Controlling cell interactions by micropatterning in co-cultures: hepatocytes and 3T3 fibroblasts. *J Biomed Mater Res* 1997. **34**(2): 189-199.

186. Hirose M, Yamato M, Kwon OH, Harimoto M, Kushida A, Shimizu T, Kikuchi A, Okano T. Temperature-Responsive surface for novel co-culture systems of hepatocytes with endothelial cells: 2-D patterned and double layered co- cultures. *Yonsei Med J* 2000. **41**(6): 803-813.

187. Yamato M, Kwon OH, Hirose M, Kikuchi A, Okano T. Novel patterned cell coculture utilizing thermally responsive grafted polymer surfaces. *J Biomed Mater Res* 2001. **55**(1): 137-140.

188. Yousaf MN, Houseman BT, Mrksich M. Using electroactive substrates to pattern the attachment of two different cell populations. *Proc Natl Acad Sci U S A* 2001. **98**(11): 5992-5996.

189. Hubbell JA. Biomaterials in tissue engineering. *Biotechnology (N Y)* 1995. **13**(6): 565-576.

190. Vacanti JP, Langer R, Upton J, Marler JJ. Transplantation of cells in matrices for tissue regeneration. *Adv Drug Deliv Rev* 1998. **33**(1-2): 165-182.

191. Engelberg I, Kohn J. Physico-mechanical properties of degradable polymers used in medical applications: a comparative study. *Biomaterials* 1991. **12**(3): 292-304.

192. Skarja GA, Woodhouse KA. Synthesis and characterization of degradable polyurethane elastomers containing and amino acid-based chain extender. *J Biomater Sci Polym Ed* 1998. **9**(3): 271-295.

193. Skarja GA, Woodhouse KA. Structure-property relationships of degradable polyurethane elastomers containing an amino acid-based chain extender. *J Appl Polym Sci* 2000. **75**(12): 1522-1534.

194. Pett SB, Jr., Follis F, Allen K, Temes T, Wernly JA. Posterior ventricular septal rupture: an anatomical reconstruction. *J Card Surg* 1998. **13**(6): 445-450; discussion 451-442.

195. Ogiwara M, *et al.* [Clinical result of left ventricular free wall rupture resulting from acute myocardial infarction]. *Kyobu Geka* 1995. **48**(4): 286-289.

196. Murata H, *et al.* Oozing type cardiac rupture repaired with percutaneous injection of fibrin-glue into the pericardial space: case report. *Jpn Circ J* 2000. **64**(4): 312-315.

197. Dapper G, *et al.* Attachment of gelatin films to tissue using argon beam coagulator. *J Biomed Mater Res* 1998. **43**(2): 89-98.

198. Zogno M, La Canna G, Ceconi C, Ferrari M, Latini L, Lorusso R, Sandrelli L, Alfieri O. Postinfarction left ventricular free wall rupture: original management and surgical technique. *J Card Surg* 1991. **6**(3): 396-399.

199. Coletti G, Torracca L, Zogno M, La Canna G, Lorusso R, Pardini A, Alfieri O. Surgical management of left ventricular free wall rupture after acute myocardial infarction. *Cardiovasc Surg* 1995. **3**(2): 181-186.

200. Yamazaki Y, Eguchi S, Miyamura H, Hayashi J, Fukuda J, Ozeki H, Yoshimura T, Fujita Y, Tsuchiya A. Replacement of myocardium with a Dacron prosthesis for complications of acute myocardial infarction. *J Cardiovasc Surg (Torino)* 1989. **30**(2): 277-280.

201. Lijoi A, Scarano F, Parodi E, Dottori V, Secchi GL, Delfino R, Tallone M, Venere G. Subacute left ventricular free wall rupture complicating acute myocardial infarction. Successful surgical repair with a sutureless technique. *J Cardiovasc Surg (Torino)* 1996. **37**(6): 627-630.

202. Deutsch J, Motlagh D, Russell B, Desai TA. Fabrication of microtextured membranes for cardiac myocyte attachment and orientation. *J Biomed Mater Res* 2000. **53**(3): 267-275.

203. Polonchuk L, Elbel J, Eckert L, Blum J, Wintermantel E, Eppenberger HM. Titanium dioxide ceramics control the differentiated phenotype of cardiac muscle cells in culture. *Biomaterials* 2000. **21**(6): 539-550.

204. Folliguet TA, Rucker-Martin C, Pavoine C, Deroubaix E, Henaff M, Mercadier JJ, Hatem SN. Adult cardiac myocytes survive and remain excitable during long-term culture on synthetic supports. *J Thorac Cardiovasc Surg* 2001. **121**(3): 510-519.

205. Marsh JD. The cultured heart cell: a useful model for physiological and biochemical investigation. *Int J Cardiol* 1983. **3**(4): 465-468.

206. Jacobson SL, Piper HM. Cell cultures of adult cardiomyocytes as models of the myocardium. *J Mol Cell Cardiol* 1986. **18**(7): 661-678.

207. Mitcheson JS, Hancox JC, Levi AJ. Cultured adult cardiac myocytes: future applications, culture methods, morphological and electrophysiological properties. *Cardiovasc Res* 1998. **39**(2): 280-300.

208. Israel DA, Barry WH, Edell DJ, Mark RG. An array of microelectrodes to stimulate and record from cardiac cells in culture. *Am J Physiol* 1984. **247**(4 Pt 2): H669-674.

209. Connolly P, Clark P, Curtis AS, Dow JA, Wilkinson CD. An extracellular microelectrode array for monitoring electrogenic cells in culture. *Biosens Bioelectron* 1990. **5**(3): 223-234.

210. Denyer MC, Riehle M, Britland ST, Offenhauser A. Preliminary study on the suitability of a pharmacological bio-assay based on cardiac myocytes cultured over microfabricated microelectrode arrays. *Med Biol Eng Comput* 1998. **36**(5): 638-644.

211. Pancrazio JJ, *et al.* Description and demonstration of a CMOS amplifier-based-system with measurement and stimulation capability for bioelectrical signal transduction. *Biosens Bioelectron* 1998. **13**(9): 971-979.

Vita

Todd C. McDevitt was born in Atlanta, Georgia in 1974. He grew up in Laurel Springs, NJ (outside of Philadelphia) until 1986, when his family moved to Naperville, IL (outside of Chicago). He received his Bachelor of Science in Engineering degree at Duke University in May 1997 with a double major in biomedical and electrical engineering. At Duke, he conducted independent research under Dr. W. M. Reichert working on optimization of a multi-analyte biosensor. In October of 2001, he earned his Doctor of Philosophy in Bioengineering from the University of Washington. He is continuing his formal training with a post-doctoral research fellowship at the University of Washington working with Dr. Charles E. Murry and Dr. Stephen D. Hauschka. Todd anticipates pursuing a career in tissue engineering, most likely in academia.